Extragalactic Novae and Their Progenitors

Steven Charles Williams

A thesis submitted in partial fulfilment of the requirements of

Liverpool John Moores University

for the degree of

Doctor of Philosophy.

April 2014

Declaration

The work presented in this thesis was carried out at the Astrophysics Research Institute, Faculty of Science, Liverpool John Moores University. Unless otherwise stated, it is the original work of the author.

While registered as a candidate for the degree of Doctor of Philosophy, for which submission is now made, the author has not been registered as a candidate for any other award. This thesis has not been submitted in whole, or in part, for any other degree.

Steven Charles Williams
Astrophysics Research Institute
Liverpool John Moores University
IC2, Liverpool Science Park
146 Brownlow Hill
Liverpool
L3 5RF
UK

April 2014

Abstract

Novae are binary systems containing a white dwarf (WD) and a less-evolved companion star, either a main-sequence, sub-giant or red giant star. The WD accretes matter from the companion through Roche lobe overflow or via a stellar wind. As material is accreted, the pressure and temperature at the base of the accreted envelope increase until a thermonuclear runaway occurs. This causes a sudden increase in brightness (the outburst), which ranks among the most luminous stellar astrophysical phenomena.

Following the outburst, some novae form detectable dust in the ejecta. Observationally, there is a correlation between the dust-formation timescale and the time it takes the nova to fade optically by two magnitudes, which was emphasised in a study of infrared emission from novae in the Andromeda Galaxy (M31). In the first part of this thesis, a simple theoretical model is presented, which considers the higher-energy photons produced by the nova being absorbed by neutral hydrogen in the ejecta, before they can reach the potential dust-formation sites. This new model successfully replicates the observed trend between these two parameters and agrees well with the observational data.

The majority of novae are thought to consist of a WD and a main-sequence star, although some systems harbour a sub-giant (SG-novae) or red giant (RG-novae) companion instead. In the Milky Way galaxy, relatively few RG-novae have been confirmed, although in many systems, the evolutionary state of the secondary is simply not known. There is evidence that the progenitors of some Type Ia supernovae (SNe Ia) may be RG-nova systems (e.g. SN PTF11kx), therefore it is important to understand the population of such systems. In this thesis, archival *Hubble Space Telescope*

(*HST*) data are used to search for RG-novae in M31. Many more novae are discovered in M31 each year ($\sim$30) than in the Milky Way ($\sim$10). Distance determination is a major complication when studying Galactic novae. However, at the distance of M31 all the novae may be considered to be at the same distance, making M31 an excellent environment for studying nova populations.

We conducted a survey of 38 spectroscopically confirmed M31 novae in quiescence. We determined that 11 of these systems had a coincident progenitor candidate whose probability of being a chance alignment with a resolved source in the *HST* data was $\leq 5\%$. As the main sequence and the majority of the sub-giant branch are not resolvable in the *HST* data, this implies that a significant proportion of these systems contain red giant secondaries. The light curves of several M31 novae are also presented here, some of which use *HST* data to extend the light curves far deeper than is typically possible for extragalactic systems.

A statistical study was then carried out to test the results of the survey and derive an estimate of the proportion of M31 novae associated with a resolved source in the *HST* data. This includes, for example, models of the spatial distribution, speed class and peak magnitude of the M31 nova population, as well as considering biases introduced by the *HST* coverage of M31. The initial results suggest $0.38^{+0.16}_{-0.12}$ of M31 novae are associated with a source in the *HST* data, a class of objects expected to be dominated by RG-novae. This is a much greater proportion than that observed so far in our Galaxy, and will be important when considering such systems as potential SN Ia candidates. The spatial distribution of novae that have resolved progenitor candidates is consistent with these systems being associated with the M31 disk, rather than the bulge.

The method used to locate the progenitors of M31 novae was also used to study three additional systems. The M31 nova, M31N 2008-12a, which appears to be a recurrent nova (RN) with a very short inter-outburst period, produced an outburst in November 2013. This outburst was studied and a candidate progenitor system was found in *HST* data when it was apparently in quiescence, supporting its classification as a RN with a high accretion rate. The method was also used to explore upper limits on the brightness of the progenitor of SN 2014J, a SN Ia in M82, although no progenitor was found, a

RG-nova (or in-fact any type of system) could not be ruled out due to the limitations of the data. For the M31 transient TCP J00403295+4034387, which showed an unusual spectrum, archival *HST* data were used to show the object was probably a blend of two objects with a very small apparent separation. Finally, the thesis is summarised, and future work on both dust formation and the progenitor search are discussed.

Publications

Refereed Journals:

Williams, S. C., Bode, M. F., Darnley, M. J., Evans, A., Zubko, V. and Shafter, A. W., 2013, ApJ, 777, L32 – *Rapid Dust Formation in Novae: The Speed Class–Formation Timescale Correlation Explained*

Henze, M., Ness, J.-U., Darnley, M. J., Bode, M. F., **Williams, S. C.**, Shafter, A. W., Kato, M. and Hachisu, I., 2014, A&A, 563, L8 – *A remarkable recurrent nova in M31: The X-ray observations*

Darnley, M. J., **Williams, S. C.**, Bode, M. F., Henze, M., Ness, J.-U., Shafter, A. W., Hornoch, K. and Votruba, V., 2014, A&A, 563, L9 – *A remarkable recurrent nova in M31: The optical observations*

Williams, S. C., Darnley, M. J., Bode, M. F., Keen, A. and Shafter A. W., 2014, ApJS, accepted (arXiv:1405.4874) – *On the Progenitors of Local Group Novae - I. The M31 Catalog*

Williams, S. C., Darnley, M. J., Bode, M. F. and Shafter, A. W., ApJ, in preparation – *On the Progenitors of Local Group Novae - II.*

Telegrams:

Shafter, A. W., Darnley, M. J., Bode, M. F., **Williams, S. C.**, Hornoch, K. and Ciardullo, R., 2011, ATel, 3806 – *Spectroscopic observations of the M31 optical transient, TCP J00403295+4034387*

Williams, S. C., Darnley, M. J., Bode, M. F. and Shafter, A. W., 2013, ATel, 5611 – *A Candidate Recurrent Nova in M31: The Progenitor System?*

Henze, M., Ness, J.-U., Bode, M. F., Darnley, M. J. and **Williams, S. C.**, 2013, ATel, 5627 – *A Candidate Recurrent Nova in M31: A fast supersoft X-ray counterpart found with Swift XRT*

Henze, M., Ness, J.-U., Bode, M. F., Darnley, M. J., **Williams, S. C.** and Shafter, A. W., 2013, ATel, 5633 – *A Candidate Recurrent Nova in M31: X-ray and UV short-term variability with Swift*

Henze, M., Ness, J.-U., Bode, M. F., Darnley, M. J., **Williams, S. C.** and Shafter, A. W., 2013, ATel, 5687 – *A recent M 31 nova found as a supersoft X-ray source with Swift*

Williams, S. C., Darnley, M. J., Bode, M. F., Shafter, A. W., Zhang, J. J., Mazzali, P. and Pian, E., 2014, ATel, 5723 – *Spectroscopic Classification of the M31 Nova Candidate PNV J00425172+4118142*

Williams, S. C., Darnley, M. J., Bersier, D. F., Bode, M. F., James, P. A. and Mazzali, P., 2014, ATel, 5824 – *SN 2014J: HST archival observations do not preclude Recurrent or Classical Nova progenitor system*

Conference Proceedings:

Darnley, M. J., Bode, M. F., Harman, D. J., Hounsell, R. A., Munari, U., Ribeiro, V. A. R. M., Surina, F., Williams, R. P. and **Williams, S. C.**, 2013, in Stella Novae: Future and Past Decades, P. A. Woudt & V. A. R. M. Ribeiro (eds), ASPCS, in press

(arXiv:1303.2711) – *On the Galactic Nova Progenitor Population*

Williams, S. C., Darnley, M. J., Bode, M .F., Shafter, A. W., 2013, in Stella Novae: Future and Past Decades, P. A. Woudt & V. A. R. M. Ribeiro (eds), ASPCS, in press (arXiv:1303.1980) – *On the M31 Nova Progenitor Population*

Williams, S. C., Bode, M .F., Darnley, M. J., Zubko, V., Evans, A. and Shafter, A. W., 2013, in Stella Novae: Future and Past Decades, P. A. Woudt & V. A. R. M. Ribeiro (eds), ASPCS, in press – *Rapid Dust Formation in Novae: Speed Class and Grain Formation Timescale*

Acknowledgements

First and foremost, I would like to thank my supervisors, Dr Matt Darnley and Prof. Mike Bode for their help, support and guidance throughout these last three and a half years.

I would like to extend these thanks to everyone at the ARI, past and present, that made my time here enjoyable. I would particularly like to thank fellow students Matt Prescott, Rob Barnsley, Dave Eden, Rich Harrison and Joe Lyman. The many pub trips, and the laughs and adventures we've had along the way, is what has made my stay in Liverpool really enjoyable.

I would also like to thank Liverpool John Moores University and the Science & Technology Facilities Council for giving me the opportunity to study for a doctorate.

Finally, I would like to thank my parents Arnie and Heather, siblings Lisa and Andrew, and grandmothers Joyce and Amy, for their love and support during my PhD.

Contents

List of Tables

List of Figures

Chapter 1

Novae

1.1 Introduction

Novae are a type of cataclysmic variable star (CV; Kraft, 1964) and are produced by a white dwarf (WD) accreting matter from its companion star. When sufficient pressure and temperature are reached at the base of the accreted envelope, the accreted matter will undergo a thermonuclear runaway reaction (TNR). The energy produced during the TNR leads to the ejection of material from the WD surface and causes a vast increase in luminosity, which is observed as the outburst. The word *nova* itself is derived from the Latin *nova stella* meaning *new star*, as they were originally thought to be new stars appearing in the sky. The outburst of a typical bright nova in the Andromeda Galaxy (M31) is shown in Figure 1.1.

Novae have been noted since ancient times. A list of pre-telescopic novae and supernovae (SNe) compiled from various sources was published by Duerbeck (2008) giving over 90 events spanning from the 14^{th} century BC until Kepler's SN of 1604. We now know of approximately 400 novae in our Galaxy alone (Bode, 2010; Darnley et al., 2012) and over 900 candidates in M31 (Pietsch, 2010, see also their online catalogue[1]). The first extragalactic nova was discovered in M31 in 1885 and has since been

[1] `http://www.mpe.mpg.de/~m31novae/opt/m31/index.php`

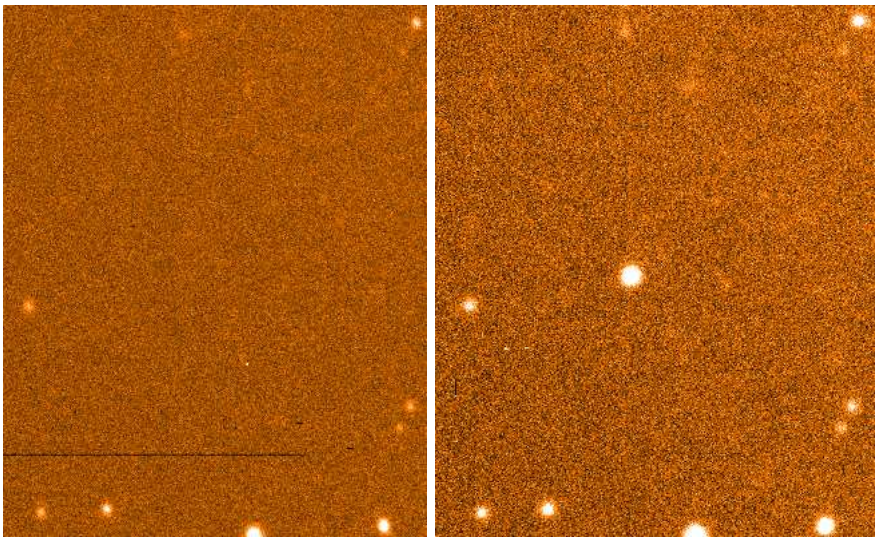

Figure 1.1: M31 nova M31N 2010-09b on *B*-band images taken by RATCam on the Liverpool Telescope during quiescence (left) and during outburst (right).

identified as a SN (1885A; see e.g. Hogg, 1937, and de Vaucouleurs & Corwin, 1985, for discussion). A number of possible extragalactic novae were discovered in the early $20^{\rm th}$ century, the first, subsequently confirmed, nova (and not a SN or other CV) was reported by Ritchey (1917, see also Shafter, 2008).

Hubble (1929) performed the first comprehensive search for extragalactic novae, identifying 63 novae in M31. Walker (1954) discovered that a nova that underwent outburst in 1934 (DQ Herculis) was an eclipsing binary. It was a further ten years before Kraft (1964) showed that all nova systems are probably binaries.

Novae are amongst the most energetic stellar events known. Gamma-ray bursts, SNe and some luminous blue variables surpass them, however novae are much more prevalent than these other events. For example our Galaxy is estimated to have a nova rate of about 35 per year (Shafter, 1997; Darnley et al., 2006), with the most recent estimate giving an M31 nova rate of 65^{+16}_{-15} (Darnley et al., 2006).

1.2 Nova Formation and Outburst Mechanism

1.2.1 White Dwarf Formation

During the main sequence, stars burn hydrogen to helium in their core, but their path after the main sequence is dependent on their mass. If a star has a very low mass ($\lesssim$0.5 $M_\odot$) it is thought that the core of the star will not reach sufficient temperatures to fuse helium and hence will form a He WD. However, since the age of our Universe is thought to be $\sim$13.8 billion years (Planck Collaboration et al., 2013) and stars of similar mass to the Sun take a similar timescale to evolve to WDs (a 1 $M_\odot$ star spends about 10^{10} years on the main sequence; see e.g. Iben, 1985 for a review), no such systems are likely to have formed yet, unless a significant amount of material gets accreted by a companion star for example. Stars with higher masses will be able to fuse helium through the triple-alpha process forming carbon and oxygen. Outside the helium-burning core, there is also a hydrogen-burning shell.

The low and medium mass stars cannot reach a sufficient temperature to continue nuclear burning to form higher mass elements, so the star can no longer be supported and contracts. This contraction continues until it is halted by electron degeneracy pressure (EDP). EDP is a consequence of the Pauli exclusion principle, which states that two identical fermions cannot occupy the same quantum state at a given time. During this contraction the star will expel its outer layers leaving behind a core composed of mainly degenerate carbon and oxygen (CO WD). The upper mass limit for the progenitor of this group is around 9 $M_\odot$ (Siess, 2006), but it can depend on the amount of mass shed by the star during its evolution. Slightly more massive stars ($\sim 9 - 12$ $M_\odot$; Siess, 2006) may reach a high enough temperature to fuse carbon to neon and magnesium, but not high enough to undergo further fusion to produce even higher mass elements. This group of stars will undergo a similar process as the previous group, but instead leave behind cores composed mainly of oxygen and neon (ONe WD). Stars more massive than this will not form WDs, but will evolve towards core-collapse SNe. For further information on the evolution of these low and medium mass stars, see e.g.

Iben (1985), Garcia-Berro & Iben (1994) and García-Berro (2013).

It is thought both types of WD can produce nova systems, with novae containing ONe WDs being estimated to account for about one third of all outbursts (Truran & Livio, 1986; Gil-Pons et al., 2003). However, the number of systems with an ONe WD is likely much lower than a third. This is because ONe WDs tend to be more massive, so require much less matter to be accreted for an outburst to occur and hence tend to produce outbursts more often (see also Section 1.2.3).

1.2.2 Accretion Process

There are two mechanisms by which accretion from the companion star to the WD can proceed. One method occurs when the companion is large enough to exceed its Roche lobe. The Roche lobe of a star is the space within which any material will be gravitationally bound to that star. Any material outside the Roche lobe can escape the gravitational field of the star and instead be bound either to the other body or to the centre of mass of the system (Iben & Fujimoto, 2008). Hence in novae, the matter may be accreted onto the WD. Due to angular momentum conservation, the WD is not thought to accrete the material directly from the secondary, but through an accretion disk that forms around the WD in the binary plane. Optical flickering of a quiescent nova is thought to indicate the presence of an accretion disk. The material in the accretion disk then must lose angular momentum before it can be accreted onto the WD. The angular momentum is transported outwards by viscosity within the disk (Wynn, 2008). Figure 1.2 shows an illustration of a binary system where a white dwarf is accreting matter from its companion via Roche lobe overflow. In novae where this process occurs, the WD (or at least the accretion disc) can steadily accrete gas from the outer regions of the companion star. The second method of mass transfer is via the stellar wind of the secondary star. An accretion disk is thought to form when matter is accreted via this channel too, as the material still needs to lose a large proportion of its angular momentum in order to be accreted by the WD. The processes within the accretion disk have a big effect on the accretion rate of the WD. For example, even if

the secondary is losing mass at a constant rate, the WD may not accrete at a constant rate.

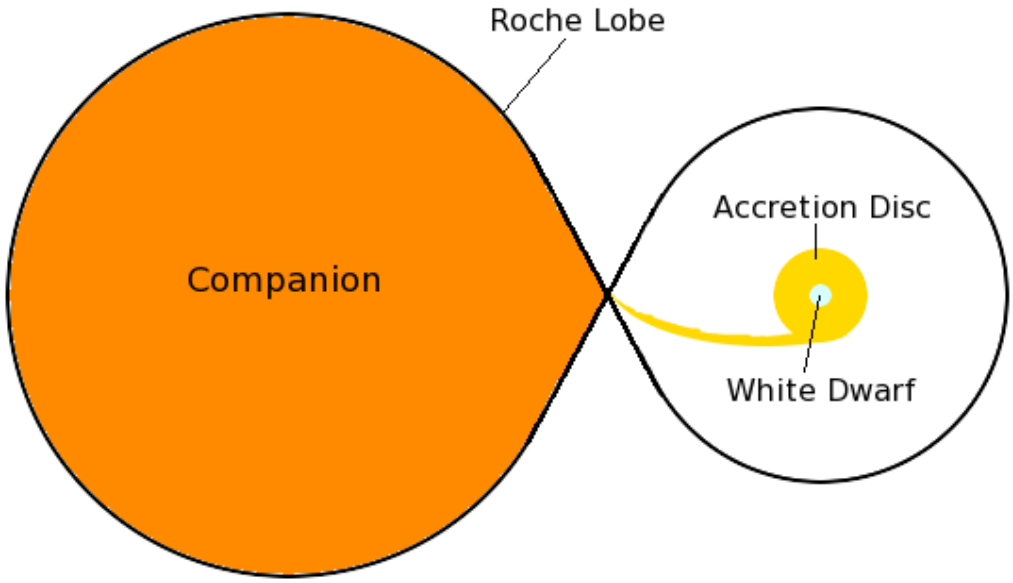

Figure 1.2: Illustration of a WD accreting matter from a higher-mass companion star via Roche lobe overflow. The Roche lobes of the two objects are represented by the black lines surrounding them. Any matter from the companion that goes beyond the Roche lobe can then be accreted by the WD; here it can be seen doing so via an accretion disk.

If the magnetic field in a CV system is strong enough, it can affect how the mass is transferred. The CVs with the strongest magnetic fields are polars, where an accretion disk is unable to form and matter is accreted via a stream following the field lines. This allows the material lost by the companion to be quickly accreted by the WD, although such systems can still show variation in their accretion rate (e.g. AM Herculis; Hessman et al., 2000). There are also intermediate polars (also known as DQ Herculis stars, after the 1934 nova of the same name), a sub-class of CVs where the magnetic field is not strong enough to prevent an accretion disk from forming, but is strong enough to disrupt it. In these systems an accretion disk is formed, but as the material in the disk gets closer to the WD, it then follows the magnetic field lines, and thus is accreted quickly by the WD (Patterson, 1994). In novae with strong magnetic fields the rotation of the WD is usually synchronised with the orbital revolution (Warner, 2008). A notable system where this is not the case is V1500 Cygni, where the difference is

believed to have been caused by its 1975 outburst (Stockman et al., 1988).

1.2.3 Thermonuclear Runaway on the White Dwarf

When a critical pressure and temperature are reached at the base of the accreted envelope, hydrogen burning is triggered. However, on the degenerate surface of a WD temperature cannot be moderated as it would be within a star. This is due to the differing relationships between temperature and pressure. In a non-degenerate star, pressure is proportional to temperature, so if the star expands (thereby lowering the pressure) the temperature will also be reduced. In degenerate material, temperature and pressure are only very weakly coupled, therefore the rate of hydrogen burning can continue to increase. If this continues it will trigger a TNR. This occurs because the accreted material is heated by the energy from the nuclear burning and the gravitational energy until an explosion occurs, and happens over a very short timescale.

The nuclear burning occurs initially through the p-p chain and then through the CNO cycle (Starrfield et al., 2008). Isotopic ratios are different in novae than in stars due to the differing timescales of the expansion (the fast expansion in novae not allowing equilibrium to be reached). The metallicity also affects the TNR, as increased metallicity gives an increased opacity. This increased opacity then traps the heat being produced by nuclear burning, triggering the TNR with less mass having been accreted than would be required at a lower metallicity (Starrfield et al., 2008). Any mixing of the WD core with the envelope increases metallicity. The mass required for a TNR to occur is lower in systems with more luminous WDs because the higher temperatures at the WD surface further heat the accreted envelope. The envelope mass required for a TNR to be triggered is also lower the more massive the WD (Starrfield et al., 2008). Due to the increased pressure at the surface of a massive WD, less material is required to achieve nuclear fusion.

An equation for the critical pressure, P_{crit}, is given by Starrfield (2008):

$$P_{\rm crit} = \frac{GM_{WD}M_{\rm ig}}{4\pi R_{\rm WD}^4},$$

where $M_{\rm WD}$ and $R_{\rm WD}$ are the mass and radius of the WD respectively and $M_{\rm ig}$ is the ignition mass of the accreted envelope. $P_{\rm crit}$ is thought to be $\sim 10^{20}$ dyne cm^{-2} (Starrfield, 2008) and as a WD's mass is related to its radius, the mass of the WD can be estimated using an accretion rate (and hence $M_{\rm ig}$) estimate. Starrfield (2008) notes however that $P_{\rm crit}$ is also dependent on accretion rate and the WD's composition.

1.2.4 The Ejecta

Evans (2001) lists five phases of the expanding ejecta, viz: 1. The fireball phase, as the optically thick ejecta expand. 2. The free-free phase, as the ejecta thin out. 3. The dust formation phase. 4. The nebular phase, where the ejecta are excited by the hot remnant. 5. The coronal phase, where coronal lines are prominent. Not all novae produce dust and not all, indeed only a minority, show a coronal phase.

The mass of the material ejected can be more or less than the total mass accreted by the WD from its secondary and typically ranges from 10^{-5} M$_\odot$ to a few 10^{-4} M$_\odot$ for classical novae (CNe; Bode, 2010), with less mass being ejected in most recurrent novae (RNe; for descriptions of RN and CN systems see Section 1.5). There is a long-standing disagreement between the mass predicted to be ejected by TNR theory and the mass actually observed to be ejected. The observed ejection masses can be up to ten times those predicted (see Starrfield et al., 2008, and references therein). Typical ejection velocities of novae are from a few hundred to a few thousand kms^{-1} (Bode, 2010). Models predict that some material dredged up from the WD core will be expelled along with the envelope (e.g. Prialnik & Kovetz, 1984; Casanova et al., 2011), hence analysis of the ejecta can indicate whether the system has an ONe or CO WD. Models by Prialnik & Kovetz (1995) suggested that the mass of the WD in a system increases with each outburst if the accretion rate $\geq 10^{-7}$ M$_\odot$ yr^{-1} and decreases with each outburst if the accretion rate $\leq 10^{-9}$ M$_\odot$ yr^{-1} independently of the WD's mass

or temperature. This leaves a significant accretion rate range where the WD mass can either increase or decrease, depending on other parameters. Figure 1.3 shows *Hubble Space Telescope* (*HST*) images of the remnant of DQ Herculis, which erupted in 1934.

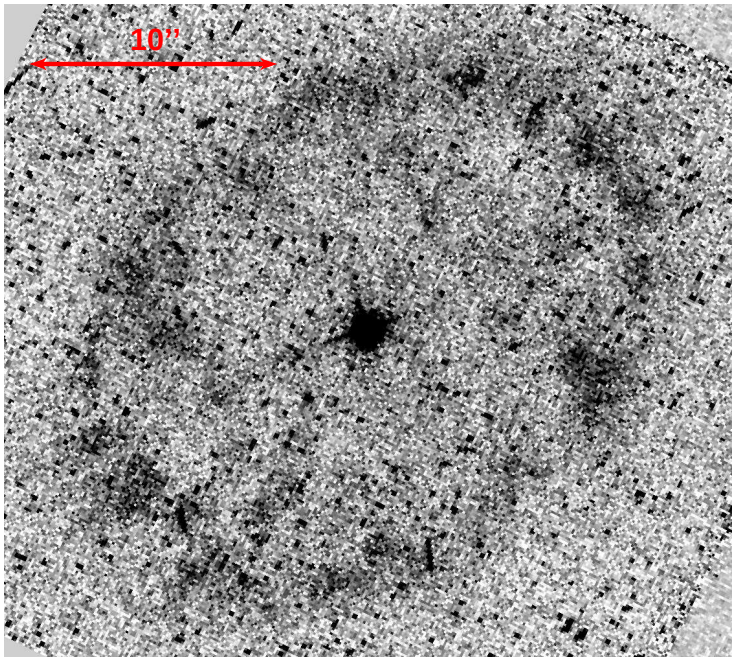

Figure 1.3: Hα image of the remnant of DQ Herculis taken on 1995 September 4 using WFPC2 on *HST* (proposal ID 6060).

From studying relative abundances, Truran & Livio (1986) arrived at several conclusions about typical abundances of novae ejecta: They have high helium to hydrogen ratio and high abundances of heavy elements. Higher helium abundances tend to occur in slower novae and substantial heavy-element enrichment tends to occur in faster novae. The abundance of nitrogen in novae is generally between 10 and 100 times the solar level, while overall metal abundances are typically 10 to 50 times greater in the ejecta (Evans, 2001). In order to produce observed abundances in the ejecta it is thought there must be some mixing of the core of the WD and the accreted envelope (and indeed there must be if the overall mass of the WD is decreasing). The composition of the ejecta may also vary with the time at which it is ejected, depending upon when the material from the WD core is dredged up. Williams & Mason (2010) suggested that there are two components to nova ejecta with different origins. They

argued that one component is the ejected gas from the outer layers of the WD and the other is pre-existing circumbinary gas that represents ejecta from the secondary or the accretion disk and expands much more slowly.

1.2.5 Post-outburst

It is thought that during a nova outburst, an accretion disk can be destroyed, or at least disrupted. This is indicated by the loss of optical flickering for a period of time. For example 241 days after the 2006 outburst of RS Ophiuchi (RS Oph), evidence of the reappearance of optical flickering was found (Worters et al., 2008). U Scorpii (U Sco) showed evidence that its accretion disk began to reform much sooner after its 2010 outburst, at only $8 - 10$ days (Mason et al., 2012). Once the accretion disk has reformed (if there was one and if it was disrupted) the accretion process then starts again, eventually leading to another outburst. This cycle can take any amount of time from one year (Darnley et al., 2014) to the order of decades for RNe up to the order of $10^4 - 10^5$ years for CNe. The upper time limit for this cycle is not known, but all novae are thought to have more than one outburst. There is also evidence that accretion discs can survive or reform very quickly (e.g. Walter & Battisti, 2011). Some novae can remain active X-ray sources long after outburst. V723 Cassiopeia, for example, was still active 12 years post-outburst. A possible explanation for this is continued hydrogen burning at the WD surface, being fed by renewed accretion (Ness et al., 2008).

1.3 Light Curves of Novae

The light curve of a particular nova can indicate a number of things about its properties. The various phases in the light curve of an outburst were described by McLaughlin (1939). An ideal light curve was plotted from this by Gaposchkin (1957) and McLaughlin (1960). A version of this ideal light curve created by Darnley (2005) is reproduced here in Figure 1.4, and the stages are also briefly described here.

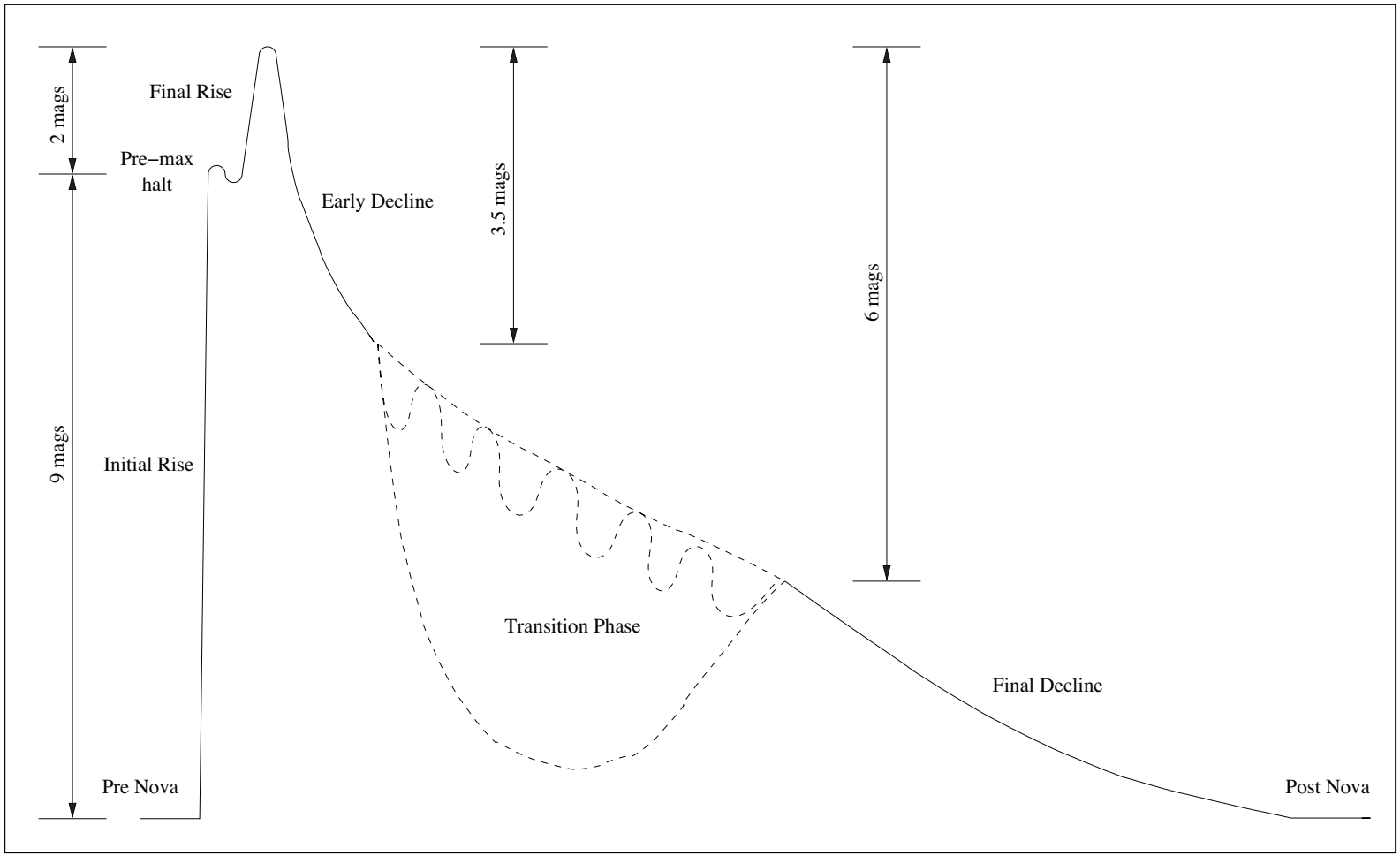

Figure 1.4: A reproduction of the ideal nova light curve adapted from Gaposchkin (1957), McLaughlin (1960) and Darnley (2005).

1.3.1 Pre-nova

Only RNe are usually studied pre-outburst, as their positions are already known. The pre-outburst stages of CN systems usually have to be studied retrospectively and hence usually in no great detail. Robinson (1975) found half of the 12 novae with well defined pre-outburst light curves he studied showed changes in their light curve 1-15 years before the outburst, with five showing an increase in brightness between 0.25 and 1.5 magnitudes. However when Collazzi et al. (2009) tested these results they found four out of the five Robinson (1975) found to have significant pre-outburst rises were due to mistakes in the old literature. Collazzi et al. (2009) did however find two cases of significant pre-outburst rises out of 22 studied. This suggests the phenomenon is much less widespread than previously believed. Adamakis et al. (2011) studied the historical light curve of RS Oph. Using wavelet analysis they found that the system appears to show a signal in the power spectrum prior to an outburst; a method that could therefore be used to predict when an outburst may occur.

1.3.2 Rise To Maximum

The initial brightness rise during an outburst is a very short phase of the light curve and is rarely observed except in slow novae. A number of novae display a pre-maximum halt in their light curve; this can be a pause in the rising brightness or even a small decrease in brightness. The cause of the pre-maximum halt is still uncertain, however recent models by Hillman et al. (2014) have suggested the pre-maximum halt is accompanied by a temporary dip in total luminosity, possibly caused by convection in the envelope becoming less efficient as it expands and thins out. It has long been noted that the length of the pre-maximum halt appears to correspond to the speed class of the nova, with the slower novae displaying longer pre-maximum halts (e.g. McLaughlin, 1939). Observations of the fast nova V463 Scuti by Kato et al. (2002) showed there are exceptions to the trend, as V463 Scuti displayed a pre-maximum halt of at least 24 days. As these early stages are often missed, whole sky surveys can be useful in retrospectively studying these early phases of bright novae (e.g. Hounsell et al., 2010).

After the pre-maximum halt (if one occurs) the increase in brightness is then resumed until the maximum is reached. This is known as the final rise and tends to be slower than the initial rise.

1.3.3 Decline From Maximum

The early decline phase can be a smooth decline or show fluctuations in brightness. The transition phase is the stage where individual novae display most differences. McLaughlin (1939) defined the three forms as: (1) an abrupt change of the curve towards a gentler slope, (2) a single broad minimum of very different depth in individual cases, followed by a recovery of light or (3) a series of strong oscillations. Attempts to further classify nova light curve declines have been made (e.g. Duerbeck, 1981; Strope et al., 2010). Robinson (1975) found that in CNe, almost uniformly, the post-outburst magnitudes were the same as the pre-outburst magnitudes. Indeed Collazzi et al. (2009) too found that the average change in magnitude from pre-outburst to post-outburst was 0.0 magnitudes. They did however find five novae where the post-outburst brightness was over ten times the pre-outburst brightness.

1.3.4 Nova Classification by Speed of Decline

In general, the more luminous a nova is the faster its luminosity will decline. Novae can be classified by the speed at which their light curve declines or t_n, the time it takes a novae to fade by n magnitudes. t_2 for very fast novae can be less than 10 days, but for very slow novae it is in the order of hundreds of days.

Gaposchkin (1957) suggested a scheme for classifying novae by the time they take to fade by two magnitudes, which is reproduced here in Table 1.1.

RNe often decline very rapidly after outburst hence outbursts can be missed simply by them occurring when the nova appears near the Sun in the sky. The light curves of individual RNe tend not to vary greatly between outbursts (Schaefer, 2010).

Novae speed classes

Speed class	t_2 (days)	$\dot{m}_V$ (mag day^{-1})
Very fast	$<$10	$>$0.20
Fast	11-25	0.18-0.08
Moderately fast	26-80	0.07-0.025
Slow	81-150	0.024-0.013
Very Slow	151-250	0.013-0.008

Table 1.1: The classification of light curve decline speeds as defined by Gaposchkin (1957).

1.3.5 Magnitude 15 Days After Maximum

It was long been believed that absolute magnitudes of novae are approximately the same 15 days after the maximum. This relationship was first noted by Buscombe & de Vaucouleurs (1955), who stated *"the mean light-curves of the combined two groups of fast novae and the combined two groups of slow novae intersect at 14 days"*. This could obviously be a useful indicator as to whether the maximum of a given nova has been missed, although recent work suggests there is no such relationship (e.g. Ferrarese et al., 2003; Darnley et al., 2006).

1.4 Infrared Emission

During outburst, a nova emits radiation over a large range of frequencies, from radio to X-rays. The overall luminosity remains approximately constant during the first phases of the outburst, but the type of radiation emitted by the nova changes. During this constant bolometric luminosity phase, as the effective photospheric radius shrinks, the effective temperature increases, causing radiation to be systematically emitted at shorter wavelengths. For example, novae are initially bright optically, but as they fade in the optical, they become bright in the UV, and then the X-ray. This is illustrated in Figure 1.5. Different frequencies indicate different processes in the outburst. For example, infrared is the most important emission when trying to detect dust formation in the ejecta and soft X-ray emission is thought to indicate continued nuclear burning on the surface of the WD.

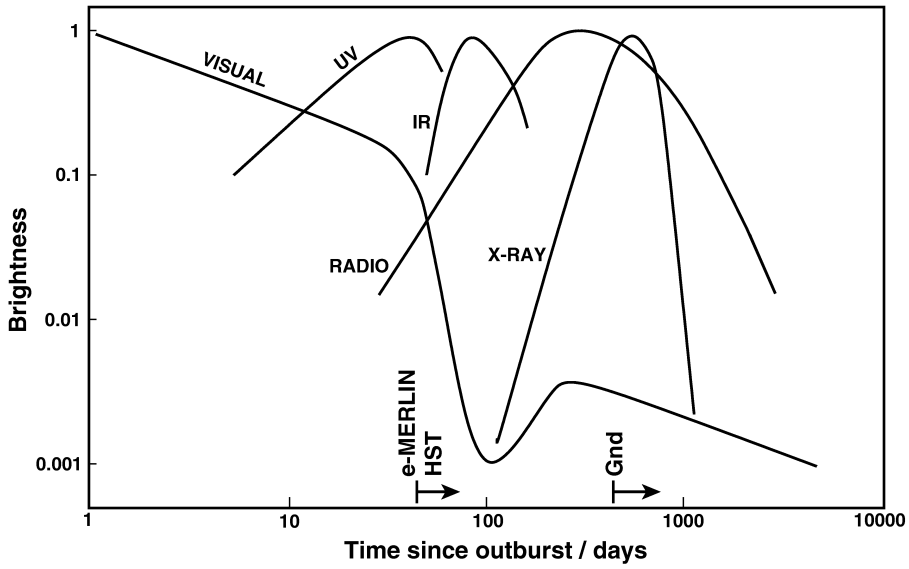

Figure 1.5: A multi-wavelength illustration showing how the emission of a typical dust-forming nova varies over the course of an outburst (from O'Brien & Bode, 2008).

The dip in the visual light curve at about 100 days in Figure 1.5 corresponds to dust formation. This is caused by the newly formed dust obscuring the central source. As the optically thick dust cloud expands and disperses, the source re-emerges and the optical emission re-brightens. This dip in the optical is accompanied by an increase in the infrared emission, caused by re-emission. In non-dust-forming novae the infrared decline would follow that of the optical, with the infrared decline being delayed. Infrared observations can be used to measure the abundances of C, O, Si and other elements in dust formed after an outburst (Gehrz et al., 1998). They can also help determine if the primary in the system is a CO or ONe WD. For example, outbursts in an ONe system produce strong Ne II infrared forbidden lines (Gehrz et al., 1998). This dip in the optical light curve and the accompanying rise in the infrared is the primary indicator of dust formation in novae.

1.5 Recurrent Novae

RNe are novae for which more than one outburst has been recorded, whereas CNe have only one recorded outburst. However, since all novae are thought to undergo

multiple outbursts, RN systems are likely just on the extreme on a continuum of recurrence times. RNe contain higher mass WDs and have high accretion rates. This is because the more massive the WD, the less matter is required on the surface of the WD in order to reach a high enough pressure for the TNR to be triggered. In order to produce recurrence times in the order of decades, high accretion rates are still required even in systems with the highest mass WDs. Due to the relatively short period between outbursts in RNe and less mass being required for a TNR to occur, RNe tend to eject much less mass when they have an outburst. Many RNe have fast light curve declines, increasing the likelihood of outbursts being missed. The WDs of many RNe are believed to increase in mass with each outburst (e.g. RS Oph, Hachisu et al., 2007; U Sco, Hachisu et al., 2000). This is the opposite to CNe that are thought to typically decrease in mass when they undergo an outburst (see e.g. Livio & Truran, 1992). della Valle & Livio (1996) estimated about 10%-25% of nova outbursts would be attributed to systems that are classed as RNe.

The RN U Sco appears to produce outbursts at regular intervals of $\sim$10 years (Schaefer, 2010). This is assuming several pre-1960 outbursts have been missed. U Sco is a very fast nova so this is not an unreasonable assumption. However, for some RNe the inter-outburst time-periods change significantly. The RN T Pyxidis (T Pyx) has outbursts recorded in 1890, 1902, 1920, 1944, 1967 (Schaefer, 2010) and recently in 2011 (Waagan et al., 2011). T Pyx is a slow nova, so outbursts are much less likely to have been missed and there were almost certainly no outbursts between 1967 and 2010 (Schaefer, 2010). T Pyx is thought to be atypical among the RN class of objects. The nova shell around T Pyx appears to originate from the first observed outburst in 1866 (Schaefer et al., 2010a). The low ejection velocities and high ejecta mass also imply this was a CN type outburst with a very long quiescent period before the 1866 eruption (Schaefer et al., 2010a).

Darnley et al. (2012) proposed a new classification scheme for novae. This scheme is based on the evolutionary state of the secondary, rather than outburst properties. The classification of novae into the CN or RN group depends not only on WD mass, but on properties such as accretion rate (which can change) and even observational biases

(i.e. some CNe could have produced more than one outburst in the last 100 years, yet are not classified as RNe). Darnley et al. (2012) propose three types: Those with main-sequence companions (MS-novae), those with sub-giant companions (SG-novae) and those with red giant companions (RG-novae).

1.5.1 Types of Recurrent Novae

There are currently only 10 known Galactic RNe (Schaefer, 2010). With 3 known in the LMC (e.g. Shore et al., 1991; Bode et al., in preparation) and a few candidates in M31 (e.g. Henze et al., 2008a; Shafter et al., 2010a; Darnley et al., 2014; Shafter et al., in preparation). From this small sample, there appears to be distinct subtypes into which the known RNe can be categorised. The properties of each group as described by Anupama (2008), Bode (2010) and references therein are briefly given here.

RS Oph/T CrB type (hereafter RS Oph type) RNe have orbital periods in the order of hundreds of days and contain red giant secondaries. Members of the group are fast novae and have high initial ejection velocities ($\gtrsim$ 4000 km s^{-1}). The ejected mass is typically a few 10^{-6} M$_{\odot}$.

U Sco type RNe are very fast novae and contain sub-giant secondaries. They typically have orbital periods in the order of hours and ejection velocities $\sim$ 10000 km s^{-1}, ejecting about 10^{-7} M$_{\odot}$.

T Pyx type RNe contain main-sequence secondaries and are the slowest class of RNe, in the moderately fast to slow range (see Table 1.1). Their ejection velocities are in the range of 800 - 2500 km s^{-1} and they have much higher ejection masses ($\sim 10^{-5}$ M$_{\odot}$), approaching those of some CNe. Indeed T Pyx itself is thought to be decreasing in mass with each outburst. Selvelli et al. (2010) estimated the total accreted mass to be $\sim 5.2 \times 10^{-7}$ M$_{\odot}$, with the ejected mass being at least 10^{-5} M$_{\odot}$.

These sub-groups of RNe also fit well into the classes that Darnley et al. (2012) proposed. RS Oph type RNe are RG-novae, U Sco type RNe are SG-novae and T Pyx type RNe are MS-novae, with majority of CNe also thought to be members of the MS-nova

group.

1.5.2 Predicting Outbursts of Recurrent Novae

The outbursts of RNe can, in principal, be predicted using data from previous outbursts (such as the mass required to trigger the TNR) and the accretion rate during the inter-outburst period. This was displayed when the outburst of RN U Sco was predicted to occur on 2009.3 ± 1.0 by Schaefer (2005) and it occurred at 2010.1 (Schaefer et al., 2010b). However, this currently unreliable, as illustrated when Schaefer (2005) incorrectly predicted that T Pyx would erupt in 2052 ± 3, which was then extended by Schaefer et al. (2010a) to be later than the year 2225. However the outburst actually occurred in 2011. It should be noted that within the small sample of confirmed RNe, T Pyx does not appear typical. As noted in Section 1.3.1, Adamakis et al. (2011) showed that it may be possible to predict outbursts of RS Oph up to a few hundred days before eruption through wavelet analysis.

1.6 Novae as Distance Indicators

Novae can be used as distance indicators, due to the link between the maximum magnitude of a nova and the rate at which its visible light declines. The trend of bright novae declining faster was first noted by Hubble (1929). The relationship between peak brightness and speed of decline was defined by McLaughlin (1945) and is known as the maximum magnitude, rate of decline (MMRD) relationship. Prior to this, the average brightness of several novae in a galaxy was used to estimate the distance. Novae have advantages over Cepheids in the determination of galaxy distances. Novae are brighter than all but the longest period Cepheids and long-period Cepheids are concentrated in the spiral arms, where overcrowding and absorption is a problem (van den Bergh & Pritchet, 1986). However, using the MMRD relation to measure distance can be difficult due to the time period that a nova must be observed for to measure its decline.

Pritchet & van den Bergh (1987) observed over 15 nights in 1986 and detected 9 novae in the Virgo cluster. Using six novae with reasonably well observed light curves they estimated the distance of the Virgo cluster to be 19.5 ± 3.9 Mpc. This is consistent with modern estimates (e.g. 18.0 ± 1.2 Mpc, Fouqué et al., 2001; 17.6 ± 1.0 Mpc, Jerjen et al., 2004)

1.7 Spectroscopic Classification

Williams (1992) proposed that novae could be split into two classes based on whether they had stronger Fe II or He and N emission lines; designated as "Fe II" novae and "He/N" novae. Williams (1992) suggested that the He/N type spectra are formed in the shells that are ejected at the optical maximum, with the Fe II type spectra being formed later on, in the winds. Hence he deduced that the parameters of the shell and the wind dictate which emission dominates for a given nova. Apart from the Fe II or He/N emission, one of the main spectral differences are the relatively narrow lines of the Fe II spectra compared to the relatively broad lines of the He/N spectra. Spectra of Fe II type novae also often display P Cygni absorption profiles. P Cygni profiles are characterised by strong emission lines with blue-shifted corresponding absorption lines.

There is also a group of novae that initially exhibit Fe II type spectra, but then develop into displaying He/N type spectra. These novae are known as hybrid novae, often (and hereafter) denoted as Fe IIb novae. Another spectral class was proposed by Shafter et al. (2011f), narrow-lined He/N novae (He/Nn). He/Nn type novae produce narrow lines, but display neither Fe II or nitrogen lines. Examples of the two main classes, Fe II and He/N, are shown in Figure 1.6. Shafter et al. (2011f) classified $\sim$82% of novae in M31 as Fe II type. Although in both the Large Magellanic Cloud (LMC; Shafter, 2013) and M33 (Shafter et al., 2012a) a much lower proportion of novae appear to be of Fe II type. This indicates that the faster He/N type novae may generally be associated with a younger stellar population (see Section 1.9 for further details). As both He/N and Fe II type novae can produce Ne lines, it is thought both types can contain ONe WDs

(Shafter et al., 2011f).

1.8 Galactic Novae

As would be expected for such bright objects, novae have been observed in our Galaxy since ancient times (see e.g. Ze-Zong & Shu-Jen, 1966; Duerbeck, 2008). Indeed, naked-eye novae are not uncommon. Nova Aquilae 1918 (V603 Aql), for example, reached around magnitude -1 at its peak and was the brightest nova of the $20^{\rm th}$ century. More recently KT Eridani (KT Eri), which produced an outburst in 2009, reached magnitude 5.4 (Yamaoka et al., 2009; Hounsell et al., 2010). There were two naked-eye novae in 2013, with V339 Delphini reaching ~ 4.4[2] and V1369 Centauri getting to ~ 3.5[2]. The novae rate of the Galaxy is estimated to be 34^{+15}_{-12} (Darnley et al., 2006). However, as we are in the Galaxy the majority of these are not observable, with about ten novae being discovered each year.

Duerbeck (1990) suggested two different populations of novae, those associated with the Galactic disk and those associated with the bulge. Further observations (e.g. della Valle et al., 1992) confirmed this, with the disk novae tending to be faster and brighter than those associated with the bulge.

della Valle & Livio (1998) found that 63% of Galactic novae belonged to the Fe II spectroscopic class. They also suggested that He/N type novae tend to be near the disk, whereas Fe II type tend to be distributed uniformly throughout the Galaxy, although the latter trend does not appear to be true for M31 (see Section 1.9.3). A more recent examination of all Galactic novae with spectroscopic information indicated a higher proportion of novae were of Fe II type ($\sim$79%; see Shafter et al., 2011f).

[2] `http://www.aavso.org`

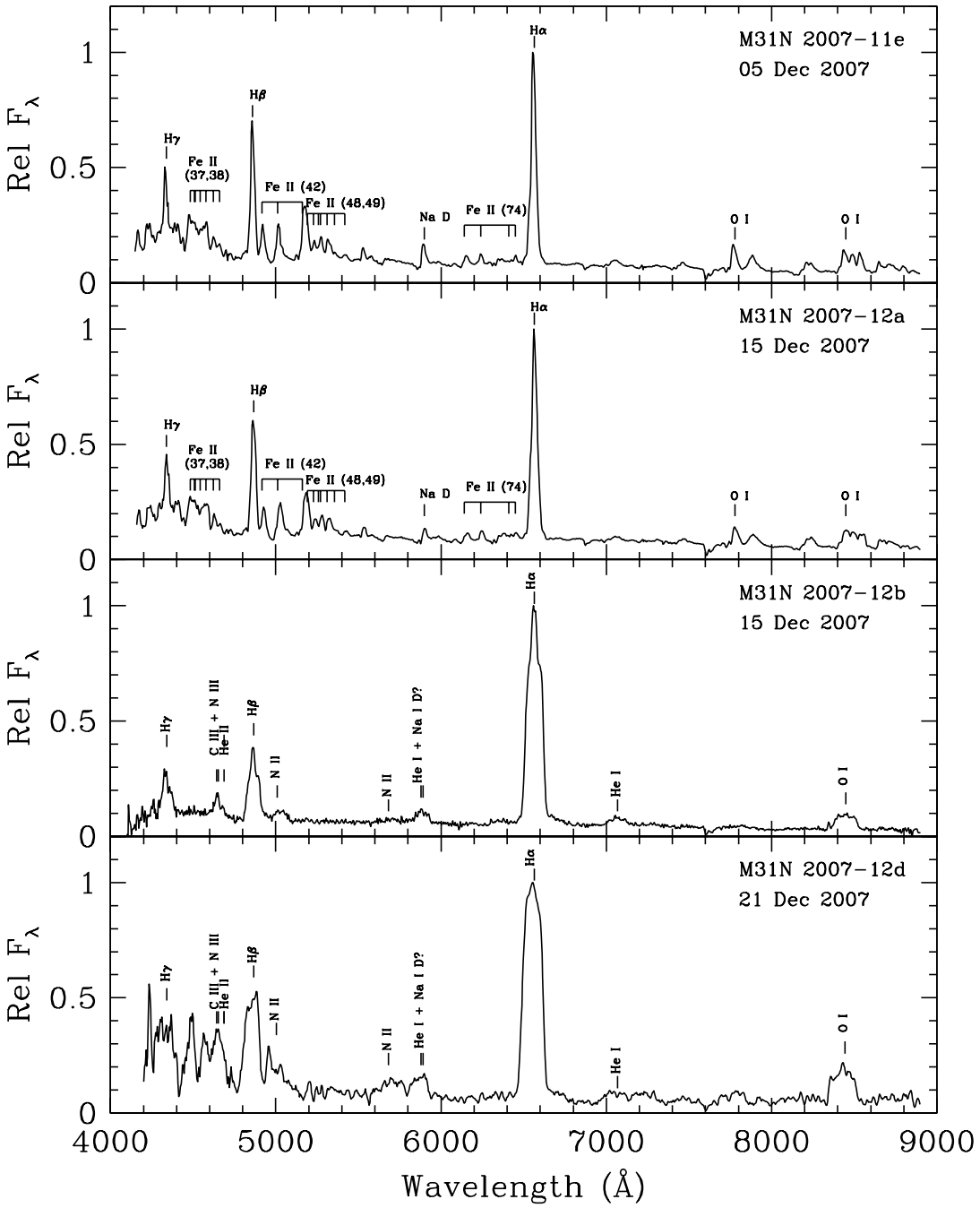

Figure 1.6: Spectra of M31 novae M31N 2007-11e, 2007-12a, 2007-12b and 2007-12d from Shafter et al. (2011f). M31N 2007-11e are 2007-12a are examples of Fe II type novae, whereas M31N 2007-12b and 2007-12d are both He/N novae. ©AAS. Reproduced with permission.

1.9 Extragalactic Novae

Novae are bright enough to be studied in the Local Group and detected far beyond. One of the main advantages of studying extragalactic novae is that, within a given galaxy, they can all be assumed to be at a similar distance. Also, with only about ten Galactic novae discovered per year, studying extragalactic systems substantially increases the sample size. Observing novae in external galaxies has shown that the faster He/N type novae tend to be associated with a younger stellar population that those belonging to the Fe II spectroscopic class (see below). Here the nova populations of the LMC, Small Magellanic Cloud (SMC), M31 and M33 are briefly reviewed and the more distant galaxies are also looked at.

1.9.1 Novae in the LMC

The first nova candidate to be discovered in the LMC was in 1926 (Luyten, 1927; Henize et al., 1954). Since that date there have been a further 42 candidates discovered[3], with 18 of these having sufficient data for their spectral types to be determined (Shafter, 2013). Novae in the LMC tend to fade quicker than novae in either our Galaxy or M31 (Shafter, 2013). Shafter (2013) also showed that approximately 50% of LMC novae appear to belong to the Fe II spectroscopic class, a lower proportion than in our Galaxy.

Three of the novae in the LMC are suspected to be recurrent. The first discovered RN was LMCN 1990-02a, whose position was coincident with LMCN 1968-12a (Williams et al., 1990). The outbursts of LMCN 2004-10a and LMCN 2009-02a are also believed to be the second observed outbursts of older novae (Bond et al., 2004; Liller, 2009). LMCN 2009-02a, which is associated with LMCN 1971-08a, has also been observed in quiescence. Bode et al. (in preparation) classified its secondary as a sub-giant, and thus it is the first extragalactic SG-nova to be discovered.

[3] `http://www.mpe.mpg.de/~m31novae/opt/lmc/index.php`

1.9.2 Novae in the SMC

The first nova candidate to be discovered in the SMC was in 1897. After this first nova there was only one further candidate (in 1927) before 1950 (Henize et al., 1954), but we now tend to see one every few years. In total, as of 2014, there are 17 nova candidates in the galaxy, with five of these being spectroscopically confirmed[4].

1.9.3 Novae in M31

As the largest galaxy in the Local Group, M31 is vital for studying extragalactic novae. It was the host galaxy of SN 1885, which was then simply classified as a nova. The first observed CN outburst candidate in M31 occurred in 1909 and was reported by Ritchey (1917). The first large survey of novae in M31, or indeed extragalactic novae as a whole, was conducted by Hubble (1929), who identified 63 novae in the galaxy. We now know of over 900 nova candidates in M31[5] and the majority of novae in the last decade have been spectroscopically confirmed (e.g. Shafter et al., 2011f). Shafter & Irby (2001) calculated a nova rate of 37^{+12}_{-8} and Darnley et al. (2006) derived a rate of 65^{+16}_{-15} per year for M31. However, M31 is difficult to observe with professional telescopes for several months of the year. Due to this and other factors about 30 novae are observed each year, which is still much more than any other galaxy. The distribution of all discovered M31 nova candidates (up to August 2013)[6] is shown in Figure 1.7. Shafter et al. (2011f) found that approximately 80% of M31 novae belonged to the Fe II spectroscopic class, consistent with our Galaxy. The same authors found some evidence to support the Galactic trend of faster novae being more associated with the disk than slower novae. However they found no evidence of spectral class being dependent on galactic position as has been suggested in our Galaxy (see Section 1.8). Several M31 novae appear to be recurrent, however due the the number of novae recorded, some of these will probably be chance alignments (see e.g. Shafter et al., 2013 and Shafter et al., in preparation).

[4] `http://www.mpe.mpg.de/~m31novae/opt/smc/index.php`
[5] see Pietsch (2010) and `http://www.mpe.mpg.de/~m31novae/opt/m31/index.php`
[6] Created from data from `http://www.mpe.mpg.de/~m31novae/opt/m31/index.php`

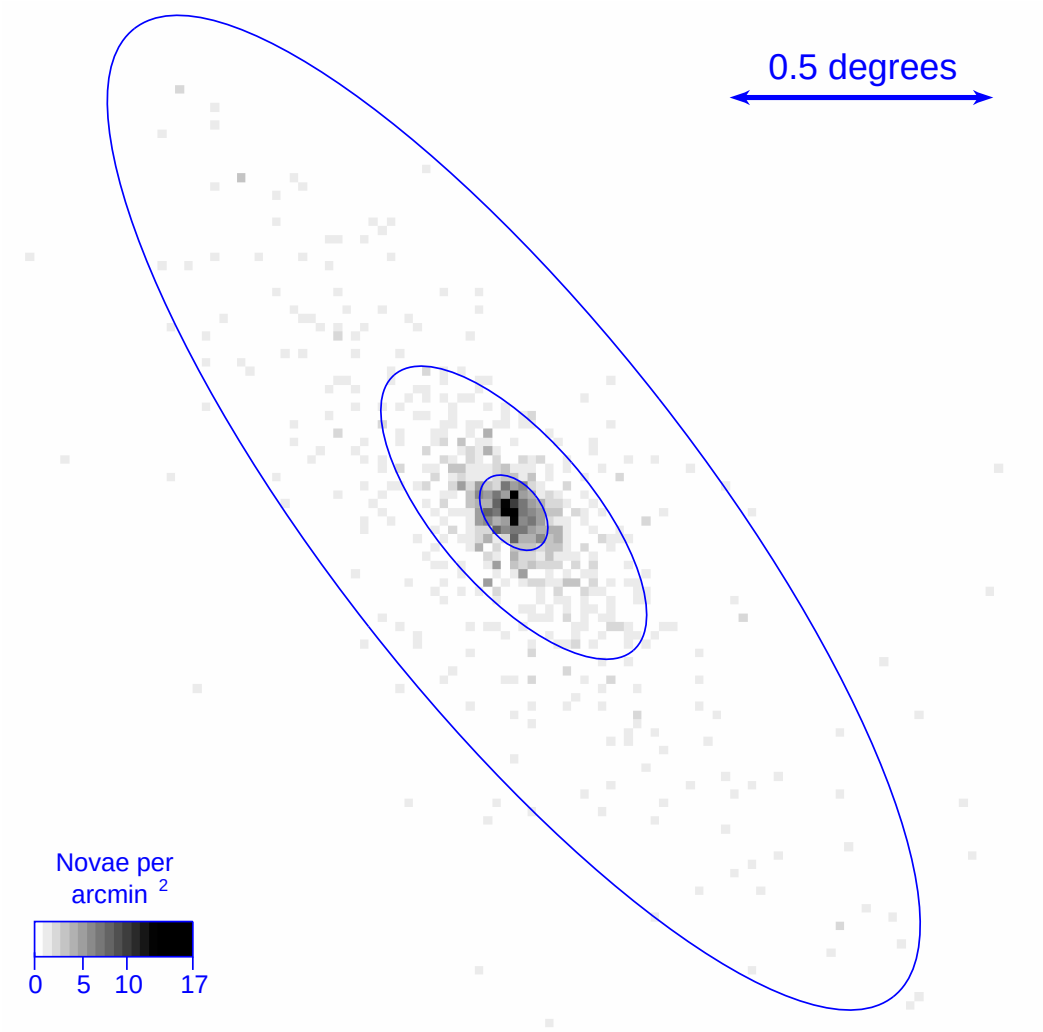

Figure 1.7: The distribution of all discovered nova candidates in the central two square degrees of M31 up to the end of August 2013, with the darker shades of grey representing higher number densities. The figure has a one arcminute resolution. The blue ellipses are isophotes from the surface photometry of Kent (1987).

Bode et al. (2009) discovered the first extragalactic nova progenitor system when they used *HST* data to observe M31N 2007-12b in quiescence. The work presented in Chapter 3 of this thesis used a similar method to those authors to conduct a survey of 38 quiescent novae in M31 to search for RG-novae. This work has now been submitted for publication in a refereed journal.

We also occasionally observe novae in M32 and NGC 205 (satellite galaxies of M31), for example, M32N 2006-07a (Leonard et al., 2006) and NGC205N 1997-11a (Qiao et al., 1997). However, Neill & Shara (2005) suggested that the nova rate in the two galaxies may be relatively high, possibly one or two per year in both M32 and NGC 205.

1.9.4 Novae in M33

The first nova observed in M33 was M33N 1919-12a, reported by Hubble (1926). The galaxy is near to M31 in the sky, but fainter and has a much smaller stellar population. The nova rate is $2.5^{+1.0}_{-0.7}$ (Williams & Shafter, 2004) and the number of novae we observe each year is third only to M31 and the Milky Way within the Local Group, although it is subject to the same observational difficulties as M31 and we see one or two per year on average. Including the most recent, M33N 2014-02a, there have been 41 nova candidates discovered in M33[7]. Shafter et al. (2012a) found that only three of the eight novae with available spectra were Fe II novae. This would initially suggest a similar ratio of Fe II type to He/N type novae to that of the LMC. As both the LMC and M33 have a generally younger stellar population than the Galaxy and M31, the findings of these extragalactic surveys suggest that the He/N type novae are more associated with these younger stellar population that those of Fe II type.

[7] `http://www.mpe.mpg.de/~m31novae/opt/m33/index.php`

1.9.5 Novae Beyond the Local Group

The only galaxy outside the Local Group where novae are observed regularly is M81. M81 is believed to have a nova rate of 33^{+13}_{-8} (Neill & Shara, 2004) and approximately 5 or 10 are actually observed each year. Many more of these relatively nearby galaxies are predicted to have reasonably high nova rates, but are not observed systematically enough for regular discoveries. For example M101, the host galaxy of SN 2011fe, has a predicted nova rate of $11.7^{+1.9}_{-1.5}$ (Coelho et al., 2008), yet few novae have been discovered in this galaxy outside of such surveys as that of the authors and Shafter et al. (2000). There are examples of novae being readily discovered even further afield, past 15 kpc. Ferrarese et al. (2003) displayed how many novae can be found with dedicated observing time on powerful telescopes. They found nine novae in M49 on images taken at 19 epochs over a 55 days, yielding a expected nova rate of roughly 100 per year. The giant elliptical M87 is believed to have a similarly high nova rate (Shafter et al., 2000).

1.10 Type Ia Supernovae

The only type of SNe that are not caused by the collapse of a massive star are Type Ia SNe (SNe Ia). SNe Ia are caused by stars that would have been low or medium mass stars whilst on the main sequence and hence formed WDs after helium burning had ceased. The progenitors of SNe Ia are still largely uncertain (see Section 1.10.1), but they are thought to occur when the total mass of a CO WD exceeds the Chandrasekhar limit ($\sim$1.38 $M_{\odot}$) and it can no longer be supported by EDP, so collapses further and explodes. SNe Ia can be identified by their singly ionized silicon line at 615nm and their lack of hydrogen.

There are two main candidates for progenitors of SNe Ia; the single degenerate model and the double degenerate model. These are explained in Section 1.10.1.

1.10.1 Progenitors of Type Ia Supernovae

The single degenerate model of SNe Ia progenitors involves a WD accreting matter from a less evolved (i.e. main-sequence, sub-giant or red giant) secondary. The WD accretes matter from the secondary and increases in mass (e.g. Whelan & Iben, 1973). Eventually the WD mass approaches the Chandrasekhar limit and the SN explosion occurs when the carbon ignites. One of the leading progenitor candidates are novae, particularly those classified as RNe, due to their high WD masses and low ejection masses. Thoroughgood et al. (2001) called U Sco "the best Type Ia SN progenitor currently known" and estimated that it is likely to explode within $\sim$700 000 years, although Mason (2011) suggested the U Sco system may contain a ONe WD. It is believed that nova systems with ONe WDs do not produce SN Ia, but instead collapse to form a neutron star (Gutierrez et al., 1996). Super-soft sources (SSSs) are other possible progenitor candidates. They have steady burning on the WD surface, but this requires a very high accretion rate. The main problem with the single degenerate model concerns the occurrence rate of SNe Ia versus the occurrence rate of likely progenitors via this method. As most WDs in RNe systems are thought to be increasing in mass with each outburst they are prime candidates for the progenitors of SNe Ia. However as most CNe are thought to be decreasing in mass as they undergo outburst, they are unlikely candidates for progenitors of SNe Ia (Starrfield et al., 2012; Newsham et al., 2013). T Pyx type RNe are not thought to produce SNe Ia due to their inability to maintain a high accretion rate (Schaefer et al., 2011). The composition of the WDs in RN systems are largely not known with any degree of certainty. This is important in assessing their merit as likely candidates for SNe Ia progenitors. As ONe WDs are formed by more massive stars, the WDs with higher initial mass tend to be ONe WDs. Therefore if RNe can only be formed in systems with massive ONe WDs and not by increasing the mass of a CO WD, they are unlikely SNe Ia progenitors.

Ruiz-Lapuente et al. (2004) studied the proper motion of stars in remnant of SN 1572, Tycho's SN, and suggested one of the stars, named Tycho G, a G0$-$G2 star, appeared to be a surviving companion from the SN. González Hernández et al. (2009) found that Tycho G has an overabundance of Ni relative to Fe as well as a high Li abundance. The

overabundance of Ni could indicate the star has been contaminated by the ejecta from the SN 1572 explosion. The reason for the high abundance of Li is less clear, although it is a feature that is in common with companions of neutron stars and black holes (i.e. core-collapse SN events; González Hernández et al., 2009). Kerzendorf et al. (2009, 2013) have argued against Tycho G being the surviving companion, stating the proper motion and rotation is consistent with stars in the SN 1572 field; further, they could not detect the high Li abundance claimed by González Hernández et al. (2009). Conversely, Bedin et al. (2014) used further *HST* observations to constrain the proper motion and supported Tycho G being the companion star. After considering all factors, such as velocity, metallicity and relative abundances, they state the probability of Tycho G being a chance alignment to be $\lesssim 0.00037$.

In 2011 a SN Ia, SN 2011fe, exploded in the nearby galaxy M101, for which Li et al. (2011) used pre-outburst images to rule out a single-degenerate system harbouring a luminous red giant as the progenitor, but could not constrain it further, although Darnley et al. (2013) pointed out that this analysis did not exclude fainter RG-nova systems such as T Coronae Borealis (T CrB). Nugent et al. (2011) proposed that it was most likely from a system with a CO WD and a MS secondary. Dilday et al. (2012) suggest that a single degenerate system with a red giant companion was the progenitor of SN PTF 11kx. Several other SNe (e.g. SN 2002ic, SN 2006X and SN 2007le) show features consistent with what would be expected from RG-nova systems (Dimitriadis et al., 2014).

The double degenerate model involves the merger of two WDs, with their combined mass exceeding the Chandrasekhar limit. However during a merger of two CO WDs it is thought the disruption of the less massive WD and accretion onto the more massive would instead form a ONe WD (e.g. Podsiadlowski, 2010). However Nomoto & Iben (1985) suggested that in some cases this may be avoided by the formation of a thick disk during the merger and a low accretion rate. The mass could then exceed the Chandrasekhar mass before carbon ignition occurred. Piersanti et al. (2003) suggested that rotation could also help avoid a ONe WD forming (thus allowing a SN Ia). Schaefer & Pagnotta (2012) could find no resolvable companion star in the SN

Ia remnant SNR 0509−67.5 in the SMC and neither could González Hernández et al. (2012) for the Galactic SN 1006. This implies these SNe at least were produced by double-degenerate systems, although the searches do not rule out some main-sequence secondary stars, if a suitable mechanism was put forward.

In January 2014, SN 2014J exploded in M82 and was the nearest SN Ia for decades (Zheng et al., 2014). This SN gives an opportunity to learn more about the progenitors of SN Ia, or the progenitor of this particular SN Ia at least, and some work on constraining the progenitor of SN 2014J is presented as part of this thesis, in Chapter 6.

1.11 This Work

Prompted by results contained in the first infrared survey of novae in M31 (Shafter et al., 2011b), this thesis first examines the theoretical relationship between dust-formation timescale and rate of optical decline in novae. Observational evidence shows that novae that fade quicker tend to form dust quicker. However, the previous basic theory did not replicate this, predicting the two parameters to be effectively independent of each other. By considering neutral hydrogen within the ejecta (for which there is observational evidence), the basic theory was modified by assuming the dust formation sites only see emission long-ward of the Lyman limit (91.2 nm), with that at shorter wavelengths being absorbed by the neutral hydrogen. Much of this work has already been published in Williams et al. (2013). Chapter 2 shows the results of this work and how it compares to the observational data.

The thesis then looks more broadly towards extragalactic novae and their progenitors. Chapter 3 presents the use of Liverpool Telescope (LT; Steele et al., 2004) and archival *HST* data to search for 38 spectroscopically-confirmed M31 novae in quiescence. Photometry of the novae in quiescence is also published for systems where likely progenitor candidates are found. In Chapter 4, light curves of eighteen M31 novae are presented, several of which contain *HST* data, allowing for those light curves to be extended to fainter magnitudes than is normally possible for extragalactic sys-

tems. Additionally, a spectrum of M31N 2013-12b taken a few days after discovery is shown.

In Chapter 5, the statistics of the catalogue are explored. A model is produced that considers many potential biases, such as the *HST* coverage of M31 and the speed-class distribution, as well as the probability of being observed in outburst and getting spectroscopic confirmation for a given nova. After taking these biases into account an estimate is derived for the proportion of novae in M31 likely to be associated with a source in the *HST* data – a group expected to be dominated by RG-novae.

Chapter 6 outlines the use of the same technique as the nova survey to help determine the nature of the three additional extragalactic variables. Firstly, the chapter focuses on a RN in M31 that may have a recurrence time of approximately one year. This object, M31N 2008-12a, was first observed as a nova in 2008, but this work focuses on photometry of the 2013 outburst and the search for a progenitor candidate. The same progenitor-location method is also used to derive magnitude limits on the progenitor of SN 2014J, a SN Ia in M82. Lastly the chapter looks at the M31 optical transient TCP J00403295+40343877, which after being classified as a nova candidate displayed an unusual spectrum. Finally, Chapter 7 summarises the work presented in the thesis and looks at the future work planned for both the dust formation and progenitor search work.

Chapter 2

An Investigation into the Relationship between Speed Class and Dust Formation in Novae

The majority of the work presented in this chapter has been published in Williams, S. C., Bode, M. F., Darnley, M. J., Evans, A., Zubko, V. and Shafter, A. W. (2013, ApJ, 777, L32)

2.1 Introduction

Dust formation has been observed in Galactic novae for over 40 years (Geisel et al., 1970; see Bode & Evans, 1989 for a review of the early observations), but observations have only recently extended to the potentially much larger sample of extragalactic novae (e.g. Shafter et al., 2011b). Dust formation typically occurs between 1 and 5 months post-outburst and appears to depend on the speed class of the nova (e.g. Gehrz et al., 1998; Evans & Rawlings, 2008; Shafter et al., 2011b). A nova outburst of a system containing a CO WD (CO nova) can produce silicates, silicon carbide, carbon or hydrocarbons, or indeed a combination of these (Gehrz et al., 1998). The

grains formed in novae can be larger ($\simeq$0.5 μm; Evans et al., 1997) than those in the interstellar medium (ISM; $\lesssim$0.2 μm; Evans, 2001). However Evans et al. (2005) found an upper limit on the grain size in V705 Cassiopeiae to be only $\simeq$0.06 μm and suggested if the grains in this particular nova were not anomalously small, grains sizes may have been overestimated in novae with optically thick dust shells. Only a small portion of the ISM dust (probably $\lesssim$0.3%; Gehrz et al., 1998) of a galaxy is dust that originated in novae, but novae may be an important source of some elements and isotopes. Indeed they are predicted to be the major source of ^{13}C, ^{15}N and ^{17}O (Starrfield et al., 1972; Jose & Hernanz, 1998; Starrfield et al., 2008). Neon novae, however, produce little or no detected dust. It may be that CO novae generally produce more dust because they involve lower mass WDs, hence an outburst involves more mass ejected at lower speeds (Gehrz et al., 1998).

The relative ratio of carbon to oxygen is important in dust formation, because carbon monoxide is a very stable molecule. Generally this leads to the least abundant of the two molecules being almost entirely used up in CO formation and hence unavailable for forming dust. Hence simplistically it would be expected that if C $>$ O, carbon rich dust would form and if O $>$ C, oxygen rich dust would form. However this does not appear to be the case in novae, with CO saturation only occurring during early times after the outburst (Pontefract & Rawlings, 2004).

In novae, CO is produced by two paths:

$$\mathrm{C + H_2 \longrightarrow CH + H}$$
$$\mathrm{CH + O \longrightarrow CO + H}$$

$$\mathrm{C^+ + H_2 \longrightarrow CH^+ + H}$$
$$\mathrm{CH^+ + O \longrightarrow CO^+ + H}$$
$$\mathrm{CO^+ + H \longrightarrow CO + H^+}$$

(Evans & Rawlings, 2008)

Nova ejecta are much hotter than the ISM and any dust is subjected to the strong radiation fields from the nova. However some factors of the environment in nova ejecta

are favourable to dust formation, such as the high densities in the ejecta. Many reaction rates are also higher at the higher temperatures in the ejecta (Evans & Rawlings, 2008).

Data from Gehrz et al. (1998), Evans & Rawlings (2008), Shafter et al. (2011b) and references therein suggest that the timescale on which dust formation occurs in novae, $t_{\rm cond}$, is longer for slower novae. Indeed Shafter et al. (2011b) show that there appears to be a strong relationship between $t_{\rm cond}$ and the time it takes for the brightness of a nova to decline by two magnitudes, t_2. This is shown in Figure 2.1.

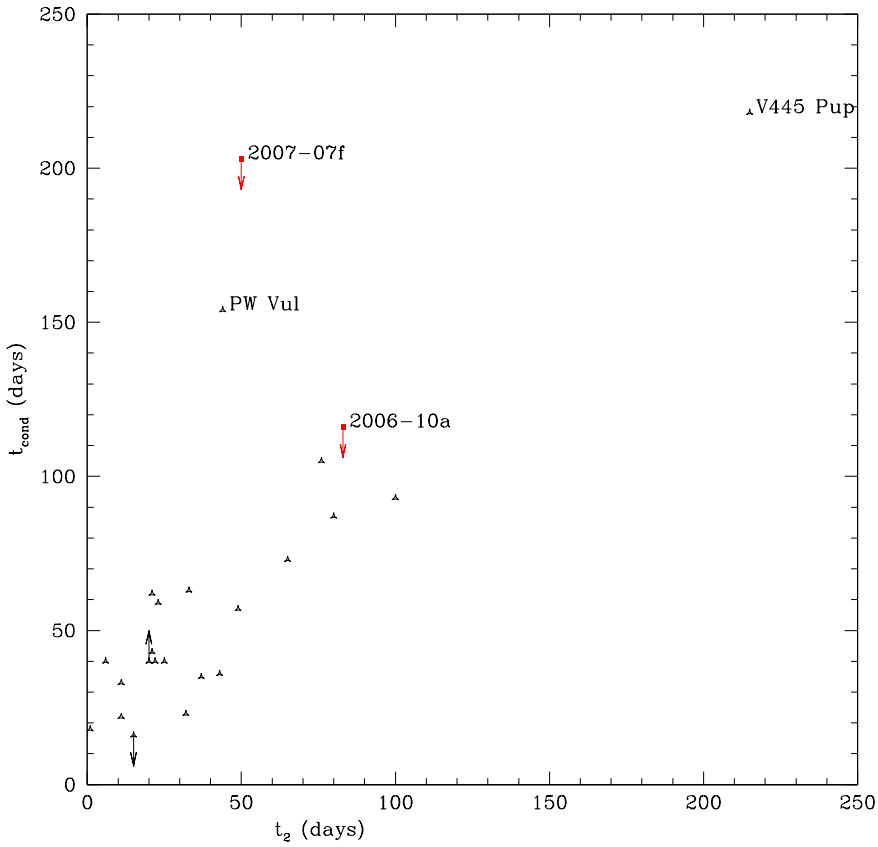

Figure 2.1: A reproduction of the plot produced by Shafter et al. (2011b) showing the dust condensation time against the speed the visual brightness declines in novae. The Galactic novae are shown as triangles, whilst the two suspected dust producing novae in M31 are squares. ©AAS. Reproduced with permission.

This work aims to better understand the relationship between dust formation timescale and speed class. During a nova outburst the underlying continuum spectrum evolves as the temperature of the pseudo-photosphere increases. At higher temperatures more

radiation is systematically emitted at higher energies than the Lyman limit and therefore can be absorbed by neutral hydrogen. Using this simplistic hypothesis, the basic theory described in Section 2.2 is modified and the initial results are compared to observational data.

2.2 The Simplistic Model

From energy balance considerations, Evans & Rawlings (2008) find the dust formation timescale, $t_{\rm cond}$, is given by

$$t_{\rm cond} = \left[\frac{L}{16\pi V_{\rm ej}^2 \sigma T_{\rm cond}^4} \frac{\langle Q_{\rm a} \rangle}{\langle Q_{\rm e} \rangle} \right]^{\frac{1}{2}}, \tag{2.1}$$

where L is the luminosity of the nova as seen by the grains (usually assumed to be the bolometric luminosity – see Section 2.4), $V_{\rm ej}$ is ejection velocity, $\langle Q_{\rm a} \rangle$ is Planck mean absorptivity, $\langle Q_{\rm e} \rangle$ is the Planck mean emissivity and $T_{\rm cond}$ is the dust condensation temperature. Hence, from Equation (2.1)

$$t_{\rm cond} \propto L^{1/2} V_{\rm ej}^{-1}. \tag{2.2}$$

Using the MMRD, Warner (2008) states absolute magnitude, *M*, is given by

$$M = b_{\rm n} \log t_{\rm n} + a_{\rm n}$$

where $t_{\rm n}$ is in days. This means that

$$2.5 \log L \propto - \log t_2^{b_2}$$

and thus if $b_2 \simeq 2.5$ (Warner, 2008), then

$$L \propto t_2^{-1}. \tag{2.3}$$

An empirically determined relationship from Warner (2008) gives

$$\log V_{\rm ej} = 3.57 - 0.5 \log t_2, \tag{2.4}$$

where $V_{\rm ej}$ is in kms^{-1} and t_2 is in units of days. In a survey of M31 novae, Shafter et al. (2011f) find a similar relationship from line widths. Therefore

$$V_{\rm ej} \propto t_2^{-0.5}. \tag{2.5}$$

Substituting Equations (2.3) and (2.5) into Equation (2.2) shows $t_{\rm cond}$ is then predicted to be approximately independent of t_2. Taking, for example, the value of $b_2 = 2.55 \pm 0.32$ from Downes & Duerbeck (2000) results in the t_2 dependency of:

$$t_{\rm cond} \propto t_2^{-0.01 \pm 0.06}.$$

However, as can be seen in Figure 2.1, this is clearly not the case and this basic analysis needs modifying. The modification of the theory is described below.

2.3 What if there was no MMRD?

If there was no significant MMRD relationship, as discussed by Kasliwal et al. (2011), $t_{\rm cond}$ would be dependent on t_2 and would be given by

$$t_{\rm cond} \propto t_2^{0.5}.$$

A full quantitative analysis then reveals however that even if very low luminosities

are assumed (which are more conducive to earlier dust formation), dust is predicted to form far later than is ever observed. An example of an unrealistically low luminosity of 10^{30} W (see the initial luminosities in Figure 2.3 for an indication of realistic bolometric luminosities of novae) and an unrealistically large grain size of 0.01 μm (see Equation 2.9 for realistic grain sizes; assuming $T_{\rm cond} \simeq 1200$ K) is shown in Figure 2.2. It can be seen that even in this example, the relationship does not fit the data well.

2.4 The Effect of the Evolving Underlying Nova Spectrum on Dust Formation

As a first step in refining the simplistic model described above, it is assumed that the grain nucleation sites only see emission at wavelengths longer than the Lyman limit (see e.g. Evans & Rawlings, 1994), with neutral hydrogen internal to the dust formation sites absorbing all radiation at wavelengths shorter than the Lyman limit. Although simple uniform-chemistry models predict that the ejecta would be fully ionised before dust formation takes place (e.g. Mitchell & Evans, 1984), it is well known that the chemistry leading to the formation of nucleation sites needs dense, cool, neutral clumps (see Evans & Rawlings, 2008 and references therein). Indeed, there is strong observational evidence – in the form of Na I (ionisation potential 5.14 eV) and CO emission (e.g. Evans et al., 1996; Rudy et al., 2003; Das et al., 2009; Raj et al., 2012) shortly before dust formation – for the presence of cool hydrogen-neutral clumps which are likely at the outer edge of the ionised wind; nucleation sites in such clumps will indeed be exposed only to radiation long-ward of the Lyman limit. In the analysis presented here it is assumed the dust is formed at the outer extremities of the ejected shell.

The initial step is to take the bolometric luminosity as constant (e.g. Warner, 2008) and defined by the speed class and then we find the fraction of this luminosity that is red-ward of the Lyman limit for any given nova at any given time. We define the peak absolute magnitude, M_V, of a given nova using the MMRD relation

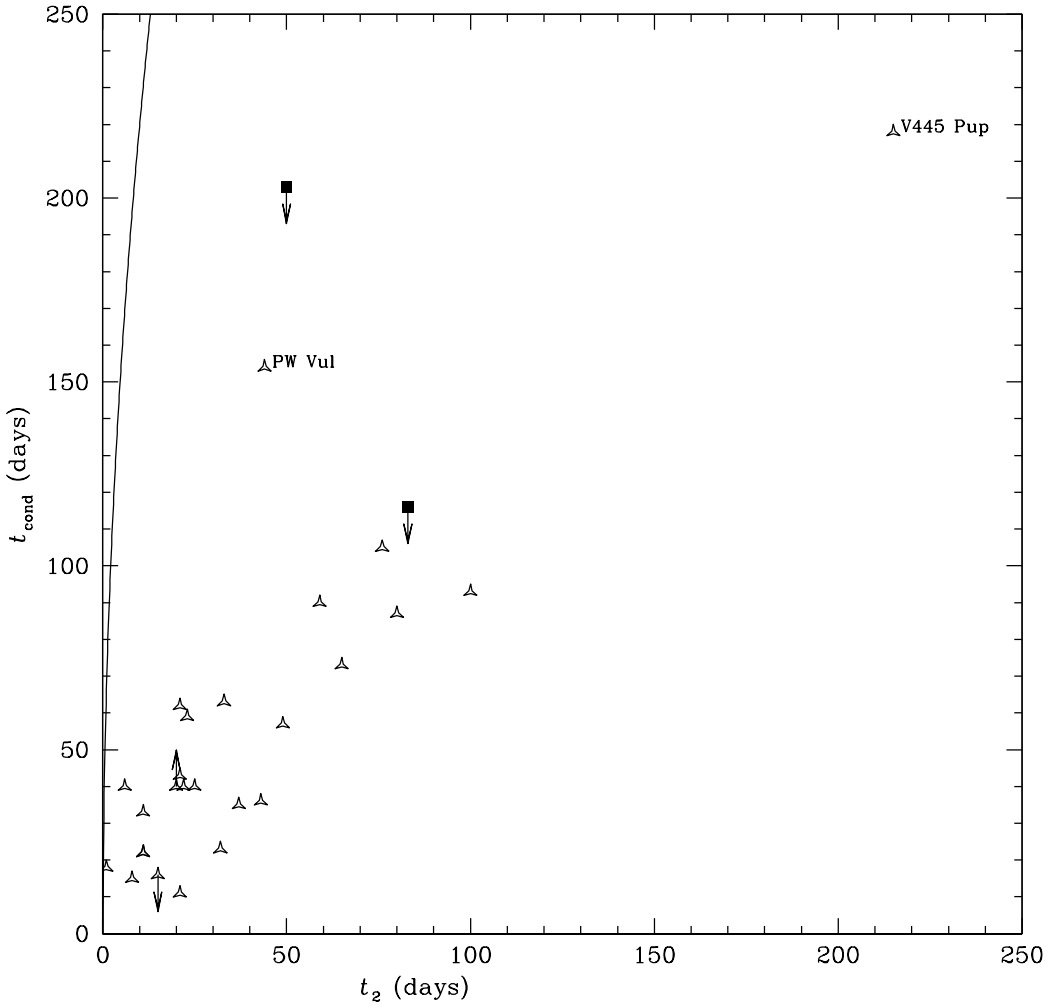

Figure 2.2: The $t_2 - t_{\rm cond}$ relationship assuming no MMRD. The black line represents the relationship derived if a luminosity of 10^{30} W and a grain size of 0.01 μm is assumed, as discussed in the text. The points represent observational data from dust-forming nova identical to those presented and discussed later in Figure 2.5 and Section 2.2.

$$M_V = 2.5 \log t_2 - 11$$

(see Warner, 2008, and references therein). Assuming the bolometric correction BC = 0 at the peak of the visual light curve (as it seems most novae at maximum have an effective photospheric temperature of about 8000K – see Evans et al., 2005), M_V is then converted to luminosity to give the bolometric luminosity, $L_{\rm bol}$, corresponding to each t_2.

The temperature of the pseudo-photosphere is at a minimum at the time of visual maximum, which is in turn reached within the first few days of outburst in most novae. At this time, almost all of the radiation is at wavelengths longer than the Lyman limit. The fraction of radiation red-ward of the Lyman limit can be calculated from the effective temperature, $T_{\rm eff}$, given by the following equation from Bath & Harkness (1989):

$$T_{\rm eff} = T_0 \times 10^{\Delta V/2.5},$$

where T_0 is the pseudo-photospheric temperature at visual peak ($= 8000$ K as noted above, Evans et al., 2005) and ΔV is the change in magnitude from peak. In order to find $T_{\rm eff}$ as a function of time, model optical light curves were produced for each t_2 value.

To do this, first the outburst amplitude, A, for each t_2 value was estimated using the 57° line in the amplitude$-$log t_2 relationship plot in Warner (1995, the average flux observed from thin accretion disks with a random distribution of inclinations will be equal to that of a 57° system). The time after outburst corresponding to each ΔV was calculated by assuming a standard exponential decay, change in magnitude, ΔV, can be expressed as:

$$\Delta V = A - Ae^{-xt} \tag{2.6}$$

Where *A* is the outburst amplitude (in magnitudes), *x* is a decay constant and *t* is time

after outburst. So:

$$t = \frac{\ln A - \ln(A - \Delta V)}{x}.$$

For t_2:

$$x = \frac{\ln A - \ln(A - 2)}{t_2},$$

hence

$$t = \frac{\ln A - \ln(A - \Delta V)}{\ln A - \ln(A - 2)} t_2.$$

How the luminosity red-ward of the Lyman limit, L_{Ly}, declined over time was then calculated for each t_2 value. Assuming the nova emits as a black body (although this is a first approximation for the purposes of this work – see Hauschildt, 2008), the blackbody function was integrated to find the luminosity red-ward of the Lyman limit that is received by the nucleation sites at a given time, L_{Ly}.

$$L_{\mathrm{Ly}} = 4\pi^2 R^2 \int_{91.2\ \mathrm{nm}}^{\infty} B_\lambda(T) d\lambda,$$

where R is radius of the pseudo-photosphere. Figure 2.3 shows L_{Ly} against t for various t_2 values. It can be seen from the figure that, as expected, L_{Ly} drops much faster for faster novae. For example, potential dust formation sites in a $t_2 = 40$ days nova see more central source luminosity at $t = 30$ days than potential sites in a $t_2 = 25$ days nova do at the same epoch, despite the bolometric luminosity being higher for the faster nova.

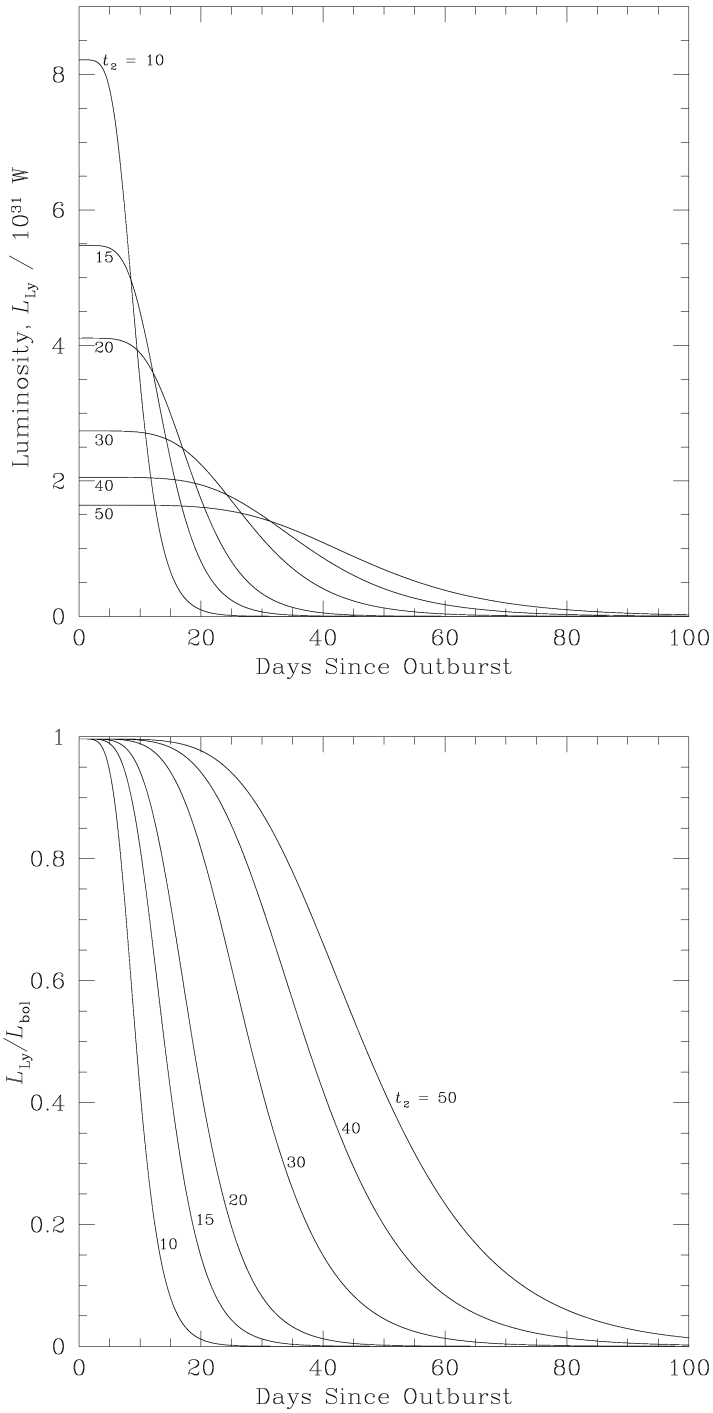

Figure 2.3: How the luminosity seen by potential dust-forming sites changes over time for different speed classes. The top plot shows the luminosity produced by a nova that will be seen by the grains for $t_2 = 10$ days (highest initial luminosity), $t_2 = 15, 20, 30, 40$ and $t_2 = 50$ days (lowest initial luminosity). The bottom plot shows the same, but expressed as a ratio of the total luminosity produced by a nova with a given t_2 value, with $t_2 = 10$ days being the fastest declining and $t_2 = 50$ days being the slowest.

2.5 The Need for $Q_{\rm abs}$ values

Assuming the nova emits as a black body, the emission red-ward of the Lyman limit was first calculated by integrating the Planck function between wavelengths 91.2nm and infinity:

$$\int_{91.2nm}^{\infty} B_\lambda(T) = \int_{91.2nm}^{\infty} \frac{2hc^2/\lambda^5}{e^{\frac{hc}{\lambda kT}} - 1} d\lambda, \tag{2.7}$$

which integrates to give:

$$\int_{91.2nm}^{\infty} B_\lambda(T) = \frac{2k^4T^4}{h^3c^3}\left[\frac{\pi^4}{15} - \sum_{n=1}^{\infty}\left(\frac{\left(\frac{hc}{\lambda_m kT}\right)^3}{n} + \frac{3\left(\frac{hc}{\lambda_m kT}\right)^2}{n^2} + \frac{6hc}{\lambda_m kTn^3} + \frac{6}{n^4}\right) e^{-\frac{nhc}{\lambda_m kT}}\right]. \tag{2.8}$$

Each $L_{\rm Ly}$ equation was substituted into Equation (2.1). Assuming graphitic carbon, $\langle Q_{\rm a}\rangle \simeq 1$, $\langle Q_{\rm e}\rangle \simeq 0.01aT_{\rm dust}^2$ and $T_{\rm cond} \simeq 1200$ K (Evans & Rawlings, 2008). As $V_{\rm ej}$ could be calculated for each t_2 value using Equation (2.4), the equation was solved using trial and error, to produce a theoretical $t_{\rm cond}$ for each value of t_2.

The initial results of this analysis showed that dust formation timescale was indeed dependent on t_2. Figure 2.4 shows the relationship calculated, but the resultant relationship appears to make $t_{\rm cond}$ far too dependent on t_2. The figure also illustrates how dependent the relationship is on the assumed grain size, however even the lower grain size estimate of 0.01 μm is an overestimate of the radius of nucleation sites.

Using an equation from Evans (1993):

$$a \lesssim \frac{1.3}{T_{\rm dust}}\mu m, \tag{2.9}$$

it can be seen that with an estimated temperature for dust formation of 1200 K the grain size would be expected to be no more than a few nm when dust formation occurs.

It is clear from Figure 2.4 that the initial analysis described in Section 2.4 produces

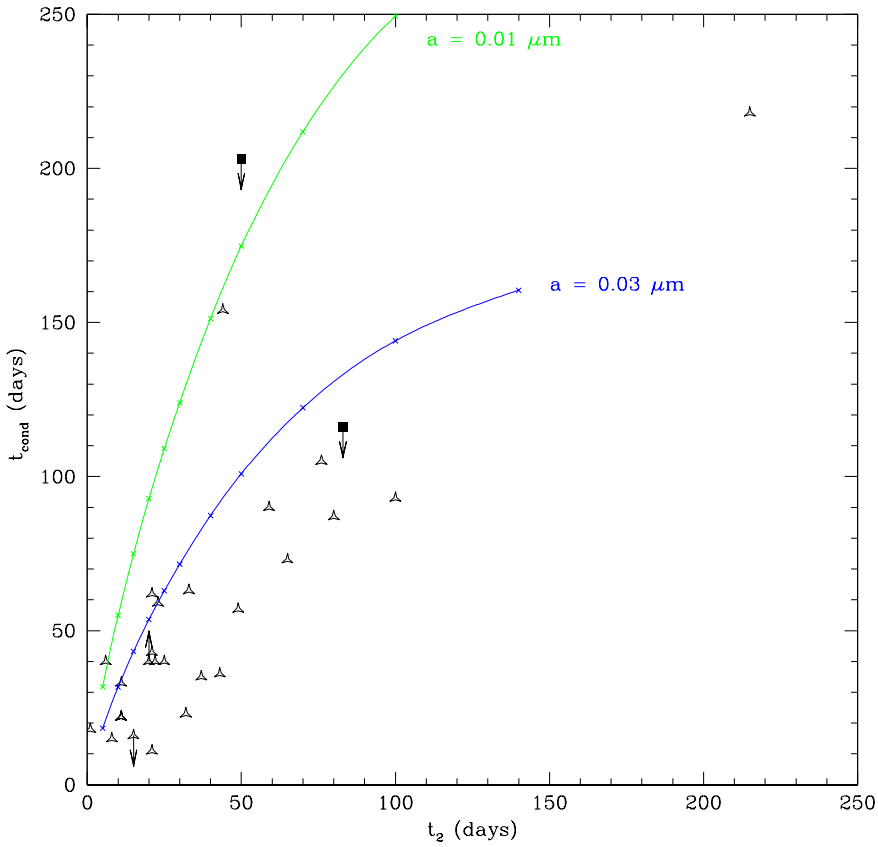

Figure 2.4: A plot showing how the initial modified theory shows that dust formation is dependent on t_2 and how dependent the relationship is on grain size. The points represent the same observational data used and described later in Figure 2.5.

a relationship where dust formation timescale is far too dependent on t_2. The main problem with the above analysis is that the mean Planck mean absorptivity, $\langle Q_{\rm a} \rangle$, and Planck mean emissivity, $\langle Q_{\rm e} \rangle$ were used. However since a complete Planck function is no longer used it is inappropriate to use these and is therefore necessary to reconsider this assumption.

The emission coefficient, $Q_{\rm em}$, is dependent only on the temperature of the nucleation centres, not the means of heating, and hence the emission is not directly governed by the wavelengths of the absorbed radiation. Therefore a Planck mean can still be used in this case. However the absorption coefficient, $Q_{\rm abs}$, will be affected, and hence $\langle Q_{\rm a} \rangle$ can no longer be used. Therefore Equation (2.8) is no longer valid and a new equation taking into account $Q_{\rm abs}$ had to be derived.

As part of the revised theoretical exploration, different types of grain material were considered, for example using data from Zubko et al. (1996). In terms of the size of nucleation centres, it was assumed that C_8 as a nucleation centre acts as a solid sphere, where grain radius, $a \sim 0.26$ nm (see Evans & Rawlings, 2008, and references therein). A Mie theory code was run by V. Zubko to generate $Q_{\rm abs}$ values for a range of grain sizes from $0.26 \leq a \leq 5$ nm over $0.05 \leq \lambda \leq 1$ μm for a condensation temperature, $T_{\rm cond}$, of 1200 K (appropriate for graphite in a 1:1 ratio C:O environment; Evans & Rawlings, 2008). Absorption efficiencies at longer wavelengths were found by extrapolation.

The carbon species that were explored were graphite and ACH2 (amorphous carbon is thought to form in H-rich environments; Zubko et al., 1996), although the formation of spherical nucleation centres is of course less likely in the case of graphite. The results showed that, as expected in the Rayleigh regime, $Q_{\rm abs} \propto a$. The Planck mean emission for graphite was calculated to be

$$\langle Q_{\rm e} \rangle \simeq 0.15 a T_{\rm d}^{1.5}$$

and that for ACH2 was

$$\langle Q_{\rm e} \rangle \simeq 400 a T_{\rm d}^{0.46},$$

where $T_{\rm d}$ is the temperature of the grains (in Kelvin) and a is in cm in each case. These Planck means are not valid over all temperatures, but sufficient for these calculations (i.e. they easily cover the range around 1200 K - the Planck mean for graphite is valid over the temperature range of approximately 500 K to 4000 K, with that of ACH2 being valid approximately between 500 K and 2000 K).

Thus, considering the energy balance between absorbed and emitted energy by a nucleation site for graphite

$$T_{\rm d} = \left[\frac{5 L_{\rm bol}}{12 a \sigma^2 T_{\rm eff}^4 V_{\rm ej}^2 t^2} \int_{91.2 \text{ nm}}^{\infty} B_\lambda(T_{\rm eff}) Q_{\rm abs}(a, \lambda) d\lambda \right]^{0.18} \tag{2.10}$$

and for ACH2

$$T_{\rm d} = \left[\frac{L_{\rm bol}}{6400 a \sigma^2 T_{\rm eff}^4 V_{\rm ej}^2 t^2} \int_{91.2 \text{ nm}}^{\infty} B_\lambda(T_{\rm eff}) Q_{\rm abs}(a, \lambda) d\lambda \right]^{0.22}. \tag{2.11}$$

Equation (2.11) was solved numerically for dust condensation temperatures in the range of 1000 K to 1400 K and Equation (2.10) was solved numerically for $T_{\rm cond} = 1200$ K for reference.

2.6 Results

The predicted $t_{\rm cond} - t_2$ relationships from the above model were compared with the data produced by Shafter et al. (2011b) using their observations and those of references therein. This is shown in Figure 2.5, with additional points added for V1425 Aquilae (Kamath et al., 1997), V1280 Scorpii (Chesneau et al., 2008), V5579 Sagittarii (Raj et al., 2011), V496 Scuti (Raj et al., 2012) and V809 Cephei (Munari et al., 2013). The graphite and ACH2 relationships shown in the figure were produced by performing the numerical integration described at the end of Section 2.4 over a range of t_2 values.

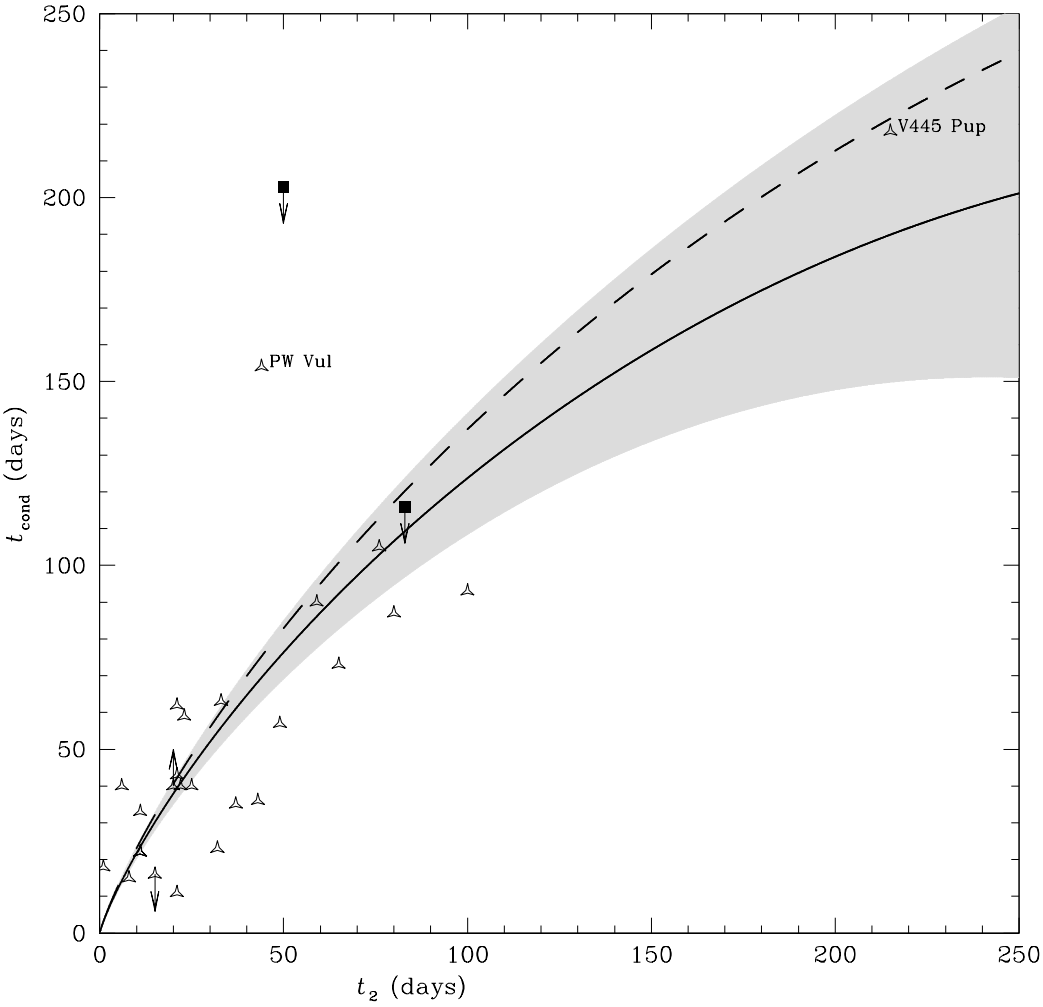

Figure 2.5: Observational data from Shafter et al. (2011b) and references therein, with the additional data points listed in the text, showing dust condensation time, $t_{\rm cond}$, against the speed of visual brightness decline, t_2, in novae. The Galactic novae are shown as open triangles, whilst the two suspected dust producing novae in M31 are shown as squares. The outlying Galactic novae PW Vulpeculae and V445 Puppis are discussed in more detail in Shafter et al. (2011b). The dashed line shows the results for the model for graphite when $T_{\rm cond} = 1200$ K. The solid line shows the results for the model for ACH2 when $T_{\rm cond} = 1200$ K, with the shaded area showing the results for ACH2 for a $T_{\rm cond}$ in the range between 1000 K and 1400 K (with the higher $T_{\rm cond}$ being the lower limit of the shaded area).

The analysis was also performed using a very simple optical decline of

$$\Delta V = \frac{2t}{t_2}, \tag{2.12}$$

which had very little effect on the final results as can be seen in Figure 2.6.

2.7 Discussion and Conclusions

As can be seen from Figure 2.5, the results for both graphite and ACH2 appear to agree well with the general trend of $t_{\rm cond}$ with t_2 from the observations, despite the simplistic assumptions made. There do not appear to be great differences between the relationships for the two types of carbon. The shaded area of the figure displays the relationship for ACH2 for $T_{\rm cond}$ between 1000 K and 1400 K. This shows that the relationship holds well for a range of $T_{\rm cond}$. Note that many specific data points at the lower t_2 values lie outside our relationship, but this reflects the simplicity of the model and the variation in parameters, including specific dust grain types, expected for individual nova outbursts.

It can also be seen in Figure 2.5, that there is a gap in observational data between $100 \gtrsim t_2 \gtrsim 200$. Note of course that the extreme case, V445 Puppis, is an unusual helium nova. The apparent gap may however be due to the relative rarity of novae of these slow speed classes, and furthermore not every nova being observed sufficiently systematically at such late times to detect the epoch of dust formation. Overall, the results of this work can be used to predict when dust will form in a nova of a given speed class and hence when, for example, infrared observations should be taken to detect the onset of dust formation.

The only known dust-forming nova where carbon-based dust has not been observed is QU Vulpeculae (QU Vul), where SiO_2 dust was formed ($t_2 = 20$ days and $t_{\rm cond} = 40$ days; Evans & Rawlings, 2008; Strope et al., 2010), although this nova still appears to match our theoretical relationships for carbon-based dust. Several novae have been

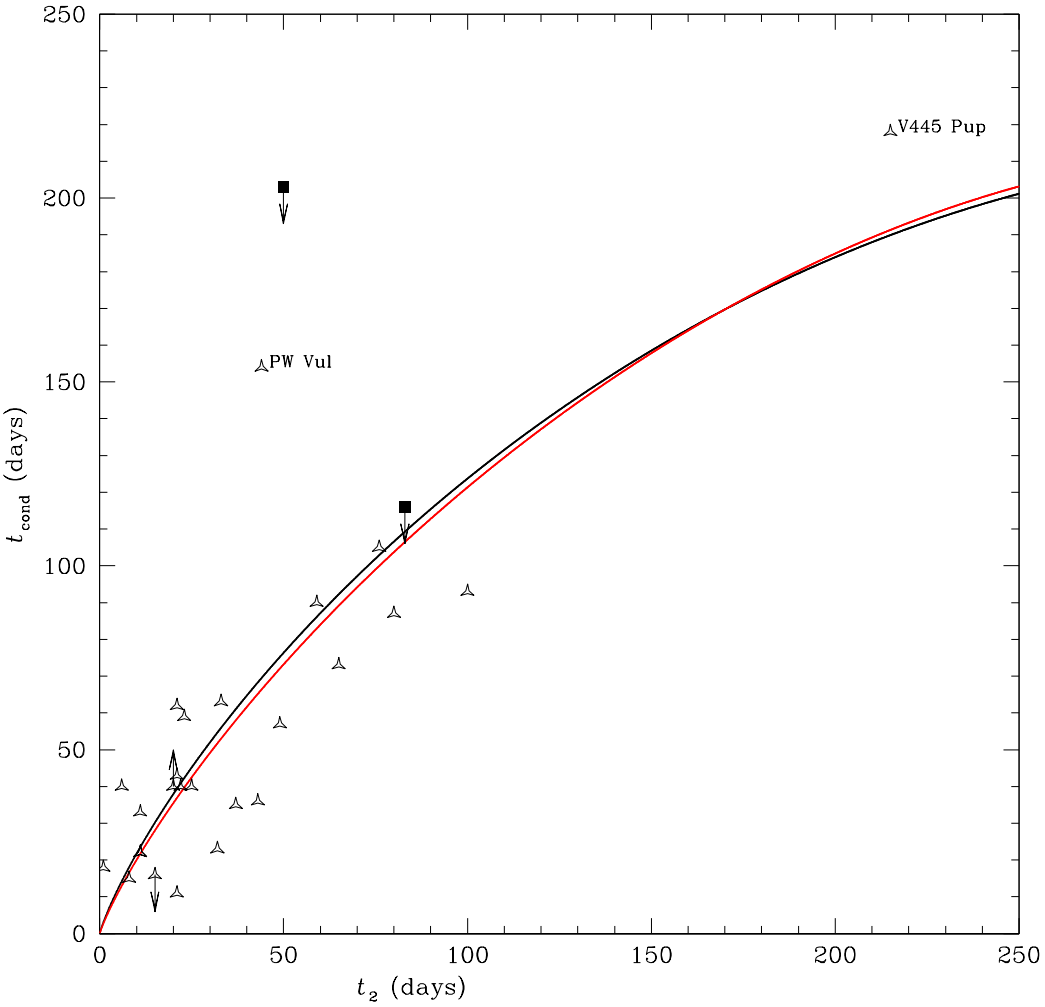

Figure 2.6: Observational data as in Figure 2.5, but showing only the model for ACH2 with $T_{\rm cond} = 1200$ K. The black line is the same ACH2 line as that presented in Figure 2.5 and the red line represents ACH2 with $T_{\rm cond} = 1200$ K, but using the simple optical decline show in Equation (2.12).

observed to form both carbon-rich and oxygen-rich dust (Evans & Rawlings, 2008), although the dust in CO novae is thought to consist mainly of amorphous carbon grains (Gehrz, 2008). The future steps to making a more realistic model are described in Section 7.2.1.

Having studied dust formation in novae, and offered a theoretical explanation for the relationship between t_2 and $t_{\rm cond}$, the thesis now moves on to present a survey for the progenitors of M31 novae, and looks at the proportion of novae with evolved secondaries.

Chapter 3

Searching for the Progenitors of M31 Novae

The majority of the work described in this chapter has been accepted for publication in Williams, S. C., Darnley, M. J., Bode, M. F., Keen, A. and Shafter, A. W. (2014, ApJS, accepted, arXiv:1405.4874)

3.1 Introduction

Many of the brighter Galactic novae can be readily observed in quiescence, even with smaller professional telescopes. However, due to the Sun's position within the Galaxy, the study of the entire nova population is hindered by the obscuring effect of dust in the Galactic plane and large uncertainties when determining distances and extinction. Approximately ten novae are discovered each year in the Milky Way, only around a third of the predicted nova rate of 34^{+15}_{-12} (Darnley et al., 2006). While some outbursts may be missed due to seasonal gaps, the majority are likely to be missed due to extinction effects. Therefore surveys of other galaxies are needed for more complete studies of nova populations.

The number of galaxies where novae will be resolvable at quiescence, even with large

telescopes, is relatively limited. RG-novae (i.e. the novae with brightest secondaries) are observable at quiescence in the Local Group and novae with luminous red giant secondaries (like RS Oph for example) are detectable further out (e.g. in the M81 Group). Whilst the Magellanic Clouds are ideal for studying individual objects (e.g. LMCN 2009-02a; Bode et al., in preparation), their nova rates are too low for any population studies of quiescent systems. M31, whilst more distant, has a predicted nova rate of 65^{+16}_{-15} (Darnley et al., 2006) and around 30 novae per year are discovered, allowing statistically significant population studies to be conducted over a much shorter timeframe than would be required for any other member of the Local Group. Whilst there are still dust extinction effects, these are generally much smaller than Galactic extinction. As is shown in Section 5.3, a considerable number of novae are likely missed due to the seasonal gap, where M31 is difficult to observe for several months. It is also shown in Section 5.3 that even just extrapolating from the novae discovered when M31 is easiest to observe yields a nova rate of ~ 48 per year. Additionally, as in any extragalactic system, novae in M31 can all be assumed to be at the same distance, therefore negating one of the main uncertainties that is encountered when studying Galactic novae.

The ability to detect multiple outbursts of a given nova system in M31, thus classifying it as a RN, is hindered by a number of factors. An outburst that occurs during the seasonal gap is less likely to be discovered, particularly if it fades quickly, as is often the case for RNe. Furthermore, a greater number of novae are now discovered in M31 each year than were a decade or so ago, when a much greater proportion were likely missed. This means that there are probably a number of systems that have produced multiple outbursts since the time of the survey of Hubble (1929), but they have simply not been discovered.

Additionally, the astrometric accuracy required to match two outbursts at the distance of M31, particularly in the bulge (more novae occur here), may be greater than was achievable for some old M31 novae. Nonetheless, there have been a number of attempts to explore the recurrent nova population of M31 by searching for multiple outbursts at similar positions (e.g. Rosino, 1973; della Valle & Livio, 1996; Ansari et al.,

2004; Henze et al., 2008b; Lee et al., 2012; Shafter et al., in preparation). However, these have all been severely limited by the large positional uncertainties of the old novae, and have only yielded a few RN candidates. Additionally, astrometric errors can give rise to incorrect association between multiple outbursts, (see Figure 4 of Bode et al., 2009, for example). This technique is further hampered by the misidentification of some long period Mira variables as M31 novae (see, for example Darnley et al., 2004; Shafter et al., 2008a,b).

Some of these problems can be overcome by using a spectroscopically confirmed sample of novae which all have well determined astrometric positions. But this essentially limits us only to M31 novae since around 2006 when spectroscopy of large samples of M31 novae in outburst became viable (see e.g. Shafter et al., 2011f). Based on the recurrence timescales of their Galactic counterparts, such a short baseline (< 10 years) is not long enough to recover a good sample of RNe using multiple outbursts alone.

Here a technique that can be used to recover the progenitor systems of novae belonging to the RG-nova class (which Galactically is dominated by confirmed and candidate RNe of the RS Oph sub-class) from a spectroscopically confirmed sample of M31 novae is proposed. In some (exceptional) cases this technique may also be able to recover SG-novae in M31 (a class dominated by RNe of the U Sco sub-class) as was recently achieved for the (albeit much closer) LMC RN LMCN 2009-02a (Bode et al., in preparation).

A number of space-based and the larger ground-based optical telescopes are capable of resolving red giant stars within M31. As such, the progenitor systems of RG-novae in M31 can in principle be directly imaged. Similar work has been used to directly image the lensed system for M31 microlensing events (see, for example Aurière et al., 2001) and indeed the nova M31N 2007-12b (Bode et al., 2009). Kasliwal et al. (2011) have also discussed such an approach.

3.2 Method

The technique employed in this work to attempt to recover the progenitor system for each nova was first outlined in Bode et al. (2009). This method relies upon accurate registration between images containing the nova in outburst and deeper (typically archival) high-resolution images where the system is likely to be in quiescence. Here a catalogue of Local Group novae selected by virtue of their spectroscopic confirmation (see e.g. Shafter et al., 2011f) and astrometric precision of the outburst was used. The input catalogue is shown in Table 3.1.

For this study, data taken using RATCam, an optical CCD camera, on the Liverpool Telescope (LT), which is on La Palma, were used to determine the outburst position of the nova and the corresponding position in archival *HST* data for the identification of the progenitor. The ground-based data were processed and analysed using a combination of Starlink[1] and IRAF[2] (Tody, 1986) software. Imaging data from the Wide-Field Planetary Camera 2 (WFPC2), the Advanced Camera for Surveys – Wide-Field Channel (ACS/WFC) and the Wide-Field Camera 3 – UVIS Channel (WFC3/UVIS) onboard *HST* were used, all three of which provide very good overlap with the $4\farcm6 \times 4\farcm6$ RATCam LT fields used for this survey. The *HST* data are again processed using Starlink and IRAF software, the *HST* photometry is performed using HSTphot (Dolphin, 2000) for the WFPC2 data and DOLPHOT[3], a photometry package based on HSTphot, for the ACS/WFC data.

[1] `http://starlink.jach.hawaii.edi`

[2] IRAF is distributed by the National Optical Astronomy Observatories which are operated by the Association of Universities for Research in Astronomy Inc., under cooperative agreement with the National Science Foundation.

[3] `http://purcell.as.arizona.edu/dolphot`

Table 3.1: The input nova catalogue: spectroscopically confirmed sample all with LT or Faulkes Telescope North (FTN) astrometry. The availability of LT and FTN outburst data along with *HST* WFPC2 and ACS/WFC quiescent data are shown for each nova. We also list the spectroscopic type and t_2 of each outburst. For novae that have a t_2 value published in more than one filter, we note the one in the filter closest to that used in this work to search for the progenitor. The table also shows the proposal IDs of the *HST* data used in this paper. The first number is for the data used to determine the position of the system, with any subsequent ID numbers being for data used in the light curves (with the latter being presented in Chapter 4).

Nova	Spectral Class[a]	t_2 (band)[a]	Outburst astrometry		Archival *HST* data		Proposal ID of
			LT	FTN	WFPC2	ACS/WFC	*HST* data used
M31N 2006-09c	Fe II[1]	23.1 ± 1.6 $(R)^2$	✓	×	✓	×	10273
M31N 2006-11a	Fe II[3]	28.7 ± 2.6 $(R)^2$	✓	×	✓	✓	10273
M31N 2007-02b	Fe II[2,4]	34.1 ± 3.6 $(R)^2$	✓	×	✓	✓	10260, 11218
M31N 2007-10a	He/Nn[2,5]	7.9 ± 0.4 $(V)^2$	✓	✓	×	✓	9719
M31N 2007-10b	He/Nn[2,6]	3.1 ± 0.4 $(R)^2$	✓	✓	×	✓	12058
M31N 2007-11b	He/Nn[2,7]	74.4 ± 16.7 $(i')^2$	✓	✓	✓	×	10273
M31N 2007-11c	Fe II[8]	11.7 ± 0.9 $(i')^2$	✓	✓	×	✓	12058
M31N 2007-11d	Fe II[9]	9.2 ± 0.5 $(i')^2$	✓	✓	×	✓	12057
M31N 2007-11e	Fe II[10]	27 $(R)^3$	✓	×	×	✓	12110
M31N 2007-12a	Fe II[11]	29.6 ± 2.0 $(i')^2$	✓	✓	✓	✓	12057

Continued on next page

Table 3.1 – continued from previous page

Nova	Spectral Class[a]	t_2 (band)[a]	LT	FTN	WFPC2	ACS/WFC	Proposal ID
M31N 2007-12b	He/N[11]	5.0 ± 0.5 $(R)^2$	✓	×	✓	✓	12058
M31N 2008-10b	Fe II[12]	98.4 ± 14.9 $(B)^2$	✓	✓	✓	✓	10006, 11833, 12058
M31N 2008-12b	Fe II[13]	24.7 ± 3.6 $(i')^2$	✓	×	×	✓	12109
M31N 2009-08a	Fe II[14]	36.7 ± 4.1 $(B)^2$	✓	×	×	✓	10760, 12058
M31N 2009-08b	Fe II[15]	26.9 ± 2.2 $(i')^2$	✓	×	×	✓	12114
M31N 2009-08d	Fe II[16]	27.9 ± 6.5 $(B)^2$	✓	×	✓	✓	10006
M31N 2009-10b	Fe II[17]	8.0 ± 0.2 $(B)^2$	✓	×	×	✓	11013, 12058
M31N 2009-10c	Fe II[18]	14.9 ± 0.8 $(B)^2$	✓	×	✓	✓	10006, 12058
M31N 2009-11a	Fe II[19]	21.7 ± 1.2 $(V)^2$	✓	×	×	✓	10273
M31N 2009-11b	Fe II[20]	74.8 ± 10.6 $(V)^2$	✓	×	✓	×	10273
M31N 2009-11c	Fe II[21]	32.5 ± 2.4 $(V)^2$	✓	×	✓	✓	10273, 12058
M31N 2009-11d	Fe II[22]	11.2 ± 0.4 $(B)^2$	✓	×	×	✓	12105
M31N 2009-11e	Fe II[23]	55.7 ± 3.1 $(R)^2$	✓	×	✓	✓	5907, 12058
M31N 2010-01a	Fe II[24]	28 ± 21 (B)[25]	✓	×	×	✓	10760, 12058
M31N 2010-05a	Fe II[26]	39 ± 17 (B)[25]	✓	×	✓	✓	10006, 12058
M31N 2010-09b	Fe II[27,28]	3.8 ± 0.2 (B)[25]	✓	×	×	✓	12073
M31N 2010-10a	Fe II[28]	$< 16 \pm 2$ (B)[25]	✓	×	×	×	12109
M31N 2010-10b	Fe II[29]	> 41[30]	✓	×	×	✓	10273
M31N 2010-10c	Fe II[31]	20[30]	✓	×	✓	✓	10407
M31N 2010-10d	Fe II[32]	23 ± 7 (B)[25]	✓	×	✓	✓	10006, 12058

Continued on next page

Table 3.1 – continued from previous page

Nova	Spectral Class[a]	t_2 (band)[a]	LT	FTN	WFPC2	ACS/WFC	Proposal ID
M31N 2010-10e	He/N[33]	> 5[29]	✓	×	✓	✓	10273
M31N 2011-10a	Fe II[34,35]		✓	×	×	✓	12058
M31N 2011-10d	Fe II[36,37]		✓	×	✓	✓	12058
M31N 2011-12a	Fe II[38]		✓	×	✓	×	10273
M31N 2012-01a	Fe II[39]		✓	×	×	✓	11647
M31N 2012-09a	Fe IIb[40]		✓	×	✓	✓	12058
M31N 2012-09b	Fe IIb[41]		✓	×	✓	✓	12058
M31N 2012-12a	Fe II[42]		✓	×	✓	✓	12058

[a] **References:** (1) Shafter et al. (2006), (2) Shafter et al. (2011f), (3) Shafter et al. (2011b), (4) Pietsch et al. (2007a), (5) Gal-Yam & Quimby (2007), (6) Rau et al. (2007), (7) Rau (2007), (8) Ciroi et al. (2007), (9) Shafter et al. (2009), (10) Di Mille et al. (2007), (11) Shafter (2007), (12) Di Mille et al. (2008), (13) Kasliwal et al. (2009), (14) Valeev et al. (2009), (15) Rodríguez-Gil et al. (2009), (16) Di Mille et al. (2009), (17) Barsukova et al. (2009), (18) Fabrika et al. (2009), (19) Hornoch et al. (2009b), (20) (Kasliwal, 2009), (21) Hornoch et al. (2009c), (22) Hornoch et al. (2009a), (23) Hornoch & Pejcha (2009), (24) Hornoch et al. (2010e), (25) this work (see Section 4), (26) Hornoch et al. (2010c), (27) Shafter et al. (2010c), (28) Shafter et al. (2010e), (29) Shafter et al. (2010f), (30) Cao et al. (2012), (31) Shafter et al. (2010d), (32) Shafter et al. (2010b), (33) Shafter et al. (2010a), (34) Cao et al. (2011), (35) Cao (2011) (36) Shafter et al. (2011c), (37) Shafter et al. (2011d), (38) Shafter et al. (2011a), (39) Shafter et al. (2012b), (40) Shafter et al. (2012d), (41) Shafter et al. (2012f), (42) Shafter et al. (2012e)

Much of the LT data were taken as part of a monitoring survey of Local Group novae in outburst (see e.g. Shafter et al., 2011f, 2012a). Observations were generally taken through B, V, r' and i' filters, with a typical exposure time per filter of 180s (each comprising 3×60s images combined by taking the median). For most of these observations the cameras were operated in a 2×2 binning mode, giving an effective pixel size of $0\farcs279$. Towards the end of this survey, the observations in the r' and i' filters were dropped in favour of first a higher cadence through the B and V filters and more recently, greater exposure times. The data used for the 2012 novae were long-exposure (typically $3\times$300s) r'-band images, specifically taken for this project. The M31 progenitor survey presented here ended in February 2013.

The accuracy of the registration between the LT data and the *HST* data is dependent upon a number of factors, including: the size of the common overlap region; the stellar density in the overlap; the seeing of the ground-based data; the luminosity of the nova, and the *HST* instrument available. Typically, it is the seeing in the ground-based data that has the largest detrimental effect, but some compromise must be reached between the ground-based seeing and the luminosity of the nova in each image. In order to minimise these effects, a number of approaches are employed. Preferentially, ground-based data in i' and r' filters were used, as these are where these telescopes are most sensitive against the unresolved M31 background light, yielding superior position measurements on fainter objects and usually more numerous objects for registration. Observations of M31 taken by the Angstrom survey using the LT (e.g. Kerins et al., 2006; Darnley et al., 2007, also Darnley private communication) indicated that the i' and r' filters gave superior contrast between M31 variable sources and the unresolved M31 background (at the typical site seeing on La Palma). Ideally WFC3/UVIS data would be used to search for the progenitor systems, however, there is little data taken of the M31 field in a suitable filter (as can be seen in Appendix A) and indeed none for the novae in this survey. Therefore ACS/WFC data is preferred over WFPC2 data. This is due to the smaller pixel size, yielding greater spatial resolution, and quantum efficiency improvement and hence better sampling of the PSF. As the ground based data are generally "red", the most appropriate *HST* filter is chosen if possible, which

was typically F814W.

3.3 Observations

The spatial distribution of the 38 novae in the catalogue is shown in Figure 3.1.

3.3.1 LT Image Selection

LT images taken using the RATCam instrument in the Sloan-like i' and r' filters along with B and V Bessel filters were used, with the images that would produce the most reliable position for each nova, taking into consideration both the seeing and brightness of the nova, being selected. The filters were also matched with those used for the *HST* images where possible. The position of each nova in the catalogue with respect to 2MASS (Cutri et al., 2003; Skrutskie et al., 2006) is shown in Table 3.2.

3.3.2 *HST* Image Selection

For this work, archival *HST* images taken with ACS/WFC and WFPC2 using the F435W, F475W, F555W, F606W, F625W, and F814W filters were used. For some novae, pre-outburst archival *HST* images were not available, but images taken long after the outburst were. In such cases it was ensured that the system was likely to be at quiescence using the speed class of the nova and the images themselves. For example, a nova with a t_2 of just a few days will clearly have faded to quiescence if the images were taken some years after the outburst. Additionally, for novae which could not be confirmed as being likely in quiescence using the previous method, multiple epochs of *HST* data (if available) were looked at. A system was assumed to be at quiescence if it had not faded between one *HST* image and the next when they are taken several months apart. For the individual novae with only post-outburst data, it is noted why the system is believed to be at quiescence in Section 3.4. A typical example of how LT images of novae in outburst coincide with the archival *HST* data is shown in Figure 3.2.

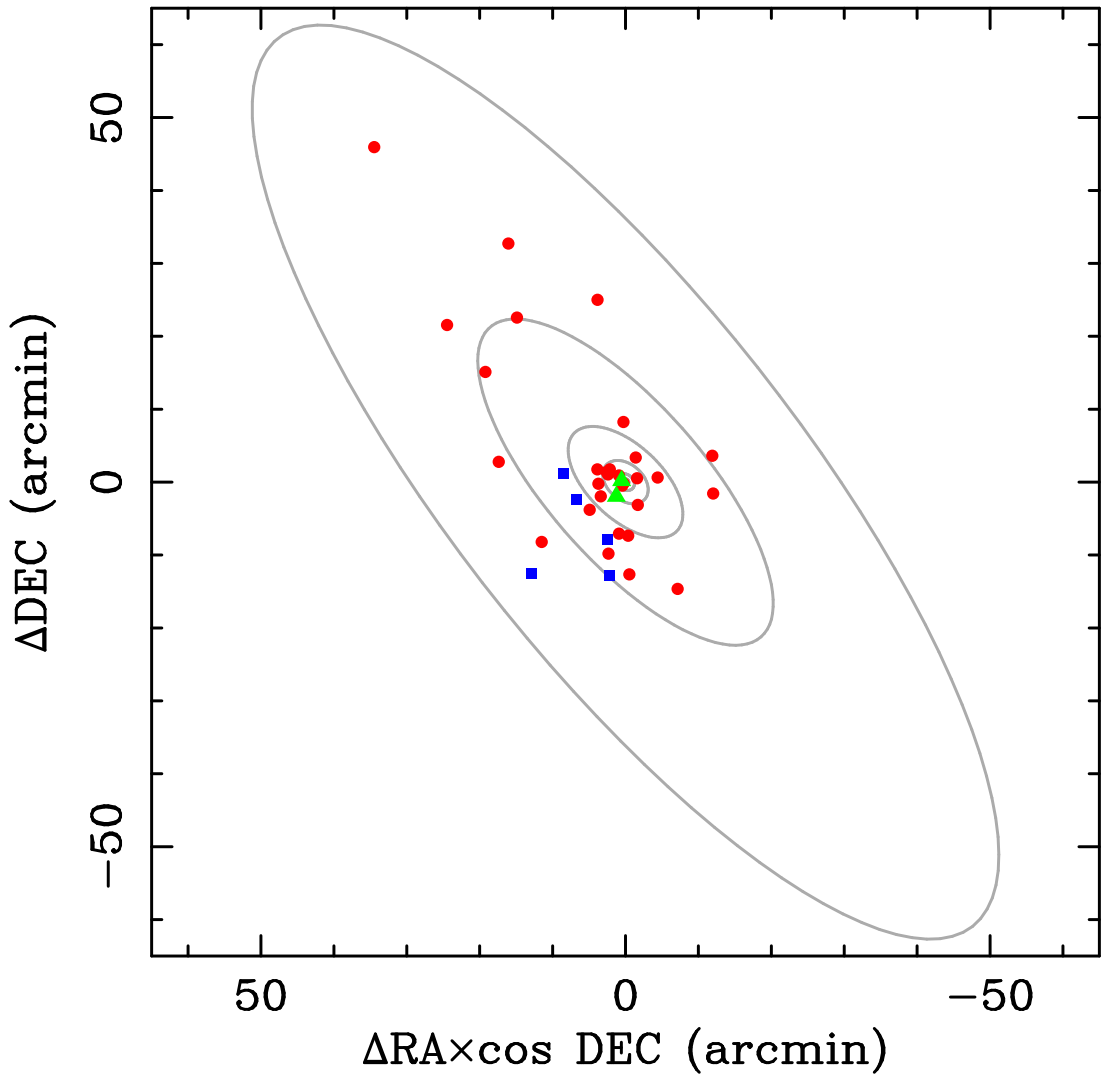

Figure 3.1: The spatial distribution of the 38 M31 novae with known spectroscopic classes examined in this study. The Fe II novae are indicated by filled red circles, the He/N novae by filled blue squares and the Fe IIb types by filled green triangles (see Shafter et al., 2011f, for a summary of each pre-2010 nova's spectroscopic type determination). The grey ellipses represent isophotes from the surface photometry of Kent (1987). ©AAS. Reproduced with permission.

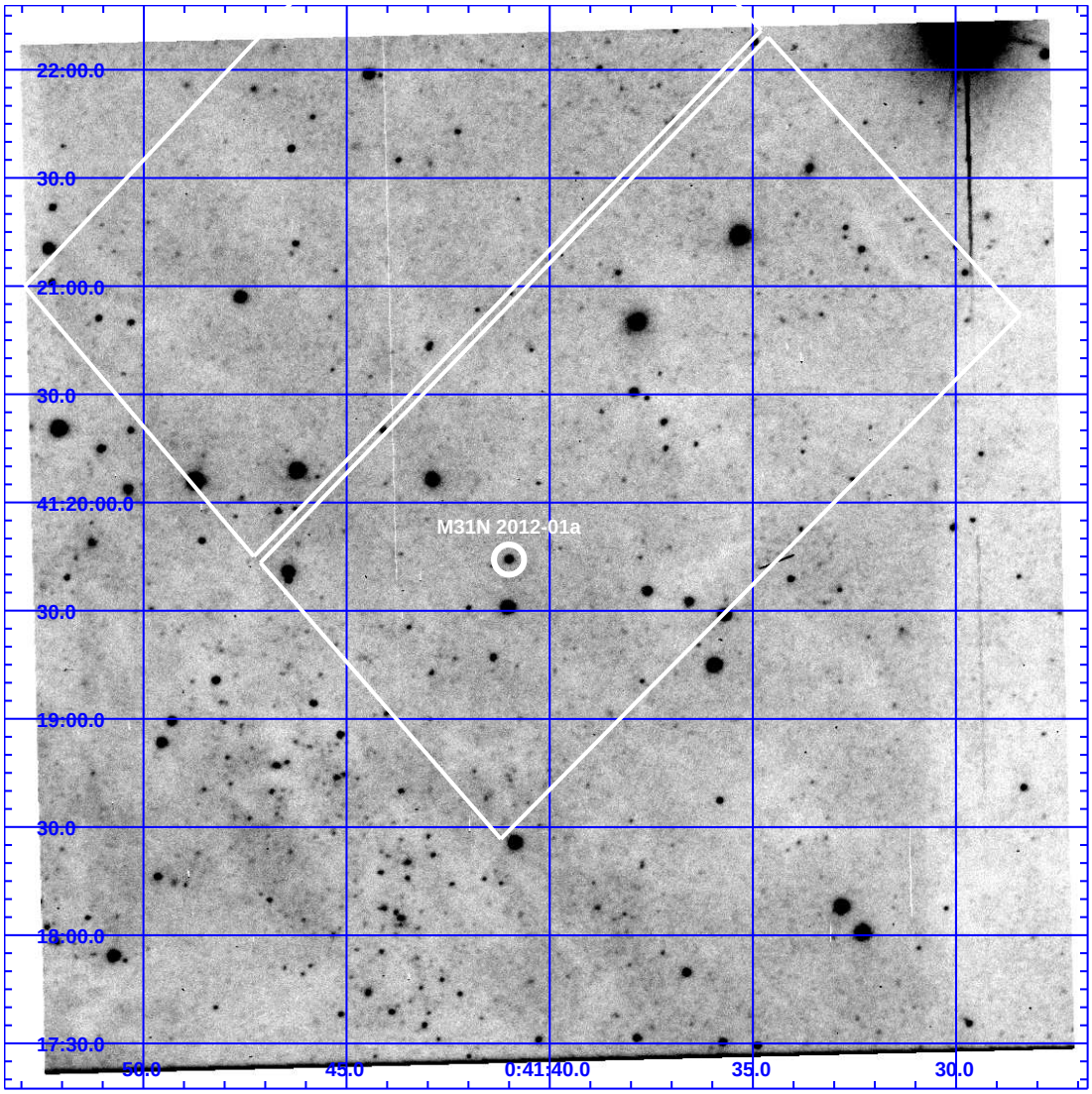

Figure 3.2: M31N 2012-01a during outburst in a V-band LT image taken on 2012 January 10.83, with the dimensions of the coincident ACS/WFC F555W *HST* image overlaid as white boxes. M31N 2012-01a is shown with the white circle (the nova being the visible source at the centre of the circle). ©AAS. Reproduced with permission.

3.3.3 Astrometry

The best images were combined for a given nova, taking into account the seeing and the brightness of the nova itself, in order to produce the most precise position possible for the system. Typically, around $25 - 30$ stars were selected and matched up with the same stars in the other images using the starfind algorithm in IRAF, which finds stars by searching an image for local density maxima with peak magnitudes greater than a given threshold above the local background. After the stars were matched in the chosen images using the xyxymatch algorithm, the necessary translation, rotation, magnification and distortion needed for the images to align were then calculated and executed using the geomap and geotran algorithms in IRAF. The newly aligned images were combined using the imcombine algorithm, with the combined image being created from the average pixel values of the individual frames. Finally the position of the nova within the combined image was measured using the imcentroid algorithm.

The positions (which were first found manually, and then the accurate positions were calculated using imcentroid) of about $15 - 25$ stars in the combined image were then recorded, as were their respective positions in the chosen *HST* image. The astrometric analysis used the drizzled (drz) *HST* images. The drizzling process is an algorithm used on *HST* data to correct for geometric distortion and cosmic rays by combining pre-processed images. The two lists of coordinates were matched and the necessary transformation to convert between the two data sets was calculated using the IRAF routines described above. The position of the nova in the LT data was then transformed into a position in the *HST* image using the geoxytran algorithm.

Using the position determined from the LT image, the coordinates of each nova were calculated using 2MASS (Cutri et al., 2003; Skrutskie et al., 2006). This was done using the same method as described above, but by using the positions of the stars in 2MASS, rather than the *HST* images. The resulting positions are more accurate than those previously published in the majority of cases and are shown in Table 3.2.

Table 3.2: A summary of the outburst images used to define the position of each nova, including the date the images were taken and the filter they were taken through. The coordinates of each nova were calculated from the LT images using positions from 2MASS (Cutri et al., 2003; Skrutskie et al., 2006).

Nova	Telescope	Date (UT)	Filter	Right Ascension	Declination
M31N 2006-09c	LT	2006 September 19.0	V	$0^{\rm h}42^{\rm m}42^{\rm s}.38 \pm 0^{\rm s}.02$	$+41°08'45''.4 \pm 0''.2$
M31N 2006-11a	LT	2007 February 9.9	i'	$0^{\rm h}42^{\rm m}56^{\rm s}.800 \pm 0^{\rm s}.009$	$+41°06'18''.3 \pm 0''.1$
M31N 2007-02b	LT	2007 February 14.9	i'	$0^{\rm h}41^{\rm m}40^{\rm s}.307 \pm 0^{\rm s}.009$	$+41°14'33''.4 \pm 0''.1$
M31N 2007-10a	LT	2007 October 10.9	V	$0^{\rm h}42^{\rm m}55^{\rm s}.947 \pm 0^{\rm s}.007$	$+41°03'21''.9 \pm 0''.1$
M31N 2007-10b	LT	2007 October 16.0	i'	$0^{\rm h}43^{\rm m}29^{\rm s}.47 \pm 0^{\rm s}.01$	$+41°17'13''.9 \pm 0''.1$
M31N 2007-11b	LT	2007 November 16.9	i'	$0^{\rm h}43^{\rm m}52^{\rm s}.99 \pm 0^{\rm s}.01$	$+41°03'35''.9 \pm 0''.1$
M31N 2007-11c	LT	2007 November 17.0	i'	$0^{\rm h}43^{\rm m}04^{\rm s}.16 \pm 0^{\rm s}.01$	$+41°15'53''.93 \pm 0''.09$
M31N 2007-11d	LT	2007 November 28.0	i'	$0^{\rm h}44^{\rm m}54^{\rm s}.59 \pm 0^{\rm s}.01$	$+41°37'39''.8 \pm 0''.1$
M31N 2007-11e	LT	2007 December 5.1	i'	$0^{\rm h}45^{\rm m}47^{\rm s}.76 \pm 0^{\rm s}.01$	$+42°02'03''.7 \pm 0''.1$
M31N 2007-12a	LT	2007 Dec 16.9, 31.8, 2008 Jan 8.9	i'	$0^{\rm h}44^{\rm m}03^{\rm s}.52 \pm 0^{\rm s}.01$	$+41°38'40''.9 \pm 0''.1$
M31N 2007-12b	LT	2007 December 14.9	i'	$0^{\rm h}43^{\rm m}19^{\rm s}.96 \pm 0^{\rm s}.02$	$+41°13'46''.3 \pm 0''.1$
M31N 2008-10b	LT	2008 October 21.0	B	$0^{\rm h}43^{\rm m}02^{\rm s}.41 \pm 0^{\rm s}.02$	$+41°14'09''.9 \pm 0''.2$
M31N 2008-12b	LT	2009 January 15.0	i'	$0^{\rm h}43^{\rm m}04^{\rm s}.85 \pm 0^{\rm s}.01$	$+41°17'51''.6 \pm 0''.2$
M31N 2009-08a	LT	2009 August 27.1, September 4.1	i'	$0^{\rm h}42^{\rm m}58^{\rm s}.105 \pm 0^{\rm s}.007$	$+41°17'29''.56 \pm 0''.06$
M31N 2009-08b	LT	2009 August 18.0	i'	$0^{\rm h}44^{\rm m}09^{\rm s}.89 \pm 0^{\rm s}.02$	$+41°48'50''.7 \pm 0''.1$

Continued on next page

Table 3.2 – continued from previous page

Nova	Telescope	Date (UT)	Filter	Right Ascension	Declination
M31N 2009-08d	LT	2009 August 20.1	B	$0^{\rm h}42^{\rm m}46^{\rm s}.74 \pm 0^{\rm s}.02$	$+41°15'37''.4 \pm 0''.1$
M31N 2009-10b	LT	2009 October 15.0	B	$0^{\rm h}42^{\rm m}20^{\rm s}.83 \pm 0^{\rm s}.02$	$+41°16'44''.3 \pm 0''.1$
M31N 2009-10c	LT	2009 October 15.0	B	$0^{\rm h}42^{\rm m}45^{\rm s}.72 \pm 0^{\rm s}.02$	$+41°15'56''.99 \pm 0''.09$
M31N 2009-11a	LT	2009 November 13.9	V	$0^{\rm h}43^{\rm m}04^{\rm s}.789 \pm 0^{\rm s}.009$	$+41°41'07''.79 \pm 0''.08$
M31N 2009-11b	LT	2009 December 6.8	V	$0^{\rm h}42^{\rm m}39^{\rm s}.596 \pm 0^{\rm s}.009$	$+41°09'02''.9 \pm 0''.1$
M31N 2009-11c	LT	2009 November 12.9	V	$0^{\rm h}43^{\rm m}10^{\rm s}.46 \pm 0^{\rm s}.01$	$+41°12'18''.5 \pm 0''.1$
M31N 2009-11d	LT	2009 November 24.0	V	$0^{\rm h}44^{\rm m}16^{\rm s}.866 \pm 0^{\rm s}.009$	$+41°18'53''.6 \pm 0''.2$
M31N 2009-11e	LT	2009 November 27.0	V	$0^{\rm h}42^{\rm m}35^{\rm s}.33 \pm 0^{\rm s}.01$	$+41°12'59''.4 \pm 0''.2$
M31N 2010-01a	LT	2010 January 15.9	B	$0^{\rm h}42^{\rm m}56^{\rm s}.70 \pm 0^{\rm s}.02$	$+41°17'20''.2 \pm 0''.1$
M31N 2010-05a	LT	2010 June 17.2	B	$0^{\rm h}42^{\rm m}35^{\rm s}.899 \pm 0^{\rm s}.008$	$+41°16'38''.24 \pm 0''.04$
M31N 2010-09b	LT	2010 October 5.1	B	$0^{\rm h}43^{\rm m}45^{\rm s}.545 \pm 0^{\rm s}.008$	$+41°07'54''.5 \pm 0''.1$
M31N 2010-10a	LT	2010 October 10.1	V	$0^{\rm h}42^{\rm m}45^{\rm s}.82 \pm 0^{\rm s}.03$	$+41°24'22''.0 \pm 0''.1$
M31N 2010-10b	LT	2010 October 11.1	V	$0^{\rm h}42^{\rm m}41^{\rm s}.55 \pm 0^{\rm s}.02$	$+41°03'27''.7 \pm 0''.1$
M31N 2010-10c	LT	2010 October 22.1	B	$0^{\rm h}44^{\rm m}26^{\rm s}.575 \pm 0^{\rm s}.008$	$+41°31'13''.6 \pm 0''.1$
M31N 2010-10d	LT	2010 October 30.0	B	$0^{\rm h}42^{\rm m}36^{\rm s}.914 \pm 0^{\rm s}.008$	$+41°19'28''.9 \pm 0''.1$
M31N 2010-10e	LT	2010 November 7.0	V	$0^{\rm h}42^{\rm m}57^{\rm s}.75 \pm 0^{\rm s}.01$	$+41°08'12''.3 \pm 0''.1$
M31N 2011-10a	LT	2011 October 26.1	B	$0^{\rm h}42^{\rm m}57^{\rm s}.13 \pm 0^{\rm s}.01$	$+41°17'10''.9 \pm 0''.1$
M31N 2011-10d	LT	2011 October 26.1	B	$0^{\rm h}42^{\rm m}55^{\rm s}.74 \pm 0^{\rm s}.01$	$+41°17'52''.3 \pm 0''.1$
M31N 2011-12a	LT	2011 December 26.8	V	$0^{\rm h}42^{\rm m}06^{\rm s}.277 \pm 0^{\rm s}.009$	$+41°01'28''.7 \pm 0''.1$
M31N 2012-01a	LT	2012 January 10.8	V	$0^{\rm h}41^{\rm m}41^{\rm s}.01 \pm 0^{\rm s}.01$	$+41°19'44''.3 \pm 0''.1$

Continued on next page

Table 3.2 – continued from previous page

Nova	Telescope	Date (UT)	Filter	Right Ascension	Declination
M31N 2012-09a	LT	2012 September 10.0	r'	$0^{\mathrm{h}}42^{\mathrm{m}}47^{\mathrm{s}}.16 \pm 0^{\mathrm{s}}.01$	$+41^{\circ}16'19''.63 \pm 0''.07$
M31N 2012-09b	LT	2012 September 18.2	r'	$0^{\mathrm{h}}42^{\mathrm{m}}50^{\mathrm{s}}.98 \pm 0^{\mathrm{s}}.02$	$+41^{\circ}14'09''.7 \pm 0''.2$
M31N 2012-12a	LT	2012 December 20.9	r'	$0^{\mathrm{h}}42^{\mathrm{m}}49^{\mathrm{s}}.13 \pm 0^{\mathrm{s}}.02$	$+41^{\circ}17'02''.5 \pm 0''.1$

3.3.4 Photometry

Crowded field photometry was carried out on the *HST* data available for each nova using the specific ACS/WFC modules for the DOLPHOT photometry software[4] and the HSTphot software (Dolphin, 2000) for the WFPC2 data. These software packages create catalogues of all objects (above a certain detection threshold; 3σ above the local background in this case) simultaneously across all available filters for each data-set. For the purpose of this work HSTphot and DOLPHOT were essentially run as "black-boxes" following the standard procedure and parameters given in the manuals/cookbooks. Often multiple *HST* observations are taken during a given observation group and when this was the case, photometric data for a given filter was combined using a weighted mean, with the associated errors propagated with the weights in mind.

The results of this photometry were first used to determine the position of all objects in the vicinity of the nova eruption, and from this the position of the most likely (statistically closest) matching object is drawn. The resolved sources (in the *HST* data) from the region around a given nova were also used, in conjuction with a Monte Carlo technique, to test the significance of any detected progenitor candidates. In this Monte Carlo technique, positions were randomly generated (in a $5'' \times 5''$ square centred on the position of the nova) and the distance to the nearest resolved source (in the actual *HST* data of that particular region) was measured for each randomly seeded point. Once the measurements for all these seeded points were combined, it gave us the probability of a resolved source being within a certain distance from the position of the nova. This probability was used to examine how significant the detection of any progenitor candidates, which appear to be coincident with the nova, may be. There is also an analytical solution to this, which is discussed in Section 5.8.

The HSTphot/DOLPHOT software also computes photometry for each object in each catalogue. This photometry is presented in the native *HST* photometric/filter system, and where photometry in at least two filters is available for a particular object, these data were converted from the native *HST* system to the *UBVRI*$_C$ system using the

[4] `http://americano.dolphinsim.com/dolphot`

relations from Dolphin (2009) and Sirianni et al. (2005) for the WFPC2 and ACS/WFC data respectively. Additionally the extinction internal to M31 that the novae may be subject to was calculated for each individual system based on its apparent position within the galaxy. The extinction estimates were based on the extinction map of M31 published by Darnley (2005). This extinction map gives the r'-band extinction for an object positioned at the far side of M31. The extinction law from Cardelli et al. (1989) was then used to estimate the equivalent *B*, *V*, *R* and I_C extinction. It was assumed that the actual internal extinction is between this value and zero, allowing the effects of internal extinction to be incorporated into the magnitude and colour measurements of the quiescent systems. The effects of extinction towards M31 are not taken into account for the numbers presented in the text, but are applied to catalogue Galactic stars when analysing the progenitor candidates in the context of colour−magnitude diagrams, such as in Figure 3.24 (i.e. the magnitudes of Galactic stars are shifted to the distance of M31, with the appropriate extinction towards M31 of $E_{B-V} = 0.1$ mag; Stark et al., 1992; applied).

Figure 3.3 shows the colour−magnitude diagram for an ACS/WFC *HST* field positioned along the semi-major axis of M31, approximately 1.3 degrees out from the centre. The photometry of each source in the field was calculated using DOLPHOT. This is compared to *Hipparcos* data (Perryman & ESA, 1997) shifted to the distance of M31. Although, the sources in the M31 field do not follow the expected sequence as tightly as the *Hipparcos* data, it can clearly be seen that the red-giant branch is fully resolved. Sources were included in this plot if they had ≤ 0.5 magnitude error on their colour, which introduces some scatter. Additional scatter is introduced by the extinction internal to M31, which will vary between individual sources, and although the field is dominated by M31 stars, there may also be some contamination by foreground Galactic objects. It could also be possible that DOLPHOT may incorrectly associate some fainter objects in one filter with faint objects in the other filter if they have a small apparent separation.

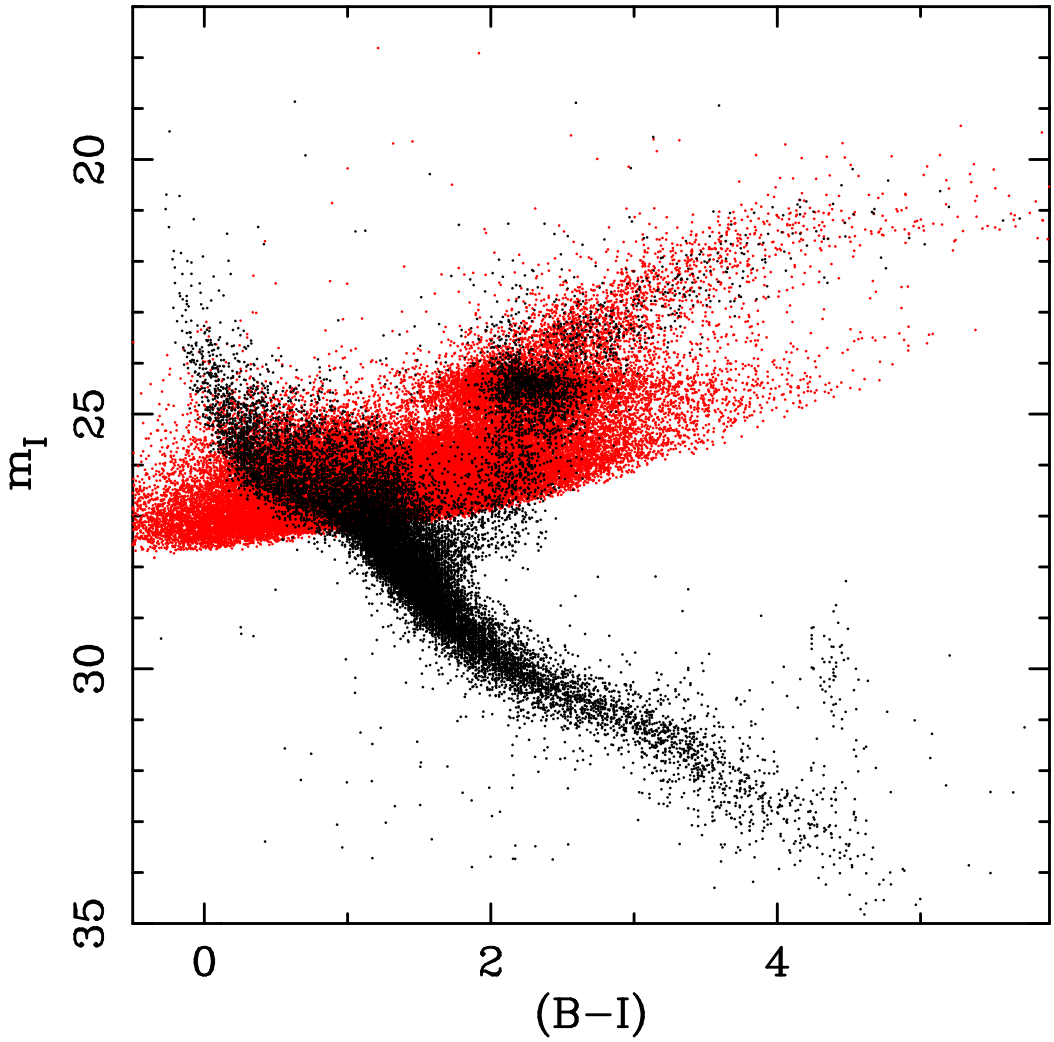

Figure 3.3: The regions of the *I* vs. $(B - I)$ colour-magnitude diagram of M31 resolved by ACS/WFC on *HST*. The M31 field used for this plot is ~ 1.3 degrees along the semi-major axis away from the centre of M31, with data having been taken using F475W and F814W filters. The red points represent the sources in the *HST* data, with the overlaid black points representing the *Hipparcos* data (Perryman & ESA, 1997) shifted to the distance of M31, assuming $(m{-}M)_0 = 24.43$ (Freedman & Madore, 1990) and extinction of $E_{B-V} = 0.1$ mag towards M31 (Stark et al., 1992).

3.4 Progenitor Systems

The positional information for the most likely matching objects for each nova, along with the probability of coincidence are summarised in Table 3.3. We present below the results of each individual nova in the catalog.

Table 3.3: The distance from the calculated nova position in arcsecs and σ (to nearest 0.05σ; the σ value is derived from the error in the positional transformation) for each progenitor candidate, along with the probability of the detection being a chance alignment. The table shows all candidates within 3σ of the calculated position or if no source is within 3σ we show the closest source. The two progenitor candidates at the bottom of the table were found using *HST* images taken during outburst. In both of these systems, the progenitor candidate found is the same source identified using LT data.

Nova	Distance from nova position		Offset	Coincidence	Limiting
	Pixels	Arcsec	(σ)	probability	magnitude (filter)
2006-09c	1.688	$0.168''$	3.90	0.285	23.8 (F814W)
2006-11a	2.825	$0.142''$	3.95	0.580	26.1 (F814W)
2007-02b	0.325	$0.016''$	0.30	0.011	26.6 (F814W)
2007-10a	0.517	$0.026''$	1.00	0.027	26.3 (F814W)
2007-10b	3.842	$0.193''$	1.85	0.811	25.4 (F814W)
2007-11b	0.319	$0.032''$	1.75	0.0005	22.3 (F814W)
2007-11c	2.317	$0.117''$	2.80	0.422	24.7 (F814W)
2007-11d	0.181	$0.009''$	0.25	0.003	26.3 (F814W)
...	2.018	$0.102''$	1.75	0.344	...
2007-11e	0.786	$0.040''$	1.40	0.042	26.4 (F814W)
2007-12a	0.446	$0.022''$	1.30	0.017	26.1 (F814W)
2007-12b	0.684	$0.034''$	0.95	0.043	25.5 (F814W)
2008-10b	1.815	$0.091''$	2.95	0.309	26.4 (F435W)
2008-12b	1.431	$0.072''$	1.75	0.180	26.0 (F475W)[1]
2009-08a	1.118	$0.056''$	1.40	0.121	26.0 (F435W)
2009-08b	2.830	$0.142''$	3.25	0.571	26.6 (F814W)
2009-08d	3.236	$0.163''$	2.95	0.627	25.9 (F435W)
2009-10b	1.803	$0.091''$	4.30	0.291	26.7 (F435W)
2009-10c	2.128	$0.107''$	2.40	0.287	25.9 (F435W)

Continued on next page

Table 3.3 – continued from previous page

Nova	Distance from nova position		Significance	Coincidence	Limiting
	Pixels	Arcsec	(σ)	probability	magnitude (filter)
2009-11a	3.999	$0.201''$	3.45	0.683	26.5 (F814W)
2009-11b	1.971	$0.197''$	4.15	0.386	23.8 (F814W)
2009-11c	2.975	$0.150''$	3.35	0.550	25.8 (F814W)
2009-11d	0.505	$0.025''$	0.60	0.022	26.4 (F814W)
2009-11e	1.104	$0.110''$	0.80	0.099	22.8 (F814W)
2010-01a	1.058	$0.053''$	1.45	0.094	26.1 (F435W)
2010-05a	1.939	$0.098''$	2.20	0.369	25.8 (F435W)
2010-09b	0.579	$0.029''$	0.55	0.026	26.3 (F814W)
...	2.264	$0.114''$	2.05	0.363	...
2010-10a	1.181	$0.059''$	1.20	0.112	26.7 (F814W)
2010-10b	1.968	$0.099''$	3.60	0.334	26.1 (F814W)
2010-10c	1.083	$0.055''$	1.05	0.124	27.1 (F606W)
...	1.988	$0.100''$	1.90	0.385	...
...	2.084	$0.105''$	2.00	0.416	...
...	3.405	$0.171''$	3.00	0.786	...
2010-10d	2.992	$0.151''$	4.25	0.656	26.3 (F435W)
2010-10e	1.216	$0.061''$	0.80	0.156	25.9 (F814W)
...	1.859	$0.094''$	1.45	0.344	...
...	4.310	$0.217''$	2.75	0.923	...
2011-10a	2.540	$0.128''$	4.80	0.468	26.1 (F475W)[1]
2011-10d	1.400	$0.070''$	3.25	0.164	26.1 (F475W)[1]
2011-12a	1.129	$0.113''$	1.15	0.036	24.2 (F814W)
2012-01a	1.712	$0.086''$	2.50	0.220	26.2 (F814W)
2012-09a	2.152	$0.108''$	3.65	0.328	25.8 (F475W)[1]
2012-09b	3.659	$0.184''$	10.55	0.784	24.6 (F814W)
2012-12a	1.532	$0.077''$	2.00	0.199	25.6 (F475W)[1]
2009-08a	0.516	$0.026''$	2.85	0.024	26.0 (F435W)
2010-01a	0.641	$0.032''$	2.65	0.038	26.1 (F435W)

[1]Due to problems with the F814W photometry, short exposure images had to be used, leading to a relatively bright limiting magnitude. For F814W limiting magnitudes see text for each nova.

3.4.1 M31N 2006-09c

Nova M31N 2006-09c was discovered independently by K. Itagaki[5] and R. Quimby on 2006 September 18 (Quimby, 2006). A spectrum showed the transient to be an Fe II type nova (Shafter et al., 2006, 2011b) and it had an R-band t_2 of 23.1 ± 1.6 days (Shafter et al., 2011f). The LT outburst detection images used to determinte the position of the system in the archival data were taken using a V-band filter on 2006 September 19.0 UT, with the position of the nova calculated to be $0^{\rm h}42^{\rm m}42^{\rm s}.38 \pm 0^{\rm s}.02$, $+41^\circ08'45''.4 \pm 0''.2$. The *HST* images used were taken using WFPC2 with F814W and F555W filters on 2004 August 22. There is no resolvable source within 3σ of the calculated position, with the nearest object being 1.688 WFPC2 pixels, $0''.169$ or 3.90σ away from the defined position. The local population density suggests there is a 28.5% probability of an object alignment this close occurring by chance. Note that due to the data being taken with WFPC2, which cannot resolve sources as faint as ACS/WFC, there may be sources that would have been visible in ACS/WFC closer to the position of the nova than $0.169''$. Therefore the 28.5% coincidence probability is valid for objects with a F814W magnitude brighter than 23.8. From the overall distribution of stars in the M31 field in ACS/WFC data, it would be expected that a source would be at least as close as $0''.169$ to a random point in a typical ACS/WFC image about 69% of the time. The location of the quiescent system is shown in Figure 3.4.

3.4.2 M31N 2006-11a

Nova M31N 2006-11a was discovered by K. Itagaki on frames taken on 2006 November 21.657 UT[6]. Shafter et al. (2011b) classify it as an Fe II type nova and Shafter et al. (2011f) derive an *R*-band t_2 of 28.7 ± 2.6. LT data were taken using an i'-band filter on 2006 February 9.9 UT and the position of the novae was calculated to be $0^{\rm h}42^{\rm m}56^{\rm s}.800 \pm 0^{\rm s}.009$, $+41^\circ06'18''.3 \pm 0''.1$. The region where the quiescent nova M31N 2006-11a lies is covered by *HST* images that were taken with ACS/WFC using

[5] `http://www.cbat.eps.harvard.edu/CBAT_M31.html#2006-09c`
[6] `http://www.cbat.eps.harvard.edu/CBAT_M31.html#2006-11a`

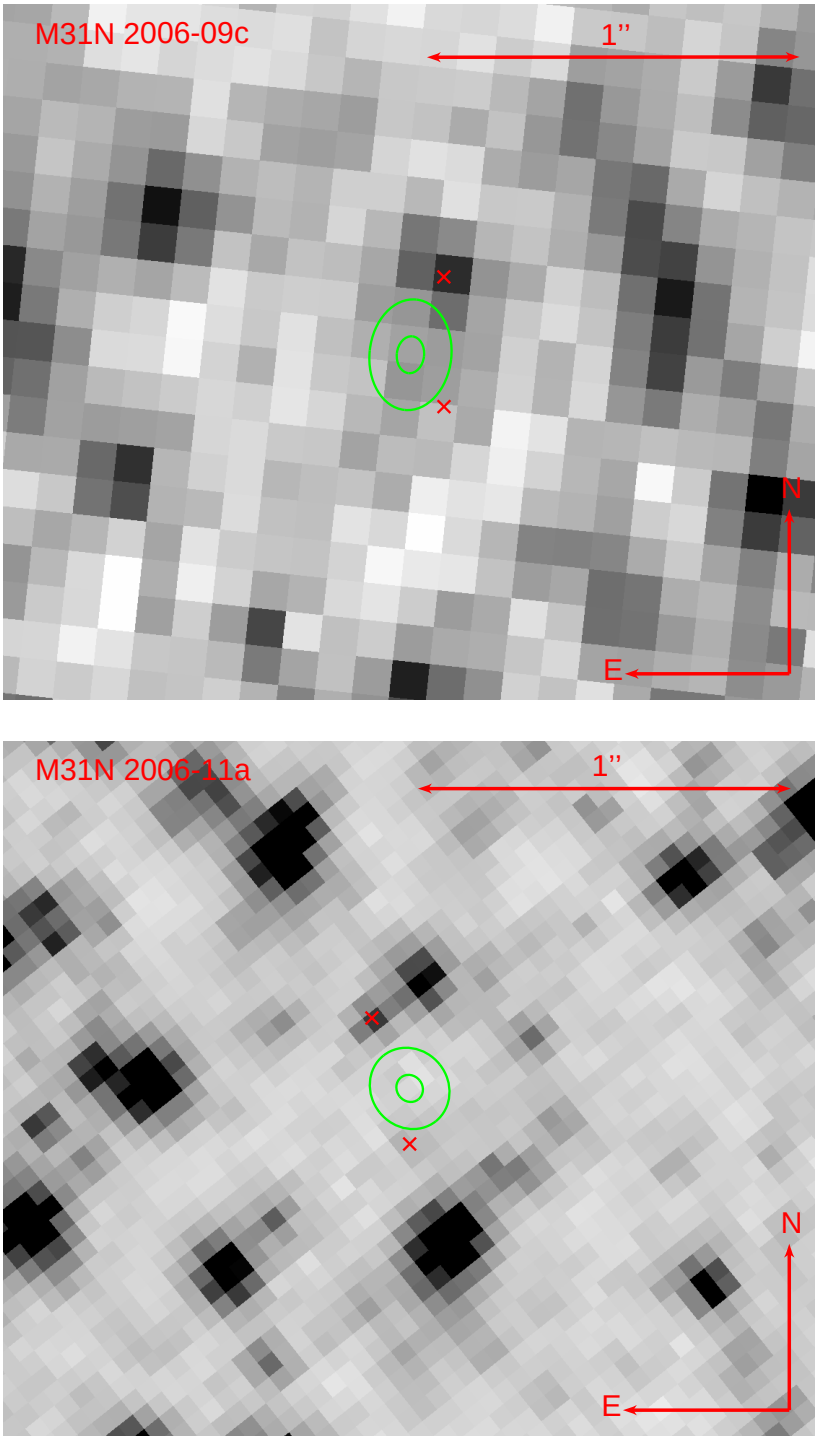

Figure 3.4: *HST* images of the $\sim 2.2'' \times 1.9''$ region surrounding each nova. Top: WFPC2 F555W image, M31N 2006-09c progenitor position determined from LT V-band data. Bottom: ACS/WFC F814W image, M31N 2006-11a progenitor position determined from LT i'-band data. In each case, the inner green ellipse indicates the 1σ radius uncertainty of the outburst position, the outer ellipse the 3σ region. The red $\times$ indicates the position of any candidate progenitor systems.

F814W and F555W filters on 2004 August 17. No resolvable source is found within 3σ of the calculated position, with the closest resolvable source being 2.825 ACS/WFC pixels, $0.141''$ or 3.95σ away from the defined position. The local population density suggests that the coincidence probability at this separation is 58.0%. The limiting F814W magnitude is 26.1. The region where this system lies is shown in Figure 3.4.

3.4.3 M31N 2007-02b

Nova M31N 2007-02b was discovered on 2007 February 3 by K. Hornoch[7] and had an *R*-band t_2 of 34.1 ± 3.6 (Shafter et al., 2011f). The first published spectrum, taken on 2007 February 13 by Pietsch et al. (2007a) indicated it may be an Fe IIb nova, although in their spectroscopic and photometric survey of M31 novae, (Shafter et al., 2011f) used an earlier spectrum and suggested it was most likely an Fe II outburst. The nova also became a SSS, still visible two years after the initial outburst (Henze et al., 2011). On 2007 February 14.9 UT, i'-band LT images were obtained, which gave the position of the nova to be $0^{\rm h}41^{\rm m}40^{\rm s}.307 \pm 0^{\rm s}.009$, $+41°14'33''.4 \pm 0''.1$. The archival *HST* images of this position were taken with ACS/WFC using an F814W filter on 2004 July 4 and an F606W filter on 2004 August 2. There is a resolvable source within 1σ of the calculated position and no other resolvable source within 3σ. The source is 0.325 ACS/WFC pixels, $0.016''$ or 0.3σ away from the defined position. The local population density, which is resolved down to an F814W magnitude of 26.6, suggests there is only a 1.1% chance of coincidence at such a separation. The candidate had an F814W magnitude of 24.82 ± 0.03 on 2004 July 4 and an F606W magnitude of 25.95 ± 0.05 on 2004 August 2. Assuming the source remained at a constant brightness between the two dates, this gives a *V*-band magnitude of 26.39 ± 0.06, *I*-band magnitude of 24.83 ± 0.04 and $(V - I)$ colour of 1.55 ± 0.07. We can see from Darnley (2005) that a nova at the apparent position of M31N 2007-02b would be subject to r'-band extinction of $A_{r'} = 0.69$ if it were at the far side of the galaxy. Using the extinction law from Cardelli et al. (1989) this equates to maximum *I*-band extinction of $A_I = 0.46$ and *V*-band extinction of $A_V = 0.80$. If we take this into account we derive a *V*-

[7] `http://www.cbat.eps.harvard.edu/CBAT_M31.html#2007-02b`

band magnitude of 26.0 ± 0.4, *I*-band magnitude of 24.6 ± 0.2 and $(V - I)$ colour of 1.4 ± 0.2. This system is shown in Figure 3.5. M31N 2007-02b was also observed in outburst with WFPC2 on 2007 September 13, which is described in Section 4.3.1. As the nova is relatively faint at this time any attempt to calculate the position of the system in the quiescent *HST* image from the outburst *HST* image is dominated by the error on the position in the WFPC2 outburst image.

3.4.4 M31N 2007-10a

Nova M31N 2007-10a was a He/Nn nova (Gal-Yam & Quimby, 2007; Shafter et al., 2011f) with a *V*-band t_2 of 7.9 ± 0.4 (Shafter et al., 2011f) that was discovered on 2007 October 5[8]. LT images were taken on 2007 October 10.9 UT, in *V*-band, with the position of the nova calculated to be $0^{\rm h}42^{\rm m}55^{\rm s}.947 \pm 0^{\rm s}.007$, $+41^\circ03'21''.9 \pm 0''.1$. The region where M31N 2007-10a lies is covered by *HST* images that were taken with ACS/WFC using an F625W filter on 2003 August 5. There is a resolvable source near 1σ of the calculated position and no other resolvable source within 3σ. The source is 0.517 ACS/WFC pixels, $0.026''$ or 1.00σ away from the defined position, with the local population density suggesting that the coincidence probability at this separation is 2.7%. The source had an F625W magnitude of 22.397 ± 0.008 at this time. The *HST* images were only taken in one filter, so it was not possible to calculate the colour of the source, although it can be estimated to have an *R*-band magnitude of $\sim$22.3 with internal extinction in M31 taking it to $\sim$22.0. The location of this system is shown in Figure 3.5.

3.4.5 M31N 2007-10b

Nova M31N 2007-10b was discovered on 2007 October 13.255 UT by Burwitz et al. (2007). The outburst faded rapidly, with an *R*-band t_2 of 3.1 ± 0.4 (Shafter et al., 2011f) and its spectrum classified it as an He/Nn nova (Rau et al., 2007; Shafter et al., 2011f).

[8] `http://www.cbat.eps.harvard.edu/CBAT_M31.html#2007-10a`

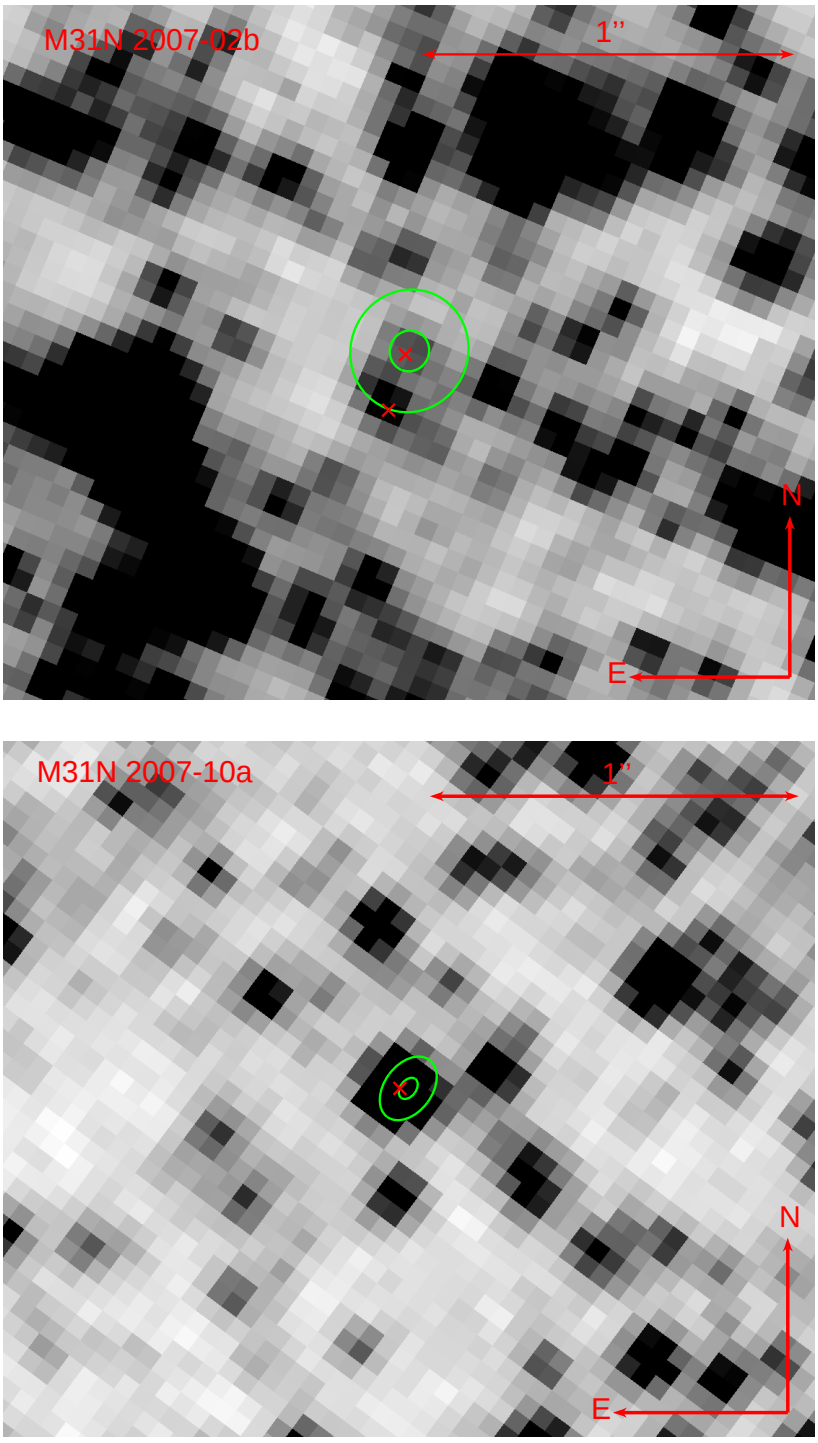

Figure 3.5: As Figure 3.4. Top: ACS/WFC F814W image, M31N 2007-02b progenitor position determined from LT i'-band data. Bottom: ACS/WFC F625W image, M31N 2007-10a position determined from LT V-band data. ©AAS. Reproduced with permission.

On 2007 October 16.0 UT, i'-band LT images were obtained, giving the position as $0^{\rm h}43^{\rm m}29^{\rm s}.47 \pm 0^{\rm s}.01$, $+41°17'13''.9 \pm 0''.1$. The location of the quiescent M31N 2007-10b was observed by *HST* with ACS/WFC using F814W and F475W filters on 2010 July 22. There are no resolvable sources within 3σ of the calculated position, with the nearest resolvable source being 3.842 ACS/WFC pixels, $0.193''$ or 4.40σ away from the defined position. The local population density suggests that the coincidence probability at this separation is 81.1%. There is also a source closer to the position of the nova resolvable in the F475W image that is not detected in the F814W image, which has a limiting magnitude of 25.4. The source is 1.529 ACS/WFC pixels, $0.076''$ or 1.85σ away from the defined position. At the separation of $0.076''$, the coincidence probability is 21.2%. The location of this quiescent system is shown in Figure 3.6.

3.4.6 M31N 2007-11b

Nova M31N 2007-11b was discovered on 2007 November 9[9] and later classified as a He/Nn nova (Rau, 2007; Shafter et al., 2011f) with an i'-band t_2 of 74.4 ± 16.7 (Shafter et al., 2011f). LT data were taken on 2007 November 16.9 UT with an i'-band filter, giving the nova position as $0^{\rm h}43^{\rm m}52^{\rm s}.99 \pm 0^{\rm s}.01$, $+41°03'35''.9 \pm 0''.1$. Although the area of M31 where M31N 2007-11b lies has not been observed with ACS/WFC, *HST* images were taken with WFPC2 using F814W and F555W filters on 2005 February 18. There is a resolvable source within 2σ of the calculated *HST* position and no other resolvable source within 3σ. The source is 0.319 WFPC2 pixels, $0.032''$ or 1.75σ away from the defined position, with the local population density suggesting a coincidence probability at this separation of only 0.05%. However these images have a F814W limiting magnitude as bright as 22.3. Therefore the 0.05% coincidence probability is valid for objects with a F814W magnitude < 22.3. The candidate had an F555W magnitude of 22.6 ± 0.1 and F814W magnitude of 20.44 ± 0.06 at this time. This gives an *I*-band magnitude of 20.30 ± 0.06 and *V*-band magnitude of 22.6 ± 0.1, with $(V-I)$ colour of 2.3 ± 0.2. Darnley (2005) showed that a nova at the apparent position of M31N 2007-11b would be subject to r'-band extinction of approximately $A_{r'} = 0.52$

[9] `http://www.cbat.eps.harvard.edu/CBAT_M31.html#2007-11b`

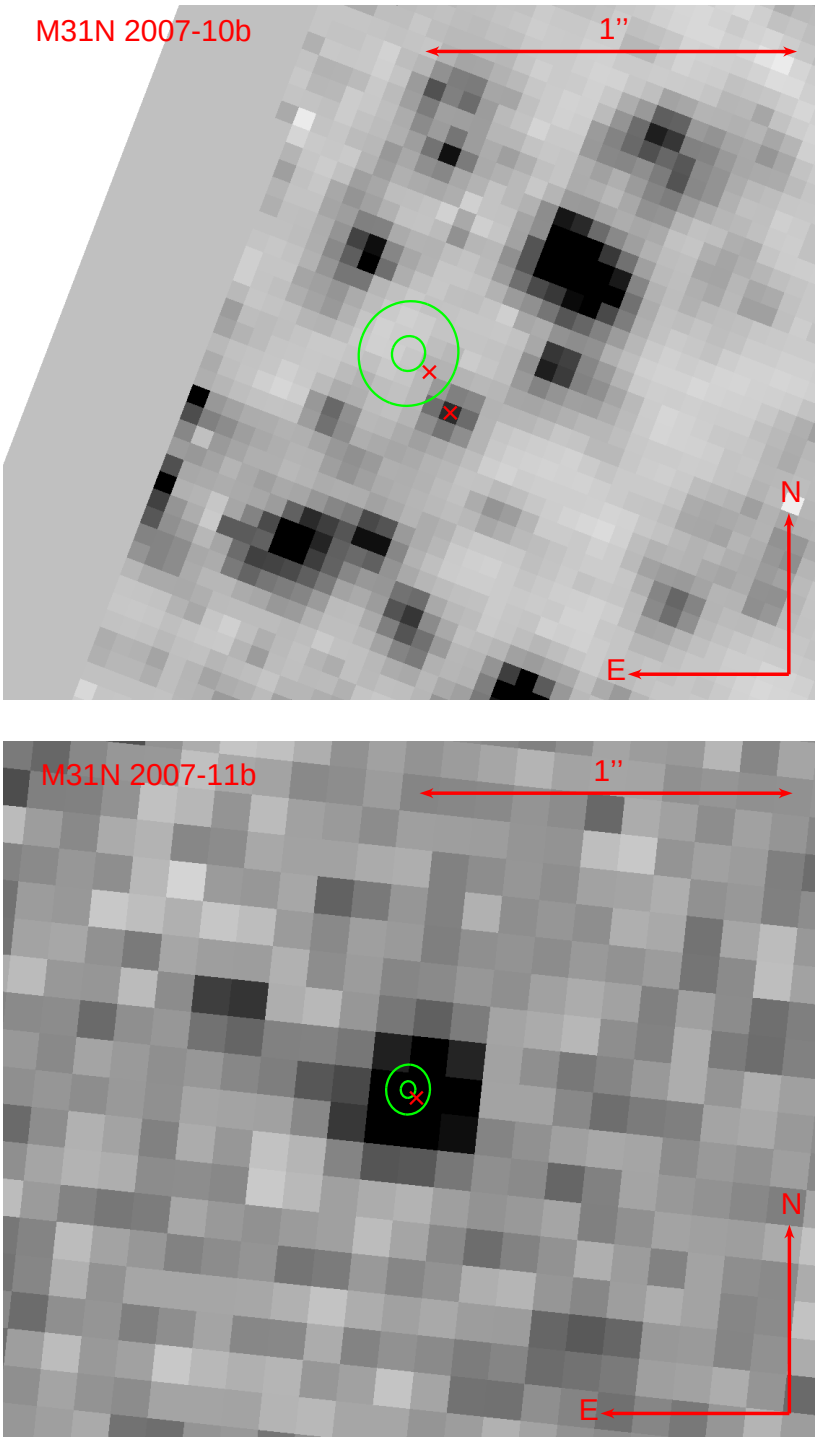

Figure 3.6: As Figure 3.4. Top: ACS/WFC F814W image, M31N 2007-10b progenitor position determined from LT i'-band data. Bottom: WFPC2 F814W image, M31N 2007-11b position determined from LT i'-band data. ©AAS. Reproduced with permission.

if it were at the far side of the galaxy. Therefore a *V*-band magnitude of 22.3 ± 0.3, *I*-band magnitude of 20.1 ± 0.2 and $(V - I)$ colour of 2.1 ± 0.2 are derived. Notably, from the overall distribution of stars in the M31 field in ACS/WFC, a source would be expected to be at least as close as $0''.032$ in a typical ACS/WFC image only about 4% of the time. M31N 2007-11b is shown in Figure 3.6.

3.4.7 M31N 2007-11c

Nova M31N 2007-11c was a Fe II nova (Ciroi et al., 2007) with an i'-band t_2 of 11.7 ± 0.9 (Shafter et al., 2011f) that was discovered on 2007 November 13. The LT data used to define the position in the archival *HST* data were taken using an i'-band filter on 2007 November 17.0 UT, from which the position of the nova was calculated to be $0^{\rm h}43^{\rm m}04^{\rm s}.16 \pm 0^{\rm s}.01$, $+41^\circ15'53''.93 \pm 0''.09$. This location was observed by *HST* with ACS/WFC using F814W and F475W filters on 2010 July 21 and there is one resolvable source just within 3σ of the calculated position. The source is 2.317 ACS/WFC pixels, $0.115''$ or 2.80σ away from the defined position. The local population density, which is resolved down to an F814W magnitude of 24.7, suggests there is a 42.2% chance of coincidence at such a separation. The location of this quiescent system is shown in Figure 3.7.

3.4.8 M31N 2007-11d

Nova M31N 2007-11d was discovered by K. Nishiyama and F. Kabashima on 2007 November 17.57 UT (Nakano, 2007). The nova had an i'-band t_2 of 9.2 ± 0.5 days (Shafter et al., 2011f) and was a member of the Fe II spectroscopic class (Quimby et al., 2007; Shafter et al., 2009). The nova had a relatively slow rise to optical maximum, but was one of the most luminous novae observed in M31 (Shafter et al., 2009). The LT observations used in this work were obtained using an i'-band filter on 2007 November 28.0 UT and gave the position of the nova to be $0^{\rm h}44^{\rm m}54^{\rm s}.59 \pm 0^{\rm s}.01$, $+41^\circ37'39''.8 \pm 0''.1$. *HST* images were taken of the position where M31N 2007-11d lies with ACS/WFC

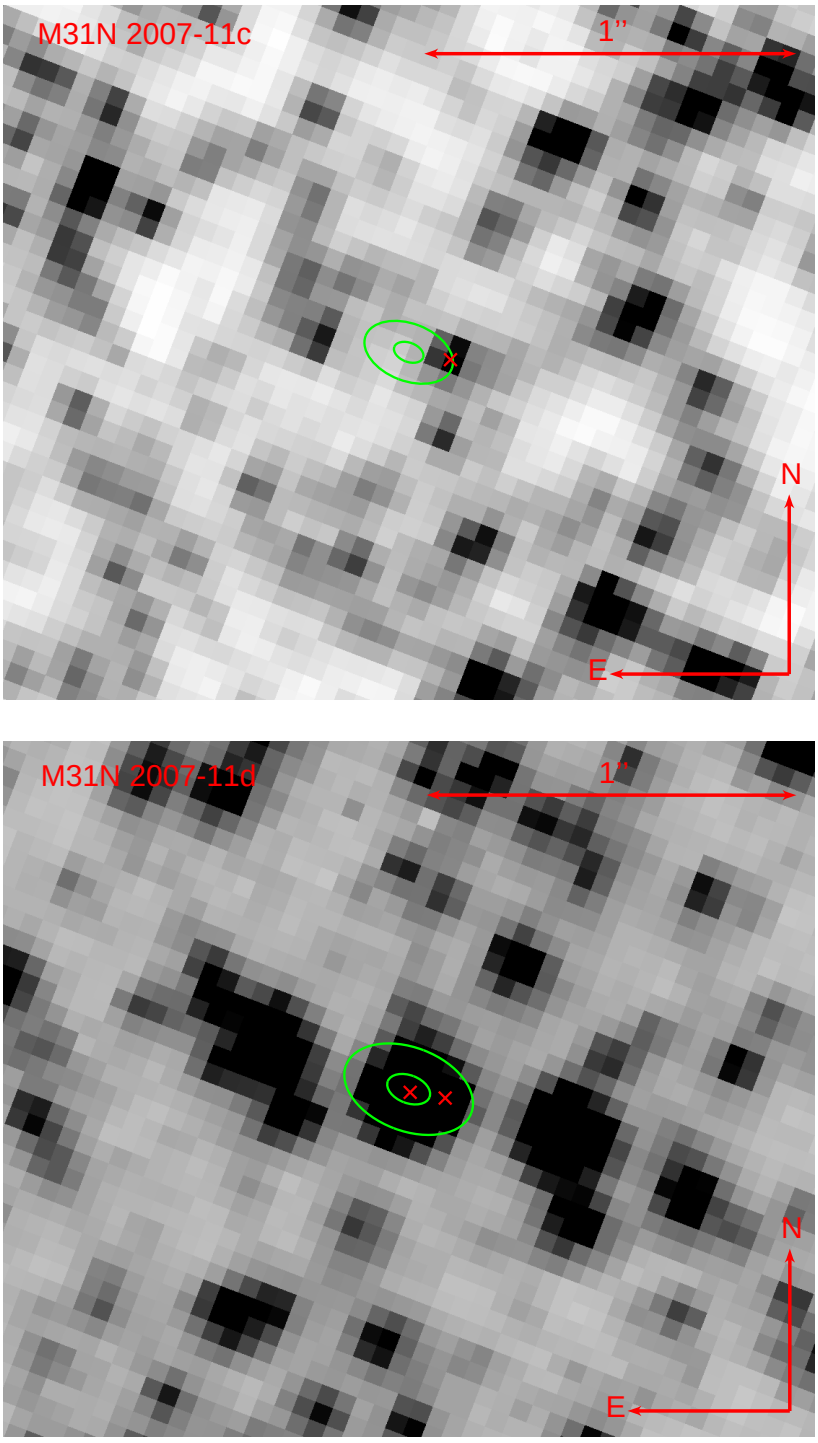

Figure 3.7: As Figure 3.4. Top: ACS/WFC F814W image, M31N 2007-11c progenitor position determined from LT i'-band data. Bottom: ACS/WFC F814W image, M31N 2007-11d progenitor position determined from LT i'-band data.

using F814W and F475W filters on 2010 July 13, by which time such a fast nova should have faded back to quiescence. There is a resolvable source within 1σ of the calculated position and another within 2σ. The closest candidate is 0.181 ACS/WFC pixels, $0.009''$ or 0.25σ away from the defined position. The local population density, which is resolved down to an F814W magnitude of 26.3, suggests there is only a 0.3% chance of coincidence at such a separation. This candidate had an F475W magnitude of 24.46 ± 0.04 and F814W magnitude of 21.387 ± 0.005, which gives an *I*-band magnitude of 21.44 ± 0.05, *B*-band magnitude of 25.43 ± 0.07 and a $(B - I)$ colour of 3.99 ± 0.09. The other candidate is 2.018 ACS/WFC pixels, $0.101''$ or 1.75σ away from the defined position, with a 34.4% chance of coincidence at this separation. We can see from Darnley (2005) that a nova at the apparent position of M31N 2007-11d would be subject to r'-band extinction of $A_{r'} = 0.58$ if it were at the far side of the galaxy. Taking this into account gives a *B*-band magnitude of 25.0 ± 0.5, *I*-band magnitude of 21.3 ± 0.2 and ($B - I$) colour of 3.8 ± 0.3 for the closer of the two progenitor candidates. If indeed the *HST* images were detecting the tail of the nova outburst it would be expected to be blue in colour, as can be seen by the late-time post-outburst *HST* data described in Chapter 4. Furthermore, the candidate is still clearly bright in ACS/WFC observations taken 2013 August 4, over three years later than the *HST* data used to search for the progenitor system. M31N 2007-11d is shown in Figure 3.7.

3.4.9 M31N 2007-11e

Nova M31N 2007-11e was Fe II nova (Di Mille et al., 2007) with an R-band t_2 of 27 days (Shafter et al., 2011b) discovered on 2007 November 28 (Yuan et al., 2007). i'-band LT data were taken on 2007 December 5.1 UT and the position of the nova was calculated to be $0^{\rm h}45^{\rm m}47^{\rm s}.76 \pm 0^{\rm s}.01$, $+42^\circ02'03''.7 \pm 0''.1$. *HST* images were taken with ACS/WFC using F814W and F475W filters on 2012 February 5, over four years after the outburst, that encompass the position of M31N 2007-11e. There is a resolvable source within 2σ of the calculated *HST* position and no other resolvable sources within 3σ. The candidate is 0.786 ACS/WFC pixels, $0.039''$ or 1.40σ away from the defined position of the nova and has an F814W magnitude of 24.19 ± 0.03 and F475W magni-

tude of 25.5 ± 0.1. This gives an *I*-band magnitude of 24.19 ± 0.04, *B*-band magnitude of 26.3 ± 0.1, with a $(B - I)$ colour of 2.1 ± 0.1. From Darnley (2005) it is estimated that a nova at the apparent position of M31N 2007-11e may be subject to a maximum r'-band extinction of $A_{r'} = 0.42$. Taking this into account gives a *B*-band magnitude of 26.0 ± 0.3, *I*-band magnitude of 24.1 ± 0.1 and ($B - I$) colour of 1.9 ± 0.2 for the progenitor candidate. If this is the nova, it is confirmed to be in quiescence by earlier *HST* observations, which show the progenitor candidate to have an F814W magnitude of 24.30 ± 0.03 on 2011 July 26. At the separation of $0.039''$, the local population density suggests a coincidence probability of 4.2%. These images have an F814W limiting magnitude of 26.4. M31N 2007-11e is shown in Figure 3.8.

3.4.10 M31N 2007-12a

Nova M31N 2007-12a was discovered by K. Nishiyama and F. Kabashima on 2007 December 5.52 UT[10]. The nova was a member of the Fe II spectroscopic class (Shafter, 2007) and had an i'-band t_2 of 29.6 ± 2.0 days (Shafter et al., 2011f). The data used to calculate the outburst position of the nova was taken with the LT using an i'-band filter on 2007 December 16.9, 31.8 and 2008 January 8.9 UT, with the position derived being $0^{\rm h}44^{\rm m}03^{\rm s}.52 \pm 0^{\rm s}.01$, $+41°38'40''.9 \pm 0''.1$. The *HST* images that were used to locate M31N 2007-12a were taken with ACS/WFC using F814W and F475W filters on 2010 December 31. There is only one resolvable source within 3σ of the calculated position. The candidate is 0.446 ACS/WFC pixels, $0.022''$ or 1.30σ away from the defined position, with an F475W magnitude of 25.98 ± 0.08 and F814W magnitude of 25.3 ± 0.1. This gives an I-band magnitude of 25.3 ± 0.1 and B-band magnitude of 26.14 ± 0.08, with a $(B - I)$ colour of 0.9 ± 0.1. It can be seen from Darnley (2005) that a nova at the apparent position of M31N 2007-12a would be subject to r'-band extinction of about $A_{r'} = 0.61$ if it were at the far side of the galaxy. Therefore a *B*-band magnitude of 25.7 ± 0.5, *I*-band magnitude of 25.1 ± 0.2 and a ($B - I$) colour of 0.6 ± 0.3 were derived. The local population density, which has an F814W limiting magnitude of 26.1, suggests there is a 1.7% chance of coincidence at such a separation.

[10] `http://www.cbat.eps.harvard.edu/CBAT_M31.html#2007-12a`

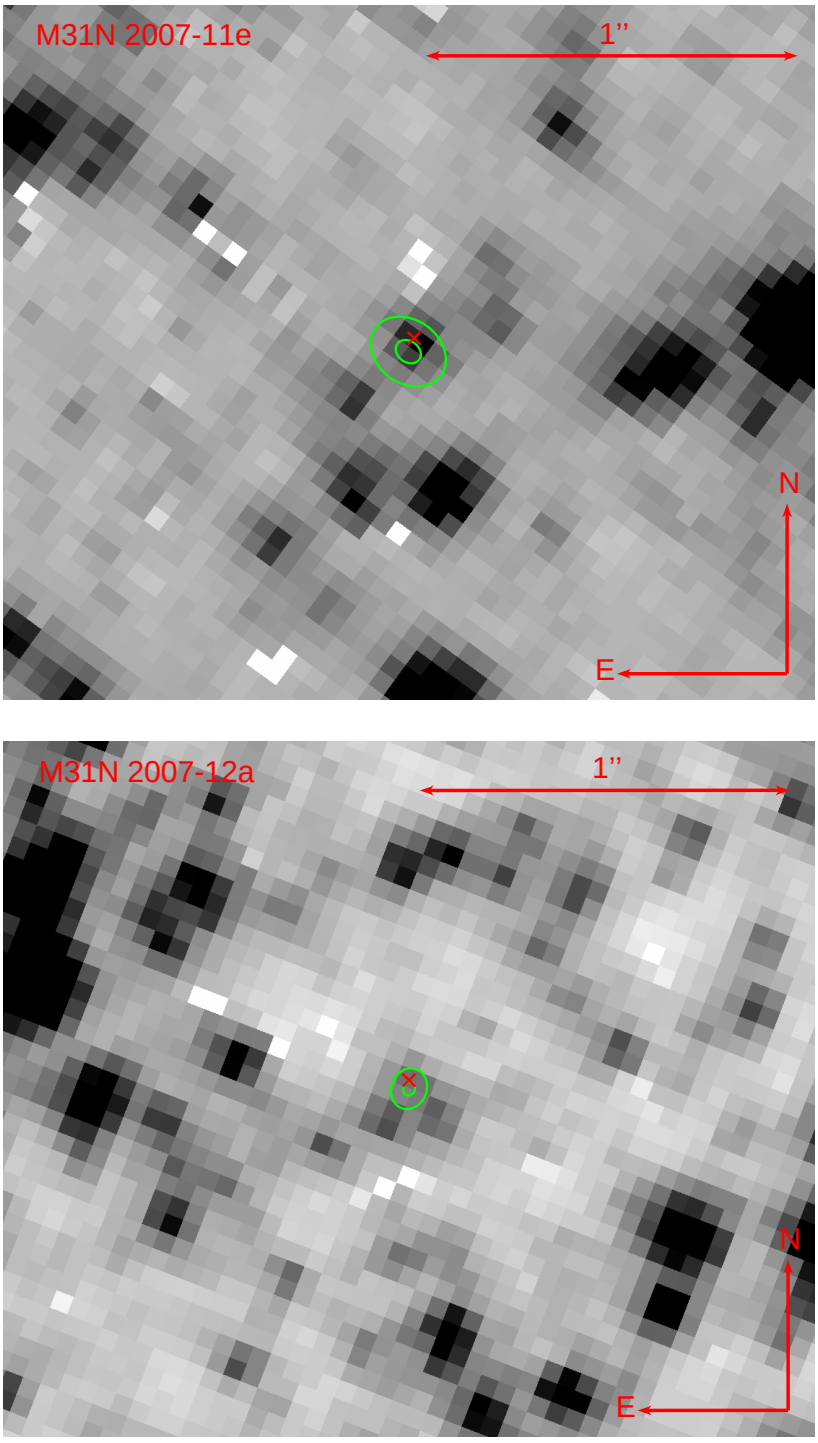

Figure 3.8: As Figure 3.4. Top: ACS/WFC F814W image, M31N 2007-11e progenitor position determined from LT i'-band data. Bottom: ACS/WFC F814W image, M31N 2007-12a progenitor position determined from LT i'-band data.

This nova is shown in Figure 3.8.

3.4.11 M31N 2007-12b

Nova M31N 2007-12b was a fast He/N nova (Bode et al., 2009) with an *R*-band t_2 of 5.0 ± 0.5 days (Shafter et al., 2011f) and was discovered on 2007 December 9[11]. The position of this nova was near the reported position of an outburst in 1969, although Bode et al. (2009) revealed the two outbursts were caused by two separate systems. The same authors found a likely progenitor candidate in archival *HST* data, implying this system may be a RG-nova. The SSS phase started between 21 and 30 days after the optical discovery, was still active 60 days post-outburst, but not detectable 120 days post-outburst (Pietsch et al., 2011). The same authors used dips in three X-ray observations to suggest a possible orbital period of 4.9 or 9.8 hours, contradicting the nova's assignment as a RG-nova, which would be expected to have a much longer orbital period. They also suggested it to be an intermediate-polar system. Bode et al. (2009) estimated the mass of the WD to be at least about 1.3 $M_\odot$, whereas Pietsch et al. (2011), who estimated an ejected mass of 2×10^{-6} $M_\odot$, derived a WD mass of 1.2 $M_\odot$.

From i'-band images taken using the LT on 2007 December 14.9 UT, the position of the nova was calculated to be $0^{\rm h}43^{\rm m}19^{\rm s}.96 \pm 0^{\rm s}.02$, $+41^\circ13'46''.3 \pm 0''.1$. The location of M31N 2007-12b was observed by *HST* with ACS/WFC using F814W and F475W filters on 2010 July 21 and 22, when this very fast nova is likely to have returned to quiescence. There is a resolvable source within 1σ of the calculated position and no other resolvable sources within 3σ. The candidate is 0.684 ACS/WFC pixels, $0.034''$ or 0.95σ away from the defined position, with the local population density suggesting there is a 4.3% chance of coincidence at such a separation. The progenitor candidate had an F475W magnitude of 25.36 ± 0.04 and F814W magnitude of 23.79 ± 0.04 at this time, which gives an I-band magnitude of 23.80 ± 0.04, B-band magnitude of 26.14 ± 0.06 and $(B - I)$ colour of 2.34 ± 0.07. This is the same candidate identified

[11] `http://www.cbat.eps.harvard.edu/CBAT_M31.html#2007-12b`

by Bode et al. (2009), who used a different set of *HST* images and found that the probability of a star being as close by change was 3.4%. They found the candidate to have I-band magnitude of 22.33 ± 0.04 and $(V-I)$ colour of 2.3 ± 0.1 in August 2004, although they note that the F814W data may have been affected by a cosmic ray. This comparison clearly shows that the nova had indeed returned to quiescence by the time the *HST* observations used here were taken. The location of the quiescent M31N 2007-12b is shown in Figure 3.9. Darnley (2005) found that a nova at the apparent position of M31N 2007-12b would be subject to r'-band extinction of $A_{r'} = 0.65$ if it were at the far side of the galaxy, which gives a *B*-band magnitude of 25.7 ± 0.5, *I*-band magnitude of 23.6 ± 0.2 and ($B-I$) colour of 2.1 ± 0.3.

3.4.12 M31N 2008-10b

Nova M31N 2008-10b was discovered on 2008 October 18, but was visible as early as October 6 (Henze et al., 2008c). A spectrum taken by Di Mille et al. (2010) showed it to be a Fe II type nova. The nova had a *B*-band t_2 of 98.4 ± 14.9, although the light curve suggests the nova initially faded quickly and then re-brightened, before undergoing a slower decline (Shafter et al., 2011f). The LT images used to determine the position of the quiescent system in the archival *HST* data were taken with a *B*-band filter on 2008 October 21.0, from which the position of the nova was found to be $0^{\rm h}43^{\rm m}02^{\rm s}.41 \pm 0^{\rm s}.02$, $+41^\circ 14' 09''.9 \pm 0''.2$. *HST* images coincident with this position were taken with ACS/WFC using a F435W filter on 2004 October 2. There is one resolvable source within 3σ of the calculated position. The candidate is 1.815 ACS/WFC pixels or 2.95σ away from the defined position. The local population density, which is resolved down to an F435W magnitude of 26.4, suggests there is a 30.9% chance of coincidence at such a separation. The location of M31N 2008-10b is shown in Figure 3.9, but it is clear from the post-outburst F435W *HST* images taken on 2010 January 1 (see Section 4.3.2) that the source listed above is not the nova.

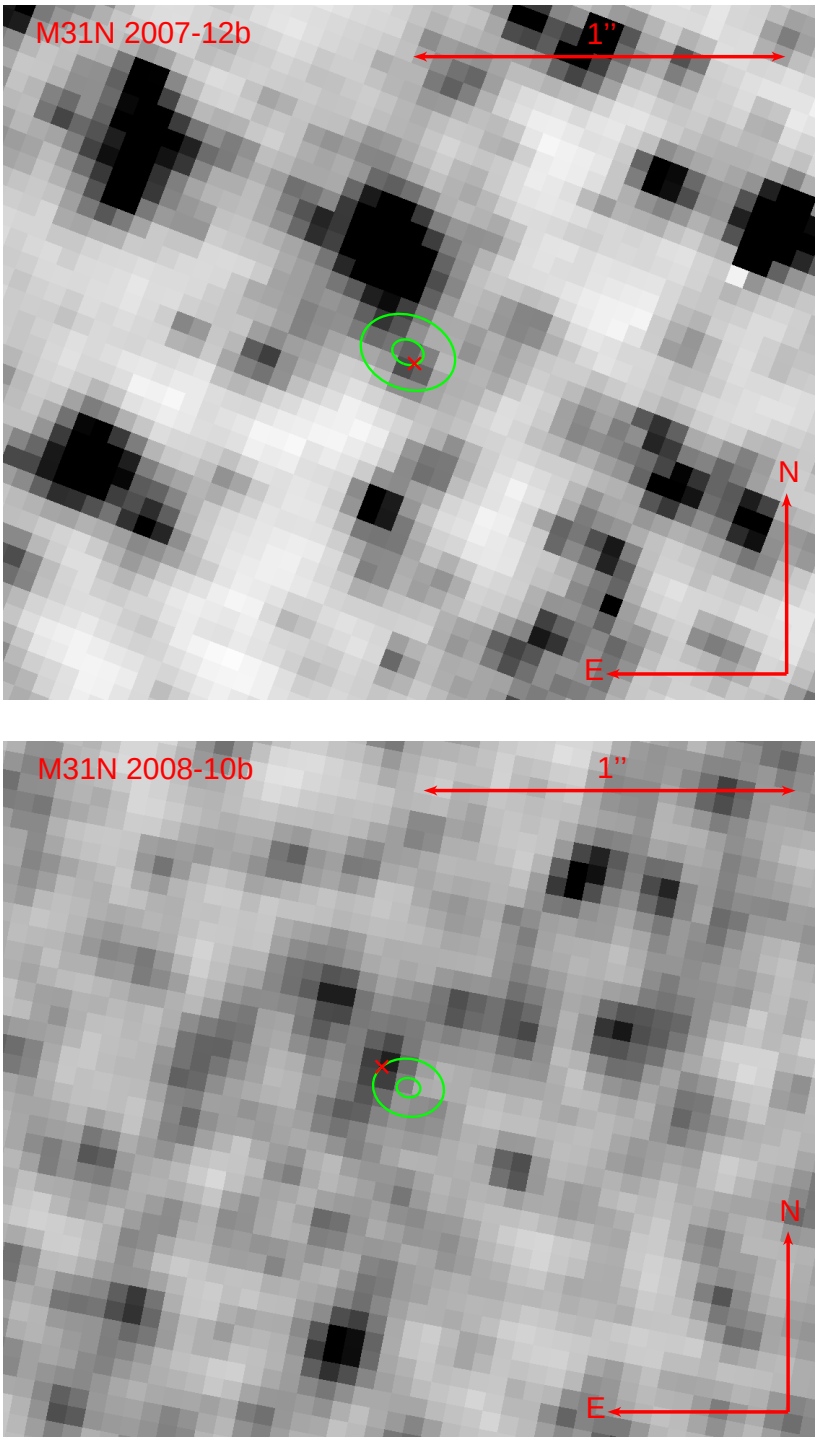

Figure 3.9: As Figure 3.4. Top: ACS/WFC F814W image, M31N 2007-12b progenitor position determined from LT i'-band data. Bottom: ACS/WFC F435W image, M31N 2008-10b progenitor position determined from LT B-band data. ©AAS. Reproduced with permission.

3.4.13 M31N 2008-12b

Nova M31N 2008-12b was discovered on 2008 December 30[12]. It was a member of the Fe II spectroscopic class (Kasliwal et al., 2009) and had an i'-band t_2 of 24.7 ± 3.6 days (Shafter et al., 2011f). On 2009 January 15.0, i'-band LT data were obtained, giving the position as $0^{\rm h}43^{\rm m}04^{\rm s}.85 \pm 0^{\rm s}.01$, $+41^\circ 17' 51''.6 \pm 0''.2$. The location of nova M31N 2008-12b was observed by *HST* with ACS/WFC using F814W and F475W filters on 2012 July 9. The closest resolvable source, and the only one within 3σ, is 1.431 ACS/WFC pixels, $0.072''$ or 1.75σ away from the defined position. It has F475W magnitude of 24.75 ± 0.05, but is not detected in the F814W data. However, it should be noted that due to problems with the photometry and a short-exposure F814W image having to be used, the limiting F814W magnitude was 22.7, whereas the F475W magnitude limit was 26.0. The local population density suggests that there is a 18.0% probability of such an alignment occurring by chance. The closest source resolvable in the F814W data was 4.558 ACS/WFC pixels, $0.228''$ or 5.80σ away from the defined position. The location of this quiescent system, including the candidate only visible in the F475W image, is shown in Figure 3.10.

3.4.14 M31N 2009-08a

M31N 2009-08a was an Fe II type nova (Valeev et al., 2009) discovered on 2009 August 4 by Pietsch et al. (2009a), with a *B*-band t_2 of 36.7 ± 4.1 (Shafter et al., 2011f). Using i'-band LT data taken on 2009 August 27.1 and September 4.1, the position $0^{\rm h}42^{\rm m}58^{\rm s}.105 \pm 0^{\rm s}.007$, $+41^\circ 17' 29''.56 \pm 0''.06$ was calculated for the nova. The *HST* images used to locate the quiescent M31N 2009-08a were taken with ACS/WFC using an F435W filter on 2007 January 10. There is a resolvable source within 2σ of the calculated position and no other resolvable sources within 3σ. The source is 1.118 ACS/WFC pixels, $0.056''$ or 1.40σ away from the defined position, with the local population density suggesting there is a 12.1% chance of coincidence at such a separation. The source has an F435W magnitude of 25.50 ± 0.05 and the images have a limit-

[12] `http://www.cbat.eps.harvard.edu/CBAT_M31.html#2008-12b`

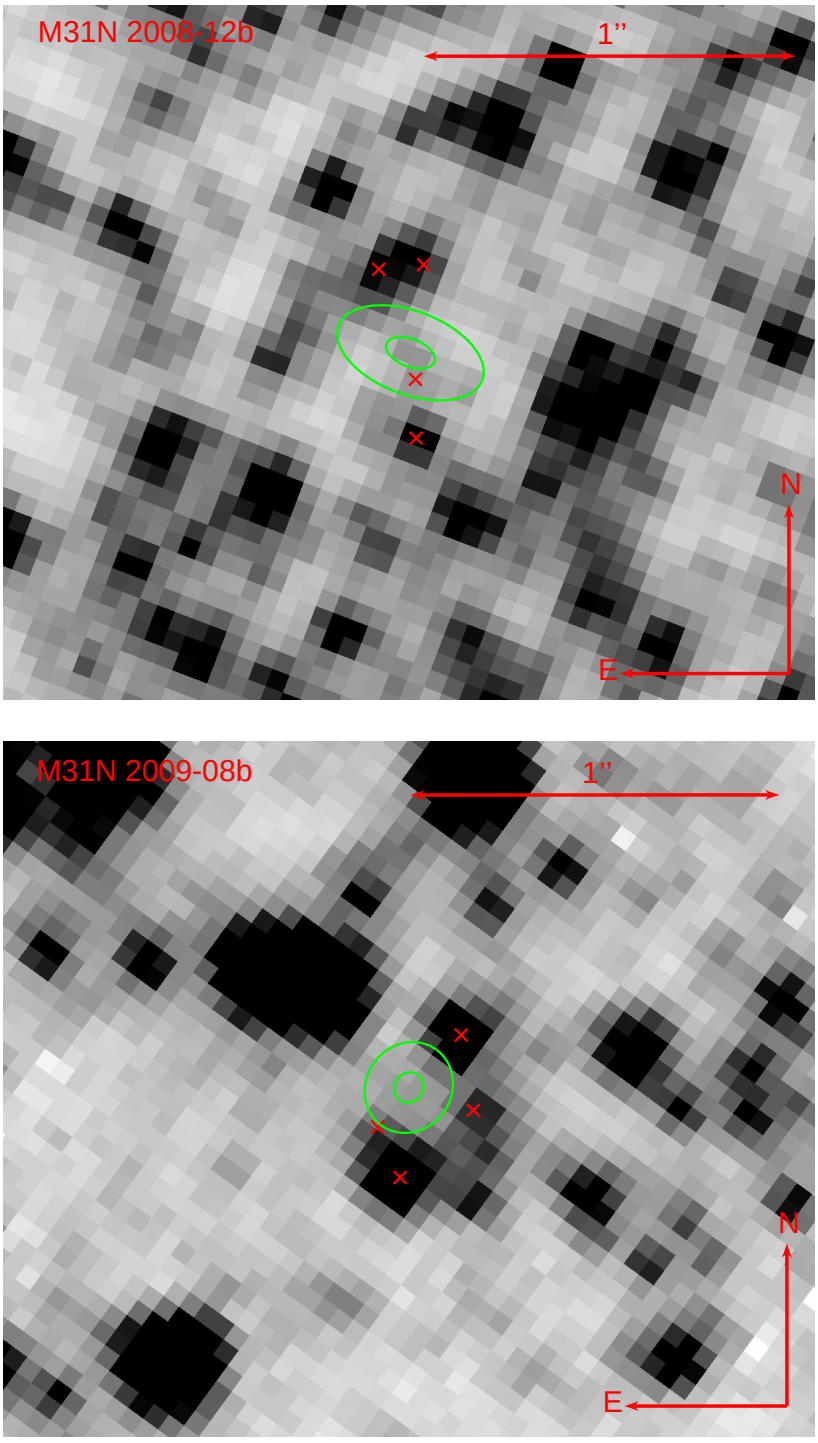

Figure 3.10: As Figure 3.4. Top: ACS/WFC F814W image, M31N 2008-12b progenitor position determined from LT i'-band data. Bottom: ACS/WFC F814W image, M31N 2009-08b progenitor position determined from LT i'-band data. ©AAS. Reproduced with permission.

ing magnitude of 26.0. The *HST* images were only taken in one filter, so it was not possible to calculate the colour of the source, although it is estimated to have a *B*-band magnitude of ∼25.5 with internal extinction in M31 taking in to ~ 25.2. The position of the system, as determined from the LT images, is shown in Figure 3.11. M31N 2009-08a was also observed in outburst with ACS/WFC on 2010 July 21 and December 14, which is described in Section 4.3.3. Using this post-outburst *HST* data, it was possible to determine the position of the progenitor without using LT data. Here the same method as previously described was employed, but the photometrically determined positions for the transformations from DOLPHOT were used. The closest resolvable source is 0.516 ACS/WFC pixels, $0.026''$ or 2.85σ away from the defined position of the nova, with a 2.4% probability of a chance alignment. Due to the small errors associated with the transformation and the source being relatively faint, the errors on the position of the pre-outburst source may be more significant than in the regular transformations using LT data. The position of the nova, as determined from the post-outburst *HST* data, is also shown in Figure 3.11.

3.4.15 M31N 2009-08b

Nova M31N 2009-08b was discovered to be in outburst by K. Nishiyama and F. Kabashima on frames taken on 2009 August 9.78 UT and was independently discovered by both K. Itagaki and R. Ferrando[13]. The nova was a member of the Fe II spectroscopic class (Rodríguez-Gil et al., 2009) and had an i'-band t_2 of 26.9 ± 2.2 (Shafter et al., 2011f). The nova was calculated to be at $0^{\rm h}44^{\rm m}09^{\rm s}.89 \pm 0^{\rm s}.02$, $+41^\circ48'50''.7 \pm 0''.1$ from LT i'-band images taken on 2009 August 18.0. *HST* images, coincident with the position of M31N 2009-08b, were taken with ACS/WFC using F814W and F475W filters on 2013 January 6. The closest resolvable source is 2.830 ACS/WFC pixels, $0.142''$ or 3.25σ away from the defined position. The local population density, which is resolved down to an F435W magnitude of 26.6, suggests there is a 57.1% chance of coincidence at such a separation. Additionally, it is noted that there is a source visible around the 1σ area in the F475W drz image, but it is too faint to determine the PSF and

[13] `http://www.cbat.eps.harvard.edu/CBAT_M31.html#2009-08b`

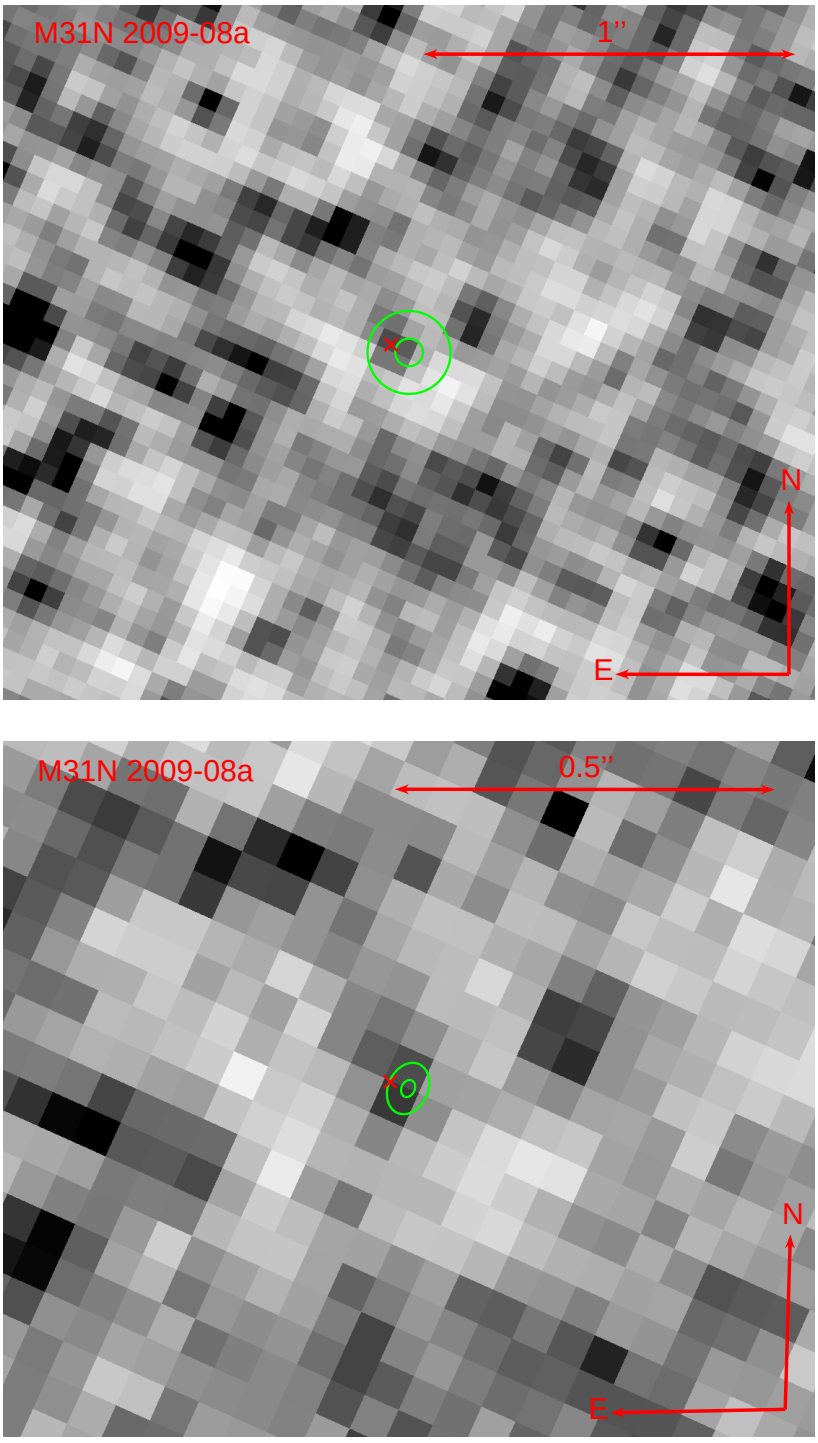

Figure 3.11: As Figure 3.4. Top: ACS/WFC F435W image, M31N 2009-08a progenitor position determined from LT B-band data Bottom: F435W FLT image with M31N 2009-08a progenitor position determined from post-outburst F475W data.

hence perform photometry or accurate astrometry. The location of M31N 2009-08b is shown in Figure 3.10.

3.4.16 M31N 2009-08d

Nova M31N 2009-08d was discovered by K. Hornoch and P. Zasche on 2009 August 12[14]. It was an Fe II nova (Di Mille et al., 2009) with a *B*-band t_2 of 27.9 ± 6.5 days (Shafter et al., 2011f). LT images of the nova were taken with a *B*-band filter on 2009 August 20.1, from which its position was determined to be $0^{\rm h}42^{\rm m}46^{\rm s}.74 \pm 0^{\rm s}.02$, $+41°15'37''.4 \pm 0''.1$. The *HST* images used to locate position of the quiescent M31N 2009-08d were taken with ACS/WFC using an F435W filter on 2004 January 23. The closest resolvable source is 3.236 ACS/WFC pixels, $0.163''$ or 2.95σ away from the defined *HST* position. The local population density, which is resolved down to an F435W magnitude of 25.9, suggests there is a 62.7% chance of coincidence at such a separation. There is also a very faint source about 1.5σ away from the defined position, but it is too faint to determine a PSF. The location of M31N 2009-08d is shown in Figure 3.12.

3.4.17 M31N 2009-10b

Nova M31N 2009-08d was discovered on 2009 October 11 (Nakano & Yusa, 2009) and later confirmed as an Fe II nova (Barsukova et al., 2009) with a *B*-band t_2 of 8.0 ± 0.2 days (Shafter et al., 2011f). The nova was particularly luminous and was quite similar to M31N 2007-11d (Shafter et al., 2011f). *B*-band LT data were taken on 2009 October 15.0 and the position of the nova was calculated to be $0^{\rm h}42^{\rm m}20^{\rm s}.83 \pm 0^{\rm s}.02$, $+41°16'44''.3 \pm 0''.1$. It had coincident *HST* images taken with ACS/WFC using an F435W filter on 2009 August 25. There is no resolvable source within 3σ of the calculated position, with the closest source being 1.803 ACS/WFC pixels, $0.091''$ or 4.30σ away from the defined position. The local population density suggests there is a 29.1%

[14] `http://www.cbat.eps.harvard.edu/CBAT_M31.html#2009-08d`

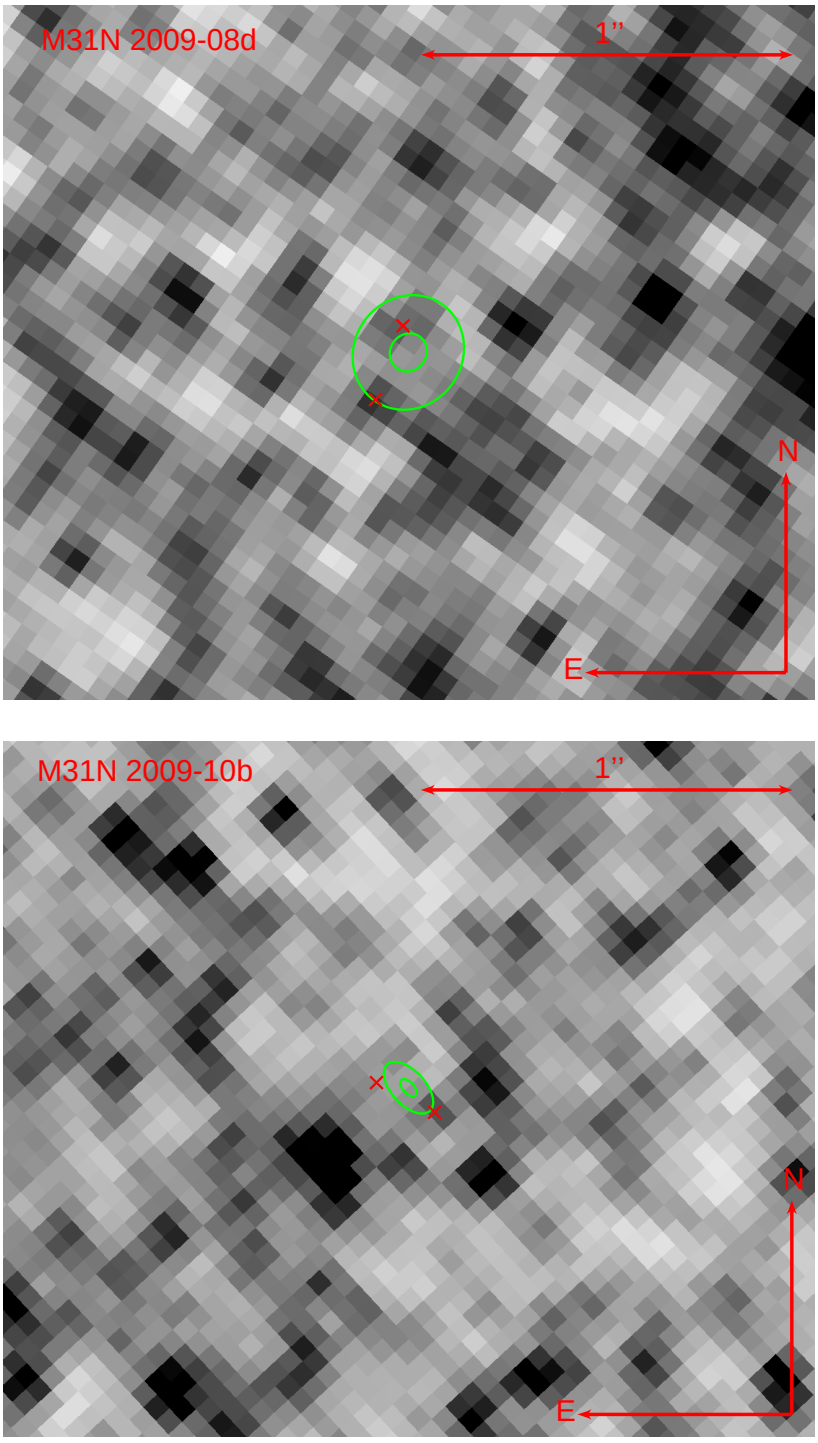

Figure 3.12: As Figure 3.4. Top: ACS/WFC F435W image, M31N 2009-08d progenitor position determined from LT B-band data. Bottom: ACS/WFC F435W image, M31N 2009-10b progenitor position determined from LT B-band data. ©AAS. Reproduced with permission.

chance of coincidence at such a separation. The data had an F435W limiting magnitude of 26.7. The location of M31N 2009-10b in quiescence is shown in Figure 3.12. It is clear from the post-outburst F475W *HST* images taken on 2010 December 26 (see Section 4.3.4) that neither of the sources shown in the figure are the nova. Note that M31N 2007-11d, which this nova is similar to in terms of peak luminosity, decline rate and spectroscopic class, does have a nearby resolved source that is likely to be the progenitor.

3.4.18 M31N 2009-10c

Nova M31N 2009-10c was discovered by Podigachoski et al. (2009a) on 2009 October 9. Fabrika et al. (2009) confirmed it as an Fe II type nova and it had a *B*-band t_2 of 14.9 ± 0.8 days (Shafter et al., 2011f). The LT data used to determine the position of the nova in the archival *HST* data were taken using a *B*-band filter on 2009 October 15.0, from which the outburst position of $0^{\rm h}42^{\rm m}45^{\rm s}.72 \pm 0^{\rm s}.02$, $+41^\circ15'56''.99 \pm 0''.09$ was also calculated. The *HST* were taken with ACS/WFC using an F435W filter on 2004 January 23. There is one resolvable source within 3σ of the calculated position. The source is 2.128 ACS/WFC pixels, $0.107''$ or 2.30σ away from the defined position, and the local population density, which is resolved down to an F435W magnitude of 25.9, suggests there is a 28.7% chance of coincidence at such a separation. The location of this system is shown in Figure 3.13. It is clear from the post-outburst F475W *HST* images taken on 2010 December 22 (see Section 4.3.5) that the source listed above is not the nova.

3.4.19 M31N 2009-11a

Nova M31N 2009-11a was discovered on 2009 November 3 (Nishiyama & Kabashima, 2009a). It was a member of the Fe II spectroscopic class (Hornoch et al., 2009b) and had a *V*-band t_2 of 21.7 ± 1.2 days (Shafter et al., 2011f). *V*-band LT data were taken on 2009 November 13.9 and the position of the nova was calculated to

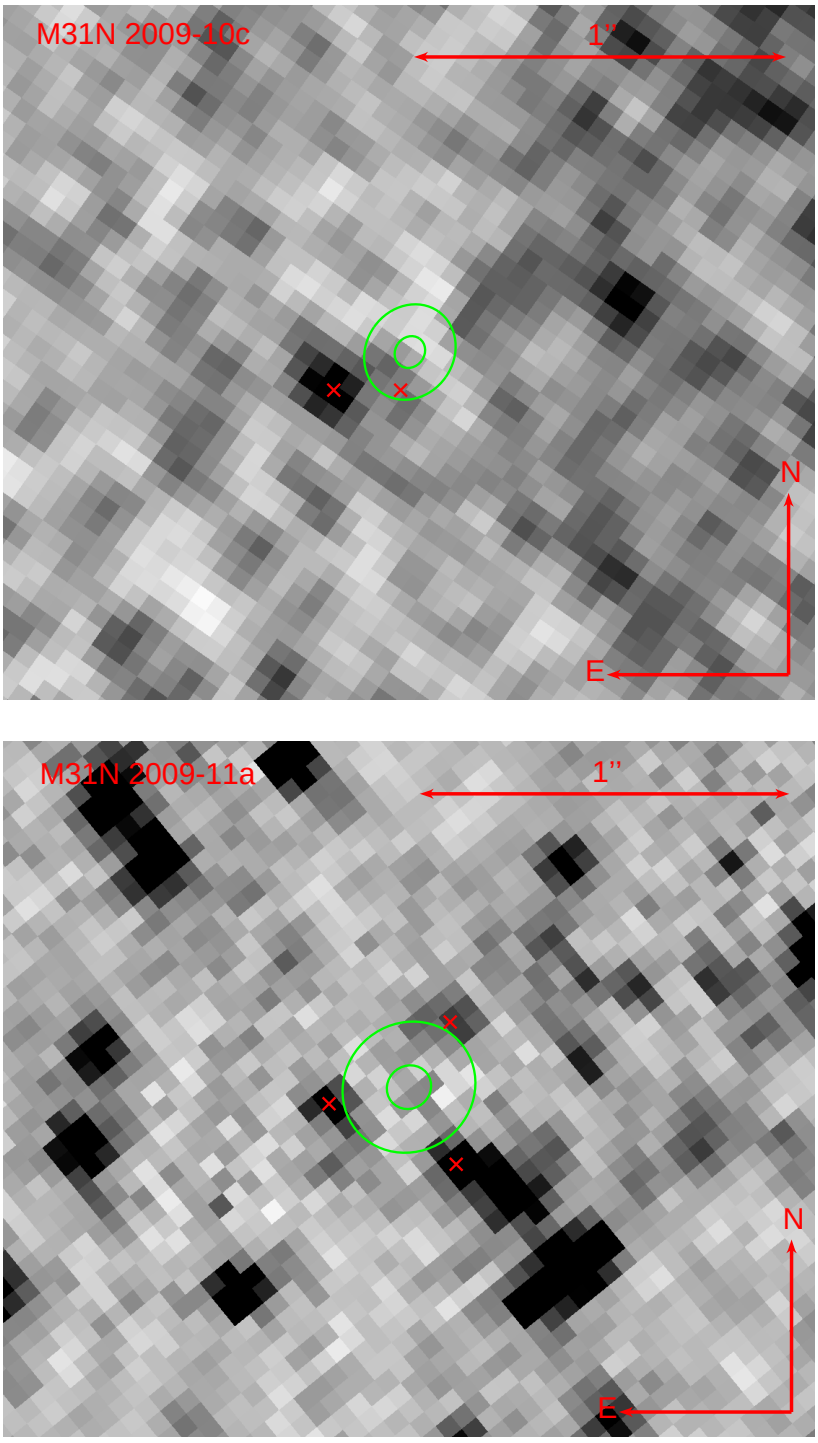

Figure 3.13: As Figure 3.4. Top: ACS/WFC F435W image, M31N 2009-10c progenitor position determined from LT B-band data. Bottom: ACS/WFC F555W image, M31N 2009-11a progenitor position determined from LT V-band data. ©AAS. Reproduced with permission.

be $0^{\rm h}43^{\rm m}04^{\rm s}.789 \pm 0^{\rm s}.009$, $+41°41'07''.79 \pm 0''.08$. *HST* images, coincident with the position of M31N 2009-11a, were taken with ACS/WFC using F814W and F555W filters on 2004 August 15. There are no resolvable sources within 3σ of the calculated position, with the closest resolvable source being 3.999 ACS/WFC pixels, $0.201''$ or 3.45σ away from the defined position. The local population density, which is resolved to an F814W magnitude of 26.5, suggests there is a 68.3% chance of coincidence at such a separation. The location of this system is shown in Figure 3.13.

3.4.20 M31N 2009-11b

K. Nishiyama and F. Kabashima discovered nova M31N 2009-11b on frames taken around 2009 November 6.523 (Nishiyama et al., 2009) and it was a member of the Fe II spectroscopic class (Kasliwal, 2009; Shafter et al., 2011f) with a *V*-band t_2 of 74.8 ± 10.6 days (Shafter et al., 2011f). M31N 2009-11b is thought to be a RN, with previous outbursts having occurred in 1997 (M31N 1997-11k) and 2001 (M31N 2001-12b) (Nishiyama et al., 2009; Henze et al., 2009; Shafter et al. in preparation). The LT images used to calculate the position of the quiescent system in the archival *HST* data were taken with a *V*-band filter on 2009 December 6.8, with the position of the nova being calculated as $0^{\rm h}42^{\rm m}39^{\rm s}.596 \pm 0^{\rm s}.009$, $+41°09'02''.9 \pm 0''.1$. *HST* observed this location with WFPC2 using F814W and F555W filters on 2004 August 22. There are no resolvable sources within 3σ of the calculated position, with the closest resolvable source being 1.971 WFPC2 pixels, $0.197''$ or 4.15σ away from the defined position. The local population density suggests there is a 38.6% probability of an object alignment this close occurring by chance, although the limiting F814W magnitude is only 23.8. If looking at a typical ACS/WFC image of M31, it would be expected that an object at a distance of $0.197''$ would have approximately an 81% chance of being aligned by chance. The location of M31N 2009-11b in the WFPC2 image is shown in Figure 3.14.

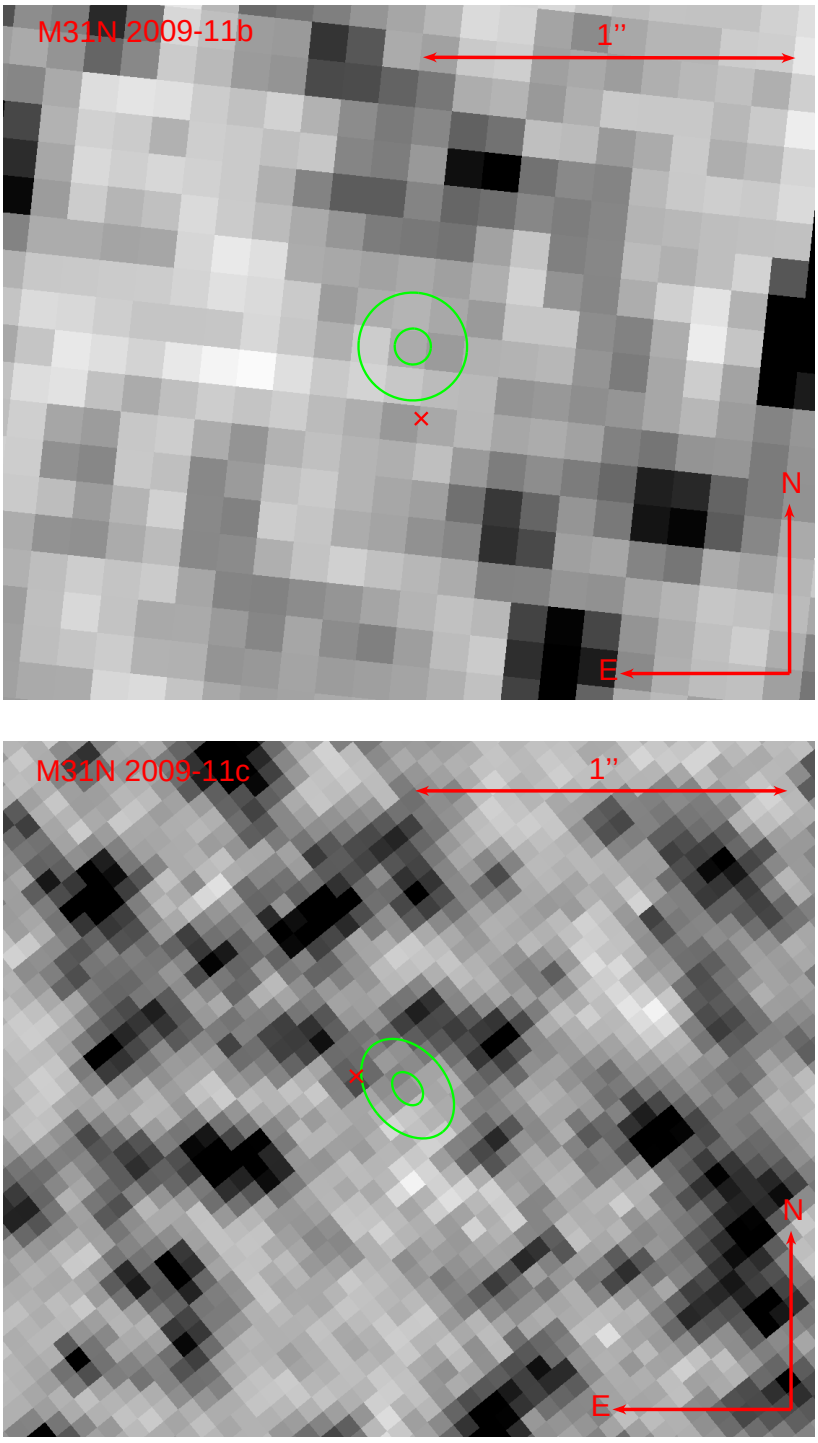

Figure 3.14: As Figure 3.4. Top: WFPC2 F555W image, M31N 2009-11b progenitor position determined from LT V-band data. Bottom: ACS/WFC F555W image, M31N 2009-11c progenitor position determined from LT V-band data. ©AAS. Reproduced with permission.

3.4.21 M31N 2009-11c

Nova M31N 2009-11c was first seen to be in outburst on images taken on 2009 October 31 (Hornoch et al., 2009d), but was not reported until several days later. The nova was of Fe II spectral type (Hornoch et al., 2009c) and had a *V*-band t_2 of 32.5 ± 2.4 days (Shafter et al., 2011f). LT data taken with an *i*-band filter on 2007 November 17.0 showed the position of the nova to be $0^{\rm h}43^{\rm m}04^{\rm s}.16 \pm 0^{\rm s}.01$, $+41^\circ15'53''.93 \pm 0''.09$. The *HST* images used to locate M31N 2009-11c in quiescence were taken with ACS/WFC using F814W and F555W filters on 2004 August 22. There are no resolvable sources within 3σ of the calculated position. The closest resolvable source is 2.975 ACS/WFC pixels, $0.150''$ or 3.35σ away from the defined position, with the local population density, which is resolved to an F814W magnitude of 25.8, suggesting there is a 55.0% chance of coincidence at such a separation. The location of this system is shown in Figure 3.7. It is clear from the post-outburst F475W *HST* images taken on 2010 July 23 (see Section 4.3.6) that the source listed above is not the nova.

3.4.22 M31N 2009-11d

Nova M31N 2009-11d was an Fe II nova (Hornoch et al., 2009a) with a *B*-band t_2 of 11.2 ± 0.4 days (Shafter et al., 2011f) discovered on 2009 November 19 (Podigachoski et al., 2009b; Nishiyama & Kabashima, 2009b). It can be seen from data published by Shafter et al. (2011f), that 51 days after peak the nova had already faded by almost five magnitudes in both g' and r'. The position of the nova was calculated to be $0^{\rm h}44^{\rm m}16^{\rm s}.866 \pm 0^{\rm s}.009$, $+41^\circ18'53''.6 \pm 0''.2$ using *V*-band LT images taken on 2009 November 24.0. The system had coincident *HST* images taken with ACS/WFC using F475W and F814W filters on 2011 December 22, more than two years after the outburst. There is a resolvable source within 1σ of the calculated position and no other source within 3σ, with the source being 0.505 ACS/WFC pixels, $0.025''$ or 0.60σ away from the defined position. The local population density, which has an F814W limiting magnitude of 26.4, suggests there is only a 2.2% chance of an object alignment this close occurring by chance. On 2011 December 22, the source had an F814W mag-

nitude of 25.1 ± 0.2 and F475W magnitude of 25.67 ± 0.04. This gives a B-band magnitude of 25.81 ± 0.06, I-band magnitude of 25.1 ± 0.2 and $(B - I)$ colour of 0.7 ± 0.2. From Darnley (2005) it can be seen that a nova at the apparent position of M31N 2009-11d would be subject to r'-band extinction of approximately $A_{r'} = 0.58$ if it were at the far side of the galaxy. This gives a *B*-band magnitude of 25.4 ± 0.4, *I*-band magnitude of 24.9 ± 0.3 and $(B - I)$ colour of 0.5 ± 0.3 when the effects of internal extinction are included. M31N 2009-11d is shown in quiescence in Figure 3.15. Further coincident *HST* observations were taken of the position of M31N 2009-11d seven months later on 2012 July 21. Between the two sets of observations the brightness of the source had varied very little and had an F475W magnitude of 25.89 ± 0.09 in the latter set, confirming that the nova was likely at quiescence in both sets of images.

3.4.23 M31N 2009-11e

Nova M31N 2009-11e was an Fe II type nova (Hornoch & Pejcha, 2009) discovered on 2009 November 20 (Pietsch et al., 2009b) with an *R*-band t_2 of 55.7 ± 3.1 days (Shafter et al., 2011f). The LT observed the nova through a *V*-band filter on 2009 November 27.0 and its position was calculated to be $0^{\rm h}42^{\rm m}35^{\rm s}.33 \pm 0^{\rm s}.01$, $+41°12'59''.4 \pm 0''.2$. This location was observed by *HST* with WFPC2 using F814W and F555W filters on 1996 February 14. There is a resolvable source within 1σ of the calculated position and no other source within 3σ, with the source being 1.104 WFPC2 pixels, $0.110''$ or 0.80σ away from the defined position. The local population density, which is only resolvable to an F814W magnitude of 22.8, suggests there is a 9.9% chance of an object alignment this close occurring by chance. If, as with previous WFPC2 images, a standard ACS/WFC image of the M31 field is considered, an object would be expected to be at least as close as $0.110''$ from a random point in the image approximately 33% of the time. The location of this system is shown in Figure 3.7. It is clear from the post-outburst F475W *HST* images taken on 2010 December 25 (see Section 4.3.7) that the source listed above is not the nova.

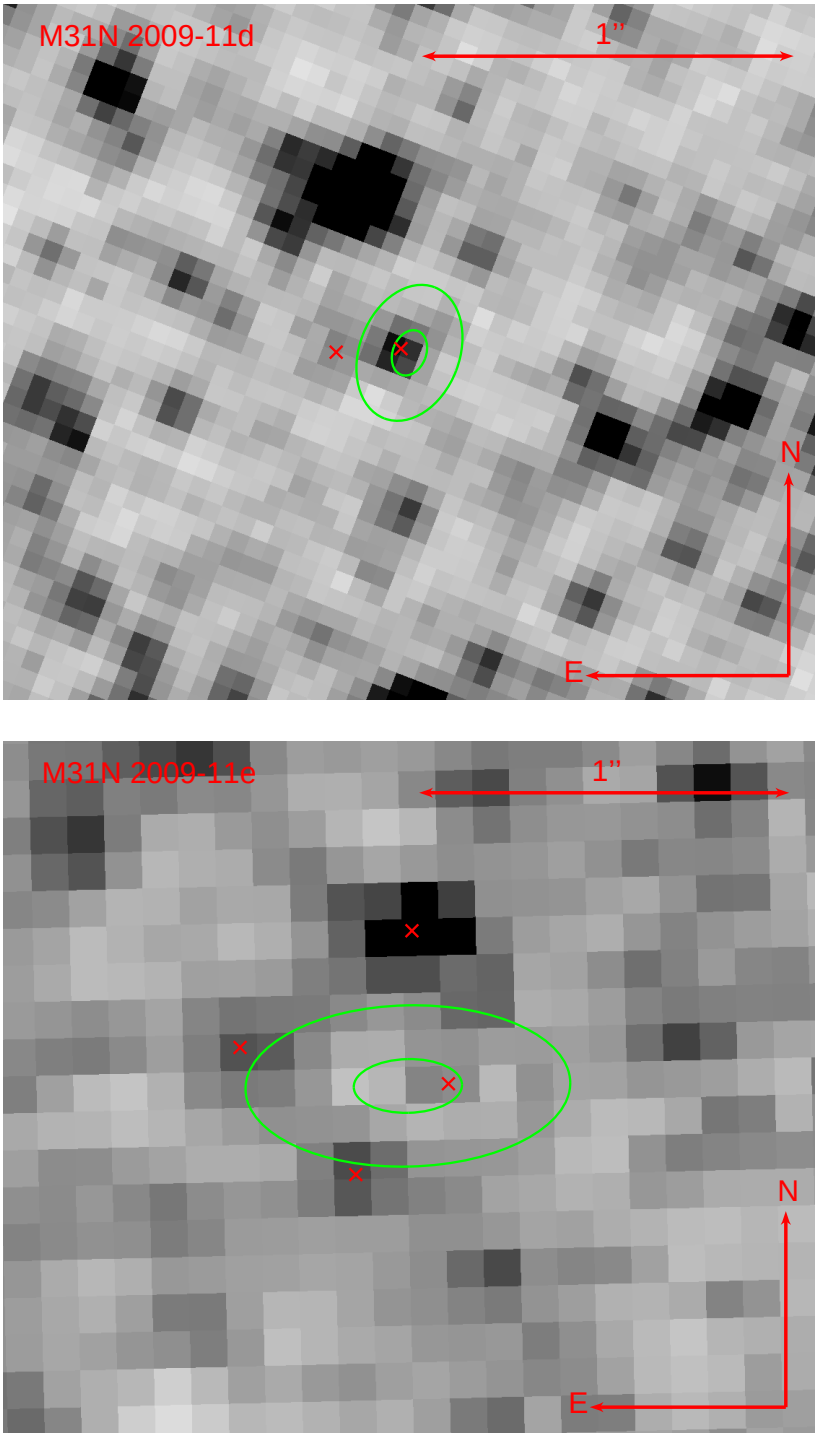

Figure 3.15: As Figure 3.4. Top: ACS/WFC F475W image, M31N 2009-11d progenitor position determined from LT V-band data. Bottom: WFPC2 F555W image, M31N 2009-11e progenitor position determined from LT V-band data. ©AAS. Reproduced with permission.

3.4.24 M31N 2010-01a

Nova M31N 2010-01a was discovered on 2010 January 11 (Burwitz et al., 2010b) and was confirmed as an Fe II type nova by Hornoch et al. (2010e). The LT images used to find the position of the quiescent system in the archival *HST* data were taken with a *B*-band filter on 2010 January 15.9, from which the position of the nova was calculated to be $0^{\rm h}42^{\rm m}56^{\rm s}.70 \pm 0^{\rm s}.02$, $+41^\circ17'20''.2 \pm 0''.1$. The *HST* images were taken with ACS/WFC using an F435W filter on 2006 February 10. There is a resolvable source within 2σ of the calculated position, which is the only object within 3σ and 1.058 ACS/WFC pixels, $0.053''$ or 1.45σ away from the defined position. The local population density, which is resolved down to an F435W magnitude of 26.1, suggests there is a 9.4% chance of an object alignment this close occurring by chance. The source has an F435W magnitude of 24.79 ± 0.04, but the *HST* images were only taken in one filter, so it was not possible to calculate the colour of the source, although it is estimated to have a *B*-band magnitude of ~ 24.8 with internal extinction in M31 taking in to ~ 24.5. The location of this nova is shown in Figure 3.16. M31N 2010-01a was also observed in outburst with ACS/WFC on 2010 July 21, which is described in Section 4.3.8. Using this post-outburst *HST* data, it was possible to determine the position of the progenitor without using LT data. Here the same method as previously described was employed, but the photometrically determined positions were used for the transformations. The closest resolvable source is 0.641 ACS/WFC pixels, $0.032''$ or 2.65σ away from the defined position of the nova, with a 3.8% probability of a chance alignment at this separation. As previously noted, due to the small errors associated with the transformation and the source being relatively faint, the errors on the position of the pre-outburst source may be more significant than in the regular transformations using LT data. The position of the quiescent nova, as determined from the post-outburst *HST* data, is also shown in Figure 3.16. Later in the year there was a nova outburst (M31N 2010-12c) very close to the position of M31N 2010-01a, however the precise positions reveal that they are not the same system (Hornoch et al., 2010d; Shafter et al. in preparation).

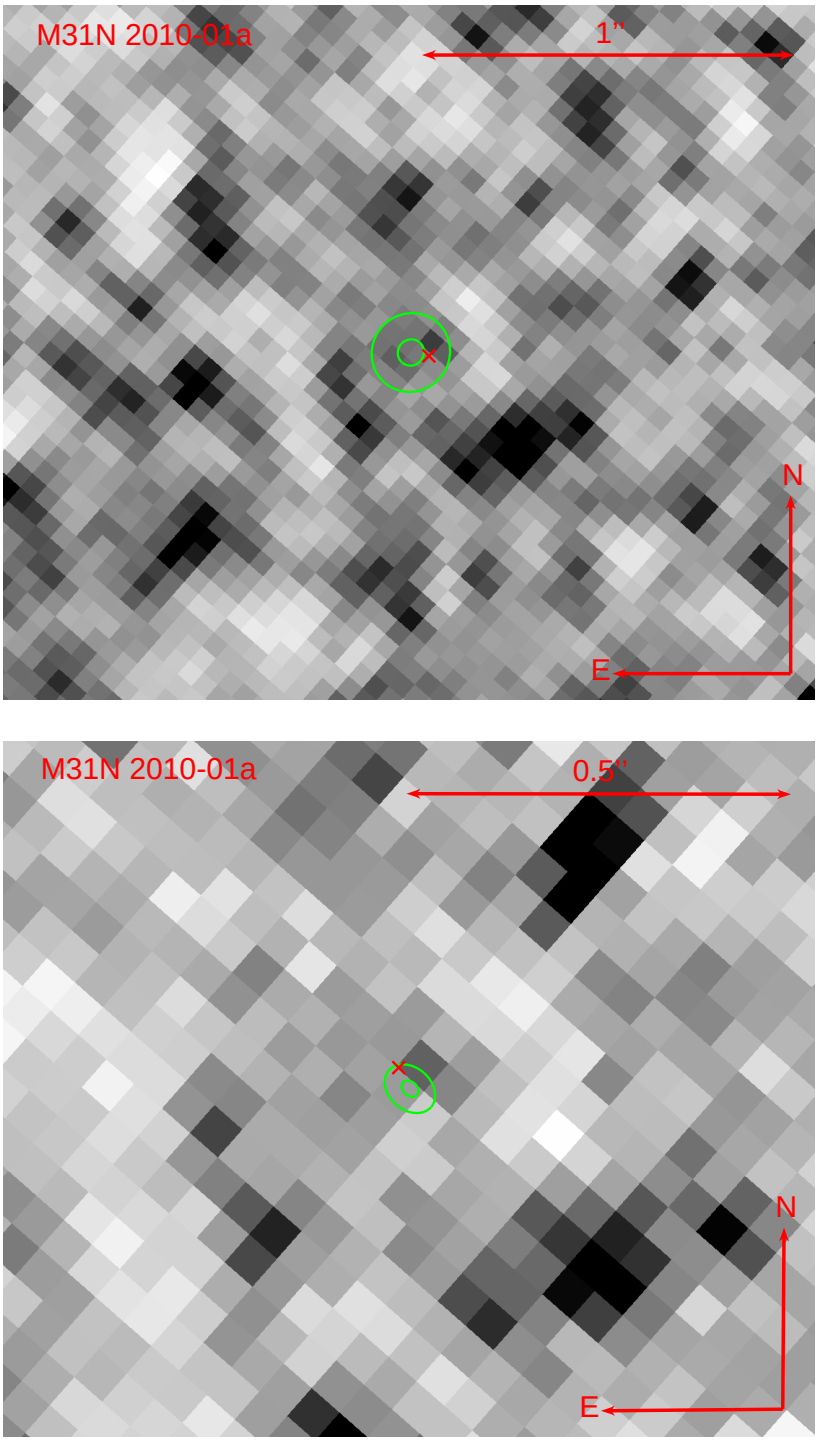

Figure 3.16: As Figure 3.4. Top: ACS/WFC F435W image, M31N 2010-01a progenitor position determined from LT B-band data. Bottom: F435W FLT image with M31N 2010-01a progenitor position determined from post-outburst F475W data. ©AAS. Reproduced with permission.

3.4.25 M31N 2010-05a

Nova M31N 2010-05a was an Fe II type nova (Hornoch et al., 2010c) discovered on 2010 May 28 (Hornoch et al., 2010f). It had a *B*-band t_2 of 39 ± 17 (see Section 4.3.9) and the position of the nova was calculated to be $0^{\rm h}42^{\rm m}35^{\rm s}.899 \pm 0^{\rm s}.008$, $+41°16'38''.24 \pm 0''.04$ from *B*-band LT data taken on 2010 June 17.2. The location of M31N 2010-05a was observed by *HST* with ACS/WFC using an F435W filter on 2004 January 23. There is one resolvable source within 3σ of the calculated position. This source is 1.939 ACS/WFC pixels, $0.053''$ or 2.10σ away from the defined position. The local population density suggests there is a 36.9% probability of an object alignment this close occurring by chance. The data has a limiting F435W magnitude of 25.8. This location of this quiescent system is shown in Figure 3.17.

3.4.26 M31N 2010-09b

Nova M31N 2010-09b was discovered on 2010 September 30 (Nishiyama et al., 2010a) and belonged to the Fe II spectroscopic class (Shafter et al., 2010c,e). A *B*-band t_2 of 3.8 ± 0.2 was calculated from LT data (see Section 4.3.10). From *B*-band LT images taken on 2010 October 5.1, a position of $0^{\rm h}43^{\rm m}45^{\rm s}.545 \pm 0^{\rm s}.008$, $+41°07'54''.5 \pm 0''.1$ was derived. The *HST* images used to locate M31N 2010-09b in quiescence were taken with ACS/WFC using F814W and F475W filters on 2011 December 9. Even though the *HST* data were taken only about 14 months after the outburst, this very fast nova should have returned to quiescence by then. There is a resolvable source within 1σ of the calculated position and another resolvable source within 2σ. The closest source is 0.579 ACS/WFC pixels, $0.029''$ or 0.55σ away from the defined position. The local population density, which is resolvable down to an F814W magnitude of 26.3, suggests there is a 2.6% chance of coincidence at such a separation. This source had an F814W magnitude of 24.7 ± 0.1 and F475W magnitude of 26.30 ± 0.07. This gives a B-band magnitude of 27.1 ± 0.1, I-band magnitude of 24.7 ± 0.1 and $(B - I)$ colour of 2.4 ± 0.1. We can see from Darnley (2005) that a nova at the apparent position of M31N 2010-09b would be subject to r'-band extinction of $A_{r'} = 0.63$ if it were

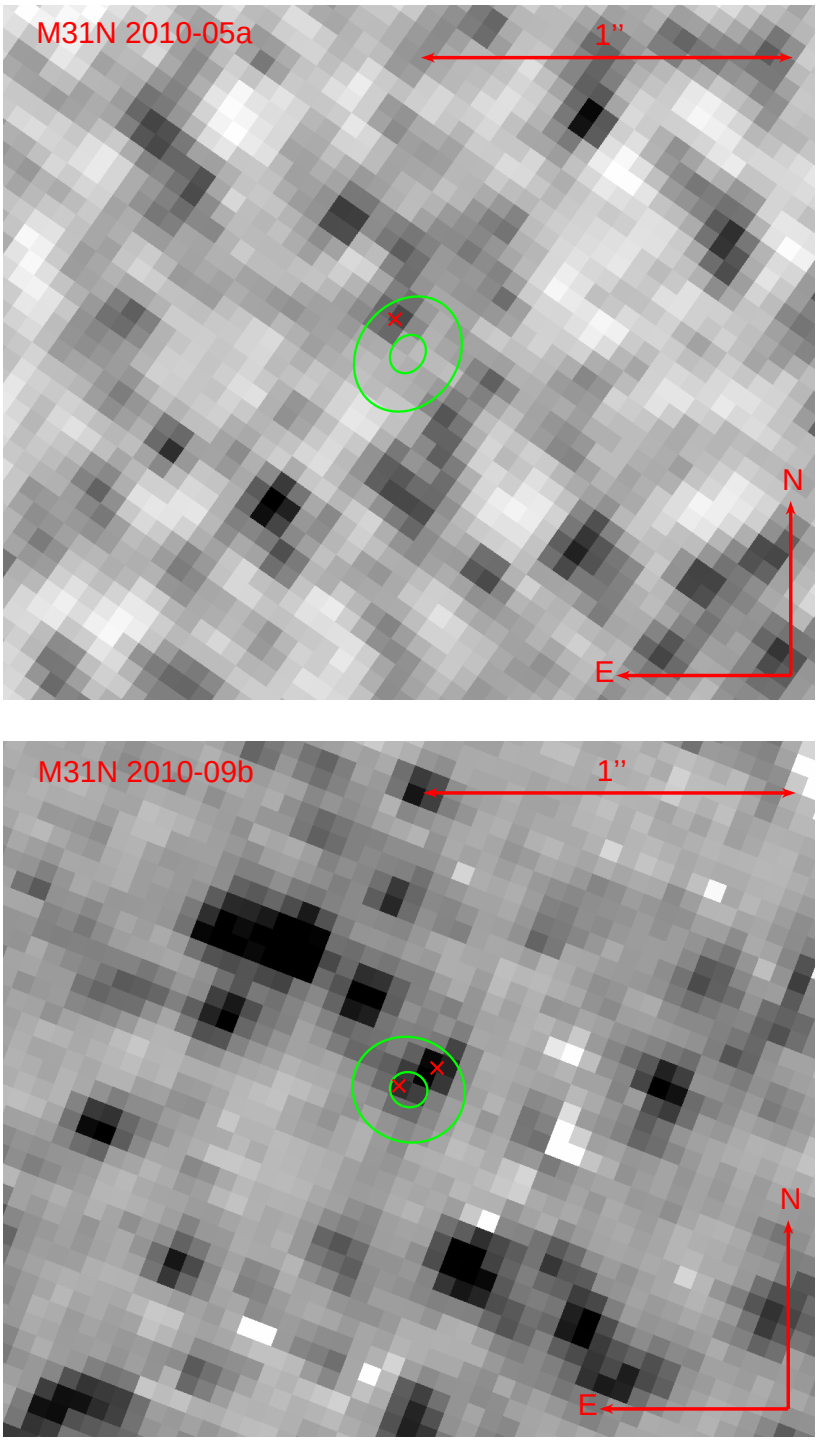

Figure 3.17: As Figure 3.4. Top: ACS/WFC F435W image, M31N 2010-05a progenitor position determined from LT B-band data. Bottom: ACS/WFC F475W image, M31N 2010-09b progenitor position determined from LT B-band data.

at the far side of the galaxy. Therefore a *B*-band magnitude of 26.6 ± 0.5, *I*-band magnitude of 24.5 ± 0.2 and $(B - I)$ colour of 2.2 ± 0.3 were calculated. The other source is 2.264 ACS/WFC pixels or 2.05σ away from the defined position. The local population density suggests there is a 36.3% chance of a resolvable source being within this distance of a random point in the image. If the closest source is the nova, it had already returned to quiescence by 2011 August 3, when *HST* data showed it to have an F814W magnitude of 25.05 ± 0.06. The location of M31N 2010-09b is shown in Figure 3.17.

3.4.27 M31N 2010-10a

Nova M31N 2010-10a was discovered on 2010 October 5 by Nishiyama et al. (2010b). Spectra taken by Shafter et al. (2010e) showed it to be an Fe II type nova. *V*-band LT data taken on 2010 October 10.1 was used to calculate the position of the nova to be $0^{\rm h}42^{\rm m}45^{\rm s}.82 \pm 0^{\rm s}.03$, $+41°24'22''.0 \pm 0''.1$. *HST* observed this location with ACS/WFC using F475W and F814W filters on 2012 December 15. Although the *HST* data were taken after the outburst (over two years), the nova has a maximum B-band t_2 of 16 ± 2 days (see Section 4.3.11), so would have faded back to quiescence by the time the *HST* data were taken. There is a resolvable source just outside 1σ of the calculated position and no other resolvable source within 3σ. The source is 1.181 ACS/WFC pixels, $0.059''$ or 1.20σ away from the defined position. The local population density suggests there is a 11.2% chance of coincidence at such a separation. The location of this quiescent system is shown in Figure 3.18.

3.4.28 M31N 2010-10b

Nova M31N 2010-10b was a member of the Fe II spectroscopic class (Shafter et al., 2010f) and was discovered on 2010 October 6.932 by Hornoch et al. (2010a). The LT images used to locate the position of the nova in the archival *HST* images were taken using a *V*-band filter on 2010 October 11.1, from which the position of the nova was

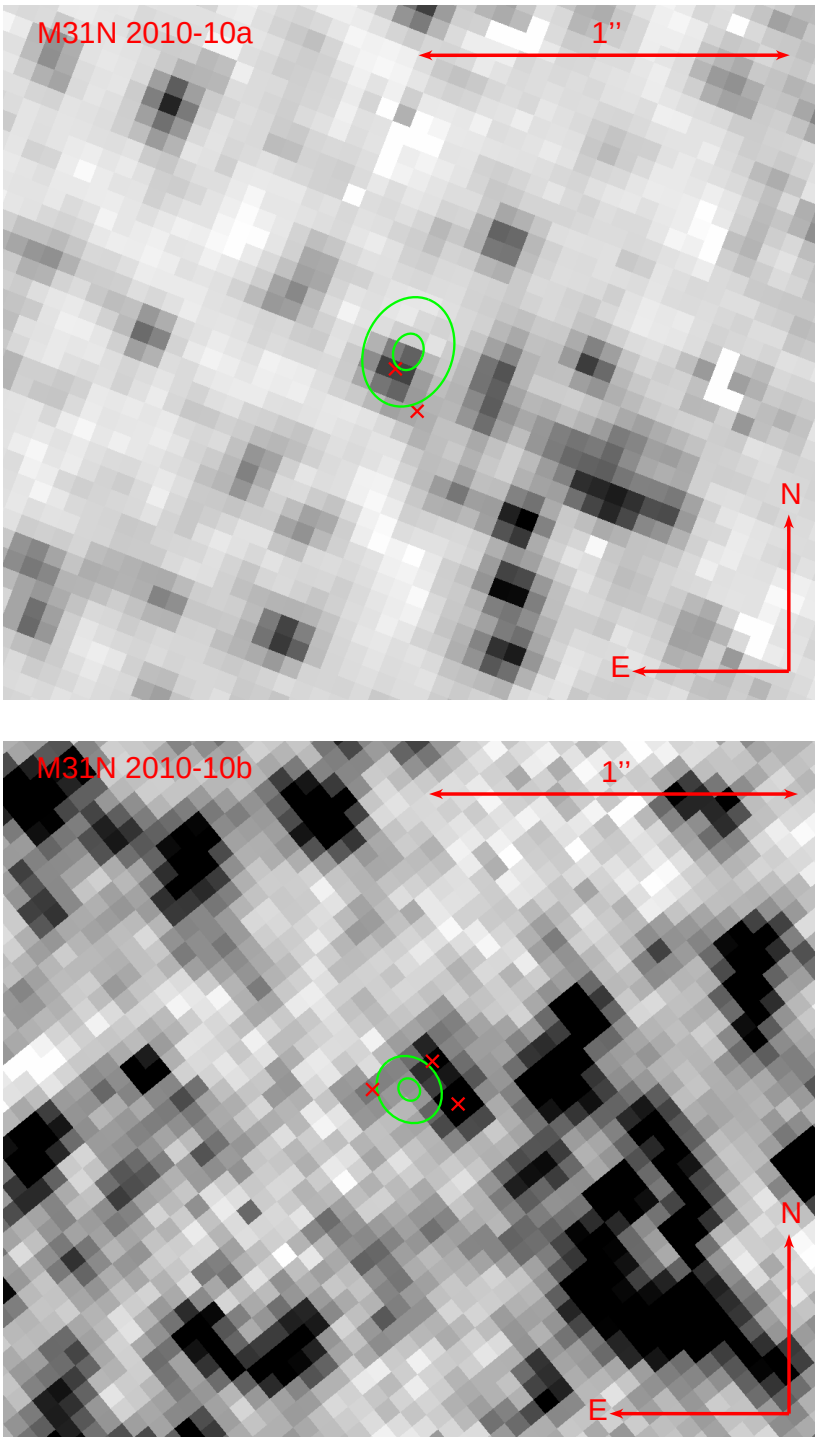

Figure 3.18: As Figure 3.4. Top: ACS/WFC F475W image, M31N 2010-10a progenitor position determined from LT B-band data. Bottom: ACS/WFC F555W image, M31N 2010-10b progenitor position determined from LT V-band data. ©AAS. Reproduced with permission.

calculated to be $0^{\rm h}42^{\rm m}41^{\rm s}.55 \pm 0^{\rm s}.02$, $+41°03'27''.7 \pm 0''.1$. The *HST* data were taken with ACS/WFC using F555W and F814W filters on 2004 August 14. There are no resolvable sources within 3σ of the calculated position, the closest resolvable source being 1.968 ACS/WFC pixels, $0.099''$ or 3.60σ away from the defined position. The local population density suggests there is a 33.4% probability of such an alignment occurring by chance, with the data being resolved down two F814W = 26.1. The location of M31N 2010-10b is shown in Figure 3.18.

3.4.29 M31N 2010-10c

Nova M31N 2010-10c was discovered by J. Ruan and X. Gao on frames taken around 2010 October 13.5566 UT (Ruan et al., 2010), with a spectrum taken a few days later confirming it as an Fe II nova (Shafter et al., 2010d). The nova was calculated to be at $0^{\rm h}44^{\rm m}26^{\rm s}.575 \pm 0^{\rm s}.008$, $+41°31'13''.6 \pm 0''.1$ from *B*-band LT data taken on 2010 October 22.1 UT. The location of M31N 2010-10c was observed by *HST* with ACS/WFC using F606W and F435W filters on 2005 July 22. There are three resolvable sources within 2σ of the calculated position and another resolvable source within 3σ. The closest resolvable source is 1.083 ACS/WFC pixels, $0.055''$ or 1.05σ away from the defined position. The local population density, which is resolvable down to an F606W magnitude of 27.1, suggests there is a 12.4% probability of such an alignment occurring by chance. The second closest resolvable source is 1.988 ACS/WFC pixels, $0.100''$ or 1.90σ away from the defined position. The local population density suggests there is a 38.5% probability of chance alignment and the third closest source is 2.084 ACS/WFC pixels, $0.105''$ or 2.00σ away from the defined position, with a 41.6% probability of chance alignment. The fourth closest resolvable source is 3.405 ACS/WFC pixels, $0.171''$ or 3.00σ away from the defined position, with a 78.6% probability of chance alignment. The location of M31N 2010-10c, with the four closest progenitor candidates, is shown in Figure 3.19.

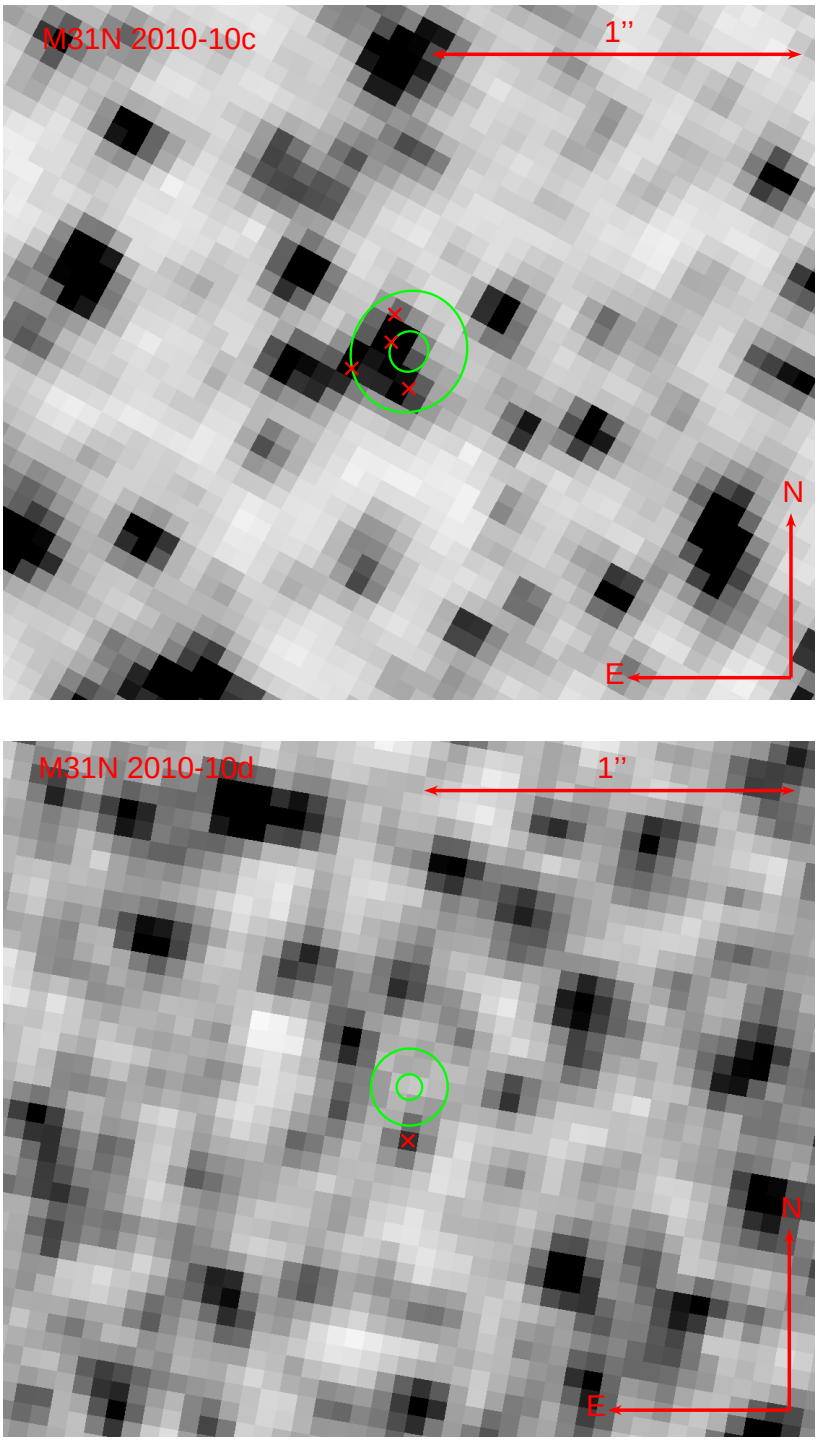

Figure 3.19: As Figure 3.4. Top: ACS/WFC F606W image, M31N 2010-10c progenitor position determined from LT V-band data. Bottom: ACS/WFC F435W image, M31N 2010-10d progenitor position determined from LT B-band data. ©AAS. Reproduced with permission.

3.4.30 M31N 2010-10d

Nova M31N 2010-10d was first observed to be in outburst on images taken on 2010 October 28 (Hornoch et al., 2010b) and was confirmed as an Fe II type nova by Shafter et al. (2010b). The position of the nova, as calculated from *B*-band LT data taken on 2010 October 30.0 UT, was $0^{\rm h}42^{\rm m}36^{\rm s}.914 \pm 0^{\rm s}.008$, $+41^\circ19'28''.9 \pm 0''.1$. The *HST* images used to locate M31N 2010-10d in quiescence were taken with ACS/WFC using an F435W filter on 2004 June 14. There are no resolvable sources within 3σ of the calculated position, with the closest resolvable source being 2.992 ACS/WFC pixels, $0.151''$ or 4.25σ away from the defined position. The local population density, which is resolved down to an F435W magnitude of 26.3, suggests that the coincidence probability at this separation is 65.6%. The location of this system is shown in Figure 3.19. It can clearly be seen from the *HST* data taken during outburst (see Section 4.3.12) that this source is not the progenitor of M31N 2010-10d.

3.4.31 M31N 2010-10e

Nova M31N 2010-10e was discovered on 2010 October 31.727 by K. Hornoch and P. Hornochova and has been suggested as another outburst of the RN candidate M31N 1963-09c (which also had coincident outbursts in 1968 and 2001; Pietsch et al., 2010a; Shafter et al., 2010a; Shafter et al., in preparation). A SSS phase was detected 15 days post-outburst (Pietsch et al., 2010b), with the X-ray spectra being consistent with a high-mass WD (Henze et al., 2014b). *V*-band observations of this 2010 outburst taken on 2010 November 7.0, gave the position of the system as $0^{\rm h}42^{\rm m}57^{\rm s}.75 \pm 0^{\rm s}.01$, $+41^\circ08'12''.3 \pm 0''.1$. The *HST* images used to search for the quiescent system were taken with ACS/WFC using F814W and F555W filters on 2004 August 17. There is a resolvable source within 1σ of the calculated position, one within 2σ and another within 3σ. The closest resolvable source is 1.216 ACS/WFC pixels, $0.061''$ or 0.80σ away from the defined position. The local population density suggests there is a 15.6% probability of such an alignment occurring by chance. The next closest source is 1.859 ACS/WFC pixels, $0.094''$ or 1.45σ away from the defined position, with a 34.4% prob-

ability of chance alignment. The third closest source is 4.310 ACS/WFC pixels, $0.217''$ or 2.75σ away from the defined position, with a 92.3% probability of chance alignment. The *HST* data are resolvable down to an F814W magnitude of 25.9. The position of M31N 2010-10e is shown in Figure 3.20. The relatively large errors on the position of the quiescent nova are caused by the nova being very faint in the LT images. This is simply because M31N 2010-10e was a fast novae and the first LT images were taken several days after discovery.

3.4.32 M31N 2011-10a

Nova M31N 2011-10a was an Fe II nova (Cao et al., 2011; Cao, 2011) discovered on 2011 October 2[15]. The LT data used to search for the progenitor system in the archival *HST* data were taken using a *B*-band filter on 2011 October 26.1, from which the position of the nova was calculated to be $0^{\rm h}42^{\rm m}57^{\rm s}.13 \pm 0^{\rm s}.01$, $+41^\circ17'10''.9 \pm 0''.1$. The *HST* images themselves were taken with ACS/WFC using F814W and F475W filters on 2010 December 14. There are no resolvable sources within 3σ of the calculated position and the closest resolvable source in the F475W image is 2.540 ACS/WFC pixels, $0.128''$ or 4.80σ away from the defined position. The source was not detected in the F814W filter due to problems with the photometry, leading to a magnitude limit of 22.6, whereas the F475W magnitude limit was 26.1. The local population density suggests that the coincidence probability at this separation is 46.8%. The location of this quiescent system is shown in Figure 3.20.

3.4.33 M31N 2011-10d

Nova M31N 2011-10d was discovered on 2011 October 20 (Ovcharov et al., 2011), with spectra confirming it as a likely member of the Fe II spectroscopic class (Shafter et al., 2011c,d). Using *B*-band LT data taken on 2011 October 26.1, the position of the nova was calculated to be $0^{\rm h}42^{\rm m}55^{\rm s}.74 \pm 0^{\rm s}.01$, $+41^\circ17'52''.3 \pm 0''.1$. This location was

[15] `http://www.cbat.eps.harvard.edu/unconf/followups/J00425701+4117095.html`

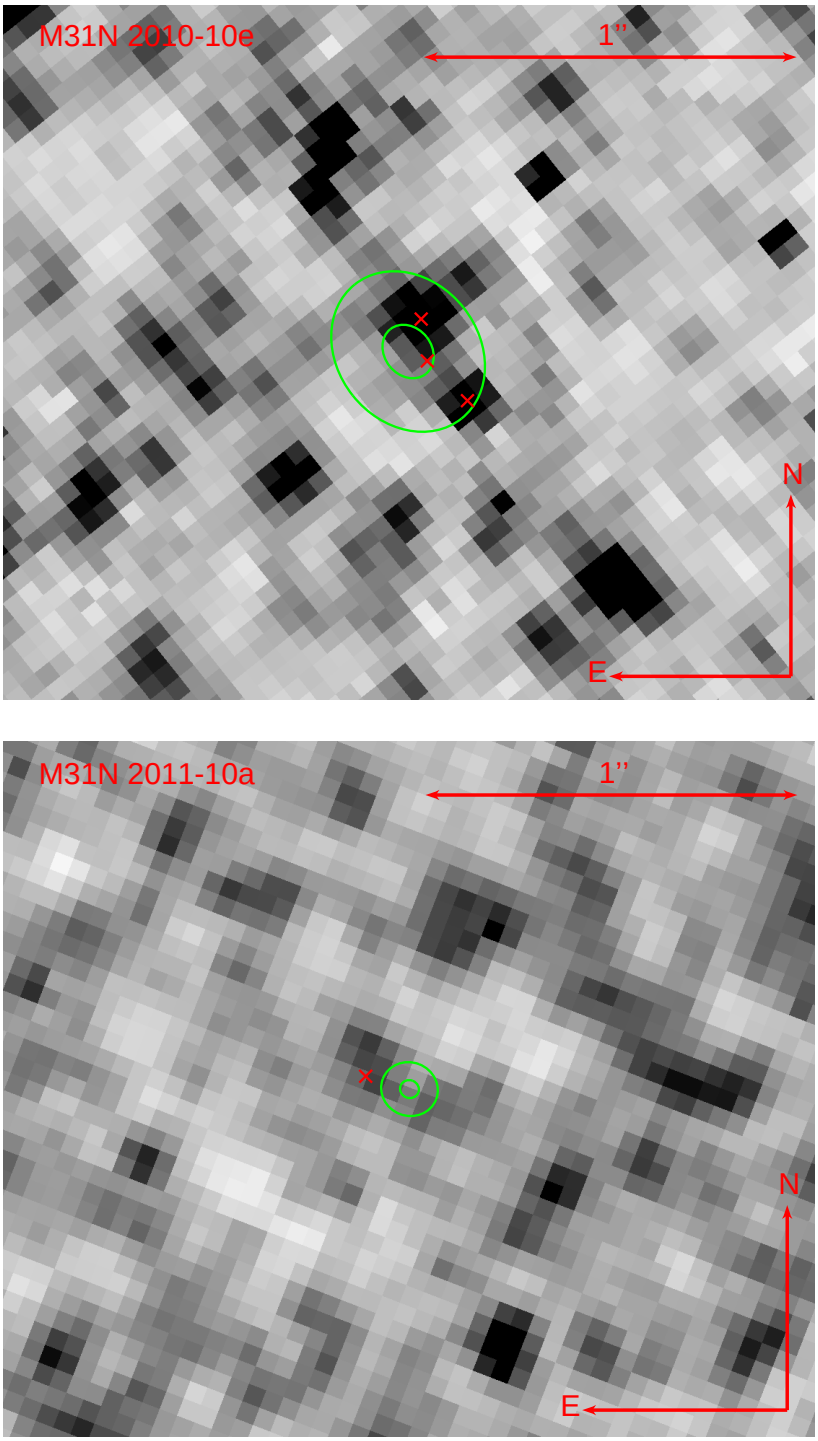

Figure 3.20: As Figure 3.4. Top: ACS/WFC F555W image, M31N 2010-10e progenitor position determined from LT V-band data. Bottom: ACS/WFC F475W image, M31N 2011-10a progenitor position determined from LT B-band data.

observed by *HST* with ACS/WFC using F814W and F475W filters on 2010 December 14. There are no resolvable sources within 3σ of the calculated position, with the closest resolvable source being 1.400 ACS/WFC pixels, $0.070''$ or 3.25σ away from the defined position. The local population density, which has an F435W limiting magnitude of 26.1, suggests there is a 16.4% probability of such an alignment occurring by chance. The images have an F475W limiting magnitude of 26.1, although as with M31N 2011-10a, the F814W limiting magnitude is only 22.6. The location of the quiescent system is shown in Figure 3.21.

3.4.34 M31N 2011-12a

Nova M31N 2011-12a was discovered on an image taken on 2011 December 7.08 UT by Cao & Kasliwal (2011). It was classified as an Fe II system, although unusually, it did show strong He I emission (Shafter et al., 2011a). *V*-band LT images taken on 2011 December 26.8 UT gave the position of the nova as $0^{\rm h}42^{\rm m}06^{\rm s}.277 \pm 0^{\rm s}.009$, $+41^\circ01'28''.7 \pm 0''.1$. M31N 2011-12a was searched for in quiescence using *HST* images taken with WFPC2 using F814W and F555W filters on 2004 August 14. There is a resolvable source within 2σ of the calculated position and no other resolvable source within 3σ. The source is 1.129 WFPC2 pixels, $0.113''$ or 1.15σ away from the defined position. The local population density, which is resolved down to an F814W magnitude of 24.2, suggests there is a 3.6% probability of such an alignment occurring by chance. The source had an F814W magnitude of 23.67 ± 0.07 and an F555W magnitude of 21.58 ± 0.03. This gives a V-band magnitude of 23.67 ± 0.07 and an I-band magnitude of 21.44 ± 0.04, with $(V - I)$ colour 2.16 ± 0.08. However, from the overall distribution of stars in the M31 field in ACS/WFC, a source would be expected to be at least as close as $0''.113$ in a typical ACS/WFC image about 35% of the time. Therefore such a detection in ACS/WFC would be relatively insignificant. For this reason M31N 2011-12a is not included in the list of systems with a high likelihood of a recovered progenitor. The location of M31N 2011-12a is shown in Figure 3.21.

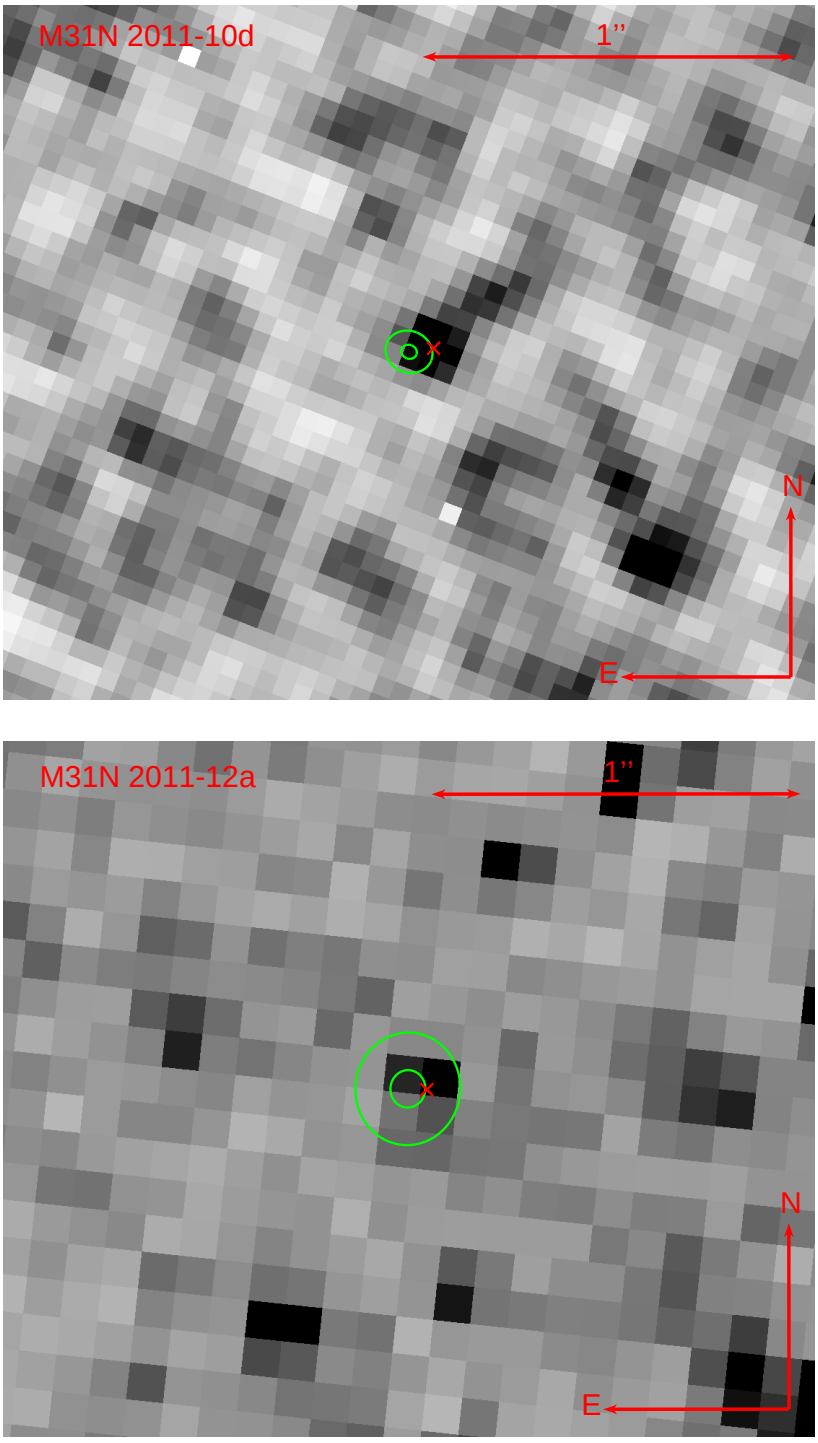

Figure 3.21: As Figure 3.4. Top: ACS/WFC F475W image, M31N 2011-10d progenitor position determined from LT B-band data. Bottom: WFPC2 F555W image, M31N 2011-12a progenitor position determined from LT V-band data. ©AAS. Reproduced with permission.

3.4.35 M31N 2012-01a

Nova M31N 2012-01a was discovered on 2012 January 6 by Cao & Kasliwal (2012) and belonged to the Fe II spectroscopic class (Shafter et al., 2012b). The position of the nova was calculated to be $0^{\rm h}41^{\rm m}41^{\rm s}.01 \pm 0^{\rm s}.01$, $+41°19'44''.3 \pm 0''.1$ from *V*-band LT data taken on 2012 January 10.8 UT. The *HST* images used to locate M31N 2012-01a in quiescence were taken with ACS/WFC using F814W and F555W filters on 2011 February 16 and there is one resolvable source within 3σ of the calculated *HST* position. The source is 1.712 ACS/WFC pixels, $0.086''$ or 2.50σ away from the defined position. The local population density suggests there is a 22.0% probability of such an alignment occurring by chance. Figure 3.2 shows the nova in the combined LT image taken during outburst and how the coincident *HST* field overlaps its position. The location of the quiescent system is shown in Figure 3.22.

3.4.36 M31N 2012-09a

Nova M31N 2012-09a was discovered on 2012 September 8.770 UT by Hornoch & Vrastil (2012), with a spectrum confirming it as an Fe IIb nova (Shafter et al., 2012d). This system is a recurrent candidate, with the first observed outburst being M31N 1984-07a (Pietsch et al., 2007b; Shafter et al., 2012d). The LT images used to locate the nova in archival *HST* images were taken using an r'-band filter on 2012 September 10.0 UT, which gave its position as $0^{\rm h}42^{\rm m}47^{\rm s}.16 \pm 0^{\rm s}.01$, $+41°16'19''.63 \pm 0''.07$. The *HST* images were taken with ACS/WFC using an F814W filter on 2010 December 20 and 24. There are no resolvable sources within 3σ of the calculated position, with the closest resolvable source being 2.152 ACS/WFC pixels, $0.108''$ or 3.65σ away from the defined position. The local population density suggests the coincidence probability at this separation is 32.8%. The F475W limiting magnitude of this data is 25.8, with that of F814W being 22.2. The location of this quiescent system is shown in Figure 3.22.

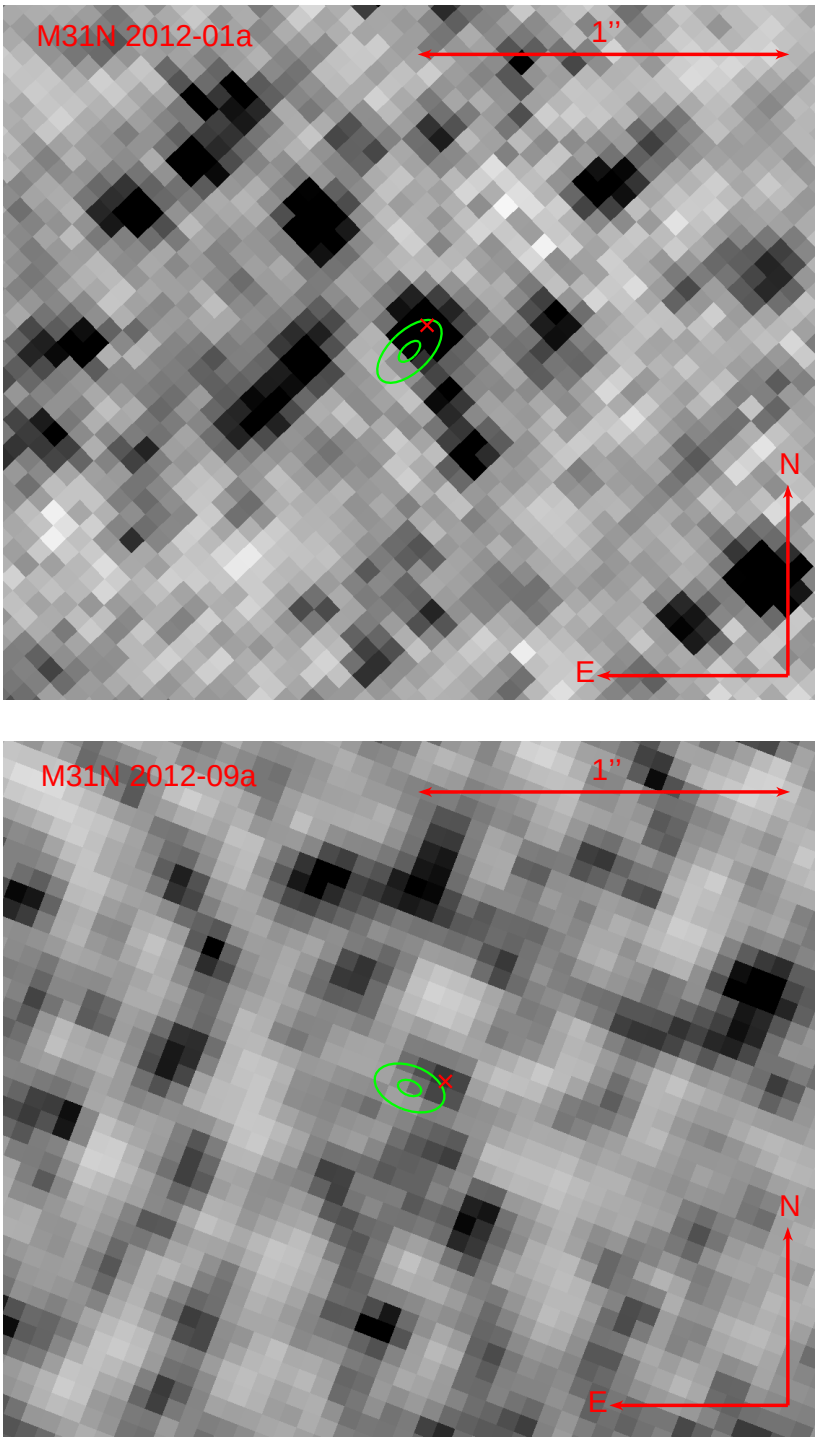

Figure 3.22: As Figure 3.4. Top: ACS/WFC F555W image, M31N 2012-01a progenitor position determined from LT V-band data. Bottom: ACS/WFC F814W image, M31N 2012-09a progenitor position determined from LT r'-band data.

3.4.37 M31N 2012-09b

Hornoch (2012) discovered M31N 2012-09b on 2012 September 17.781 UT, with Shafter et al. (2012f) classifying it as an Fe IIb type nova. LT images taken using an r'-band filter on 2012 September 18.2 UT were used to calculate a position of $0^{\rm h}42^{\rm m}50^{\rm s}.98 \pm 0^{\rm s}.02$, $+41^\circ14'09''.7 \pm 0''.2$ for the nova. The position of this quiescent nova was located using *HST* images taken with ACS/WFC using an F814W filter on 2010 December 20. There are no resolvable sources within 3σ of the calculated position. The closest resolvable source is 3.659 ACS/WFC pixels, $0.184''$ or 10.55σ away from the defined position. The local population density, which is resolvable down to an F814W magnitude of 24.6, suggests there is a 78.4% probability of such an alignment occurring by chance. The F814W limiting magnitude was 24.6, although that of F475W was 26.0 and there were no sources closer to the position of the nova in this filter. The position of this quiescent system is shown in Figure 3.23.

3.4.38 M31N 2012-12a

Nova M31N 2012-12a was an Fe II nova (Shafter et al., 2012e) first visible on images taken 2012 December 10.030 UT (Hornoch & Galad, 2012). The position of the nova was calculated to be $0^{\rm h}42^{\rm m}49^{\rm s}.13 \pm 0^{\rm s}.02$, $+41^\circ17'02''.5 \pm 0''.1$ from r'-band LT data taken on 2012 December 20.9 UT. The *HST* images used to find the position of M31N 2012-12a in quiescence were taken with ACS/WFC using F814W and F475W filters on 2010 December 14. There is a resolvable source at 3.00σ of the calculated position. The source is 1.532 ACS/WFC pixels or $0.077''$ away from the defined position, with the local population density suggesting that the coincidence probability at this separation is 19.9%. The F475W limiting magnitude is 25.6 and the F814W limiting magnitude is 22.3. The location of M31N 2012-12a is shown in Figure 3.23.

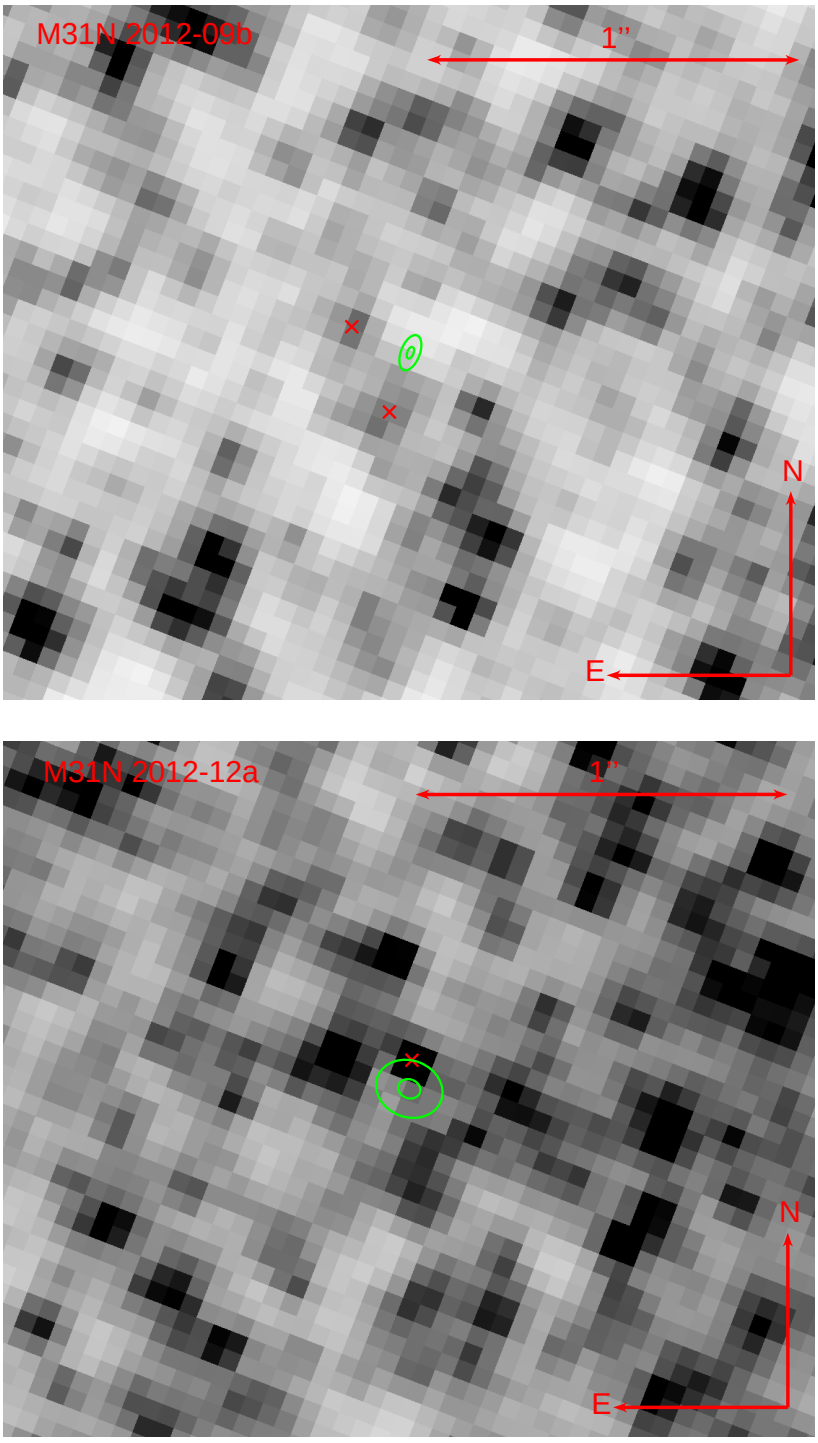

Figure 3.23: As Figure 3.4. Top: ACS/WFC F814W image, M31N 2012-09b progenitor position determined from LT r'-band data. Bottom: ACS/WFC F814W image, M31N 2012-12a progenitor position determined from LT r'-band data. ©AAS. Reproduced with permission.

3.5 Discussion

Eleven nova systems (29% of the original catalogue of 38 novae) have a resolvable source close enough for the probability of them being chance alignments to be $\leq 5\%$ in each case, and are therefore likely to be the progenitor systems. These novae with candidate progenitor systems are M31N 2007-02b, 2007-10a, 2007-11b, 2007-11d, 2007-11e, 2007-12a, 2007-12b, 2009-08a, -11d, 2010-01a and 2010-09b (the progenitor system of M31N 2007-12b had already been identified by Bode et al., 2009). The photometry of these eleven candidate progenitor systems is summarised in Tables 3.4 and 3.5.

Nova	Broadband Photometry					
	F435W	F475W	F555W	F606W	F625W	F814W
2007-02b	-	-	-	25.95 ± 0.05	-	24.82 ± 0.03
2007-10a	-	-	-	-	22.397 ± 0.008	-
2007-11b	-	-	22.6 ± 0.1	-	-	20.44 ± 0.06
2007-11d	-	24.46 ± 0.04	-	-	-	21.387 ± 0.005
2007-11e	-	25.5 ± 0.1	-	-	-	24.19 ± 0.03
2007-12a	-	25.98 ± 0.08	-	-	-	25.3 ± 0.1
2007-12b	-	25.36 ± 0.04	-	-	-	23.79 ± 0.04
2009-08a	25.50 ± 0.05	-	-	-	-	-
2009-11d	-	25.67 ± 0.04	-	-	-	25.1 ± 0.2
2010-01a	24.79 ± 0.04	-	-	-	-	-
2010-09b	-	26.30 ± 0.07	-	-	-	24.7 ± 0.1

Table 3.4: Raw photometry in native ACS/WFC or WFPC2 system of progenitor candidates that have a less than 5% probability of occurring by chance.

The Galactic RNe RS Oph (Anupama & Mikołajewska, 1999), T CrB (Kenyon & Fernandez-Castro, 1987), V3890 Sgr and V745 Sco (Harrison et al., 1993) all have confirmed red giant secondaries, with V2487 Oph (Darnley et al., 2012), also thought to be a RG-novae. Recently, the CNe V794 Oph, EU Sct and V3964 Sgr have also been spectroscopically confirmed as RG-novae (Surina, 2014). It is believed both KT Eri (Jurdana-Šepić et al., 2012) and V2487 Oph (Darnley et al., 2012) also harbour red giant companions. Therefore these RG-novae or suspected RG-novae make up only $\sim 2.5\%$ of the approximately 400 Galactic novae discovered (Darnley et al., 2012), however in many cases the systems have simply not been observed in quiescence and this suggests the RG-nova rate in the Galaxy is probably somewhat higher, with no study systematic enough to produce a reliable population estimate having yet been conducted.

Nova	Broadband Photometry				Colour	
	B	*V*	*R*	*I*	*(B-I)*	*(V-I)*
M31N 2007-02b	-	26.0 ± 0.4	-	24.6 ± 0.2	-	1.4 ± 0.2
M31N 2007-10a	-	-	~ 22.0	-	-	-
M31N 2007-11b	-	22.3 ± 0.3	-	20.1 ± 0.2	-	2.1 ± 0.2
M31N 2007-11d	25.0 ± 0.5	-	-	21.3 ± 0.2	3.8 ± 0.3	-
M31N 2007-11e	26.0 ± 0.3	-	-	24.1 ± 0.1	1.9 ± 0.2	-
M31N 2007-12a	25.7 ± 0.5	-	-	25.1 ± 0.2	0.6 ± 0.3	-
M31N 2007-12b	25.7 ± 0.5	-	-	23.6 ± 0.2	2.1 ± 0.3	-
M31N 2009-08a	~ 25.5	-	-	-	-	-
M31N 2009-11d	25.4 ± 0.4	-	-	24.9 ± 0.3	0.5 ± 0.3	-
M31N 2010-01a	~ 24.5	-	-	-	-	-
M31N 2010-09b	26.6 ± 0.5	-	-	24.5 ± 0.2	2.2 ± 0.3	-

Table 3.5: Progenitor photometry as in Table 3.4 converted to *UBVRI* system, where available. The magnitudes were transformed using conversions from Sirianni et al. (2005). These magnitude also include the extinction internal to M31.

Along with the RG-novae that have typical nova light curves, there are very slow symbiotic novae such as PU Vul and RT Ser that can take decades to evolve. A sub-class of these very slow novae are D type symbiotic novae that contain Mira variables. RR Tel and RX Pup are such systems, although V407 Cyg is also thought to contain a Mira and its light curve evolution was more typical of CNe and RNe (see Munari et al., 2011 for a discussion on its 2010 nova outburst).

Eight of the eleven candidate progenitor systems identified by this survey have quiescent photometry in two bands. As such, the positions of these systems are plotted in the colour–magnitude diagrams shown in Figure 3.24. Inspection of this figure shows that the majority of progenitor candidates (six of eight) lie on or near the red-giant branch. Of course, it should be noted that if we had simply chosen a random sample of resolved stars in *HST* data of M31 a high proportion of them would still be expected to be on the red-giant branch. The other two candidate progenitor systems (M31N 2007-12a and 2010-09b) both have $(B - I) < 1$. The colour–magnitude diagram position of these two quiescent systems is consistent with high mass, luminous main-sequence stars. However, as is also indicated in Figure 3.24, this position is similar to a pair of Galactic RG-novae. These Galactic novae are KT Eri, and the RN V2487 Oph. The particularly blue colour of KT Eri and V2487 Oph is likely due to a bright accretion disk inclined towards the observer. This pair of M31 quiescent systems is also coincident with the colour–magnitude position of a number of SG-novae or suspected SG-novae. So if we are indeed observing M31N 2007-12a and 2009-11d in quiescence

they may be RG-novae with colours affected by a strong accretion disk or they may be luminous quiescent SG-novae similar to the recurrent SG-nova U Sco.

In Figure 3.25, we show the spatial distribution of the novae in our survey as in Figure 3.1, but also indicate the eleven systems with candidate progenitor systems. This shows that a much higher proportion of novae in the disk appear to have a recovered progenitor when compared to the systems in the central bulge. Although increased crowding near the centre of M31 (rendering any detection less significant) may have some influence on this, it does not seem to be the main factor. Indeed, the relationship between the distance of the nearest source from the nova and the probability of a chance alignment is largely uniform for the regions of M31 studied in this work. This indicates that there may be a higher proportion of RG-novae in younger stellar populations. Although of course the background light is brighter near the centre of M31 and this may obscure some faint sources that would have been visible in the outer regions of the galaxy.

As is noted in Section 3.4, there are problems with using the WFPC2 data. For example, as can be seen in Section 3.4.34, M31N 2011-12a had a progenitor candidate detected that only had 3.6% probability of such an alignment occurring by chance in a WFPC2 image. However, due to the relatively bright limiting magnitude of the WFPC2 data, the same detection in a typical ACS/WFC image would be relatively insignificant. It could also be the case that, for a system where no candidate was detected in WFPC2, if the same region was imaged with ACS/WFC, it may reveal a coincident source.

The most direct method to identify RNe is to find coincident outbursts. However, due to the large population of M31 nova candidates (over 900 have been discovered over the last 100 years[16]) many coincident sources will simply be chance alignments (see Shafter et al., 2013). Therefore the positions published here may help eliminate some of the recurrent candidates that are different systems aligned by chance.

There are three RN candidates in our catalogue: M31N 2009-11b, M31N 2010-10e and

[16] See Pietsch (2010) and
`http://www.mpe.mpg.de/~m31novae/opt/m31/index.php`

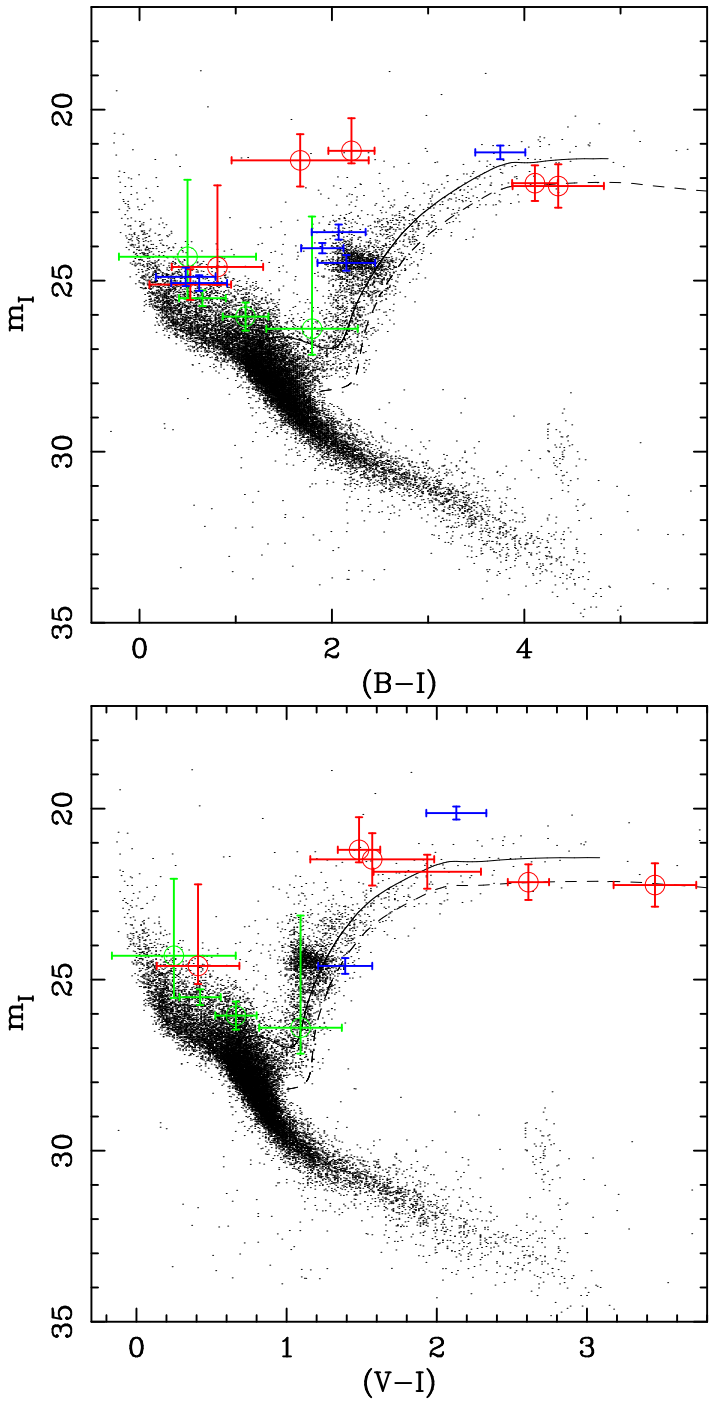

Figure 3.24: Colour−magnitude diagrams showing the *Hipparcos* data (Perryman & ESA, 1997) shifted to the distance of M31, assuming $(m-M)_0 = 24.43$ (Freedman & Madore, 1990) and extinction of $E_{B-V} = 0.1$ mag towards M31 (Stark et al., 1992). Possible extinction internal to M31 is calculated for each nova separately and is discussed in the text. The blue points show the M31 progenitor candidates found in this work. The red points represent Galactic RG-nova and the green points represent Galactic SG-novae (see Schaefer, 2010, Darnley et al., 2012 and references therein). Top plot: $(B-I)$ colour against *I*-band magnitude. Bottom plot: $(V-I)$ colour against *I*-band magnitude.

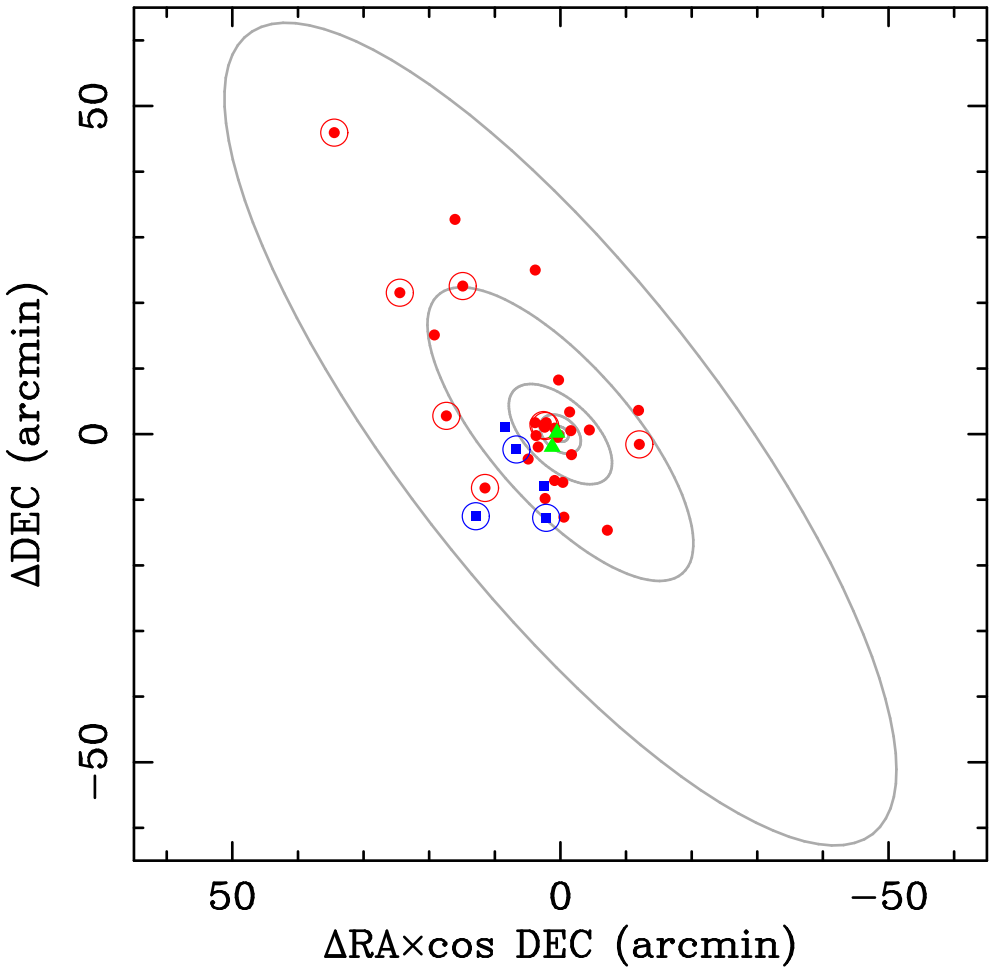

Figure 3.25: The spatial distribution and spectral class of the novae in our catalogue as in Figure 3.1, but novae that have a high likelihood of a recovered progenitor are further circled.

M31N 2012-09a (see also Section 3.4). It might be expected that these novae would have a higher chance of harbouring red giant secondaries, as in our Galaxy half of the ten RNe are RG-novae (see e.g. Darnley et al., 2012). It can be seen in Figure 3.7 that there is no resolvable source within 3σ of the position of M31N 2009-11b, although the limiting magnitude of the data is 23.8, meaning that we can exclude a luminous red giant system (such as one similar to RS Oph) as the progenitor, but it is possible that the system may contain a fainter red giant. Although M31N 2010-10e does not have a progenitor we can locate with a high confidence, it can be seen from Figure 3.9 that a red giant companion is not ruled out for this system. Indeed there is a faint candidate within 1σ and a relatively bright source just outside 1σ. M31N 2012-09a does not have any sources within 3σ of the calculated position, although the limiting magnitudes indicate a lower-luminosity red giant companion may not be resolvable in the data.

We can however all but rule out M31N 2006-11a, 2008-10b, 2009-08b, 2009-11a, 2009-11c, 2009-11e and 2010-10b as RG-novae. This was done by first ensuring all of the red-giant branch would have been resolvable in the *HST* image of the quiescent nova. Then by either the nearest source lying outside 3σ of the calculated position of the system or by using post-outburst images to compare to the respective quiescent images.

3.6 Conclusions

We have recovered the likely quiescent progenitor systems for eleven of the original 38 novae. For each of these systems the probability of the progenitor candidate being a chance alignment is $< 5\%$. These systems are M31N 2007-02b, 2007-10a, 2007-11b, 2007-11d, 2007-11e, 2007-12a, 2007-12b, 2009-08a, 2009-11d, 2010-01a and 2010-09b. Photometry of each of these progenitors is consistent with quiescent Galactic RG-novae. The archival data also allow us to all but rule out red giant secondaries for seven novae, M31N 2006-11a, 2008-10b, 2009-08b, 2009-11a, 2009-11c, 2009-11e and 2010-10b.

This chapter has presented the search for M31 nova progenitors in M31 up to February 2013 and found the likely progenitors for several novae. Given such a high proportion of these M31 novae appear to be RG-novae, compared to what has been observed so far in our Galaxy, further investigation is warranted. Therefore a statistically based analysis was conducted on the results of the survey and is presented in Chapter 5. However, the thesis first presents light curves of a number of M31 novae in outburst, further utilising archival *HST* data.

Chapter 4

M31 Nova Light Curves

Some of the work described in this chapter has been accepted for publication in Williams, S. C., Darnley, M. J., Bode, M. F., Keen, A. and Shafter, A. W. (2014, ApJS, accepted, arXiv:1405.4874)

4.1 Introduction

The light curves of M31 novae presented here are mainly from LT data. The general properties of nova light curves are discussed in Section 1.3. In addition to LT data, when archival *HST* data were searched for in the work described in Chapter 3, several novae in the survey were found to have had *HST* data taken while they were in outburst. This allowed light curves to be extended deeper than is usually possible for extragalactic systems. Several of the novae had light curves already published by Shafter et al. (2011f) and here these are simply extended with the additional *HST* points.

4.2 LT Data Photometry

The LT data were reduced using a combination of IRAF and Starlink software and calibrated using (typically six or seven) secondary standard stars from Magnier et al.

(1992), Haiman et al. (1994) and Massey et al. (2006). The time (in days) it takes a nova to fade by two magnitudes (t_2) was calculated using different methods, depending on the data available. Typically, for well populated light curves, this involved a simple linear extrapolation of the data around maximum and around *n* magnitudes below the peak. Where different approaches were employed, this is described for the respective novae in Section 4.3. Several of the earlier novae with light curves presented below have t_2 values published by Shafter et al. (2011f), which are presented in Table 3.1. Crowded field photometry was carried out on the *HST* images, which is described in Section 3.3.4.

4.3 Individual Light Curves

4.3.1 M31N 2007-02b

Nova M31N 2007-02b had *HST* WFPC2 F555W data taken on 2007 September 13 (2454356 HJD). The nova had an F555W magnitude of 23.17 ± 0.08 at that time. This was added to the light curve published by Shafter et al. (2011f) and is shown in Figure 4.1.

4.3.2 M31N 2008-10b

Nova M31N 2008-10b had ACS/WFC F435W data taken on 2010 January 21 (2455217 HJD), when the nova had a magnitude of 24.36 ± 0.02. The system also had ACS/WFC data taken on 2010 July 23 (2455400 HJD) and 24 with F475W and F814W filters. On 2010 July 23, the nova had an F475W magnitude of 23.85 ± 0.02 and on July 24, it had an F475W magnitude of 24.05 ± 0.03. The nova was not resolvable in the F814W images, but for reference an upper limit for the magnitude was added, derived simply by measuring the magnitude of a relatively faint nearby star, clearly much brighter than the nova. This produced an F814W upper limit of 24.41 ± 0.07 on July 24. The points were added to the light curve published by Shafter et al. (2011f) and are shown

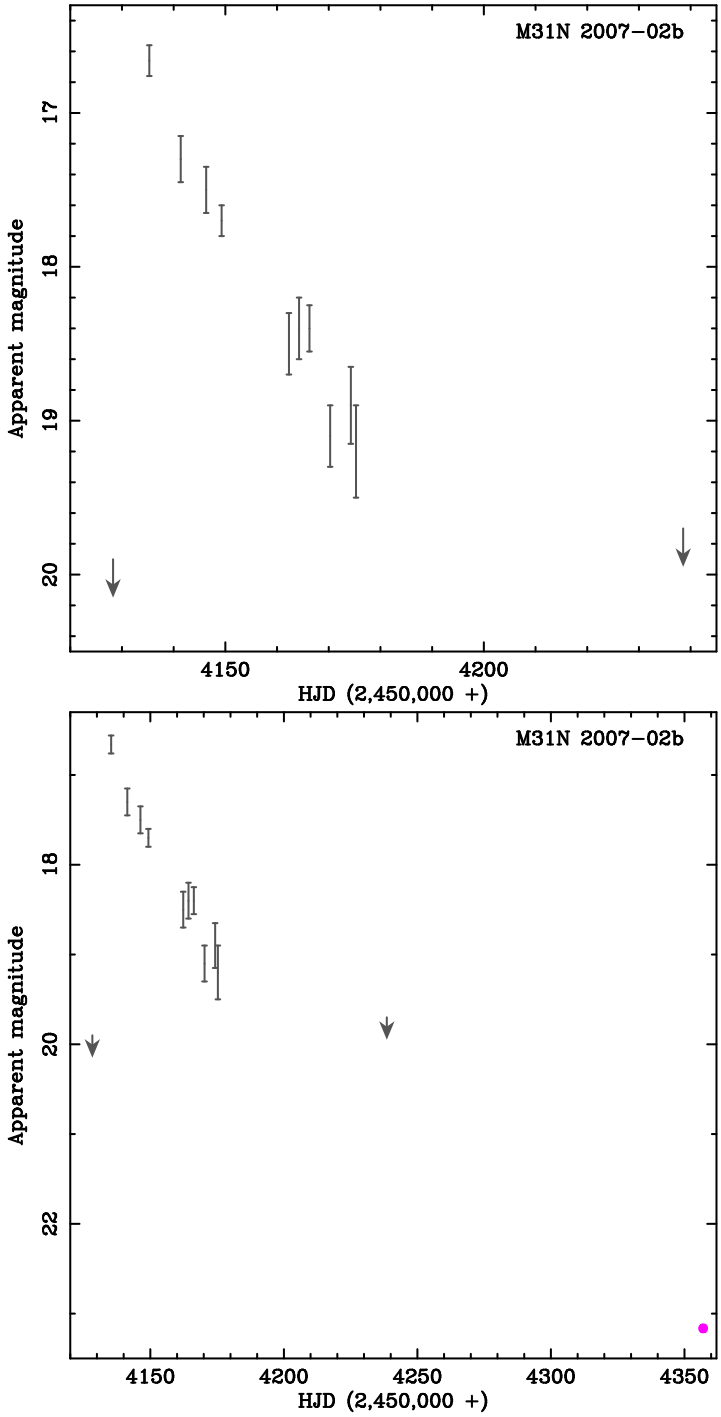

Figure 4.1: Light curve of M31N 2007-02b published by Shafter et al. (2011f), with an additional *HST* data point. Ground-based data filters are: *B*, royal blue; *V*, green; *R*, dark grey; r', red; *I*, yellow and i', black. The top figure is a reproduction of the light curve published by Shafter et al. (2011f), who used ground-based data. The bottom figure shows the same ground-based data, with an additional *HST* data point. The *HST* data were taken in F450W (purple), F475W (light blue), F555W (magenta) and F814W (orange) filters, and are furthur highlighted by filled circular points. If the error bars on the *HST* data are not visible, they are smaller than the points.

in Figure 4.2. The post-outburst *HST* data also helped constrain the progenitor of the system, as is discussed in Section 3.4.12.

4.3.3 M31N 2009-08a

Nova M31N 2009-08a had ACS/WFC F475W and F814W data taken on 2010 July 21 (2455398 HJD) and December 14 (2455544 HJD). On 2010 July 21 the system had an F475W magnitude of 22.509 ± 0.008 and on December 14 it had an F474W magnitude of 23.00 ± 0.01. The nova was not resolvable in the F814W images on either of these dates; in the first dataset an upper limit of 21.6 ± 0.1 was derived, with an upper limit of 22.1 ± 0.2 in the later set of images. These data points were added to the light curve published by Shafter et al. (2011f) and the extended light curve is shown in Figure 4.3. These post-outburst *HST* data were also used to help locate the progenitor candidate (see Section 3.4.14).

4.3.4 M31N 2009-10b

Nova M31N 2009-10b had ACS/WFC F475W and F814W data taken on 2010 December 26 (2455556 HJD). At this time the nova had an F475W magnitude of 22.378 ± 0.007 and F814W magnitude of 23.41 ± 0.07. These points were added to the light curve published by Shafter et al. (2011f) and are shown in Figure 4.4. These data were also used to rule out some nearby sources as progenitor candidates (see Section 3.4.17).

4.3.5 M31N 2009-10c

Nova M31N 2009-10c had one set of ACS/WFC F475W and F814W data taken on 2010 December 22 (2455552 HJD) and another between 2010 December 24.9 and 25.1. In the latter set of images the system had an F475W magnitude of 22.4 ± 0.2. In the images taken on 2010 December 22 the nova had an F475W magnitude of 21.40 ± 0.01. There is a source in the F814W image that has a magnitude of 21.4 ± 0.2, but

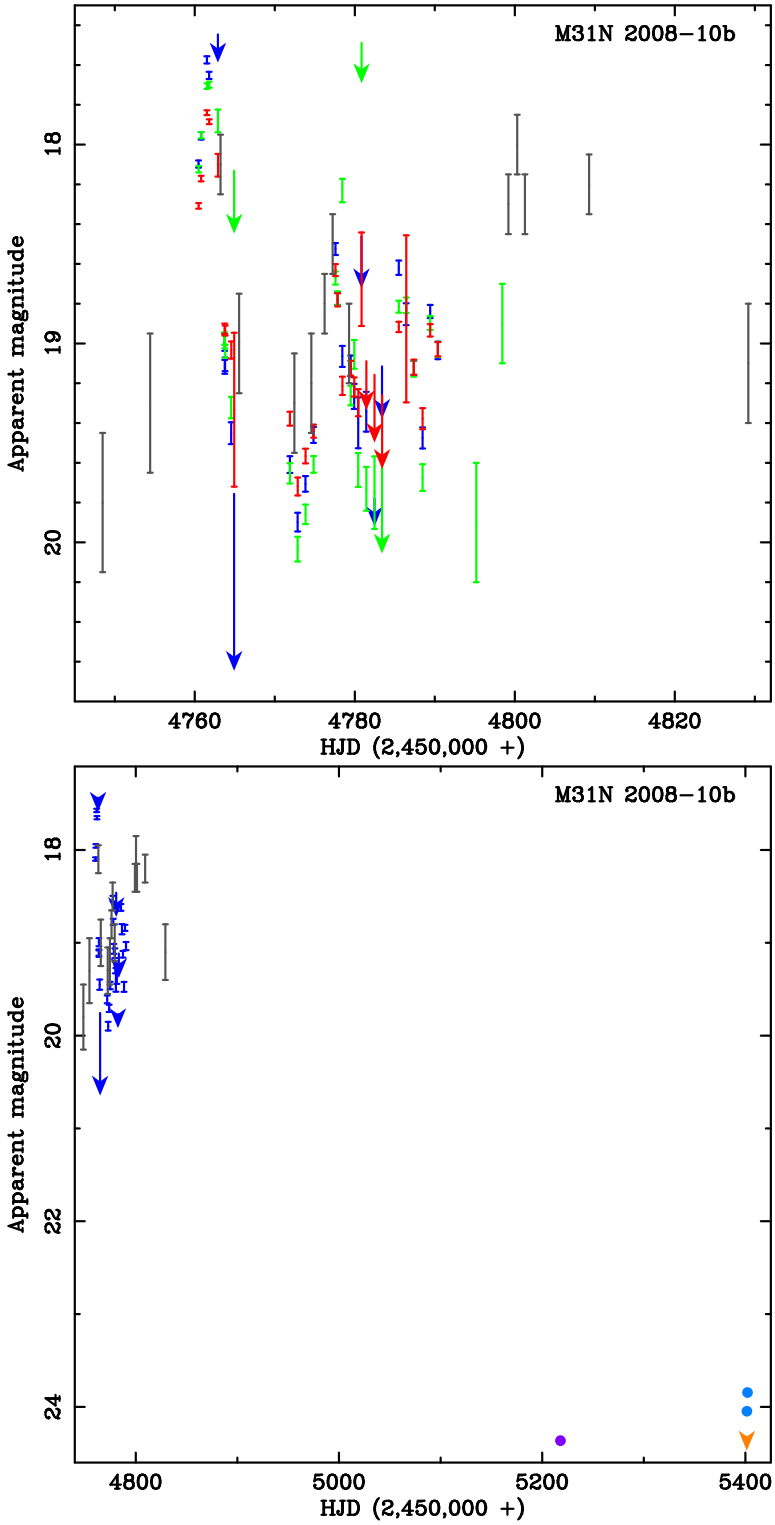

Figure 4.2: Light curve of M31N 2008-10b published by Shafter et al. (2011f), with additional *HST* data points. The top figure is a reproduction of the light curve published by Shafter et al. (2011f, ©AAS. Reproduced with permission). The bottom figure shows the same ground-based data, but only those taken in the filters closest to the *HST* data, with the additional *HST* data points. The different colour points are as in Figure 4.1.

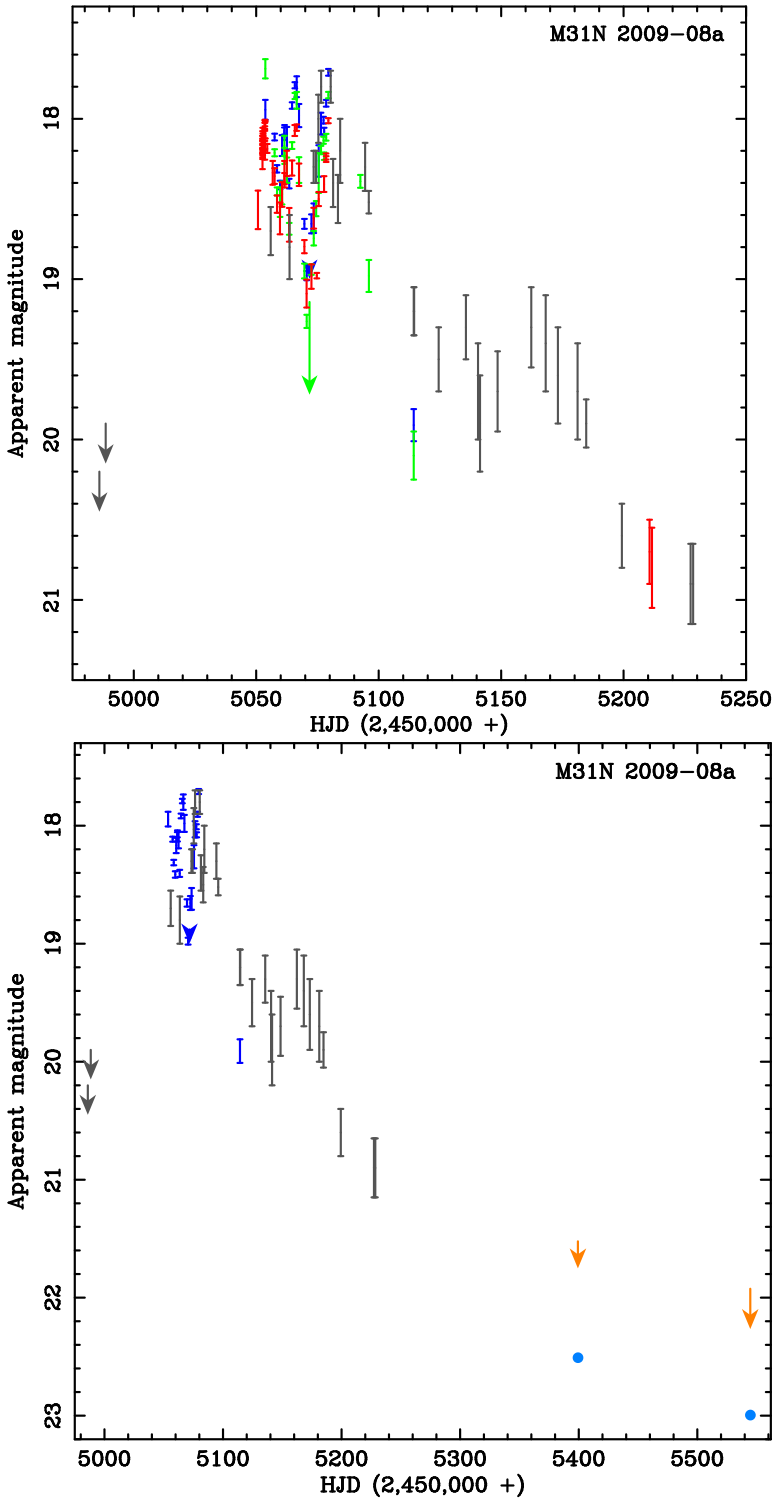

Figure 4.3: Light curve of M31N 2009-08a published by Shafter et al. (2011f), with additional *HST* data points. The top figure is a reproduction of the light curve published by Shafter et al. (2011f, ©AAS. Reproduced with permission). The bottom figure shows the same ground-based data, but only those taken in the filters closest to the *HST* data, with the additional *HST* data points. The different colour points are as in Figure 4.1.

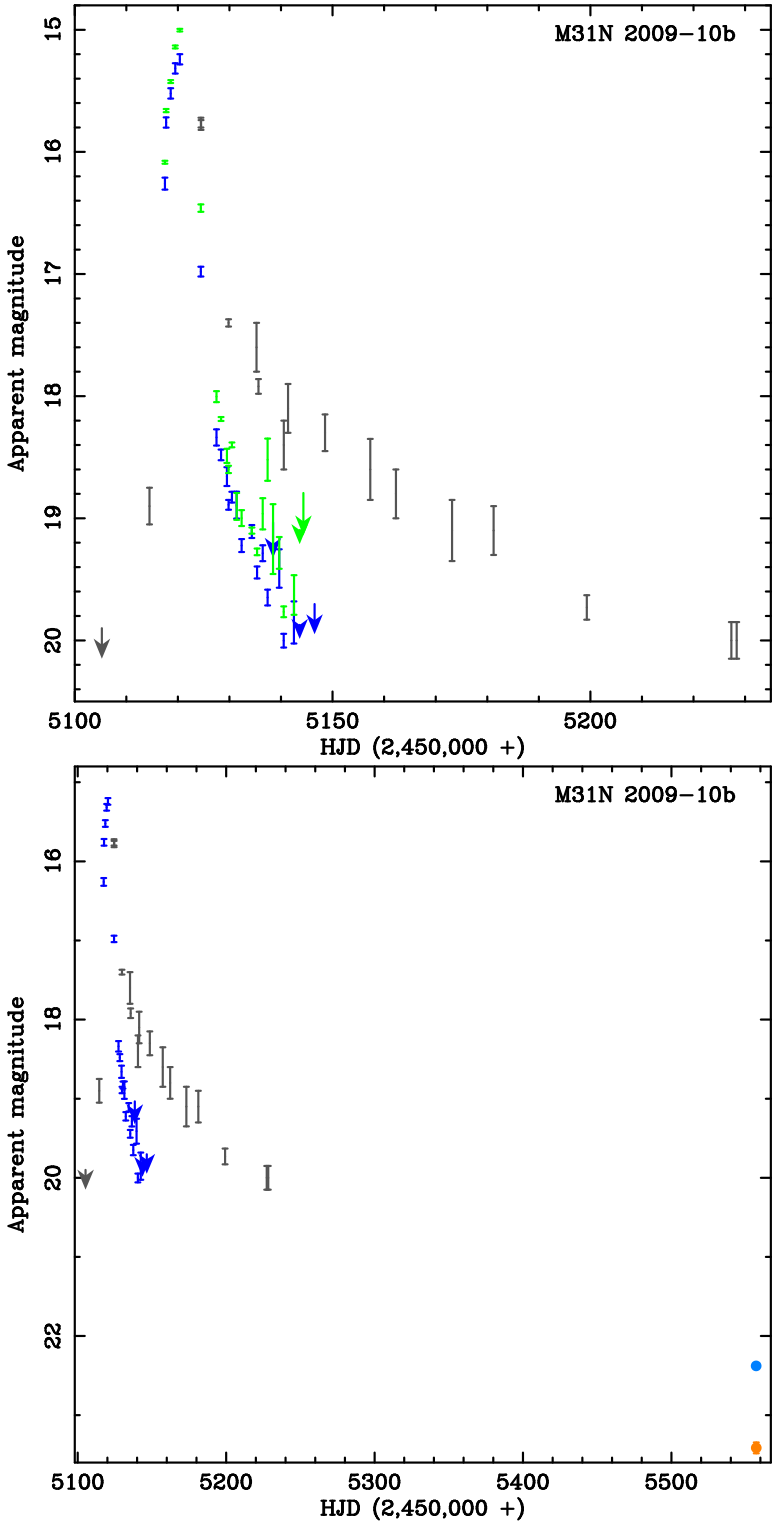

Figure 4.4: Light curve of M31N 2009-10b published by Shafter et al. (2011f), with additional *HST* data points. The top figure is a reproduction of the light curve published by Shafter et al. (2011f, ©AAS. Reproduced with permission). The bottom figure shows the same ground-based data, but only those taken in the filters closest to the *HST* data, with the additional *HST* data points. The different colour points are as in Figure 4.1.

as it is not certain (although very likely) that this is the nova itself, it is considered as an upper limit. The points were added to the light curve published by Shafter et al. (2011f) and are shown in Figure 4.5. Note that of the two F475W measurements, only the one taken on December 22 is shown. This is due to the close proximity in the time of the two measurements and the much lower error on the slightly earlier measurement. These data were also used to rule out a nearby source as the progenitor candidate for this nova (see Section 3.4.18).

4.3.6 M31N 2009-11c

Nova M31N 2009-11c had ACS/WFC F475W and F814W images taken on 2010 July 23, 24 and 25. On 2010 July 23 (2455400 HJD) the nova had an F475W magnitude of 24.40 ± 0.02. It had an F475W magnitude of 24.45 ± 0.02 on July 24 and 24.53 ± 0.02 on July 25. There is a nearby candidate with an F814W magnitude of 23.83 ± 0.03 on July 23, but as it is not certain that this is the nova, it is considered as an upper limit. These points were added to the light curve published by Shafter et al. (2011f) and are shown in Figure 4.6. These *HST* data taken during outburst were also used to rule out a nearby source as progenitor candidate (see Section 3.4.21).

4.3.7 M31N 2009-11e

Nova M31N 2009-11e had ACS/WFC F475W and F814W data taken between 2010 December 25.9 and 26.1 (2455556 HJD). At this time the nova had an F475W magnitude of 22.93 ± 0.01, but was not visible in the F814W image. For reference we have added the magnitude of a nearby faint (but clearly brighter than the nova) star as an upper limit. The points were added to the light curve published by Shafter et al. (2011f) and shown in Figure 4.7. These data were also used to rule out a nearby source as progenitor candidate (see Section 3.4.23).

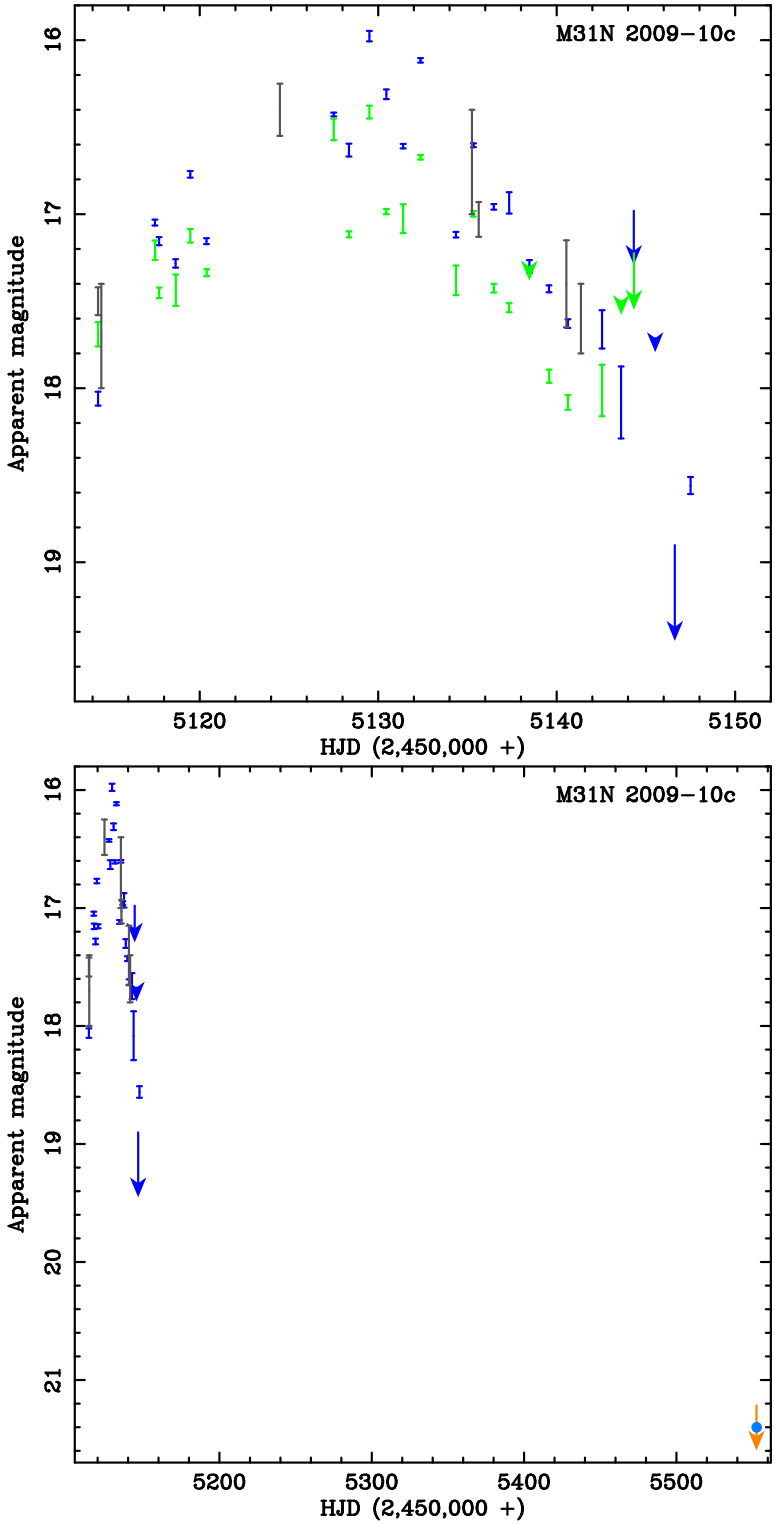

Figure 4.5: Light curve of M31N 2009-10c published by Shafter et al. (2011f), with additional *HST* data points. The top figure is a reproduction of the light curve published by Shafter et al. (2011f, ©AAS. Reproduced with permission). The bottom figure shows the same ground-based data, but only those taken in the filters closest to the *HST* data, with the additional *HST* data points. The different colour points are as in Figure 4.1.

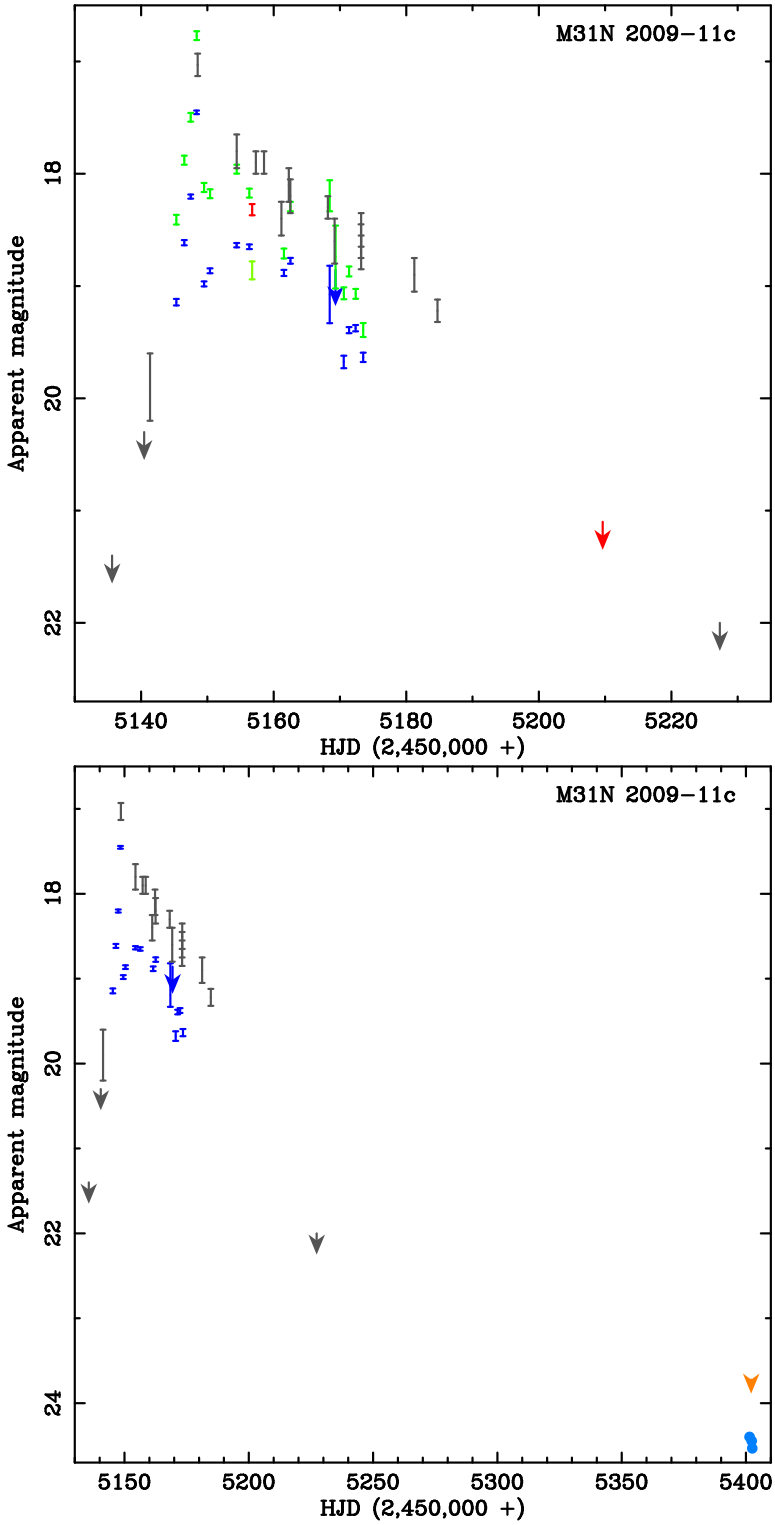

Figure 4.6: Light curve of M31N 2009-11c published by Shafter et al. (2011f), with additional *HST* data points. The top figure is a reproduction of the light curve published by Shafter et al. (2011f, ©AAS. Reproduced with permission). The bottom figure shows the same ground-based data, but only those taken in the filters closest to the *HST* data, with the additional *HST* data points. The different colour points are as in Figure 4.1.

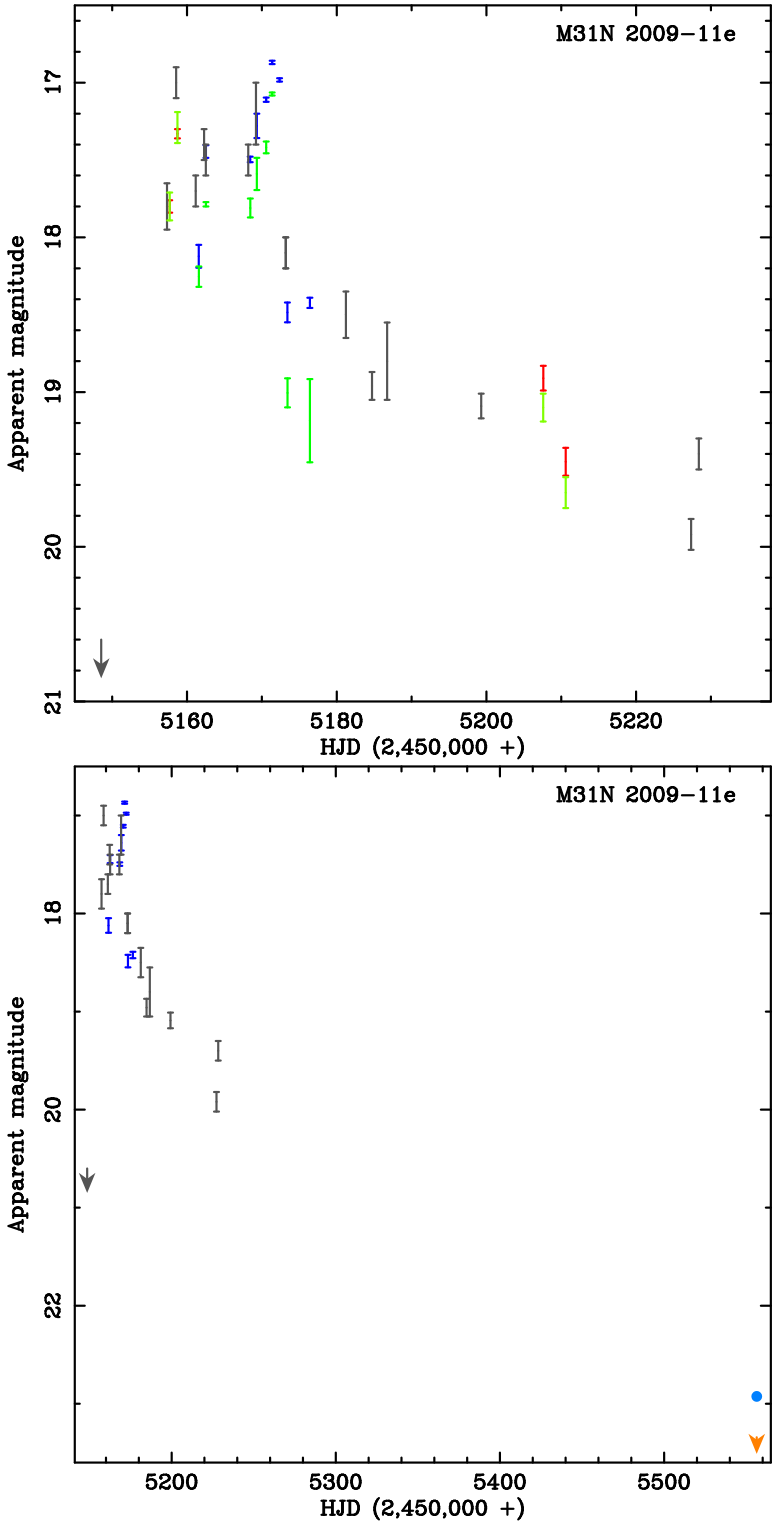

Figure 4.7: Light curve of M31N 2009-11e published by Shafter et al. (2011f), with additional *HST* data points. The top figure is a reproduction of the light curve published by Shafter et al. (2011f, ©AAS. Reproduced with permission). The bottom figure shows the same ground-based data, but only those taken in the filters closest to the *HST* data, with the additional *HST* data points. The different colour points are as in Figure 4.1.

4.3.8 M31N 2010-01a

Nova M31N 2010-01a was observed by the LT on 2010 January 13.86 (2455210.36 HJD) and 15.89 UT with *B* and *V* filters. The observations taken on January 13.86 appear to be close to the optical maximum. The object increased its *R*-band brightness between January 12.092 (2455208.59 HJD) and 13.094 UT (Burwitz et al., 2010a) and the LT observations show that the nova had started to fade by January 15.89. In addition to the LT photometry the system was observed with ACS/WFC on 2010 July 21 (2455398 HJD) and December 14 (2455544 HJD) with F475W and F814W filters. On 2010 July 21 the nova had an F475W magnitude of 23.55 ± 0.02 and F814W upper limit of 21.5 ± 0.1. On December 14 it had an F475W magnitude of 24.11 ± 0.03 and an F814W upper limit of 21.6 ± 0.1. The upper limits listed above are likely to be the nova itself, however as no quiescent F814W data are available, it cannot be certain it is the outburst, so they are listed as upper limits. The light curve showing the LT and *HST* data points is shown in Figure 4.8. From the above it is clear that the nova likely reached maximum between January 12.09 and 13.86. Therefore to calculate the lower t_2 limits we linearly extrapolate the measurements taken on January 12.092 and 13.094 and find the the magnitude this extrapolation gives at January 13.86. We then linearly extrapolate between the two LT measurements. This gives a *B* and *V* lower t_2 limit of 7 and 5 days respectively. To calculate the upper limit we extrapolate between the second LT points and the first *HST* point and take the first LT point as the maximum. This gives a *B* and *V*-band t_2 upper limits of 49 and 40 days. The *B* and *V* t_2 values are therefore 28 ± 21 and 23 ± 18 days respectively. The large errors are unsurprising given the lack of data. The *HST* data taken during outburst were also used to help locate the progenitor candidate (see Section 3.4.24).

4.3.9 M31N 2010-05a

Nova M31N 2010-05a was observed by the LT in *B* and *V* filters multiple times between 2010 June 13.15 (2455360.65 HJD) and July 4.12 (2455381.62). In these data, the nova was at its brightest in both *B* and *V*-band on June 13.15, when it had a mag-

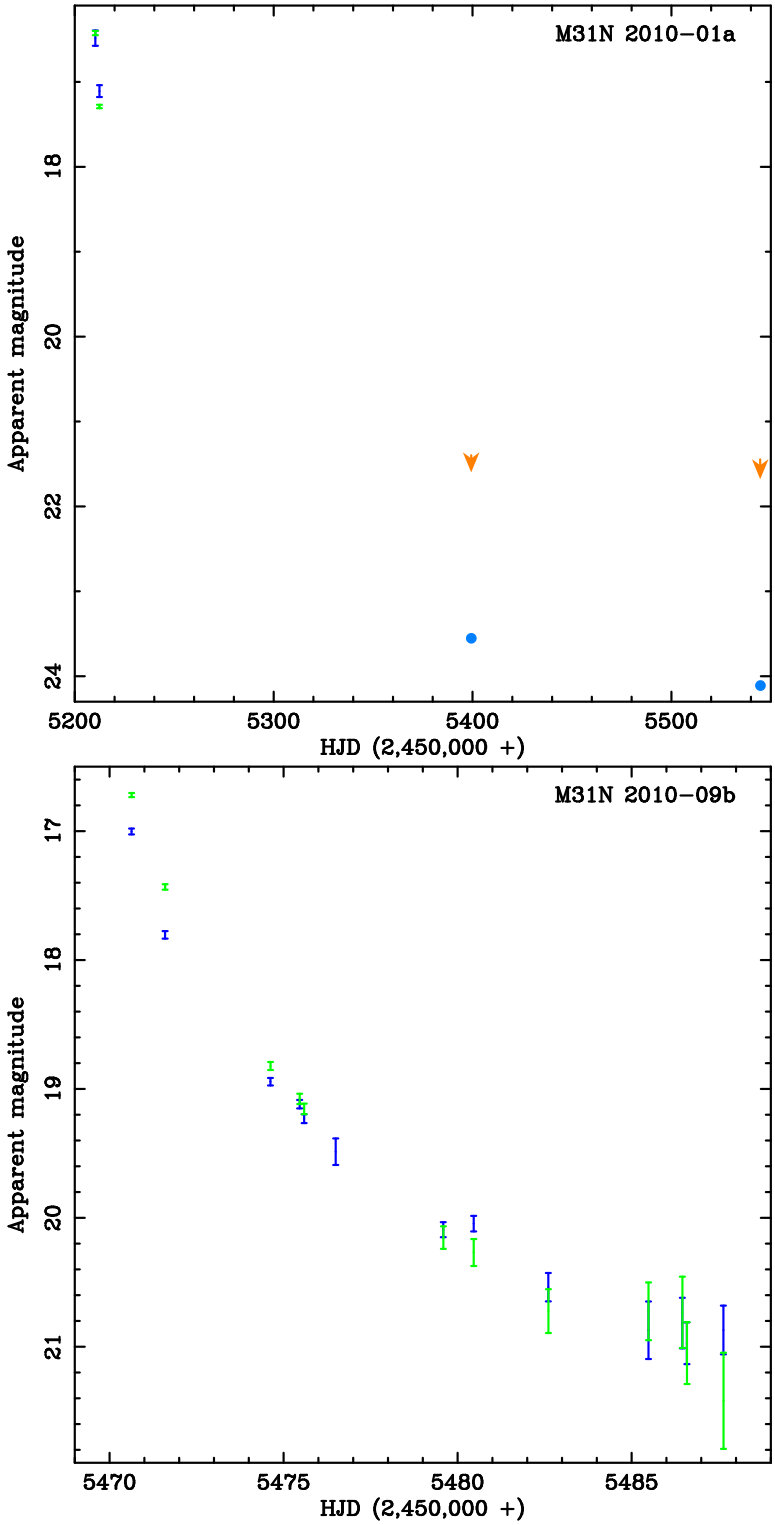

Figure 4.8: Light curves of M31N 2010-01a and M31N 2010-09b created from LT and *HST* data. The different colour points are as in Figure 4.1. ©AAS. Reproduced with permission.

nitude of 17.9 ± 0.1 in V-band and 17.53 ± 0.07 in B-band. The nova brightened in *R*-band between May 28 and June 4 (Nishiyama & Kabashima, 2010) and then appeared to remain near the maximum for several days (see Hornoch et al., 2010c,g). The LT observations appear have started just as the nova began to fade. The system was also observed by *HST* with ACS/WFC in F475W and F814W filters between 2010 December 24.88 (2455555.38 HJD) and 25.61. At this time the nova had an F475W magnitude of 22.42 ± 0.01. Although the nova was not resolvable in the F814W image, we have added an upper limit of 22.1 ± 0.2 for reference. This was calculated from a nearby faint star that was clearly brighter than the nova. A light curve of the LT and *HST* points is shown in Figure 4.9. As the nova appears to stay near maximum for a few days, it is not easy to calculate t_2 directly and there is a significant gap between the end of the LT observations and the time of the *HST* observations. To calculate the lower t_2 limit, it is assumed that the first LT observations were at maximum and then linearly extrapolate the LT points (excluding the first two measurements) until t_2 is reached. This gives a B and V lower limit of 22 and 23 days respectively. For the upper limit, it is assumed that the nova was at peak (and same magnitude as the first LT measurements) when it first appeared to plateau on June 4. Then extrapolation between the final LT point and the F475W *HST* point was used to derive the t_2. This gives a B and V upper limit of 56 and 50 days respectively. Therefore producing a B-band t_2 estimate of 39 ± 17 days and a V-band estimate of 37 ± 14 days.

4.3.10 M31N 2010-09b

Nova M31N 2010-09b was observed by the LT in *B* and *V* filters between 2010 October 1.13 (2455470.63 HJD) and 18.14 UT (2455487.64 HJD). In these data, the nova was at its brightest in both B and V filters in the images taken on October 1.13, when it had a *V*-band magnitude of 16.72 ± 0.04 and *B*-band magnitude of 17.00 ± 0.08. The nova brightened significantly in the R-band between 2010 September 30.41 (2455469.91 HJD) and October 1.18 (Pietsch et al., 2010c). The LT observations also constrain that the nova must have faded significantly by October 2.10 (2455471.60). Therefore it appears that the LT started observing the nova when it was

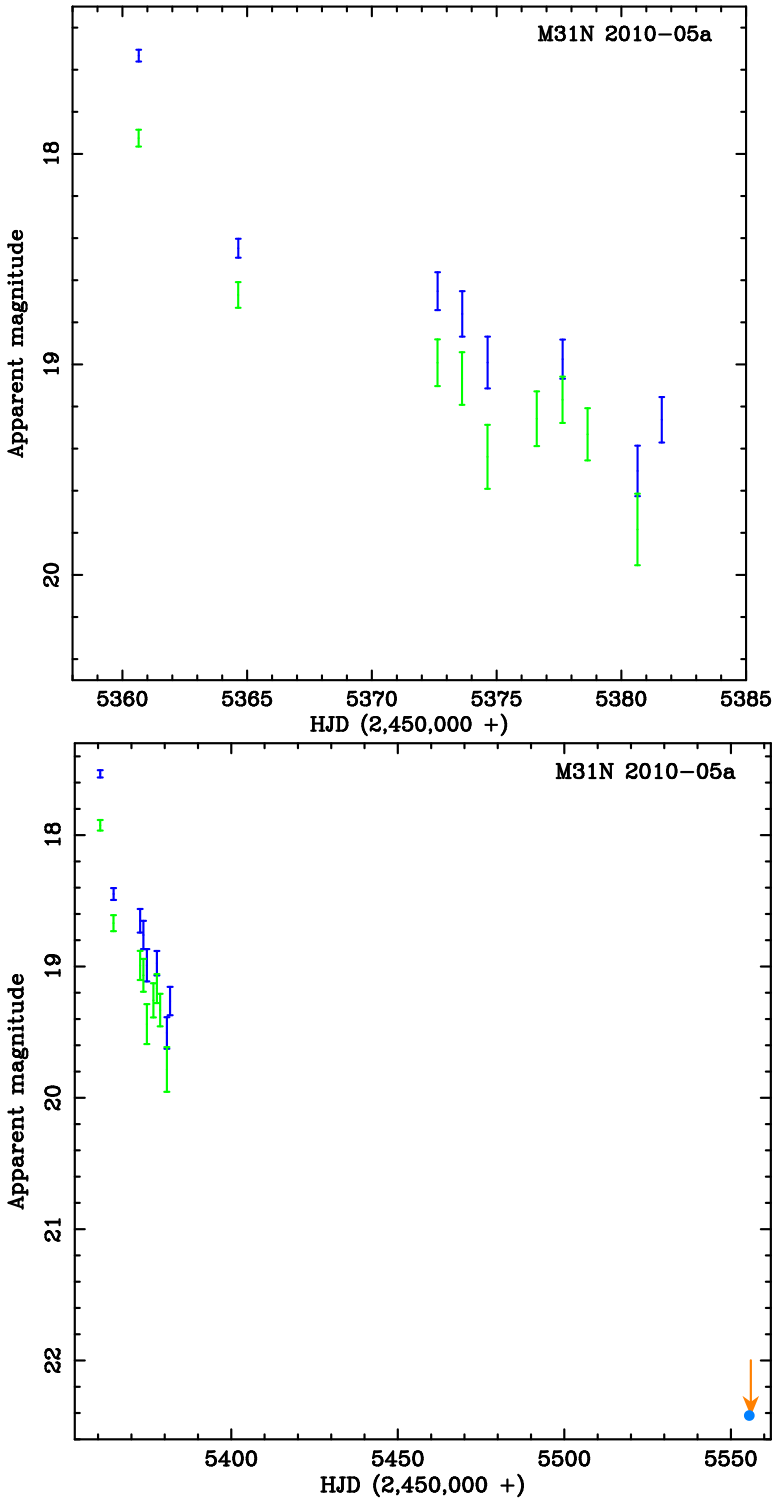

Figure 4.9: Light curve of M31N 2010-05a created from LT and *HST* data. The top figure shows only the ground-based data and the bottom figure shows the same ground-based data with the *HST* data points. The different colour points are as in Figure 4.1. ©AAS. Reproduced with permission.

at, or very close to, maximum brightness. A light curve of the LT points is shown in Figure 4.8. Assuming the first set of observations were indeed taken at maximum, a *V*-band t_2 of 3.8 ± 0.2 days and a B-band t_2 of 4.3 ± 0.6 days was derived.

4.3.11 M31N 2010-10a

Nova M31N 2010-10a was observed by the LT between 2010 October 9.22 (2455478.72 HJD) and November 7.01 UT (2455507.51 HJD) with *B* and *V* filters. The light curve for this nova is shown in Figure 4.10. The nova brightened in *R*-band between 2010 October 5.55 (2455475.05 HJD) and 6.54 UT (Nishiyama et al., 2010b). The LT images show that the nova fades in both *B* and *V*-band between October 9.22 (2455478.72 HJD) and 10.06. Therefore it is likely that the nova reached peak between October 6.54 and 9.22. As the peak may have been missed it is not possible to calculate an accurate t_2. However by calculating how long it takes the nova to fade by two magnitudes from the first LT observation, it is possible to calculate an upper limit on t_2, which for *B*-band is 16 ± 2 days and for V-band a maximum of 11 ± 5 days. From *R*-band observations Cao et al. (2012) constrained the t_2 to > 9 days.

4.3.12 M31N 2010-10d

Nova M31N 2010-10d was observed by the LT in *B* and *V* filters regularly between 2010 October 29.97 (2455499.47 HJD) and November 22.95 UT (2455523.45 HJD). It is unclear from the LT data when maximum was reached in *B*-band and there appears to be two clear peaks in *V*-band. Similarly, it is also unclear from the light curve in Cao et al. (2012) when maximum was reached. The nova was observed in F475W and F814W filters on 2010 December 16 (2455546 HJD) and 18. On December 16 the nova had an F475W magnitude of 20.906 ± 0.005 and an F814W magnitude of 20.128 ± 0.003. On December 18 it had an F475W magnitude of 20.859 ± 0.003. A light curve of the LT and *HST* points is shown in Figure 4.10. From the *V*-band maximum (i.e. the first peak) a t_2 of 22.8 ± 0.9 days was calculated. As the *B*-band

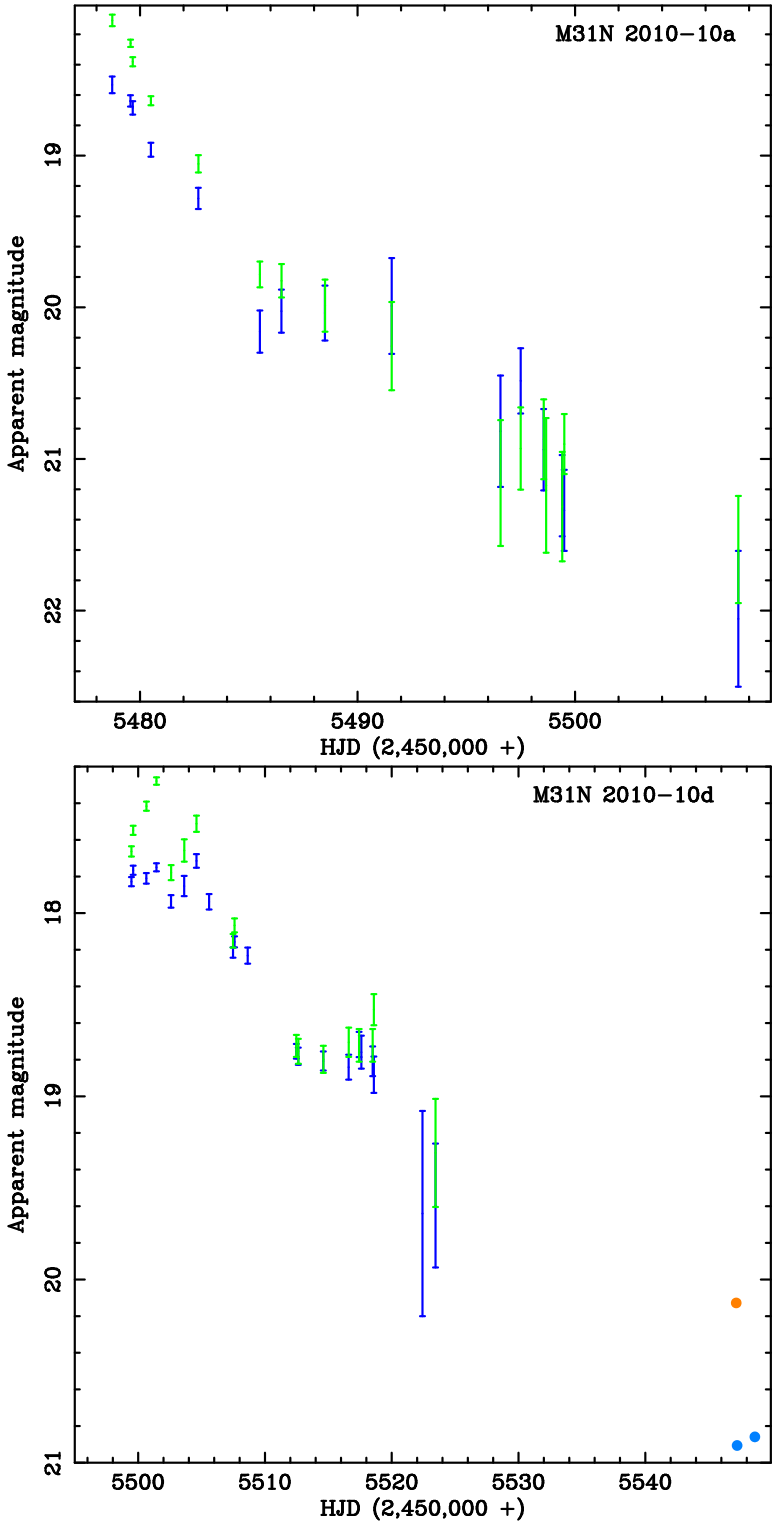

Figure 4.10: Multi-colour light curve of M31N 2010-10d from LT data, with additional *HST* points, and LT data light curve of M31N 2010-10a. The different colour points are as in Figure 4.1. ©AAS. Reproduced with permission.

LT data does not cover the nova fading by two magnitudes, an extrapolation to the first F475W data point is needed. If the *B*-band point that corresponds to the *V*-band maximum is taken, a t_2 of 25 ± 5 days is calculated. If the point of the highest *B*-band flux is taken as the maximum we calculate a t_2 of 21 ± 5 days. These are the upper and lower limits respectively, which gives a B-band t_2 of 23 ± 7 days. This is consistent with the *R*-band t_2 estimate of 20 days by Cao et al. (2012). As noted in Section 3.4.30, the *HST* data taken during outburst were also used to rule out a nearby source as a progenitor candidate.

4.3.13 M31N 2013-08a

Nova M31N 2013-08a was first discovered in ultraviolet observations by Sturm et al. (2013c) on 2013 August 6.61 UT (2456511.11 HJD). A spectrum taken a few days later confirmed it as a nova in M31 (Cao et al., 2013). In response to the ultraviolet discovery, an initial set of r'-band observations were taken on 2013 August 8.09 UT (2456512 HJD), when the nova was at $r' = 17.375 \pm 0.006$. By the time the second set of observations were taken August 10.14, M31N 2013-08a appeared to have faded significantly and was at $B = 19.12 \pm 0.02$ and $V = 19.00 \pm 0.03$. Only one further epoch (on August 15.06; 2456519.56 HJD) of data was taken before the nova had faded beyond detection. The light curve of M31N 2013-08a is shown in Figure 4.11. As the nova appears to have faded significantly before the first *B* and *V*-band observations were taken, it is difficult to derive an accurate t_2. Although it can be seen it is a very fast nova and t_2 is probably < 7 days. This is also supported by the nova being at $R = 16.8$ on August 6.79 UT (Cao et al., 2013).

4.3.14 M31N 2013-08e

Nova M31N 2013-08e was discovered on 2013 August 28 (2456532 HJD; Tang et al., 2013b) and a spectrum taken by Tang et al. (2013c) confirmed the transient to be a nova in M31. The nova was followed in *B* and *V*-bands with the LT, with a total of 17

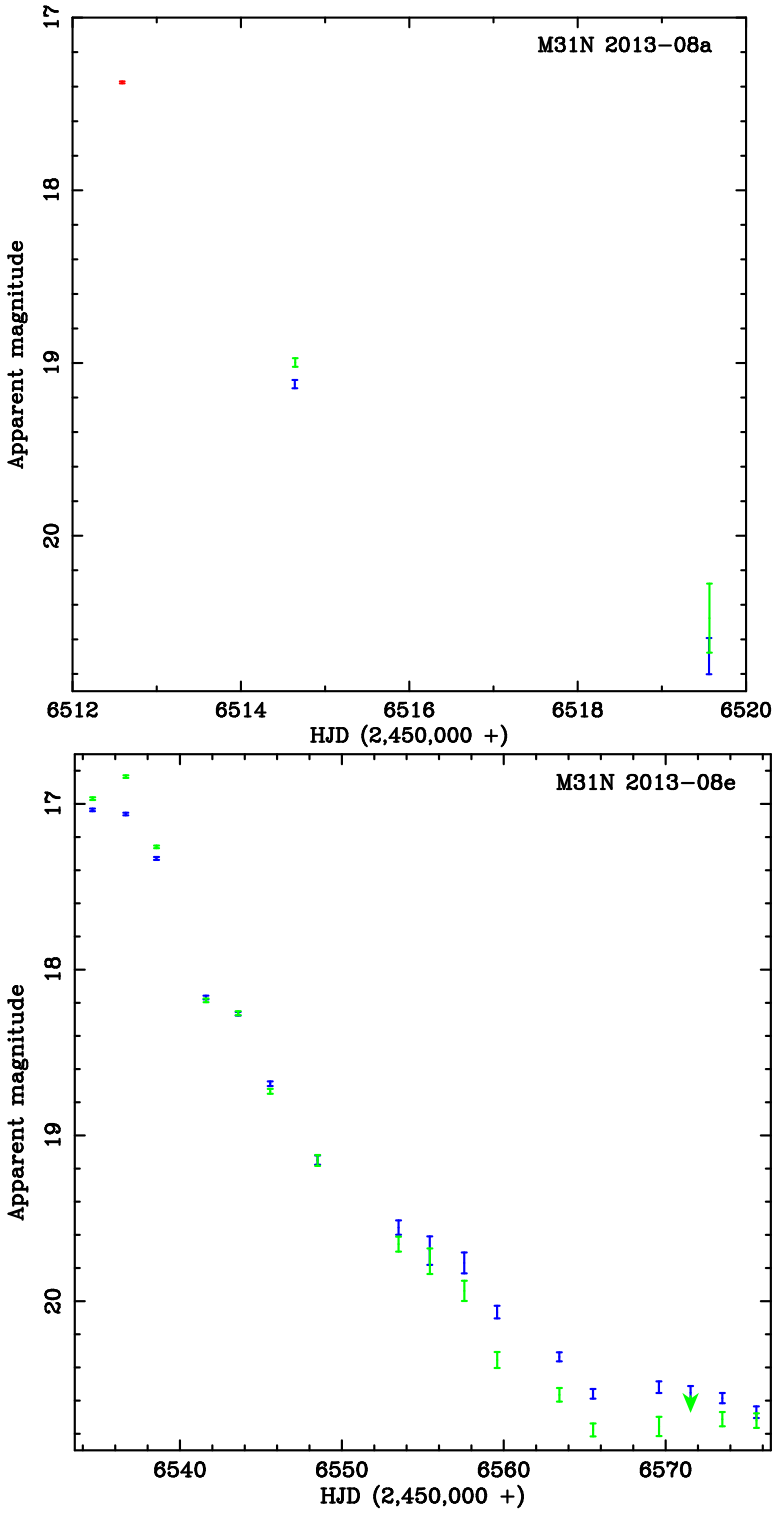

Figure 4.11: *B* and *V*-band light curves of M31N 2013-08a and M31N 2013-08e. The different colour points are as in Figure 4.1.

epochs in both filters, starting on 2013 August 30.09 UT (2456534.59 HJD). The first set of data appear to have been taken prior to the peak. Indeed in the *V*-band, the nova increases in brightness between August 30.10 (2456534.60 HJD) and September 1.16 (2456536.66 HJD). The sharp decline after September 1 also supports the peak having been reached between the first two data points. The LT light curve of M31N 2013-08e is shown in Figure 4.11. If it is assumed that maximum was reached between the first two data points in both the *B* and *V* data, the light curve shows the nova had a *B*-band t_2 of 11.4 ± 0.2 days and t_3 of 22.9 ± 0.6 days, with a *V*-band t_2 days of 9.4 ± 0.2 and t_3 of 17 ± 2 days.

4.3.15 M31N 2013-09a

Nova candidate M31N 2013-09a was discovered on 2013 September 9 (2456544 HJD) and first reported as TCP J00431492+4119128[1]. The transient was also detected in the ultraviolet by Sturm et al. (2013b). M31N 2013-09a was followed in *B* and *V*-bands by the LT. As it was in an IO:O field that was already being observed, photometric data were obtained showing the transient on the rise, prior to the discovery announcement. Additionally, *B* and *V* upper limits were calculated for two days prior to discovery. The light curve of M31N 2013-09a is shown in Figure 4.12. This light curve, accompanied by the detection of significant Hα emission (Hornoch et al., 2013) strongly supports M31N 2013-09a being classified as a nova in M31. The maximum brightness of the nova probably occurred between 2456544.48 and 2456546.48 HJD (the first two LT detections), as novae usually fade slower than they brighten. Taking this into account, the *B*-band t_2 was calculated to be 8.9 ± 0.3 days, with a t_3 of 18 ± 2 days. The nova had a *V*-band t_2 of 7.6 ± 0.7 and t_3 of 16 ± 3 days.

[1] `http://www.cbat.eps.harvard.edu/unconf/followups/J00431492+4119128.html`

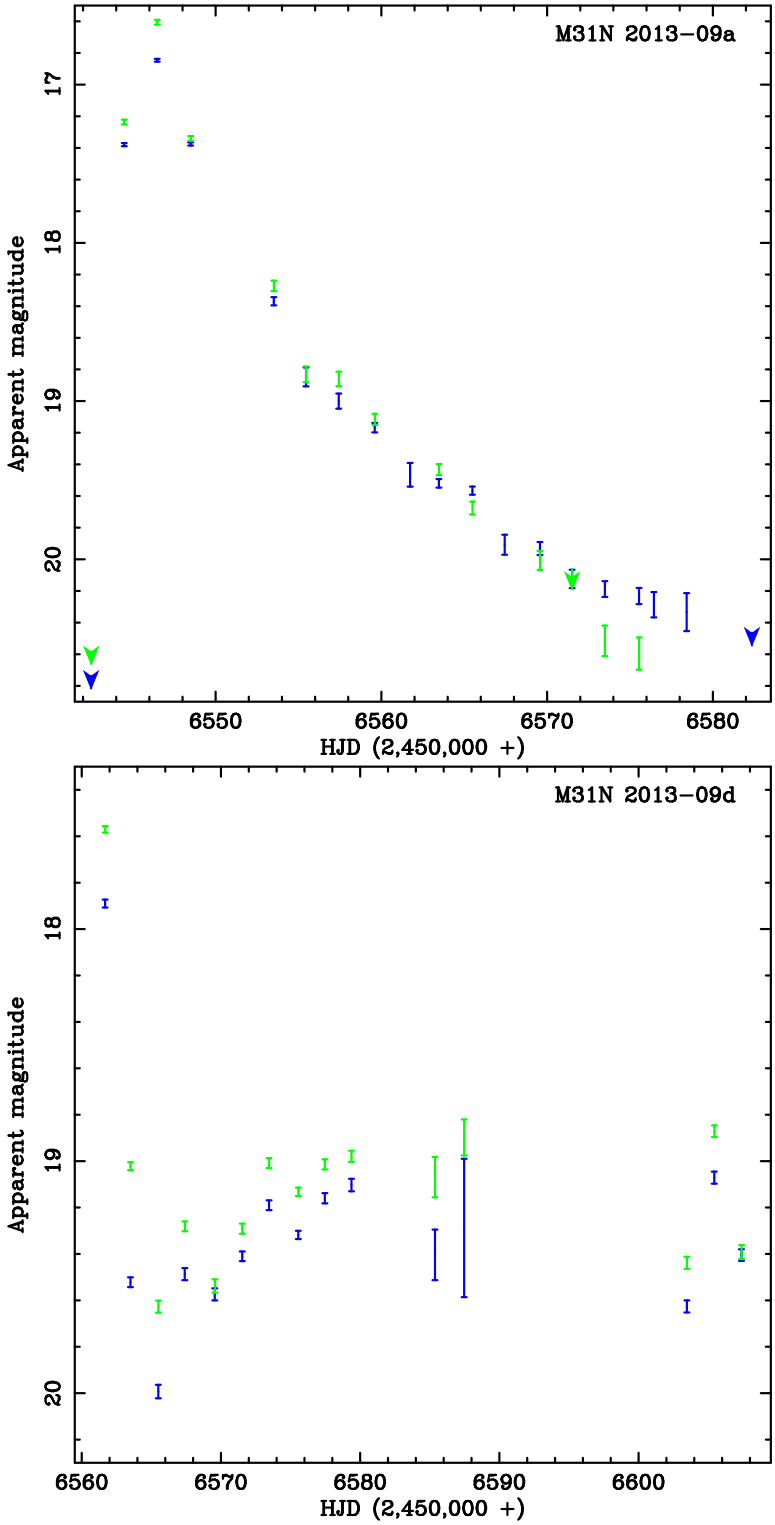

Figure 4.12: *B* and *V*-band light curves of nova candidate M31N 2013-09a and nova M31N 2013-09d. The different colour points are as in Figure 4.1.

4.3.16 M31N 2013-09d

Nova M31N 2013-09d was an Fe II nova (Valeev et al., 2013) discovered on 2013 September 24[2] (2456559 HJD). On September 25.95 UT (2456561.45 HJD) the nova had an *R*-band magnitude of 17.55 ± 0.09 (Hornoch & Kucakova, 2013b) and had brightened to $R = 17.06 \pm 0.07$ by September 26.76, but faded back to $R = 17.95 \pm 0.09$ by September 27.74. Therefore it is likely the nova peaked between September 25.95 and September 26.76. The first two epochs of LT data were taken on September 26.18 (2456561.68 HJD) and September 28.00 UT. The light curve of this nova, which can be seen in Figure 4.12, does not appear typical. It initially fades very quickly by 1.63 ± 0.03 and 1.45 ± 0.02 magnitudes in B and V respectively over just 1.82 days, then a few days later it begins to rise again, reaching about 0.9 magnitudes brighter in B and 0.6 brighter in V than the minimum. After this rise the nova appears to stay at roughly constant brightness for several weeks, although there does appear to be a significant fluctuation approximately 45 days after outburst.

4.3.17 M31N 2013-10h

On 2013 October 29.78 UT (2456595.28 HJD), an ultraviolet transient was detected by Sturm et al. (2013a). Spectra taken between 2013 November 1.67 (2456598.17 HJD) and November 2.66 UT confirmed the transient as an Fe II nova in M31 (Fabrika et al., 2013). The first set of LT observations, taken on November 4.91 UT (2456601.41 HJD), showed the nova to be very luminous, with $B = 15.716 \pm 0.007$ and $V = 15.306 \pm 0.005$. The full LT light curve of M31N 2013-10h is shown in Figure 4.13. On November 2.66 UT (2456599.16 HJD), the nova was at $B = 16.08$ and $V = 15.81$ (Fabrika et al., 2013), therefore the maximum must have occurred between November 2.66 and November 6.85 (2456603.35 HJD). It was therefore calculated that the nova had a *B*-band t_2 of 6 ± 2 days, with $t_3 = 9 \pm 2$ days and $t_4 = 15 \pm 3$ days, a *V*-band t_2 of 5 ± 2, $t_3 = 8 \pm 2$ and $t_4 = 13 \pm 3$ days.

[2] `http://www.cbat.eps.harvard.edu/unconf/followups/J00415307+4109540.html`

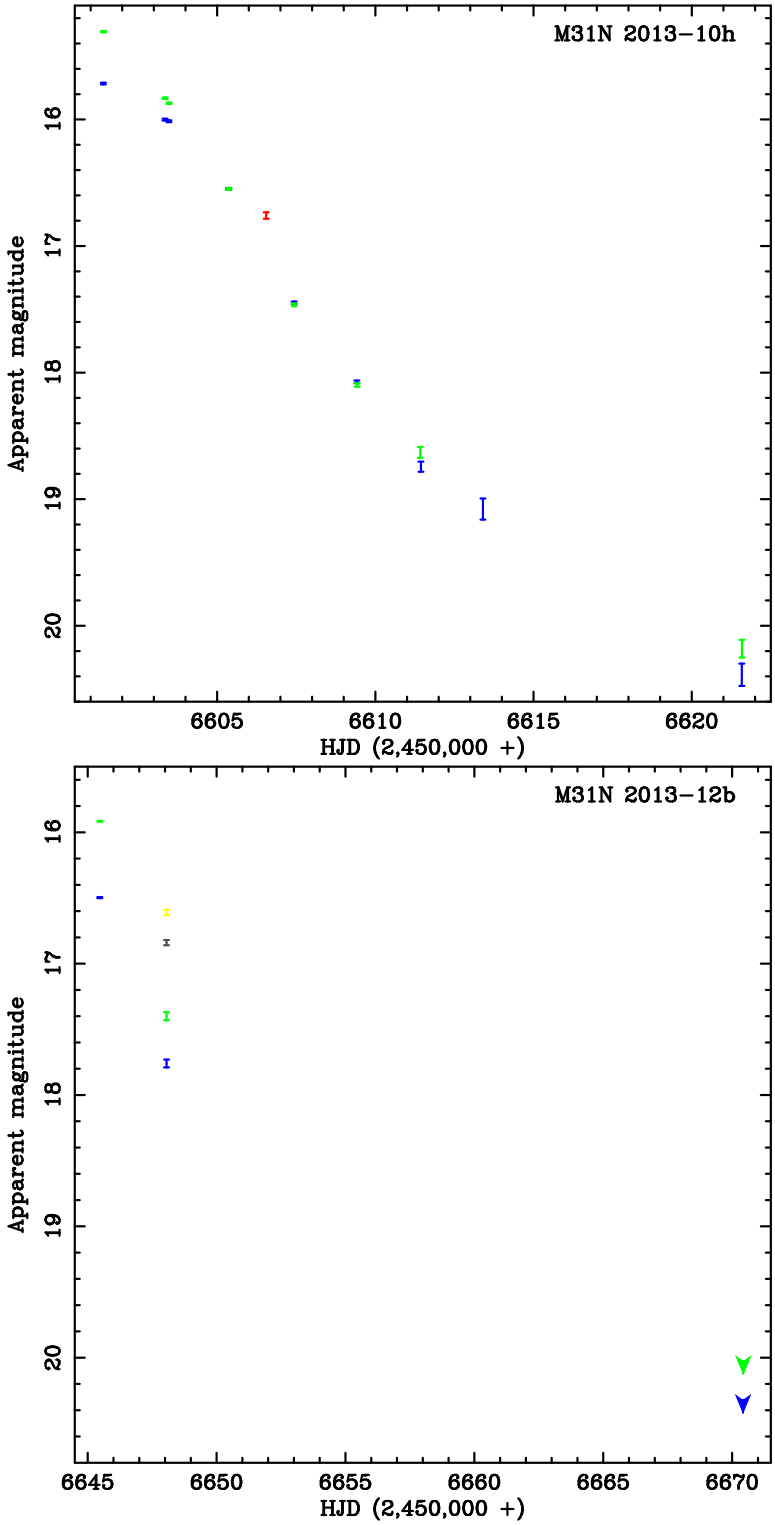

Figure 4.13: *B* and *V*-band light curves of M31N 2013-10h and multi-colour light curve of M31N 2013-12b, colours as in Figure 4.1.

4.3.18 M31N 2013-12b

Nova M31N 2013-12b was discovered on 2013 December 17.696 (2456644.20 HJD) by Hornoch & Kucakova (2013a), who observed it when it was still rising to maximum, and found it to be at $R = 17.6 \pm 0.1$ on 2013 December 17.696 and $R = 17.3 \pm 0.1$ on December 17.747. The LT observations taken just over one day later showed the nova to have brightened significantly, with $B = 16.497 \pm 0.004$ on December 18.96 (2456645.46 HJD) and $V = 15.916 \pm 0.003$ on December 18.97. By 2014 January 12.93 (2456670.43 HJD) the nova had faded further, with upper limits of $V > 20.1$ and $B > 20.4$. The light curve created from LT and Lijiang Observatory (see below) data is shown in Figure 4.14.

A spectrum of the candidate, which is shown in Figure 4.14, was obtained (by J. J. Zhang) using YFOSC on the 2.4-m telescope of Lijiang Observatory, Yunnan Observatories on 2013 December 21.567 (2456648.07 HJD). The spectrum showed Fe II emission lines, typical of novae belonging to the Fe II spectroscopic class, but also displayed relatively broad emission features and was classified as an Fe IIb type nova. This classification was supported by a later spectrum taken 14 days after the discovery, which classified the outburst as a He/N nova (Fabrika et al., 2014). Such spectral evolution is often seen in these hybrid objects (Williams, 1992).

4.4 Summary

Here the light curves of eighteen M31 novae are presented. All light curves are either previously unpublished or have added additional points to published light curves. Several of the light curves have *HST* data, allowing them to be extended much deeper than is usually possible for extragalactic systems. Also, t_2 values of several of the novae are calculated, with some of the novae having no other published t_2 value. In addition, a spectrum of M31N 2013-12b is shown, which classified the object as an Fe IIb nova.

Having studied M31 novae in both quiescence and outburst, the thesis now presents a

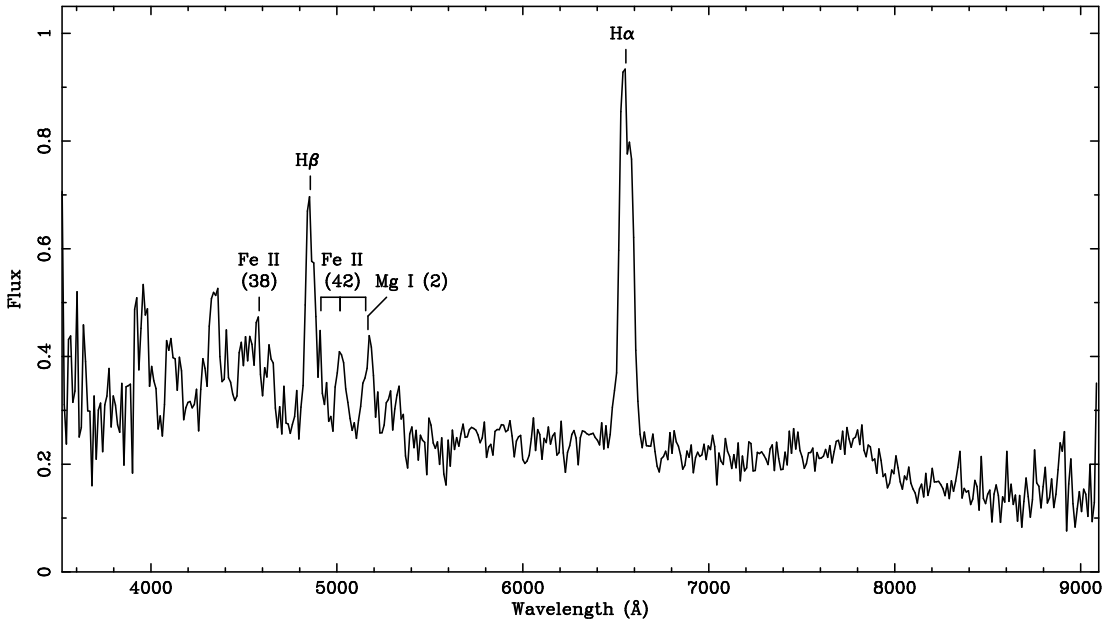

Figure 4.14: A spectrum of M31N 2013-12b, taken using YFOSC on the 2.4-m telescope of Lijiang Observatory. It shows broad Balmer, Fe II and Mg I emission features.

statistical study of the results and possible biases of the M31 progenitor survey, leading to an estimate on the proportion of novae likely to be associated with a source in the *HST* data.

Chapter 5

Analysis of the M31 Nova Progenitor Catalogue

The majority of the work described in this chapter is to be reported by Williams, S. C., Darnley, M. J., Bode, M. F. and Shafter, A. W. (ApJ, in preparation)

5.1 Introduction

The M31 nova progenitor catalogue presented in Chapter 3 found eleven of the 38 systems to be coincident with a resolvable source in the *HST* data, and thus likely to be RG-novae. However, in order to better understand the nature of the quiescent population, a statistical analysis of the survey was conducted and is presented in this chapter. In this analysis, a model was produced of the outburst population, allowing the effects of several biases to be accounted for. This model first considers the spatial distribution of both the disk and bulge M31 novae, then explores other features of the population, including speed class (t_2) distribution and its relationship to maximum brightness (MMRD). The model is then used to explore biases in LT observations, spectroscopic observations and the *HST* coverage of the M31 field. The resulting final model allows the proportion of M31 novae associated with a resolvable quiescent source in the *HST* data to be estimated. The group of novae associated with a resolved source would be

expected to be dominated by RG-novae (see discussion in Chapter 3).

In order to be included in the M31 progenitor survey, a nova outburst had to:

- Occur between August 2006 and February 2013.
- Be discovered.
- Be spectroscopically confirmed.
- Have LT data taken while still in outburst.
- Have coincident *HST* data taken when in quiescence.

Therefore the analysis of the catalogue must replicate this and the biases associated with each step, but first a model of the M31 nova population itself must be produced, which is described below.

5.2 Simulating M31 Novae

This statistical analysis aims to consider what the results for the particular novae in our catalogue tell us about the overall M31 nova population. Therefore novae are simulated that have a spacial distribution similar to that of the M31 nova population. Additionally each nova is assigned a t_2 and a peak magnitude, which are derived from the observational data of M31 novae. These considerations are described in detail below.

5.2.1 Spatial Distribution

To avoid biases in the number of simulated novae that would have been included in our survey if they were real outbursts, we must generate novae with a realistic spatial distribution. For example, many more novae occur in the central regions of M31 than in the outer disk. Figure 1.7 shows the distribution of all nova candidates discovered in

M31, but this is not a realistic map of the actual probability of a given region producing an outburst, as the number densities are far too low for the majority of the field to be statistically significant, plus it does not take into account possible selection effects, mainly those concerned with detection. Therefore, the CN eruption probability model from Darnley et al. (2006) is used to seed the simulated novae.

This model is described in detail in Darnley (2005) and Darnley et al. (2006), but is also outlined here. It first assumes that there are two fundamental nova populations. One that follows the disk light and one that follows the bulge light (see e.g. Ciardullo et al., 1987). The disk component is modelled as a thin disk inclined at 77° (de Vaucouleurs, 1958), with a smooth flux distribution across the disk. The bulge was modelled by subtracting the disk model from the galactic light (thus leaving the bulge) and using elliptical isophotes with a minor/major axis ratio of 0.6 (Ciardullo et al., 1987).

In the model of Darnley et al. (2006), the bulge and disk populations have a different eruption rate per unit r' flux, with θ being the ratio between the two rates, and it is assumed that the nova eruption probability in the disk or the bulge is proportional to the disk or bulge luminosity respectively so that

$$p_i \propto \sigma_{\rm d} f_i^{\rm d} + \sigma_{\rm b} f_i^{\rm b}$$

where p_i is the probability of eruption, $f^{\rm d}$ and $f^{\rm b}$ are the disk and bulge flux respectively, and $\sigma_{\rm d}$ and $\sigma_{\rm b}$ are the number of nova eruptions per unit time per unit r' flux for the disk and bulge populations respectively. The favoured value of $\theta = 0.18$ was calculated by comparing the disk and bulge flux to the novae detected in the POINT–AGAPE survey of M31 (Darnley et al., 2006).

The model calculates the probability of a nova eruption at a given location, Ψ_i, from

$$\Psi_i = \frac{\theta f_i^{\rm d} + f_i^{\rm b}}{\theta \sum_{j=1}^{N_{\rm bins}} f_j^{\rm d} + \sum_{j=1}^{N_{\rm bins}} f_j^{\rm b}} \tag{5.1}$$

In this equation, the numerator is concerned with the probability in bin i, whereas

the denominator acts to normalize the probabilities over all bins. The resulting model seeded $\sim 60\%$ of novae as being associated with the bulge and the distribution of bulge and disk novae produced by the model is shown in Figure 5.1.

5.2.2 Speed Class Distribution

One prospective bias is the spatial distribution of nova speed classes within M31. Shafter et al. (2011f) found some evidence that faster novae tend to be more evenly distributed throughout the galaxy (i.e. probably more associated with the disk), with slower novae being more associated with the central regions (i.e. the bulge). Figure 5.2 uses data from Shafter et al. (2011b,f), Cao et al. (2012) and Williams et al. (2014) to show how novae of different speed classes are distributed within the galaxy. The number density of novae with well defined t_2 values are too low to give an accurate distribution of t_2 against distance from the centre of M31. Therefore a single, simple t_2 distribution model was created for all the simulated novae, and was derived from the t_2 values of M31 novae from Shafter et al. (2011b,f), Cao et al. (2012) and Williams et al. (2014), with separate linear relationships for the t_2 distribution in the t_2 ranges of $0.5 - 35$ days, $35 - 60$ days and $60 - 200$ days. These relationships are shown with the observational data in Figure 5.3. From the observational data shown in the figure, there appears to be a pronounced break in the distribution around $t_2 = 60$ days. It may be more difficult to obtain t_2 values for some of the slower novae occurring near the seasonal gap of M31, but this would not be expected to produce such a sudden break, so the reason for this is not clear.

5.2.3 Peak Magnitude Distribution

The peak magnitude of a nova is linked to its speed class through the MMRD relationship. Shafter et al. (2011f) found the *R*-band MMRD in M31 to be

$$M_R = -10.89 \pm 0.12 + (2.08 \pm 0.077)\log t_2.$$

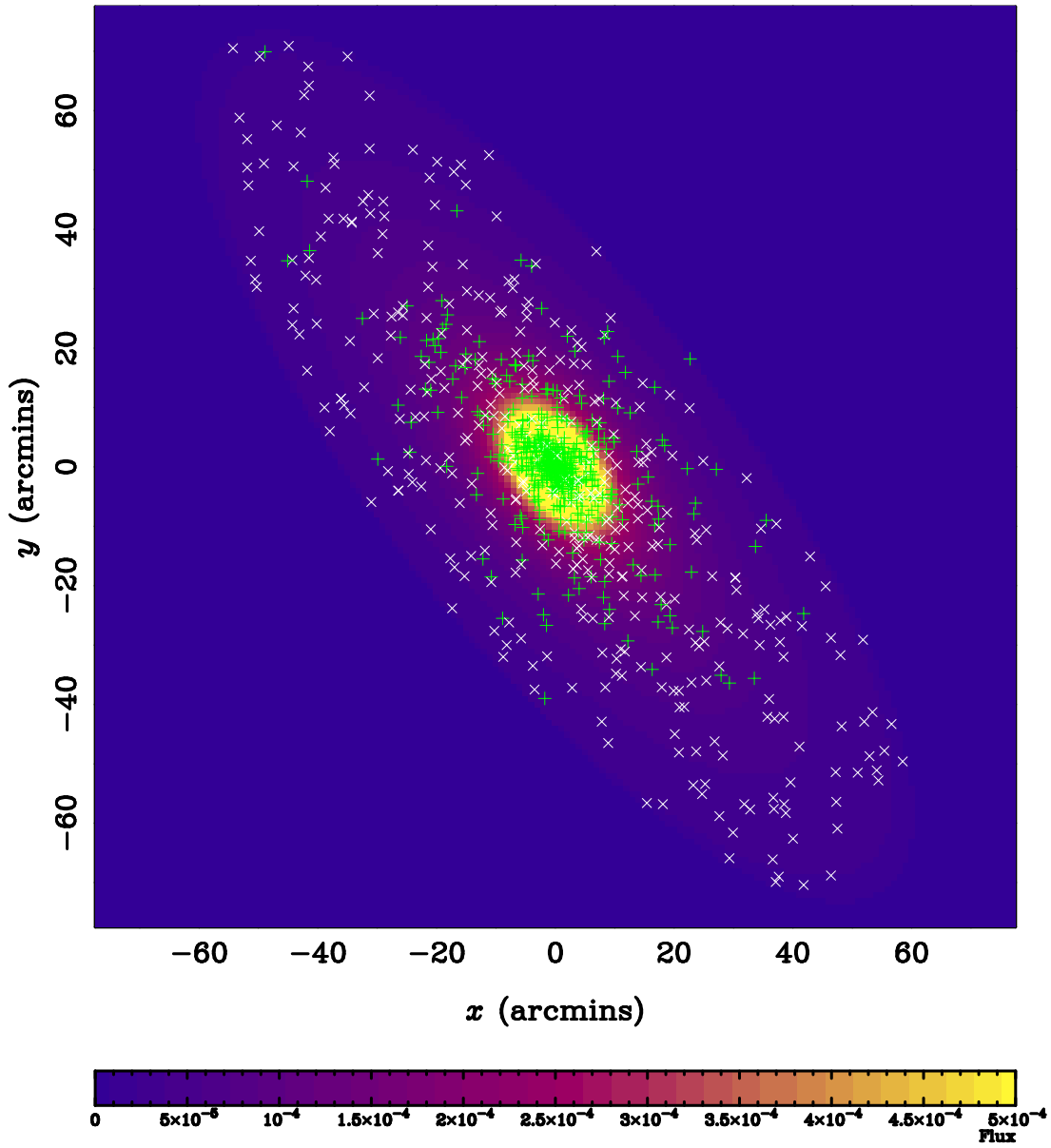

Figure 5.1: The spatial distribution of bulge (green '+') and disk (white '×') novae in M31 produced by the model from Darnley et al. (2006), with 1000 novae seeded. The background colours represent the nova rate of a given pixel (1 arcminute × 1 arcminute) indicated by the key at the bottom of the figure.

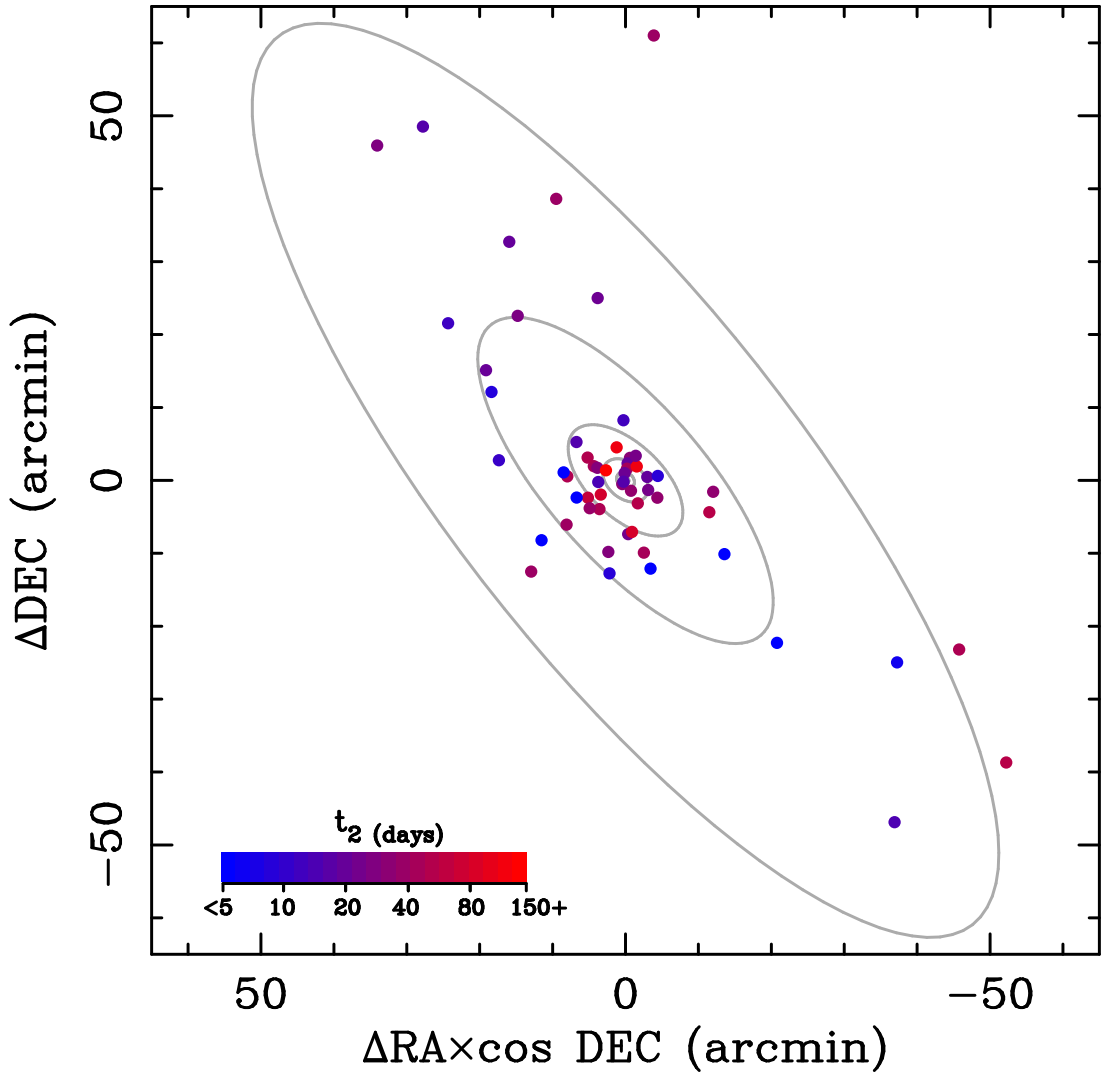

Figure 5.2: The spatial distribution of M31 novae with different t_2 values. The bluest colours represent the fastest fading novae, while the reddest colours represent the slowest novae.

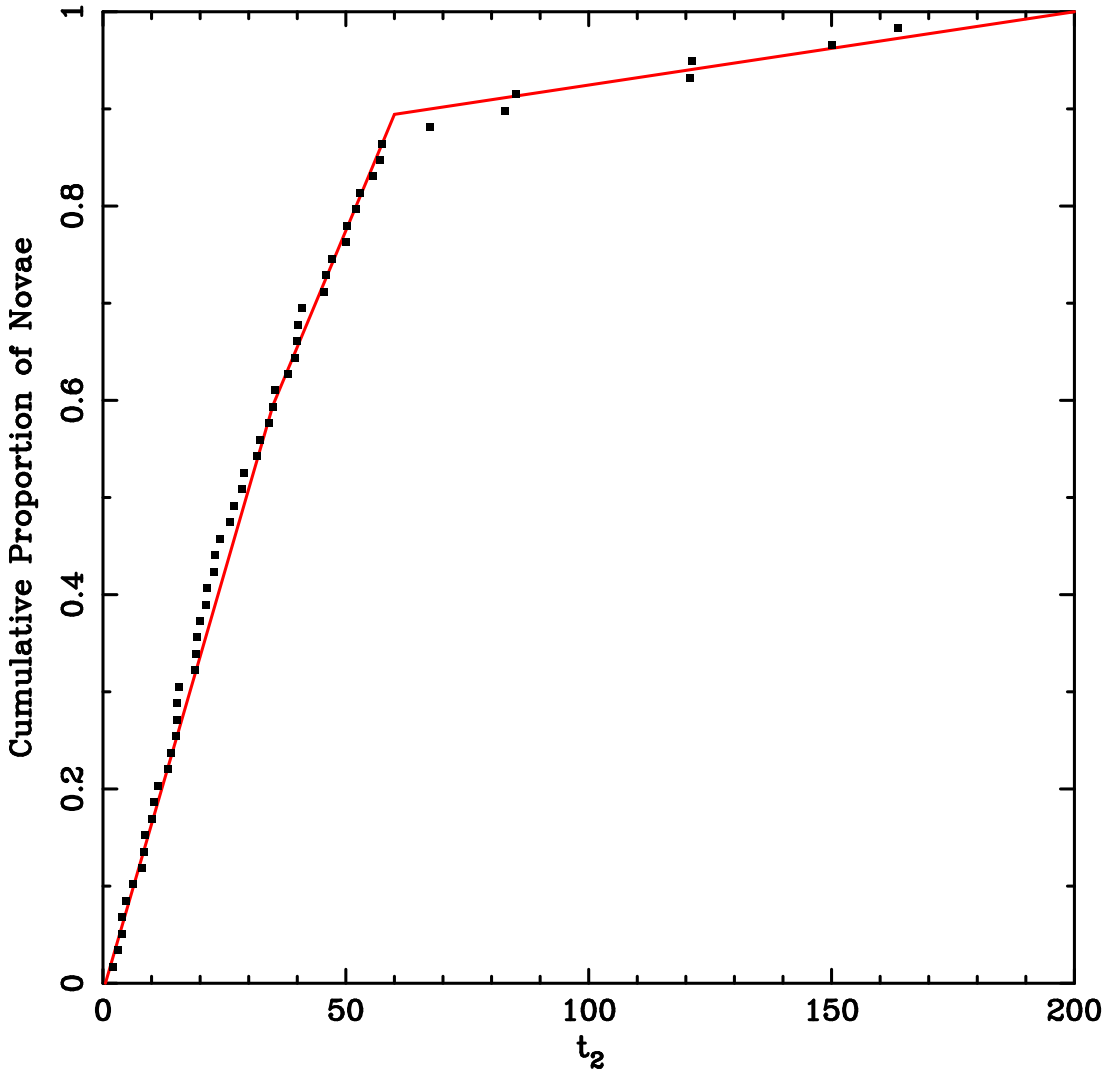

Figure 5.3: The cumulative t_2 distribution of novae in M31. The black squares represent t_2 values from Shafter et al. (2011b,f), Cao et al. (2012) and Williams et al. (2014). The red line represents the model used in this work.

The *R*-band MMRD is used, simply because that is the band with the most data. Although most of the observations used in the survey were not *R*-band, the *B* and *V*-band MMRDs found by the authors were not significantly different. Given this and the large scatter in the relationship, the *R*-band MMRD is assumed for all of the seeded novae in this model. To simulate the scatter in the relationship, a normal distribution with $\sigma = 0.70$ magnitudes was assumed. There may be two factors contributing to the observed scatter in the relationship; one, the fact that the correlation may not be intrinsically tight; and two, the novae will suffer from varying degrees of extinction internal to M31. The MMRD distribution that this produces is shown for 2500 seeded novae, plotted with the observational data from Shafter et al. (2011f) in Figure 5.4.

Having simulated a nova population, the potential biases in the catalogue are now discussed and considered below.

5.3 The Chance of Novae Being Discovered

As not every nova outburst in M31 is discovered, we needed to explore any biases in the probability of a given nova being discovered. The main problem that hinders the discovery of M31 novae is that it is difficult to observe for several months of the year. Other possible biases are faint novae being harder to detect and fast novae may possibly be missed altogether. On top of these, the available observing effort, be that dedicated surveys or the amateur community, plays a major part in the discovery efficiency. Table 5.1 shows the number of nova candidates discovered each calendar year between 2006 and 2012, with Table 5.2 showing the total number of novae discovered each calendar month between the start of 2006 and end of 2012[1].

It can be seen from Table 5.2 that only two novae have been discovered in April between 2006 and 2012. However, temporal biases in the detection are accounted for in Sections 5.4 and 5.5, so we do not need to consider them here.

The optimal months for observing M31 tend to be October and November, due to the

[1]Compiled from `http://www.mpe.mpg.de/~m31novae/opt/m31/index.php`

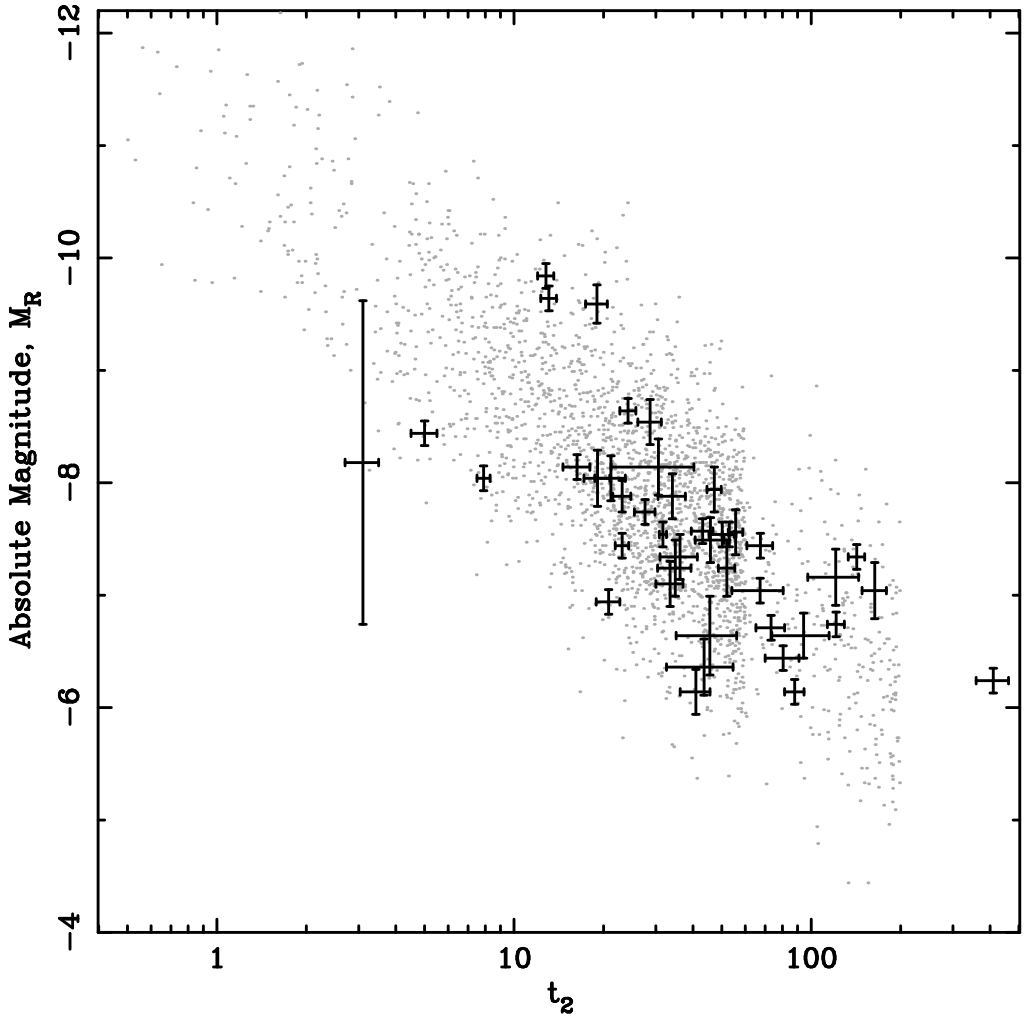

Figure 5.4: The *R*-band MMRD relationship used in the model. The black data-points represent observational data from Shafter et al. (2011f), with the grey points showing 2500 seeded novae from the model discussed in the text.

Year	Number of novae discovered
2006	19
2007	32
2008	31
2009	22
2010	28
2011	31
2012	28

Table 5.1: The number of M31 nova candidates discovered each calendar year between 2006 and 2012.

galaxy's position in the sky and the hours of darkness per night in the northern hemisphere. The year 2006 has a low discovery rate as does the latter part of 2012, probably due to lack of surveys (e.g. more novae were discovered in June 2012 than were from August to December 2012 combined). Therefore if only the novae discovered in the months of October and November from 2007 to 2011 are considered, a projected nova rate of 48 per year is derived. This also factors in that some candidates may not be novae (typically $\sim$5% of nova candidates are later found not to be novae[2]).

Some novae may not be discovered as they do not exceed the surface brightness of M31 for a given survey, others may be too far away from the centre to be covered by regular observations. The fastest novae will also be less likely to be discovered irrespective of their location, although they do tend to be brighter. Of course, the fact that fast novae may be missed makes it difficult to estimate how many actually occur. However, the effects of spatial position on the probability of discovery can be estimated by comparing the actual novae that occurred during the time of the survey to those predicted by the model described in Section 5.2.1.

During the time of the survey there were 184 nova candidates discovered (excluding transients that were subsequently found not to be novae)[3]. This is a relatively small number to explore the discovery probability as a function of radius, so only a very simple estimation can be derived. The probability of discovery as a function of distance from the centre of M31 is shown in Table 5.3.

[2]Estimated from `http://www.mpe.mpg.de/~m31novae/opt/m31/index.php`
[3]`http://www.mpe.mpg.de/~m31novae/opt/m31/index.php`

Month	Number of novae discovered	Average RA of M31 from Sun
January	15	5^{h}
February	17	3^{h}
March	9	1^{h}
April	2	1^{h}
May	14	3^{h}
June	26	5^{h}
July	15	7^{h}
August	20	9^{h}
September	14	11^{h}
October	22	11^{h}
November	24	9^{h}
December	18	7^{h}

Table 5.2: The number of M31 nova candidates discovered in each calendar month from the start of 2006 to the end of 2012 and the average difference in RA between M31 and the Sun in each month.

The probabilities of discovery listed in Table 5.3 were initially calculated with smaller bins, but the relative probability of discovery was relatively uniform out to 15 arcmin after the first 1 arcmin. The same applied for novae occurring further than 15 arcmin from the centre.

5.4 Probability of Being Observed with the LT

Table 5.2 shows that novae are rarely discovered in the month of April, however, as professional telescopes tend to be unable to observe as close to the horizon as amateur telescopes, this makes following candidates in the months near April very difficult. The LT, for example, can only observe down to an altitude of 25°. This does introduce a slight bias towards slower novae, as they can produce outbursts when M31 in not observable, yet still be detectable when M31 is visible again. Whereas the time frame where this is possible for faster novae is shorter. We can easily account for this bias in the model. As each seeded nova is assigned a t_2, we can determine for any nova occurring when M31 is unobservable, if the nova will still be bright enough to be detected when the galaxy first becomes observable again.

Distance from centre (arcmin)	Proportion of actual novae in range	Proportion of model novae in range	Relative probability of discovery based on spatial bias
$0-1$	0.04	0.11	0.27
$1-15$	0.64	0.49	1.00
$15-70$	0.31	0.38	0.67
$70+$	0.01	0.02	0.40

Table 5.3: The probability of a nova being discovered as a function of its distance from the centre of M31. The probability of discovery only considers discovery biases related to the apparent distance of novae from the centre of M31, thus is effectively normalised to 1.00. So novae occurring between $1-15$ arcmin from the centre are the most likely to be discovered, although obviously they will not actually have a 100% chance of discovery.

Some novae occurring in regions of the galaxy with high surface brightness (e.g. the centre or behind M32) may never be detectable with the LT. To account for this, a surface brightness model of M31 was created from the surface photometry of Kent (1987), assuming a seeing of $0.8''$ (the median of the LT). This surface brightness model is shown in Figure 5.5.

Additionally it is possible that very fast novae could be missed due to telescope down-time or weather. The longest period of time that the LT was unable to observe (due to either technical downtime or weather) during the epoch of our survey was 17 consecutive nights, with 10 periods lasting longer than 10 days during that time. While it is unlikely that a very fast nova would occur just as the LT had a long non-observing period, U Sco faded by around 5 or 6 magnitudes within 10 days[4]. This would make it hard to observe if such an outburst coincided with one of these periods. This was also accounted for in the model by using the observation logs of the LT[5] during the period of the survey. Any periods where no LT time was available to observe any novae were also accounted for. Also novae that produced an outburst during the seasonal gap of M31 would not have been followed by the LT, unless they were reasonably close to the time when M31 became observable again. For example novae in March and April would have effectively never been observed.

[4]Estimated from `http://www.aavso.org`
[5]Obtained from `http://telescope.livjm.ac.uk`

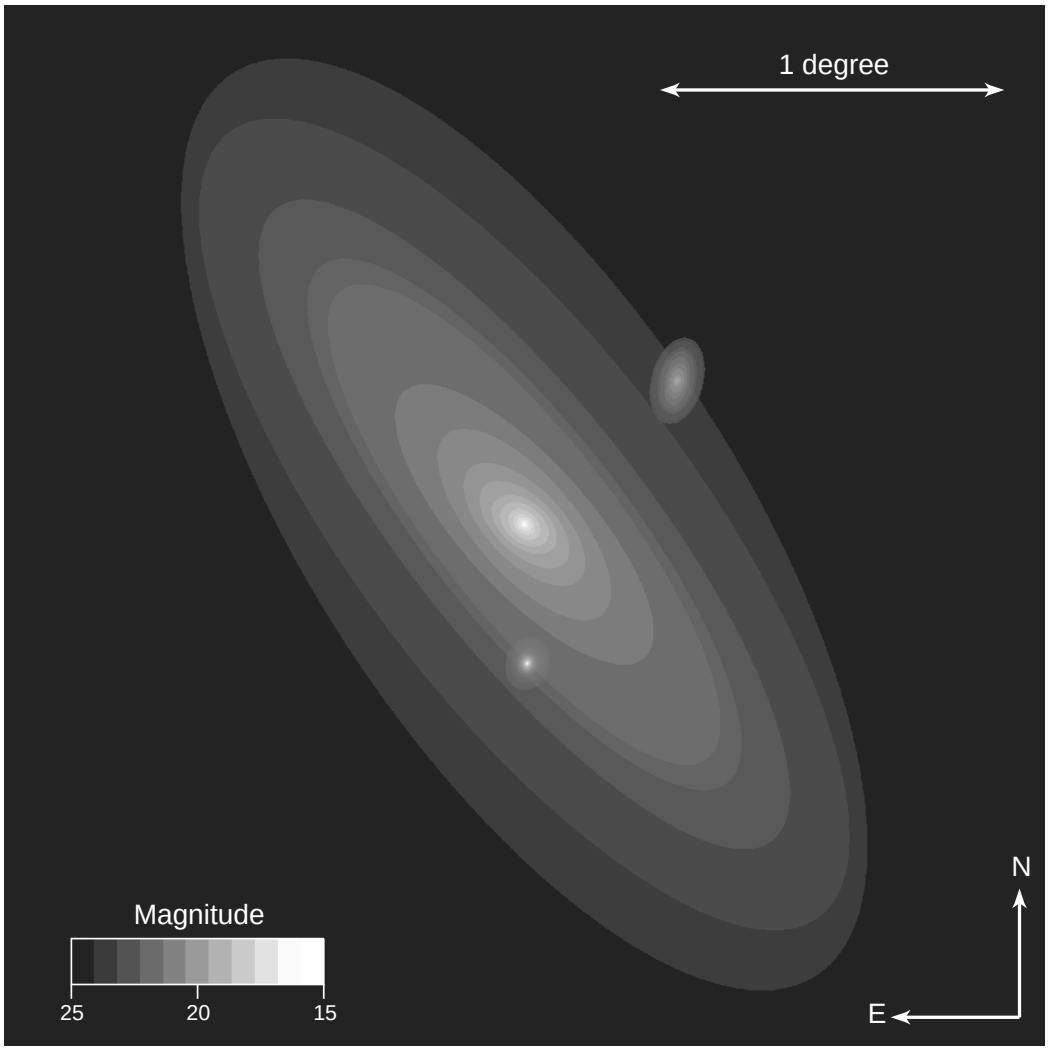

Figure 5.5: A surface-brightness map of the M31 field, also showing M32 (lower satellite) and NGC 205 (upper satellite). The scale is in magnitudes and the map was created using surface photometry from Kent (1987).

5.5 Probability of Spectroscopic Confirmation

The likelihood of a given nova being spectroscopically confirmed also needs to be considered. As with photometric data, the main factor influencing the ability to obtain spectra is the time of year an outburst occurs. As novae were included in the survey if they had any spectroscopic confirmation (i.e. using any telescope), a direct analysis could not be performed as was possible for the photometric data in Section 5.4. The best method is therefore to consider the chance of spectroscopic confirmation based on the time of year the outburst occurred. This not only accounts for the position of M31 in the sky, but also any other biases, for example, those associated with telescope semesters beginning or ending. Table 5.4[6] shows the proportion of novae in a given calendar month that were spectroscopically confirmed.

Month	Proportion of novae spectroscopically confirmed
January	0.44
February	0.29
March	0.00
April	0.00
May	0.23
June	0.63
July	0.80
August	0.70
September	0.79
October	0.86
November	0.79
December	0.78

Table 5.4: The proportion of nova candidates from August 2006 to February 2013 that had spectra taken in each calendar month.

Of course the proportions listed in Table 5.4 will not be the actual probabilities of spectroscopic confirmation, but they are the most reliable way of adding this into the model. In addition, the probability of spectroscopic confirmation may depend on the speed class and position of the nova. For example, it can be difficult to obtain spectra near the centre of M31 due to the lack of other stars in the field. Figure 5.6 shows all nova candidates discovered during the time of the survey (August 2006 – February 2013).

[6]Compiled from `http://www.mpe.mpg.de/~m31novae/opt/m31/index.php`

However, as can be seen in Table 5.4, novae occurring during certain times of the year are unlikely to be spectroscopically confirmed no matter where in the galaxy they lie. Therefore, when considering the bias in relation to spatial position, it is more helpful to consider novae that produced outbursts when M31 was at a favourable observing position. Figure 5.7 shows novae occurring between July and December (inclusive) during the time of the survey.

If the data are binned as a function of distance from the centre of M31, it can be seen in Table 5.5 that novae occurring near the galactic centre are less likely to be spectroscopically confirmed. Given the relatively small numbers, the chance of a spectrum being taken appears largely uniform at distances from the centre of M31 greater than 5 arcminutes. Some of the candidates further out may not have had spectra taken for other reasons. For example the $20' - 50'$ bin includes two non-spectroscopically-confirmed outbursts of the RN M31N 2008-12a, which fades very fast (see Chapter 6.2) and a spectrum may not have been taken in time. If it is assumed there is no spectroscopic-confirmation bias beyond $5'$, it is estimated the probability (with respect to spatial position) of a spectrum being taken of a nova less than $2'$ from the centre of M31 is 67%, with a nova between $2'$ and $5'$ from the centre having an 85% chance of spectroscopic confirmation. Note that these probabilities only consider the effect of spatial position and not parameters such as speed class and time of year, which are discussed above.

Distance from centre of M31 (arcmin)	Proportion of candidates that were spectroscopically confirmed
< 2	$0.59^{+0.11}_{-0.12}$
$2 - 5$	$0.74^{+0.08}_{-0.10}$
$5 - 10$	$0.92^{+0.04}_{-0.12}$
$10 - 20$	$0.88^{+0.05}_{-0.08}$
$20 - 50$	$0.80^{+0.07}_{-0.10}$
$50+$	$1.00^{+0.00}_{-0.12}$

Table 5.5: The proportion of nova candidates that were spectroscopically confirmed between the months of July and December from 2006 to 2012 (see text for explanation) as a function of distance from the centre of M31. The errors quoted are simply the statiscical uncertainties due to the relatively small number of novae in each bin.

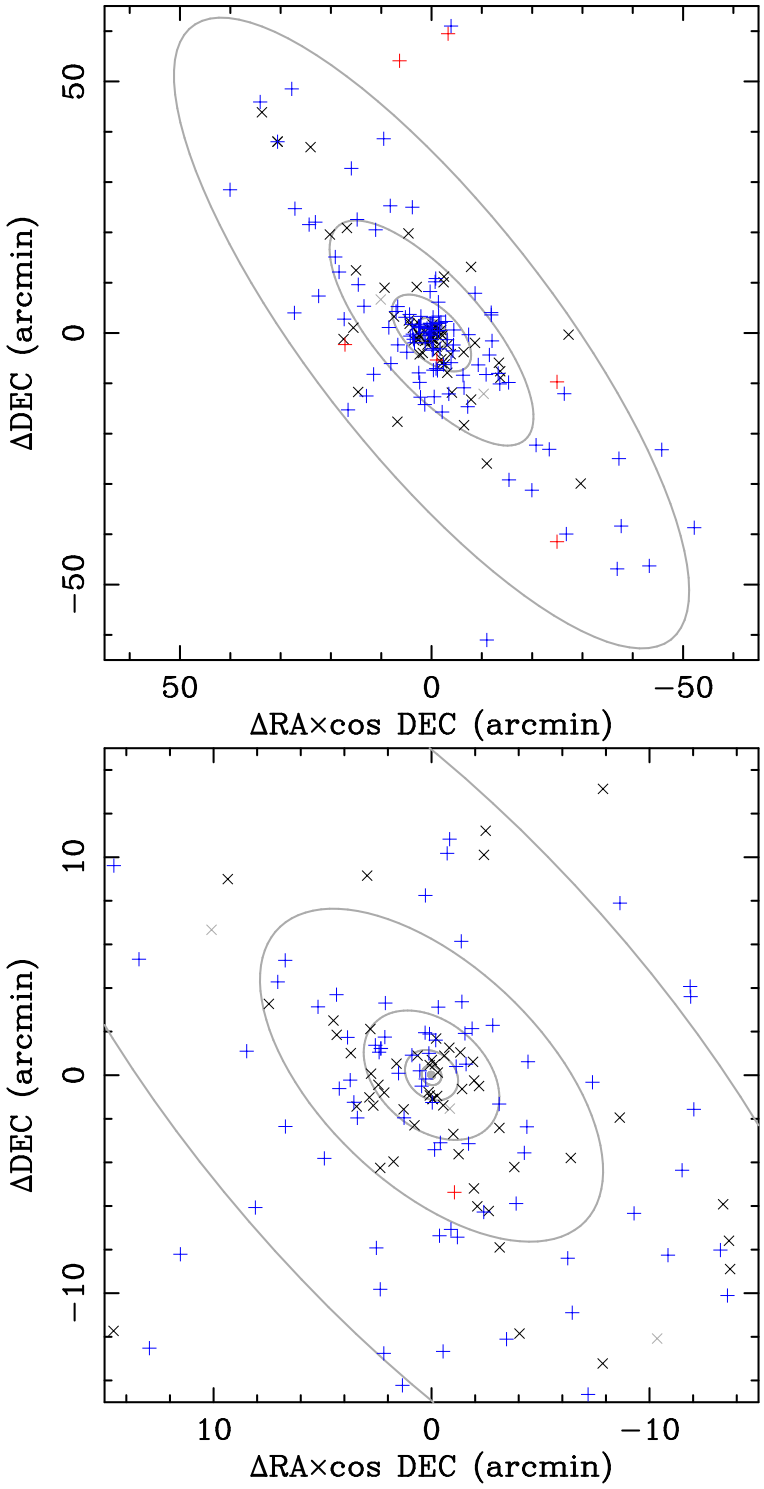

Figure 5.6: The spatial distribution of spectroscopically and non-spectroscopically-confirmed novae in M31. Spectroscopically-confirmed novae are indicated by a blue '+' and non-spectroscopically-confirmed nova candidates are shown as a black '×'. A red '+' indicates a nova candidate that had a spectrum taken, but was found not to be a nova, whereas a grey '×' indicates a nova candidate that did not have a spectrum taken, but was found not to be a nova through another method.

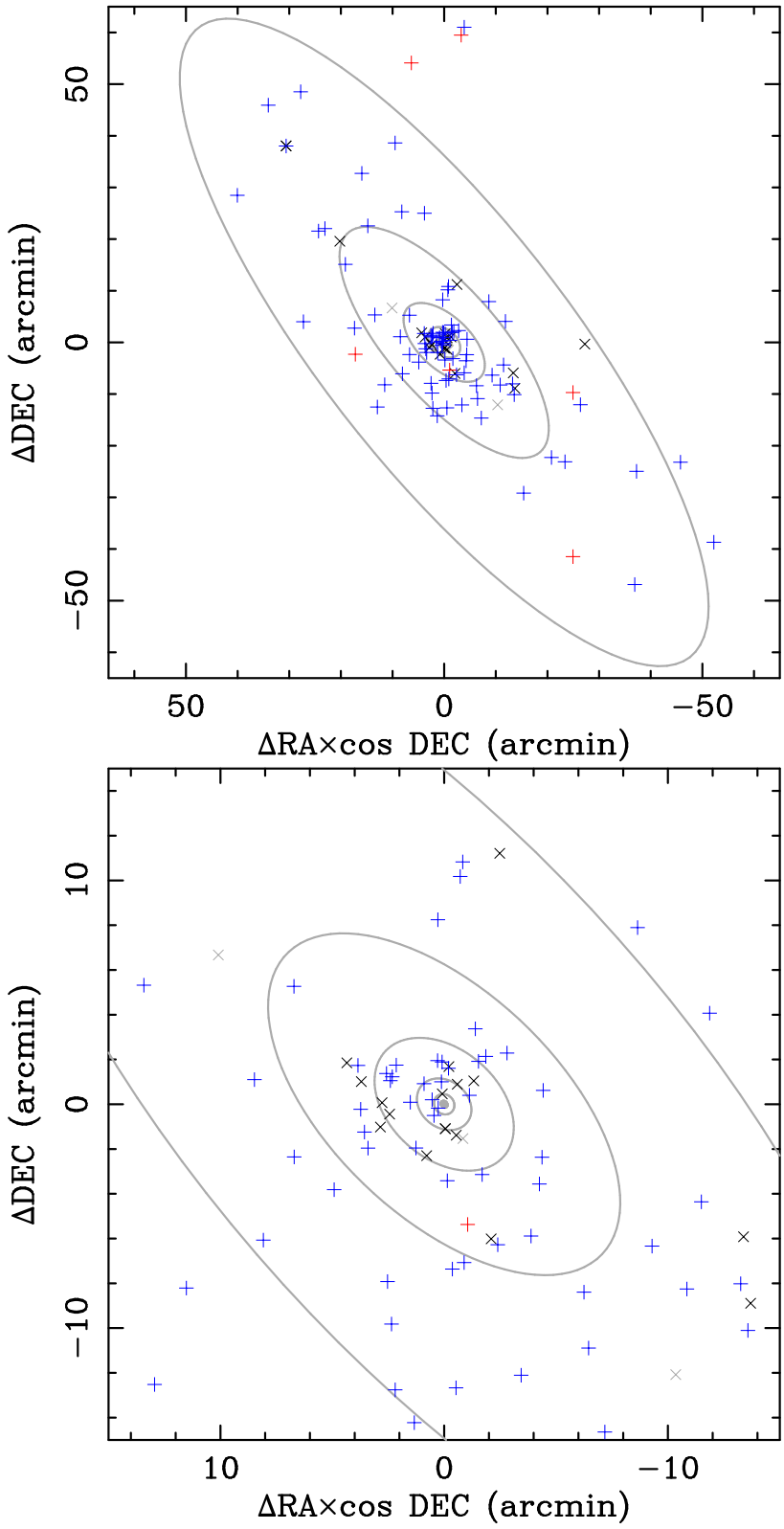

Figure 5.7: The spatial distribution of spectroscopically and non-spectroscopically-confirmed novae in M31 that occurred between the months of July and December (inclusive) during the time of the survey. Points as in Figure 5.6.

As noted above, the chance of spectroscopic confirmation is likely to depend on speed class. A nova with a t_2 of just a few days, for example, could easily fade before a spectrum is taken. However this cannot be easily accounted for, because the sample of t_2 values is biased towards spectroscopic confirmation, as many of them were from the spectroscopic and photometric survey of M31 novae published by Shafter et al. (2011f).

5.6 Archival *HST* Coverage

It was determined if each seeded nova would have suitable archival *HST* data by downloading the header information for WFC3/UVIS, ACS and WFPC2 data taken of the M31 field. The headers were searched for and acquired using the Starview program[7] hosted by the Space Telescope Science Institute. We considered data taken using F435W, F439W, F475W, F555W, F606W, F625W, F675W, F702W, F775W and F814W filters for the survey. The headers gave information on whether each point (0.1×0.1 arcmin^2) in M31 had *HST* coverage and in what filters. However, as some of the *HST* data were taken during the time-frame of this survey, the date of each *HST* images was also recorded. This allows the model to correctly handle seeded outbursts occurring within existing *HST* data.

It can be difficult to determine exactly when a nova reaches quiescence, as even while in their quiescent state, novae can show variations in their brightness. If post-outburst data were used for the progenitor search of a given nova in the M31 catalogue, it was ensured that the nova was likely to be at quiescence either using multiple *HST* observation epochs (where available), or alternatively if the data were taken a long time after a nova had produced its outburst, as described in Section 3.3.2. However, for this statistical analysis, a general rule had to be produced, which was that all novae were considered to be at quiescence two years after their outburst. Clearly this is far from the true picture and it would be expected that novae that have lower t_2 values may tend to reach quiescence sooner, however it is uncertain how tight this relationship is. For

[7] `http://starview.stsci.edu`

example RS Oph had a t_2 of 7 days and took 93 days to reach quiescence, V574 Puppis had a t_2 of 12 days and took 840 days to reach quiescence, yet IM Normae, with a t_2 of 50 days, only took 761 days to reach quiescence (Strope et al., 2010).

Figure 5.8 shows the *HST* ACS coverage of the M31 field, with 0.1 arcmin resolution. The M31 coverage in the various filters of ACS, WFPC2 and WFC3/UVIS is shown in Appendix A. For this work only ACS data are considered, as this covers 33 out of the 38 novae in the catalogue and the red-giant branch is generally resolvable in the data, whereas some of the WFPC2 data have a relatively bright limiting magnitude.

5.7 Simulating the Closest Source to a Seeded Nova

How the resolved stellar population density varies as a function of distance from the centre of M31 was found by examining the photometry of point sources in F814W and F475W ACS/WFC *HST* images in eleven fields along the semi-major axis of M31 (moving north-east from the centre). The data for these eleven fields are shown in Table 5.6. Linear extrapolation between the fields gave the resolved stellar density as a function of distance along the semi-major axis from the centre of the galaxy, which is shown in Figure 5.9.

A circular flat disk is assumed where the stellar density is uniform at any point in the disk at a given radius. The disk is assumed to be inclined with a minor/major axis ratio of 0.31, allowing the apparent population density to be calculated for any point in the disk.

The closest source to a given nova was calculated by randomly seeding points at a given density around the nova, then simply measuring which one was the closest.

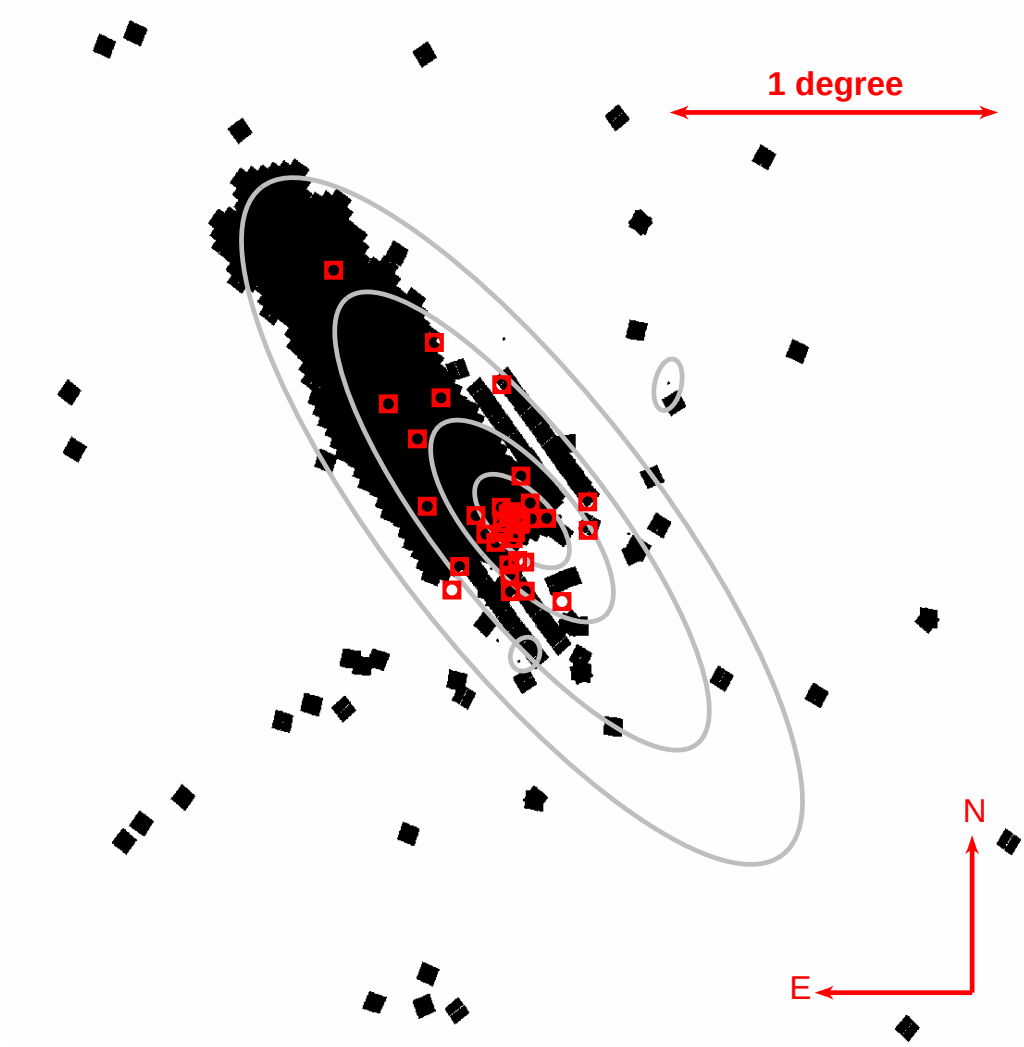

Figure 5.8: The ACS *HST* coverage of M31. Covered regions appear in black, with regions with no coverage appearing white. The red points indicate the 38 novae from the catalogue and the grey ellipses represent isophotes from the surface photometry of Kent (1987).

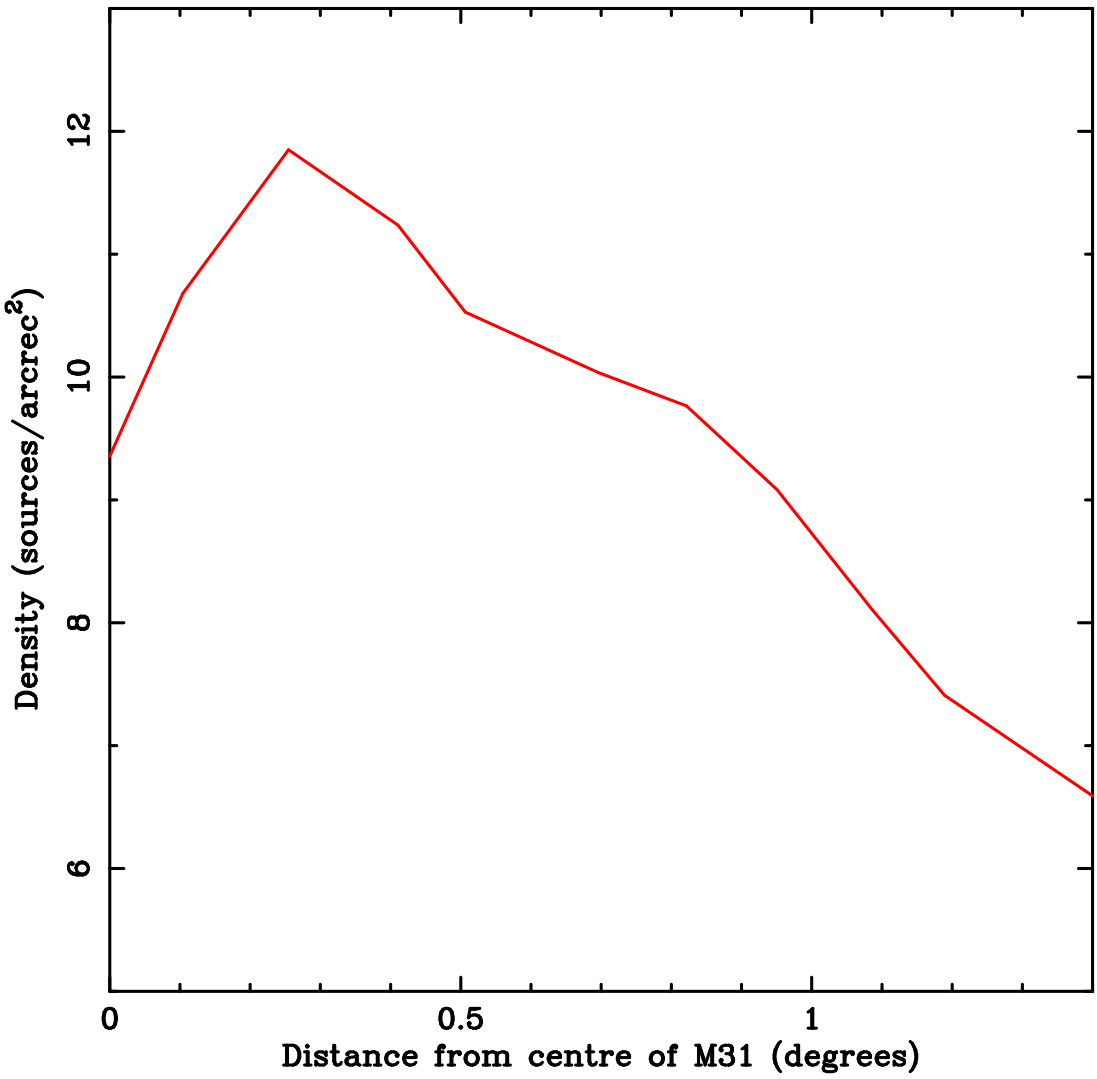

Figure 5.9: The resolved stellar population density of the M31 field as a function of distance along the major axis from the centre of the galaxy. The density was calculated from linear extrapolation of the eleven fields of *HST* data along the (north-eastern) semi-major axis presented in Table 5.6.

Distance from centre of M31 (degrees)	Resolved stellar population density (sources/arcsec^2)
1.33	6.85
1.19	7.41
1.09	8.10
0.95	9.08
0.82	9.76
0.70	10.04
0.51	10.53
0.41	11.24
0.25	11.85
0.10	10.68
0.03	9.69

Table 5.6: The resolved population density in ACS/WFC *HST* data as a function of distance along the semi-major axis from the centre of M31.

5.8 Probability of Chance Alignment

After the closest source to the position of each seeded nova has been simulated, the significance of each detection must be calculated. For the 38 systems in the catalogue, this was done using a Monte Carlo technique, but here a general mathematical solution is derived.

Considering *N* sources in an area of *A* giving a density of *n*, the probability of a source being between a radius r and $r + dr$ is $2\pi ndr$ and the probability of a source being outside the circle of radius *r* is given by

$$1 - \frac{\pi r^2}{A}$$

Therefore the probability of a source being between a radius r and $r + dr$, with that source being the closest is given by

$$P_N(r)dr = 2\pi rndr \left(1 - \frac{\pi r^2}{A}\right)^{N-1}.$$

Substituting

$$a = \left(\frac{1}{\pi n}\right)^{\frac{1}{2}} \tag{5.2}$$

gives

$$P_N(r)dr = \frac{2r}{a^2}dr\left(1 - \frac{r^2}{a^2}\frac{1}{N}\right)^{N-1}$$

If $N \to \infty$ is considered, and given

$$\left(1 + \frac{1}{x}\right)^x = e$$

when $x \to \infty$. Therefore

$$P(r) = \frac{2r}{a^2}e^{-\frac{r^2}{a^2}}.$$

So the probability of the closest source being within a radius r from a given point is given by

$$\int_0^r P(r)dr = 1 - e^{\frac{r^2}{a^2}}.$$

Substituting for *a* from Equation (5.2) leaves

$$\int_0^r P(r)dr = 1 - e^{-r^2\pi n}.$$

If the probability of chance alignment of $\leq 5\%$ is used as the criterion for likely progenitor recovery, as was done for the catalogue, then the maximum separation between a source and the nova is given by

$$\int_0^r P(r)dr = 0.05.$$

Hence the maximum distance between a source and the position of the nova so that the probability of chance alignment is $\leq 5\%$ is given by

$$r = \left(-\frac{\ln 0.95}{\pi n} \right)^{\frac{1}{2}} . \tag{5.3}$$

Equation (5.3) was then used to check if the closest source (as calculated using the method described in Section 5.7) to a given nova would be a significant detection (i.e. $\leq 5\%$ probability of being a chance alignment).

This method was tested using the nova code described in Section 5.2.1 and the M31 source density model presented in Section 5.7. If no novae are assumed to be associated with a source, 5% of novae have a coincident source classified as a significant detection ($\leq 5\%$ probability of being a chance alignment), as would be expected.

The final parameter that had to be considered was the accuracy of the transformation of the position in the LT data to the archival *HST* data. This is because if a nova is seeded to be associated with a source in the *HST* data, after transformation it would not necessarily be found to be coincident with that source to the $\leq 5\%$ accuracy required. For this the median accuracy of the 33 LT to ACS/WFC transformations in the catalogue (0.0385 arcsec) was used.

5.9 Summary of the Model

All the stages described above were added into a model, which is summarised below. Monte Carlo techniques were then used to explore the proportion of novae in M31 likely to be associated with a source in the *HST* data, a group expected to be dominated by RG-novae. As 33 systems had ACS *HST* data, the seeded novae were split into groups of this size. The likelihood of 8 out of the 33 novae being coincident with a source in the *HST* data was then tested (this is an adaptation of the nova rate determination used by Shafter & Irby, 2001). The figure of 8 out of 33 is used (rather than 11/38) because 8 out of the 33 LT to ACS/WFC transformations (i.e. the data being

modelled here) found a likely progenitor candidate. The model was run from no novae being seeded as associated with a source (i.e. no novae being RG-novae), to all novae seeded as being associated with a source in the *HST* data. In the model:

- Novae are seeded by the model from Darnley et al. (2006) and assigned t_2 values based on the overall t_2 distribution of novae in M31. These t_2 values are then used to assign peak magnitudes through the MMRD relationship.
- The discovery biases related to the spatial position of the nova are then applied, with nova outbursts less likely to be discovered if they occur in certain regions of the galaxy.
- The probability of the novae being observed with the LT is then considered, with M31 being unobservable for several months of the year. Additionally novae may not be observable due to down time of the telescope. The probability of a given nova being observed with the LT may be affected by its t_2, as the fastest novae may not be observable if their outbursts occur during telescope downtime and they have already faded by the time the telescope starts observing again.
- The probability of the novae being spectroscopically confirmed is also considered. Spectra are less likely to be taken during some parts are the year, and they are also more difficult to acquire for novae occurring near the centre of M31.
- The biases associated with the *HST* coverage of M31 are then accounted for, as a given nova would have to have coincident *HST* data taken whilst it was in quiescence, to be included in the survey.
- The model then simulates a certain proportion of novae as being associated with a source in the *HST* data. The accuracy of the LT to ACS/WFC positional transformation of the survey was used to determine how well a nova seeded with a resolved progenitor would actually be aligned with that progenitor after the transformation.
- The background resolved stellar density as a function of radius is then simulated,

producing fake stellar sources around a given seeded nova, thus simulating the possibility of chance alignments.

- The significance of each detection was then determined, whether it was a nova seeded with a resolvable progenitor or simply a chance alignment.
- A Monte Carlo model was run on random groups of 33 seeded novae to test how many groups would have 8 likely progenitors recovered. This was run from no novae, up to 100% of novae, being seeded with a resolvable progenitor.

Therefore if a nova is seeded with a resolved progenitor, it must make it through each of the bias filters. It must:

- Have been discovered.
- Be spectroscopically confirmed.
- Be visible when M31 was observable with the LT.
- Have coincident *HST* data taken when it would have been in quiescence.
- Have a simulated offset of the positional transformation (i.e. LT outburst image to *HST* image) small enough so the probability of chance alignment is $\leq 5\%$.

5.10 Results

The model was initially run using the nova generator code described in Section 5.2.1 (4.88×10^8 novae seeded), plus only the closest source and chance alignment considerations described in Sections 5.7 and 5.8 and not the various biases discussed above (i.e. assuming the catalogue sample was representative of the M31 nova population). The code was run from no novae seeded with a resolved progenitor to all novae being seeded with a resolved progenitor (in fractional steps of 0.01). The resulting distribution is shown in Figure 5.10 and shows that given the results of the survey, 0.37 is the most likely proportion of novae that are actually associated with a source in the *HST*

data. As stated previously, the group of novae associated with sources in the *HST* data would be expected to be dominated by novae with red giant secondaries. The distribution gives the 68% confidence range as $0.24 - 0.51$ and the 95% confidence range as $0.15 - 0.66$.

Given that of the 33 quiescent systems that were searched for using LT and ACS/WFC data, eight had likely progenitor candidates, the probability of no novae being actually associated with (rather than just coincident with) a source in the *HST* data is 2×10^{-5}. The probability that no more than 3% of novae (i.e. greater than the Galactic RG-nova rate observed so far) are associated with a source in the *HST* data is 3×10^{-4}. This model also tells us that the proportion of novae associated with a source in the *HST* data is greater than 0.11 to the 99% confidence level.

The model was then run again with the effects of all the biases as discussed above added in. When considering the proportion of sources that are seeded as being associated with a source in the *HST* data, this version of the code was run in steps of 0.02, as due to the filter effect of accounting for each bias, much fewer of the seeded novae get through to the final stages of the model where the novae are split into groups of 33. This model gives the proportion of sources associated with a source in the *HST* data as between $0.26 - 0.54$ to the 68% confidence level and between $0.16 - 0.70$ at the 95% confidence level, with the most likely proportion being 0.38. Note that all these figures are to the nearest 0.02 for the reasons described above. The results of this more detailed model are compared to the initial model in Figure 5.10. The results of the two models are also summarised in Table 5.7

Confidence level	Proportion of novae associated with a source in *HST* data	
	The initial model	The detailed model
Most likely	0.37	0.38
68%	$0.24 - 0.51$	$0.26 - 0.54$
95%	$0.14 - 0.66$	$0.16 - 0.70$
99%	> 0.11	> 0.10

Table 5.7: The proportion of M31 novae likely to be associated with a source in the *HST* data as defined by the statistical models of the M31 progenitor survey.

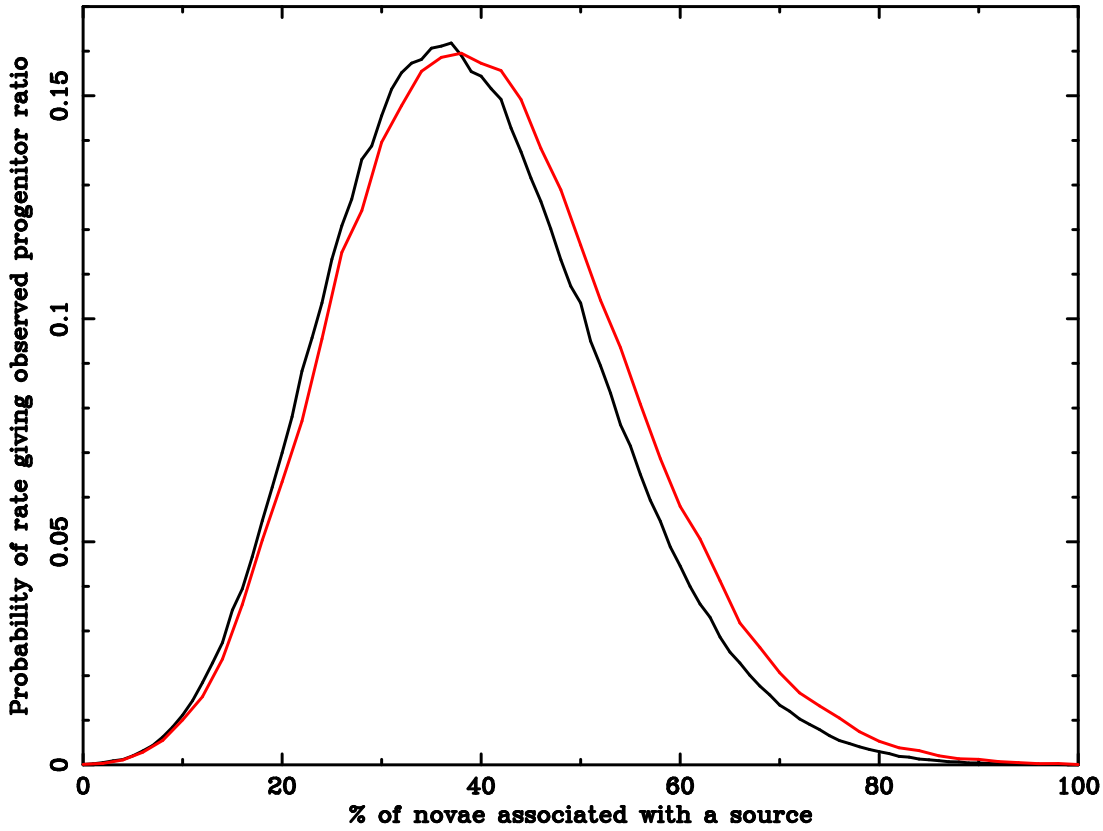

Figure 5.10: A distribution showing the proportion of novae expected to be associated with sources in the *HST* data by the model that incorporates possible biases of the survey, as well as the distribution of the novae and the accuracy of the transformation between the LT and *HST* data. The black line shows the results of the initial model, which did not consider the biases, and the red line shows the results of the more detailed model that also accounts for the possible biases in the survey.

5.11 Discussion and Conclusions

The initial results of the statistical analysis suggest that the proportion of M31 novae associated with a source in the *HST* data, a class of objects expected to be dominated by RG-novae, is $0.38^{+0.16}_{-0.12}$, where the errors represent the 68% confidence level. The model also indicated to a high level of confidence (99.95%) that the proportion of novae associated with a resolved quiescent source is > 0.04 (i.e. greater than the Galactic RG-nova rate that had been observed so far; the 0.04 cut-off, rather than 0.03 used for the initial model, is used because the more detailed version of the model was run in steps of 0.02 for the reasons described above). This is an important result for the study of nova populations, as it shows that a significant proportion of all nova systems are likely to contain an evolved companion star. As already discussed, for many of the Galactic systems, the nature of the secondary has not been determined, so it is uncertain if there is a real difference in the proportion of nova systems associated with red giant secondaries, between M31 and the Galaxy.

Recent work by Pagnotta & Schaefer (2014) attempted to identify RN candidates among the CN population. They used several parameters to try and identify these systems, including ejection velocity, evolutionary state of the secondary and white-dwarf mass. Using data for 237 CNe, they used three different methods to get the RN fraction amongst the know CNe as $24\% \pm 4\%$, $12\% \pm 3\%$ and $35\% \pm 3\%$. Notably, they suggested 16 of the 74 novae CNe where the likely nature of the secondary was able to be determined, probably contain red giant secondaires. If this is added to the 5 RG-novae among the RN population, we get a figure of 21 out of 84 (25%). This proportion is much closer to the proportion we have found in M31, particularly when considering that, although likely dominated my RG-nova, our rate may also be contaminated by some SG-novae.

The results of this work are perhaps even more important when considering its implications on RG-novae as viable SN Ia progenitors. The high proportion of novae we find likely to be associated with red giant secondaries in M31, which the results of Pagnotta & Schaefer (2014) for our Galaxy now back up, means that RG-novae could

be a much larger contributor towards the SN Ia progenitor population than previously believed.

The spatial positions of the eleven novae with recovered likely progenitors are compared to what would be expected by the model if the progenitor systems were associated with the bulge, the disk or the entire population (i.e. uniformly distributed throughout the bulge and disk) in Figure 5.11, with the archival *HST* coverage bias discussed in Section 5.6 and the discovery bias as described in Section 5.3 taken into account. The figure appears to show that the novae with recovered progenitors are more likely to be associated with the M31 disk, rather than the bulge. Note that if the catalogue of likely progenitors includes chance alignments, the spatial distribution of the progenitor candidates shown in Figure 5.11 would be expected to be shifted towards the overall nova population model (red line; i.e. further away from the disk model). A KS-test of the results reveals there that if the novae with likely progenitor candidates were associated solely with the disk population, the distribution of the novae would be expected to vary at least as much as it does 72.92% of the time. Whereas if they were uniform throughout M31 or only associated with the bulge, there is only a 0.34% and 0.01% probability, respectively, of such a variation. Therefore these initial results suggest the RG-novae are mainly or entirely associated with the M31 disk population.

If we assume that all the novae associated with a quiescent source in the *HST* data are associated with the disk and also assume 40% of nova eruptions are produced by disk novae, as predicted by the model of Darnley et al. (2006), then the results of the survey imply $0.95^{+0.05}_{-0.30}$ of disk novae should be associated with a quiescent source in the *HST* data, thus likely to be RG-novae. This is an important result as it indicates that there are two distinct nova populations, one associated with the disk and one associated with the bulge, as has been suggested in some earlier works (e.g. Duerbeck, 1990; della Valle et al., 1992). If this result is applied to galaxies dominated by younger stellar populations, such as M33, we may expect the majority of novae in such galaxies to have evolved secondaries.

This result is also important when considering RG-novae as SN Ia progenitor candidates, as it indicates that any SNe Ia that do come from RG-nova systems would not

be expected to be associated with the oldest stellar populations. It is, for example, unlikely that such a SN Ia would be found in an early-type galaxy.

Having conducted a statistical analysis of the survey for M31 progenitors, the thesis now presents the progenitor search of three additional extragalactic variable sources.

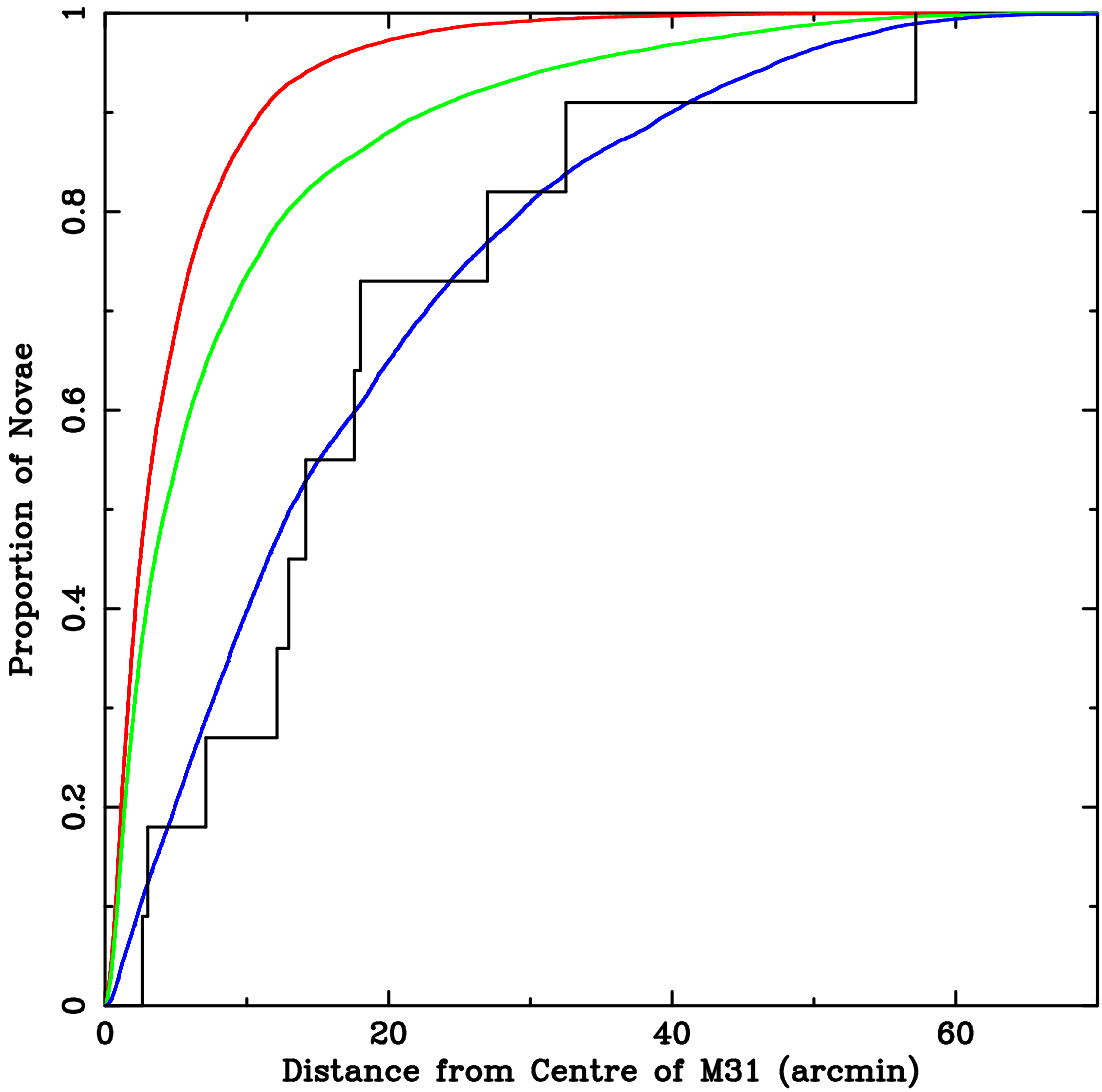

Figure 5.11: The spatial positions of the eleven progenitor candidates compared to what would be expected if such systems were associated with the bulge, the disk, or the entire stellar population of M31. The black (stepped) line shows the eleven progenitor candidates recovered in the survey. The green (middle) line represents the distribution expected from the model for M31 novae, with the blue (lower) line representing the distribution expected if the recovered progenitors are only associated with the disk, and the red (upper) line representing that expected if the progenitors were only associated with the bulge. The three model distributions also consider the *HST* coverage bias and the possible discovery biases discussed in the text.

Chapter 6

The Progenitors of Three Additional Extragalactic Variables

6.1 Introduction

The method for searching for nova progenitors described in Section 3 can also be used for other extragalactic transients that are reasonably luminous in quiescence. This chapter first looks at the extreme RN M31N 2008-12a, which appears to have an inter-outburst period of about one year, in both outburst and quiescence. In addition, the progenitor location method was used to derive upper limits on the luminosity of the progenitor of SN 2014J, a SN Ia in M82. It was also used to explore the nature of M31 optical transient TCP J00403295+40343877.

6.2 Observations of M31N 2008-12a – a Recurrent Nova with a Very Short Inter-outburst Period

The survey for the progenitors of M31 novae described in Chapter 3 ended in February 2013. However, RN M31N 2008-12a, produced an outburst in late November 2013, with coincident outbursts also having been recorded in 2008, 2011 and 2012. This

inter-outburst period is the shortest known, much less than U Sco, which at ~ 10 years, has the shortest recurrence time Galactically. The progenitor of this interesting object was searched for in archival *HST* data, but it was not included in the original catalogue presented in Chapter 3 or the statistical analysis presented in Chapter 5 because the outburst occurred after the end of the survey (no LT data were available for previous outbursts) and as the object was specifically targeted, it may bias the statistics if included.

6.2.1 The 1992, 1993 and 2001 X-ray Outbursts

An X-ray transient, named RX J0045.4+4154, was observed to be in outburst in February 1992 and again in January 1993 by White et al. (1995), who suggested it was an accreting WD, with a mass of about $1.3 - 1.4\,\mathrm{M}_{\odot}$. A further X-ray outburst, detected in September 2001, was reported by Williams et al. (2004). As no optical counterpart had been found for this system prior to 2008, it was not recognised as a nova. The transient was only linked to the RN outbursts after the 2013 eruption (Henze et al., 2014a; Darnley et al., 2014; Tang et al., 2014).

6.2.2 The 2008 Outburst

K. Nishiyama and F. Kabashima discovered an M31 nova candidate, named M31N 2008-12a, at $0^{\mathrm{h}}45^{\mathrm{m}}28^{\mathrm{s}}.80$, $+41^{\circ}54'10''.1$ on images taken on 2008 December 26.48 UT. At this point it was at an unfiltered magnitude of 18.7. They also reported the nova to have an unfiltered magnitude of 19.9 on December 27.493.[1] Unfortunately, this is the only photometry available for this outburst. The first LT data were taken on 2009 January 10.85 UT, when the nova was not visible down to a *B*-band limiting magnitude of 19.9. The nova was not visible on frames taken around January 13.93, which had a *B*-band limiting magnitude of 21.1. The nova was not visible at any other wavebands down to the following limiting magnitudes: 20.1 on January 10.85 and 21.2 on January

[1] see `http://www.cbat.eps.harvard.edu/CBAT_M31.html#2008-12a`

13.93 in *V*-band, 20.8 on January 10.84 and 21.0 on January 13.92 in r'-band, 19.8 on January 10.84 and 20.9 on January 13.92 in i'-band. It therefore seems probable that $t_2 < 20$ days.

6.2.3 The 2009 Outburst

A outburst coincident with M31N 2008-12a occurred in December 2009, but was not reported until after the 2013 outburst (Tang et al., 2014). There is little data available for this outburst, but the limited photometric data are broadly consistent with later outbursts, with the nova having faded by over two magnitudes in *R*-band by the time observations were taken ~ 7 days after the nova was first detected (Tang et al., 2014).

6.2.4 The 2011 Outburst

Another coincident outburst was discovered by S. Korotkiy and L. Elenin on unfiltered images taken on 2011 October 22.46 UT, when it was at a magnitude of 18.6 ± 0.3. They measured the position to be $0^{\rm h}45^{\rm m}28^{\rm s}.85$, $+41°54'09''.4$ to an accuracy of 0.3″. The same authors also reported that no object was visible on October 21.35 down to limiting magnitude of $R = 20.0$. Further observations reported the transient to have an unfiltered magnitude of 18.4 on October 22.99, 19.1 on October 23.43, and was not detected down to limiting magnitude of 19.7 on October 24.47. K. Hornoch measured the object have an *R*-band magnitude of 18.18 ± 0.08 on October 23.12.[2] On October 26.97, the nova candidate was measured to have a *B*-band magnitude of 20.9 ± 0.2 and *V*-band magnitude of 21.1 ± 0.2 (Barsukova et al., 2011). This outburst had an estimated g'-band t_2 of 2 days (Tang et al., 2014).

[2] see `http://www.cbat.eps.harvard.edu/unconf/followups/J00452885+4154094.html`

6.2.5 The 2012 Outburst

Almost exactly one year after the 2011 outburst, another outburst was discovered at $0^{\rm h}45^{\rm m}28^{\rm s}.84$, $+41°54'09''.5$ by K. Nishiyama and F. Kabashima. They measured it to be at an unfiltered magnitude of 18.9 on 2012 October 18.68 UT. The object, which was not visible down to a limiting magnitude of 19.8 on October 15.52, appeared to brighten to 18.6 by October 19.51.[3] The nova candidate had an *R*-band magnitude of 18.45 ± 0.04 on October 19.72 and i'-band magnitude of 18.42 ± 0.06 on October 19.73 (Shafter et al., 2012c). A spectrum of the transient was taken by Shafter et al. (2012c) on October 20.34, which was consistent with that of a nova in the M31 galaxy. The same authors classified it as a He/N type nova. After the outburst was reported, the nova was scheduled to be observed by the LT, however due to weather and scheduling constraints it was not observed until November 22.93 UT, when it was not detected in r'-band images (limiting magnitude 20.9). Therefore the t_2 of this outburst can only be constrained to < 35 days from the LT data. In four epochs between 19 and 110 days post-outburst, Swift XRT could detect no X-ray emission (Henze et al., 2013).

6.2.6 The 2013 Outburst

Another outburst of the system, which was later named M31N 2013-11f, was discovered by iPTF in 2013, when it was observed at *R*-band magnitude 18.9 on 2013 November 27.1 UT. They also reported that by November 28.1 it had further brightened to 18.3. On their *R*-band images taken on November 26, the nova was not visible (typical limiting magnitude $R \sim 21$; Tang et al., 2013a). Tang et al. (2014) estimated the *R*-band t_2 to be 2.1 days. This outburst had three spectra taken, at 1.3, 3.2 and 4.1 days after the observed peak, which confirmed the system to be a member of the He/N spectroscopic class (Tang et al., 2014).

Observations taken by the LT showed the nova to be at $B = 19.51 \pm 0.01$ on November 28.86 UT, and $B = 19.61 \pm 0.01$, $V = 19.65 \pm 0.02$ and $i' = 19.29 \pm 0.02$ on Nov 28.93.

[3] see `http://www.cbat.eps.harvard.edu/unconf/followups/J00452884+4154095.html`

Unfortunately the outburst coincided with several days of poor weather at the LT. The next set of observations showed the nova having a *B*-band magnitude of 22.2 ± 0.3 on December 4.89 and a *V*-band upper limit of 21.4 on December 4.90. Using photometry from various outbursts, Darnley et al. (2014) estimated the system to have a *V*-band t_2 of ~ 4 days. The extremely short recurrence time of this RN suggests that it likely has a high-mass WD and a high accretion rate. A light curve compiled from all the available optical data of this outburst is shown in Figure 6.1.

Swift XRT and UVOT observations were taken starting 2013 December 3.03, six days after the first optical detection, when the nova already showed a X-ray SSS, the shortest SSS turn-on time of any nova observed to that date (Henze et al., 2013). The SSS was detected after an even shorter period of time, turning on after $3 - 4$ days, during the 2014 outburst of V745 Sco (Page et al., 2014), although note that for M31N 2008-12a, the SSS had already turned on by the time of the first observation after its 2013 outburst. The source remained visible in the X-rays for about two weeks and the X-ray data suggest the temperature of the SSS to be higher than has been detected for any other M31 nova (Henze et al., 2014a). Higher SSS temperatures are predicted to be consistent with higher-mass WDs (Sala & Hernanz, 2005), as is already indicated for this system with its very short inter-outburst period.

6.2.7 The Quiescent System

As this system, with its extreme recurrence time, is such an interesting object, the progenitor system was searched for using the method described in Chapter 3. For this system the outburst images were taken using the IO:O CCD camera on the LT − the successor to RATCam, which has a wider field of view than the earlier instrument. There is no archival *HST* data of the region prior to the 2008 outburst, but there were F475W and F814W ACS/WFC data taken on 2010 August 7. This is over 8 months after the 2009 outburst, so given the system is so fast-fading, it should be at quiescence by this point. The region of the LT images covered by the above epoch of *HST* data is shown in Figure 6.2. There is a progenitor candidate at 0.9σ from the calculated posi-

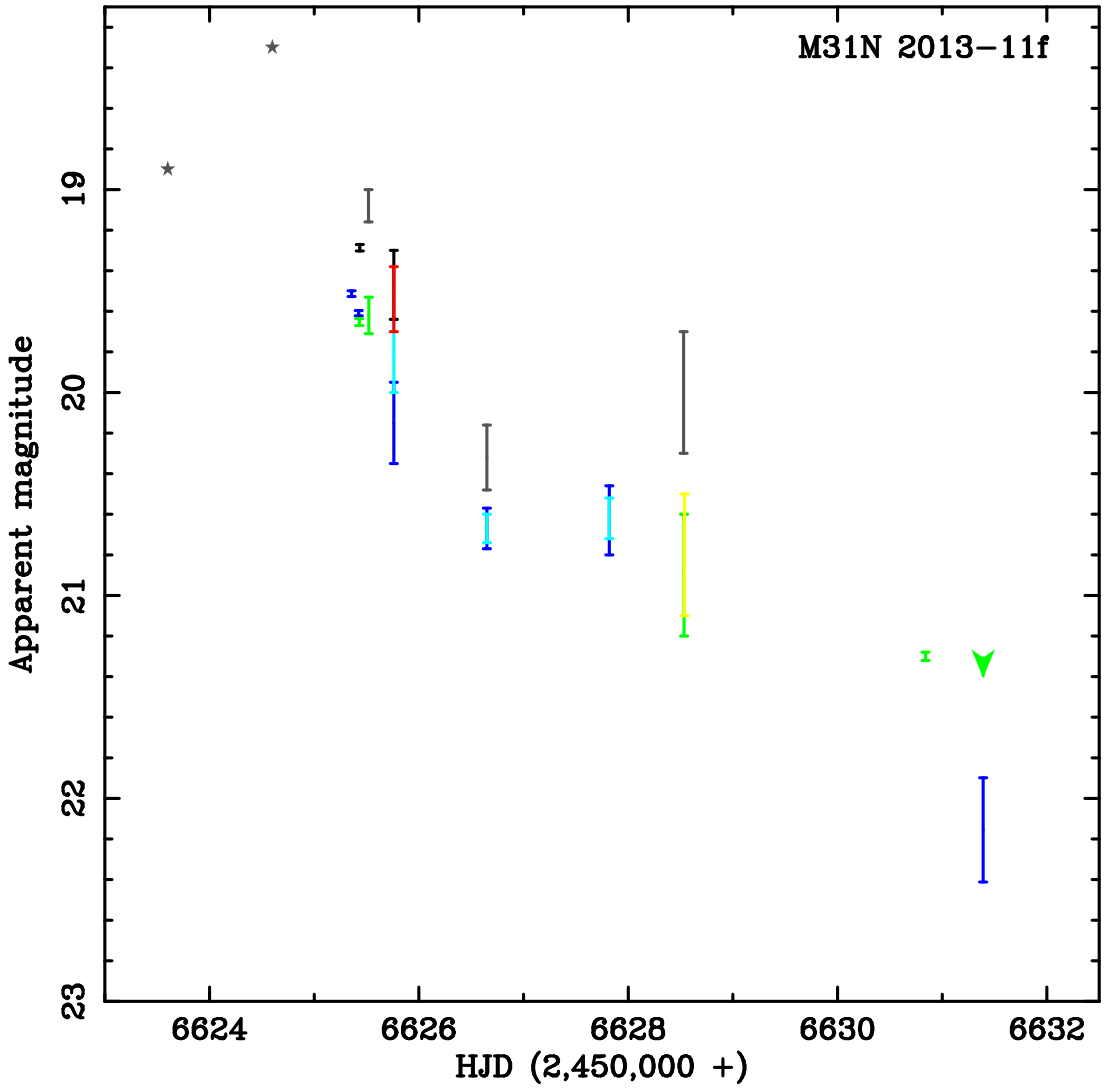

Figure 6.1: Optical light curve of M31N 2013-11f compiled using data from Tang et al. (2013a), Darnley et al. (2014), Tang et al. (2014) and those presented in the text. The stars represent data from Tang et al. (2013a), which have no published errors associated with them. Ground-based data filters are: *B*, royal blue; *V*, green; g', cyan; *R*, dark grey; r' , red; *I*, yellow and i', black, as in Figure 4.1.

tion of the quiescent nova system. The candidate is 0.557 ACS/WFC pixels or $0.028''$ away from the defined position. The local population density, which is resolvable down to an F814W magnitude of 26.1, suggests there is a 2.5% chance of coincidence at such a separation. This source had an F814W magnitude of 23.90 ± 0.02 and F475W magnitude of 24.07 ± 0.02. This gives a B-band magnitude of 24.12 ± 0.02, I-band magnitude of 23.90 ± 0.03 and ($B - I$) colour of 0.22 ± 0.03. The location of the progenitor candidate in the *HST* image is shown in Figure 6.3.

Along with the *HST* data used to search for the progenitor, there is an additional epoch of F475W and F814W data, taken less than three months after the 2011 outburst. There are also two epochs of WFC3/UVIS F275W and F336W data. Photometry on the WFC/UVIS data is performed in much the same way as for the ACS/WFC data, using DOLPHOT. Table 6.1 summarises all of this *HST* photometry of the system.

Date	Filter	Magnitude	Proposal ID
2008-12-26		*Outburst Discovered*	
2009-12-02		*Outburst Discovered*	
2010-08-07	F475W	24.07 ± 0.02	12056
...	F814W	23.90 ± 0.02	12056
2011-01-25	F275W	23.14 ± 0.06	12056
...	F336W	23.10 ± 0.03	12056
2011-08-31	F275W	22.9 ± 0.1	12106
...	F336W	22.81 ± 0.03	12106
2011-10-22		*Outburst Discovered*	
2012-01-10	F475W	24.49 ± 0.02	12106
...	F814W	24.05 ± 0.02	12106
2012-10-18		*Outburst Discovered*	
2013-11-28		*Outburst Discovered*	

Table 6.1: Summary of the brightness of M31N 2008-12a in *HST* data compared to its outbursts.

The consistency of the magnitudes in Table 6.1 further indicates that the nova would have been at quiescence when the *HST* data used to locate the progenitor were taken. Using these data, plus some near-infrared upper limits, Darnley et al. (2014) created a spectral energy distribution for the system and compared it to a selection of Galactic RNe. This figure is reproduced here in Figure 6.4. It can be seen from this figure

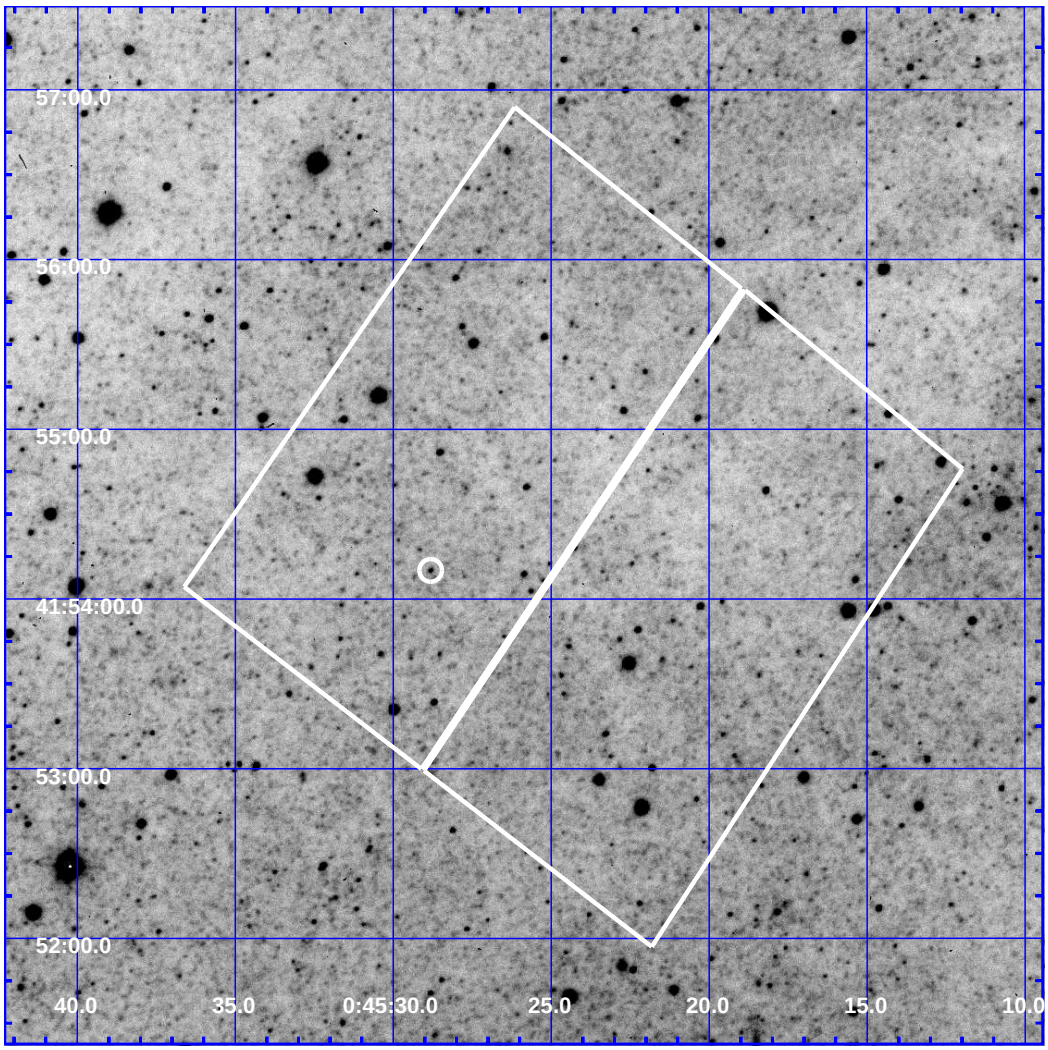

Figure 6.2: M31N 2013-11f during outburst in a i'-band LT image taken on 2013 November 28.93, with the dimensions of the coincident ACS/WFC F814W *HST* image overlaid as white boxes. M31N 2013-11f is shown with the white circle (the nova being the visible source at the centre of the circle).

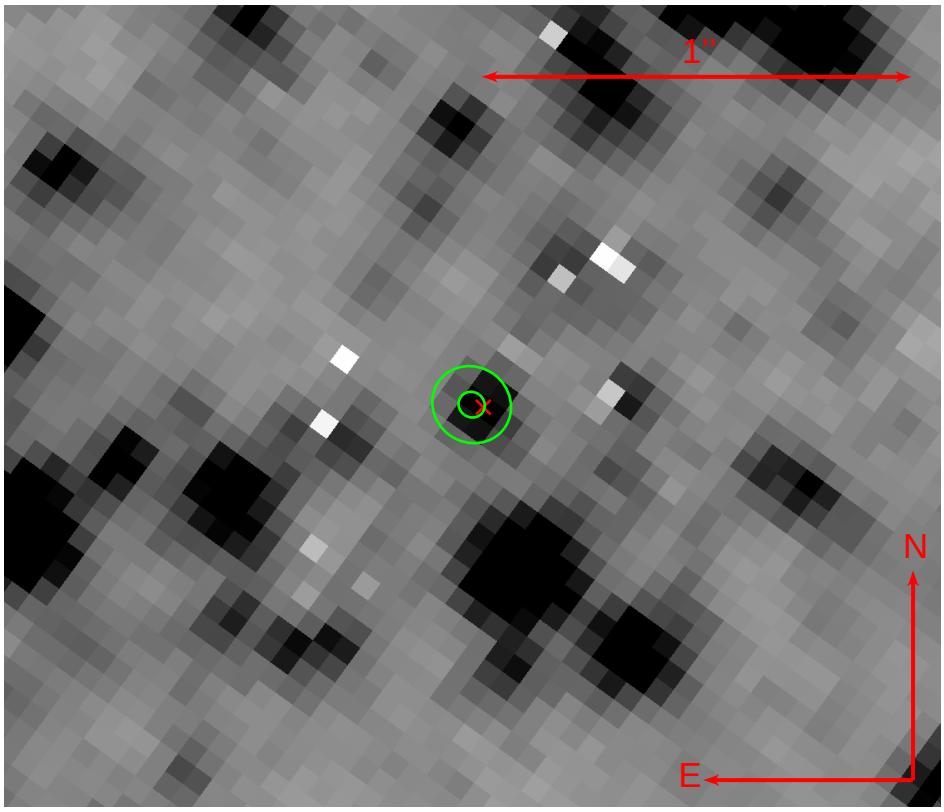

Figure 6.3: F814W ACS/WFC *HST* image of the $\sim 2.2'' \times 1.8''$ region surrounding the location of M31N 2013-11f. The inner green ellipse indicates the 1σ radius uncertainty of the outburst position and the outer ellipse the 3σ region. The red $\times$ indicates the position of the candidate progenitor system.

that, in the optical, the quiescent M31N 2008-12a appears consistent with the Galactic RG-nova RS Oph. However, as the near-infrared points are only upper limits, a less-evolved secondary can not be ruled out.

6.2.8 Discussion and Conclusions

M31N 2008-12a, as the RN with the shortest inter-outburst period, is a very important system. Galactically, the RN with the shortest recurrence time is U Sco, at ~ 10 years, although in M31, there are a few RN candidates that may produce outbursts more often than every 10 years (see e.g. Henze et al., 2009; Shafter et al., 2012d; Shafter et al. in preparation). The work described above indicates M31N 2008-12a has a high accretion rate and a high-mass WD, as would be expected for a system with such a short inter-outburst period. If the accretion rate is higher, it is thought the overall mass of the WD is more likely to increase with each nova outburst (Prialnik & Kovetz, 1995). Therefore if the system already contains a high-mass WD (and it is a CO WD), it is likely to produce a SN Ia in the future.

The nova-outburst models produced by Yaron et al. (2005) predict that a nova with a recurrence time of < 1 year would be possible in a system with a 1.25 $M_{\odot}$ WD, however this would require an extremely high accretion rate of order 10^{-6} $M_{\odot}yr^{-1}$, which they predict leads to an outburst amplitude of only 4 mag and a slowly evolving outburst. If we look at the outburst amlitude (~ 6 mag) and recurrence time of M31N 2008-12a, the best fitting of the Yaron et al. (2005) models is a system with a 1.4 $M_{\odot}$ WD with an accretion rate of order 10^{-7} $M_{\odot}yr^{-1}$, which predicts a recurrence time of 0.8 years. This model also predicts a t_3 of order 10 days, which is broadly consistent with M31N 2008-12a, and ejection velocity of order 1000 kms^{-1}, which is somewhat slower than this system (Shafter et al., 2012c). The recent theoretical work by Kato et al. (2014), which aimed to address this system specifically, reaches similar conclusions, predicting in order for a nova to have a 1 year recurrence time, the mass of the WD must be $\gtrsim 1.3$ $M_{\odot}$ and the accretion rate must be of order 10^{-7} $M_{\odot}yr^{-1}$.

Considering the likely high-mass WD and high accretion rate, when looking at known

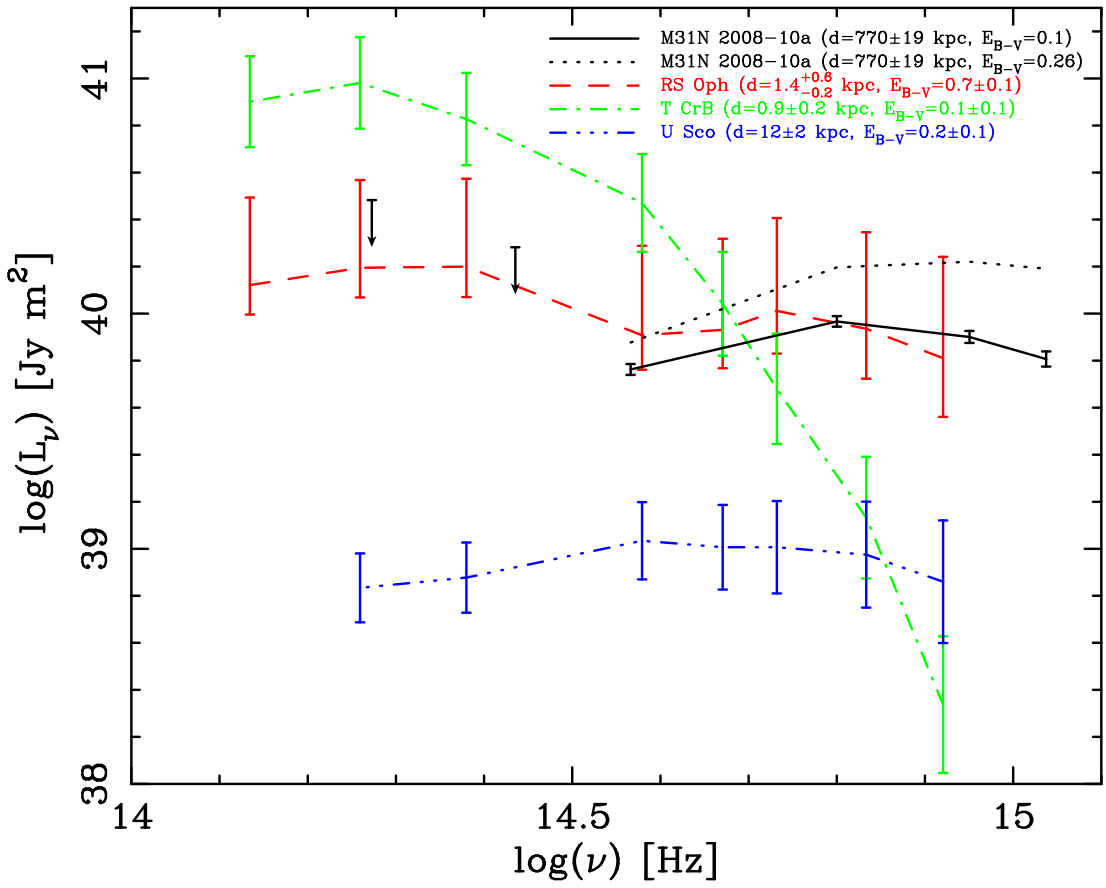

Figure 6.4: A reproduction of the spectral energy distribution of M31N 2008-12a, and comparison to the Galactic RNe RS Oph, T CrB and U Sco produced by Darnley et al. (2014). The errors on the Galactic nova points are dominated by uncertainties in the distance and extinction, however, the shapes of the spectral energy distributions should remain largely unaltered. The solid and dotted black lines represent the estimated minimum and maximum extinction respectively.

systems that are likely to produce a SN Ia in a relatively short period of time, M31N 2008-12a is probably one of the best candidates.

6.3 Upper Limits on the Magnitude of the Progenitor of SN 2014J

A SN candidate in the nearby starburst galaxy M82 was discovered on 2014 January 21.805 UT (Fossey et al., 2014), although several pre-discovery images were taken and first-light is estimated to have occurred on 2014 January 14 (Zheng et al., 2014). A spectrum taken a few hours after discovery confirmed it to be a SN Ia (Cao et al., 2014). The SN was named SN 2014J and it was the closest SN Ia for decades. It is possible to resolve part of the red-giant branch at the distance of M82, therefore an attempt was made to use archival data to search for and constrain the progenitor of SN 2014J.

6.3.1 Method

The method used to find the location of the progenitor system in the archival *HST* data is the same as that described in Chapter 3. The *HST* data used in the search were taken using ACS/WFC on 2006 March 27 with F814W, F555W and F435W filters, as part of proposal 10776. LT data were taken on 2014 January 26.91 UT, using the i'-band filter. Due to the brightness of the SN, very short exposure times had to be used for the LT observations, meaning relatively few stars in the *HST* field were also visible in the LT data. Whilst this increases the errors on the position calculated for the SN in the archival *HST* data, there were relatively few sources resolvable anyway, so the derived upper limits would remain unaltered even with a more accurate position.

6.3.2 Results

There is no resolvable source in the *HST* data within 3σ of the calculated position, as can be seen from Figure 6.5. From nearby sources, limiting magnitudes of 24.5, 23.4 and 23.3 were derived for F814W, F555W and F435W filters respectively. These upper limits are relatively high when compared to some of the limiting magnitudes of the M31 data due to a number of reasons. Firstly, the exposure times are relatively short for such *HST* observations, only 175s in F814W. Secondly, as M82 is much more distant than M31, it is more difficult to spatially resolve sources with the same pixel size. Thirdly, whilst the inclination of M31 is far from ideal, it is still more favourably aligned than M82. Fourthly, M82 suffers from high internal extinction, which is particularly noticeable in the F555W and F435W filters, which had very few resolvable non-extended sources.

6.3.3 Discussion and Conclusions

An F814W upper limit of 24.5 has been put on the apparent magnitude of the progenitor on SN 2014J. Assuming a distance to M82 of 3.5 kpc (Karachentsev & Kashibadze, 2006), this gives an absolute magnitude of $F814W = -3.2$. However, it appears that the supernova may suffer from significant extinction. If $E_{(B-V)} = 1.2$ is assumed (e.g. INAF-Astronomical Observatory of Bologna, 2014), the limit on the absolute magnitude is approximately -5.4. As can be seen from Figure 6.6, this does not exclude known Galactic nova systems with evolved companions. Analysis of near-infrared WFC3 data by Elias-Rosa et al. (2014), could also not rule out a RG-nova progenitor system.

Gerke et al. (2014) looked at 21 epochs between 2008 and 2014 and found no variable source coincident with the SN. Henze & Meusinger (2014) conducted a similar analysis with data going back to 1961, but they could not find an outburst either. However, the nova with the shortest recurrent time, M31N 2008-12a (see Chapter 6.2), fades so quickly that these data far from rule out a nova-type outburst in this period. A more

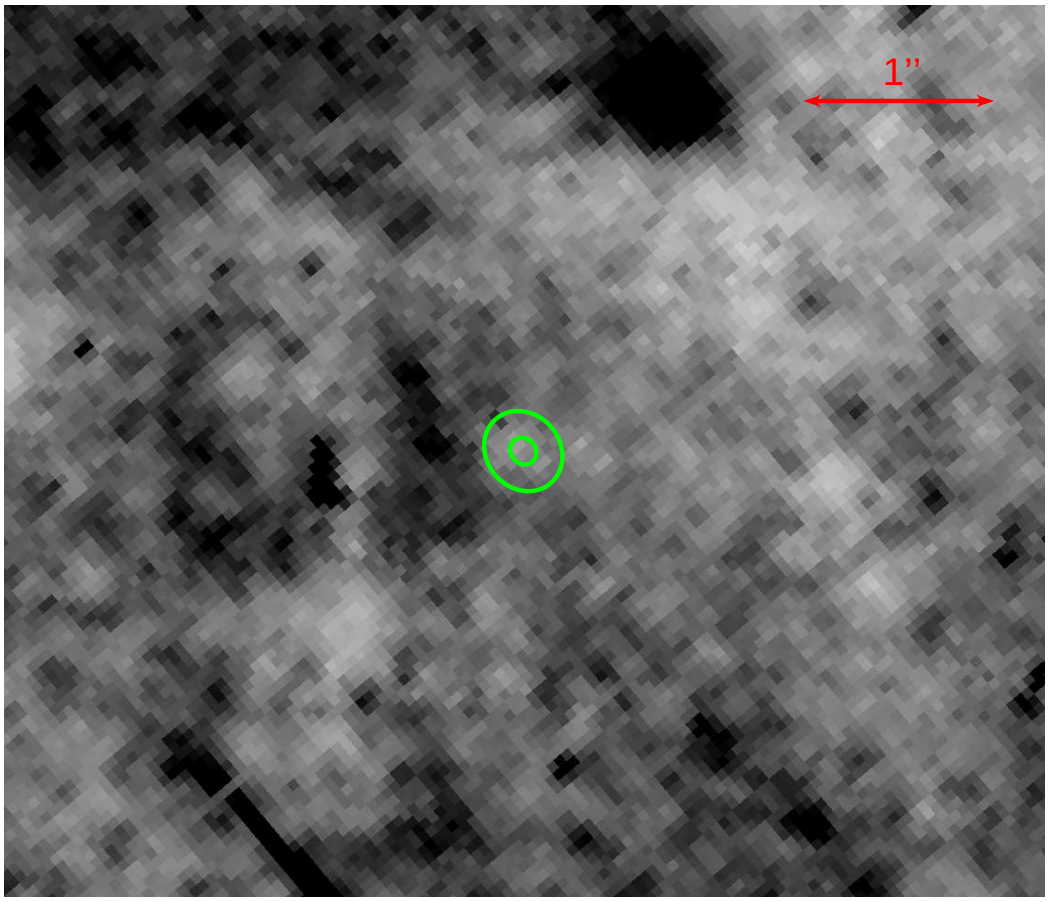

Figure 6.5: The location of SN 2014J in (negative) archival F814W ACS/WFC *HST* image. The green ellipses represent the 1σ and 3σ errors on the position as calculated from the LT images.

in-depth study of the archival data was conducted by Kelly et al. (2014), who used the flux at the position of SN 2014J to constrain the progenitor further. However, the analysis could only rule out RG-novae with the most luminous red giant secondaries, similar systems to RS Oph.

6.4 A Search for the M31 Optical Transient TCP J00403295+40343877

On 2011 November 14.5, K. Nishiyama and F. Kabashima discovered an M31 nova candidate, TCP J00403295+403438, at around magnitude 18.3 on unfiltered CCD frames using a Meade 200R 0.40-m f/9.8 reflector. They found no source down to a limiting magnitude of 20 on 2011 November 7.5[4]. The spectrum of the source showed it was not a nova, so archival *HST* images were used to help classify the object.

6.4.1 The Spectrum of TCP J00403295+40343877

A spectrum of the nova candidate TCP J00403295+40343877, designated M31N 2011-11d, was obtained by Shafter et al. (2011e) using the Hobby-Eberly Telescope on 2011 November 30.23, which revealed an unusual energy distribution. It had a red component which dominated at longer wavelengths, accompanied by a blue continuum that rose short-ward of 570 nm. Additionally the source had narrow Balmer and He II 468.6 nm line, as well as 615.0, 705.4, and 766.6 nm TiO bands (Shafter et al., 2011e).

6.4.2 *HST* Data for the Transient in Quiescence

These spectral features indicated that the transient may not be a single object, but a composite of two or more objects. Therefore archive *HST* data were used to try and find any quiescent sources. There had been data taken of the region by WFPC2 on

[4] `http://www.cbat.eps.harvard.edu/unconf/followups/J00403295+4034387.html`

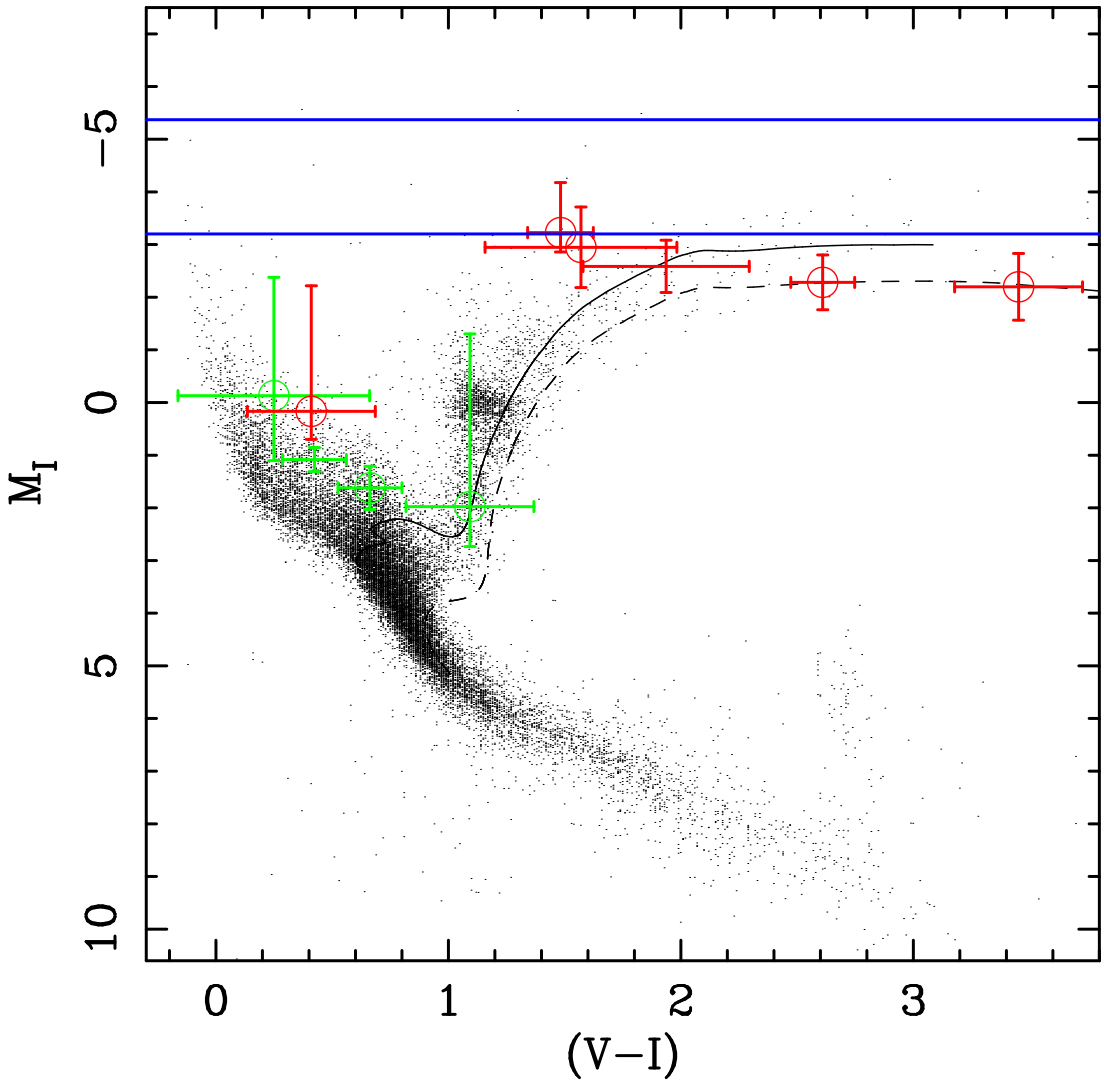

Figure 6.6: Colour-magnitude diagram showing the upper limits of the F814W brightness of the progenitor of SN 2014J. The bottom blue line assumes $E_{(B-V)} = 0.0$, with the top blue line assuming $E_{(B-V)} = 1.2$. Note that although these lines are plotted on a I vs $(V - I)$ colour-magnitude diagram, they represent F814W limits. The black dots represent Hipparcos stars, the red points represent Galactic RG-novae and the green points represent Galactic SG-novae.

2007 June 30 with F450W and F814W filters (proposal ID 10818). There does indeed appear to be two sources separated by $0.9''$ coincident with the position of transient TCP J00403295+4034387. The variable is shown in outburst in an image taken on the 0.65-m telescope at Ondrejov (see Shafter et al., 2011e) and in quiescence in the above mentioned F814W *HST* image in Figure 6.7

Photometry was performed on the two sources using HSTphot. The slightly more southerly source (see Figure 6.7) has an F450W magnitude of 23.16 ± 0.06 and an F814W magnitude of 18.857 ± 0.007. The other source has an F450W magnitude of 20.53 ± 0.01, with an F814W magnitude of 20.29 ± 0.03. The bluer source appears to be LGGS J004032.97+403439.0 in the catalogue published by Massey et al. (2006), who report it to have a *V*-band magnitude of 20.498 with a $(B - V)$ colour of -0.11 and a $(B - I)$ colour of 0.081. As suggested in Shafter et al. (2011e), the red source may be a Mira whose variation has caused the increase in brightness. Shafter et al. (2011e) also published *R*-band magnitudes for the system, with it being at magnitude 18.2 ± 0.1 on November 14.8, 19.0 ± 0.2 on November 28.7, 19.7 ± 0.2 on December 1.7, 18.9 ± 0.3 on December 8.7 and 19.1 ± 0.2 on December 10.7. A light curve created from this outburst photometry is shown in Figure 6.8.

Having looked at the progenitors of these three additional objects, this chapter concludes the research presented in this thesis. The following chapter summarises the work presented and discusses possible future work.

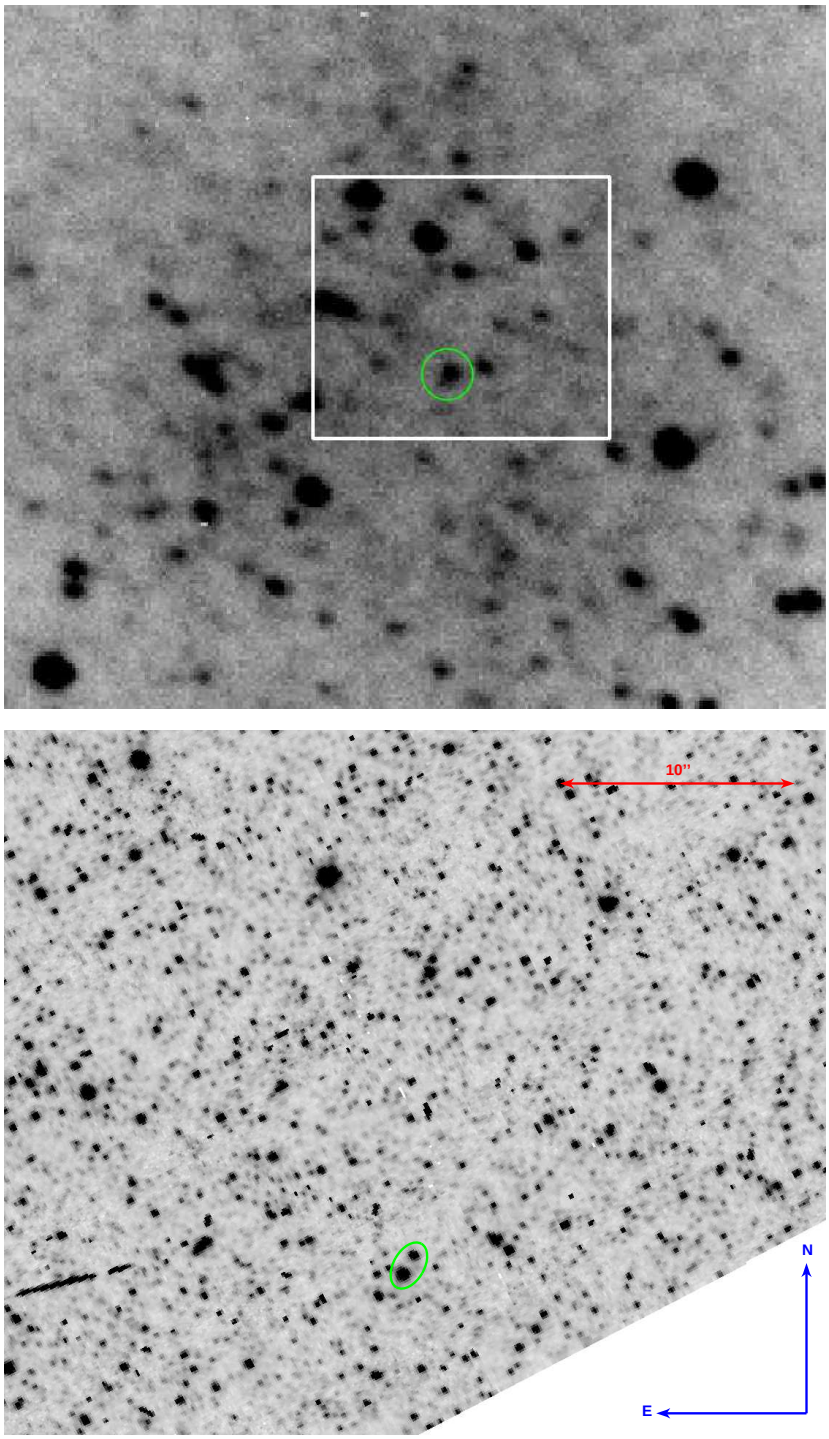

Figure 6.7: Top: TCP J00403295+4034387 (green circle) seen in outburst on image taken by 0.65-m telescope at Ondrejov, with the white box indicating the approximate region encompassed by the *HST* image below. Bottom: The location of the quiescent sources (green ellipse) in F814W *HST* image taken on 30 June 2007.

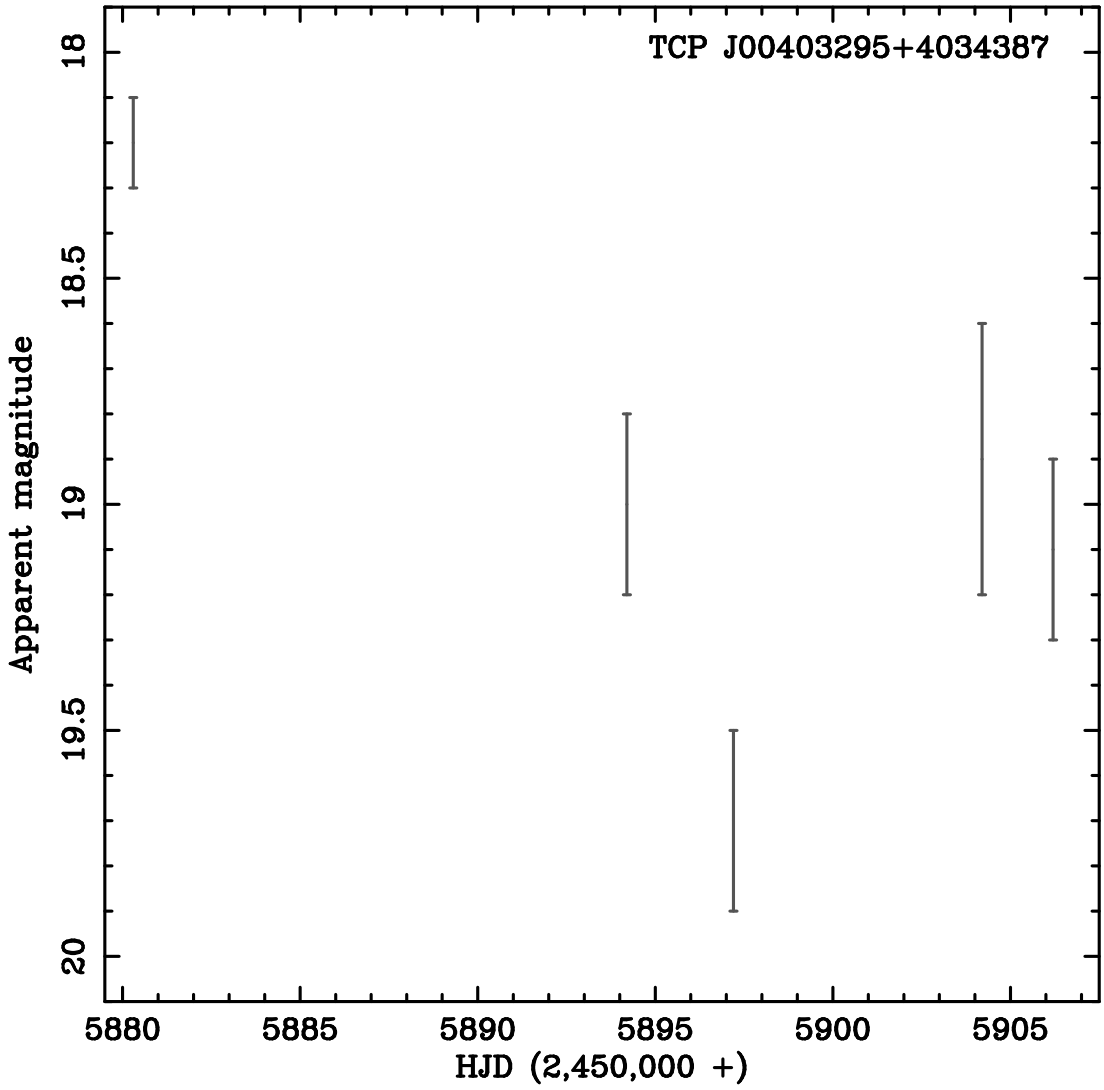

Figure 6.8: *R*-band light curve of TCP J00403295+40343877 created using photometry from Shafter et al. (2011e).

Chapter 7

Summary and Future Work

7.1 Summary

7.1.1 The Relationship Between Dust Formation and t_2 in Novae

A simple theoretical analysis was conducted to help understand the observed relationship between the onset of dust formation and the time it takes a nova to fade by two magnitudes following an outburst, t_2. The analysis assumed all the emission produced by the nova short-ward of the Lyman limit is absorbed by neutral hydrogen before it can reach the potential dust-formation sites. As the effective temperature of the central source increases with time, a lower proportion of the emitted radiation reaches these sites, allowing potential nucleation centres to reach the condensation temperature quicker. As faster novae evolve more rapidly, this allows dust to form sooner in such systems. The quantitative analysis described in this thesis offers an explanation for the observed $t_2 - t_{\rm cond}$ correlation, with the theoretical results appearing to match the observational data well.

7.1.2 The Search for the Progenitors of M31 Novae

Following the method first outlined by Bode et al. (2009), outburst images taken using the LT were used to search for the progenitors of 38 spectroscopically-confirmed M31 novae in archival *HST* data. The survey found eleven of these 38 systems (M31N 2007-02b, 2007-10a, 2007-11b, 2007-11d, 2007-11e, 2007-12a, 2007-12b, 2009-08a, 2009-11d, 2010-01a and 2010-09b) had a coincident source in the archival data, where the probability of such an alignment occurring by chance was $< 5\%$ in each case. The group of recovered nova progenitors would be expected to be dominated by RG-novae, as at the distance of M31, the red-giant branch is resolvable. However, only the brightest SG-novae would be expected to be observable in quiescence. Therefore this potential RG-nova rate appears much higher than has been observed so far Galactically, where only $2 - 3\%$ of the ~ 400 novae are thought to be associated with a red giant secondary, although many of the Galactic systems have simply not been classified.

7.1.3 Light Curves of M31 Novae

During the survey for M31 nova progenitors, several of the novae were found to have coincident *HST* data that had been taken whilst they were still in outburst. This allowed several pre-2010 light curves published by Shafter et al. (2011f) to be extended to fainter magnitudes than is normally possible for extragalactic systems. In addition, a number of light curves were published for novae that produced outbursts between 2010 and 2013, as well as a spectrum taken of M31N 2013-12b.

7.1.4 Statistical Analysis of the M31 Nova Progenitor Catalogue

A Monte Carlo model was used to analyse the statistics and biases of the M31 nova progenitor catalogue. Biases associated with chance of discovery, spectroscopic confirmation, obtaining outburst images and the nova having coincident archival *HST* data were all considered. The initial results of this analysis suggest $0.38^{+0.16}_{-0.12}$ of M31 novae are associated with a resolvable source in the archival *HST* data, a group expected to

be dominated by RG-novae. The model also indicates with a high degree of confidence that the proportion of novae associated with a quiescent source is greater than the RG-nova rate that had been observed so far in our Galaxy. However, the recent work by Pagnotta & Schaefer (2014) now supports a relatively high RG-nova rate in our Galaxy too. As well as being important for the study of nova populations, the results could have implications regarding the progenitors of SNe Ia. If a high proportion of novae are RG-novae, such systems may make a larger contribution to the SN Ia progenitor population that previously thought.

The results of the survey show that RG-novae are more likely to be associated with the disk of M31, rather than the bulge, and indeed are consistent with RG-novae being entirely with the M31 disk. This could also be important when considering RG-novae as SN Ia progenitor candidates, as it predicts that SNe Ia originating from RG-nova systems would be much less likely to occur in older stellar populations, for example early-type galaxies.

7.1.5 The Progenitors of Three Additional Extragalactic Variables

The method used to search for the progenitors of the 38 M31 novae was used to explore the nature of three additional systems, the RN M31N 2008-12a, the SN Ia SN 2014J, and the optical transient TCP J00403295+40343877. M31N 2008-12a has an extremely short inter-outburst period of approximately one year. Its 2013 outburst was studied here and a likely progenitor was recovered in archival *HST* data. The progenitor candidate system implies a high accretion rate, and as it also appears to have a high-mass WD, it is a possible SN Ia progenitor. Archival *HST* data were also used to search for the progenitor of the nearby SN Ia SN 2014J. No coincident candidate was found down to a limiting magnitude of F814W = 24.5, which is not deep enough to rule out the RG-nova progenitor channel. The optical transient TCP J00403295+40343877 produced an outburst in 2011 and showed an unusual spectrum. A search for the progenitor in archival *HST* data, when compared to the spectrum, revealed the transient may have been a blend of two objects, with the increase in brightness caused by a

long-period Mira.

7.2 Future Work

7.2.1 The Relationship Between Dust Formation and t_2 in Novae

The model described in Chapter 2 is more advanced than the basic theory and appears to agree well with the observational data. However, the model is still relatively simplistic and further refinements could include more realistic spectral energy distributions for the emission seen by the grains and consider the effects of non-spherical geometry (e.g. Chesneau et al., 2012). An advanced model should also consider the possible effects of re-emission of photons within the clumps.

Many novae have been observed to form both carbon-rich and oxygen-rich dust (Evans & Rawlings, 2008), although only one dust forming nova has been observed to produce only silicates – QU Vul. It would be feasible to conduct a similar analysis to that described in Chapter 2 for silicates, although these form later than carbon-rich dust where both types are formed in the same nova (Gehrz, 2008). Therefore, since $t_{\rm cond}$ measures the onset of dust formation, a silicate analysis may not be important for the majority of novae. Future infrared observations of novae in M31, which need 8m-class telescopes such as Gemini, could help refine the $t_2 - t_{\rm cond}$ relationship further.

7.2.2 The Search for the Progenitors of Local Group Novae

The search for M31 nova progenitors described in Chapter 3 has so far provided very interesting results. This catalogue can be expanded significantly from the 38 systems currently included. Through continued LT follow-up of M31 novae since the end of the catalogue (early 2013) and into the future, the catalogue can be expanded to include the most recent novae and by exploring the use of alternative outburst images, it may also be possible to add further pre-2013 novae to the catalogue. The expansion of the

catalogue will in turn help further constrain the RG-nova rate of M31.

M31 is the best galaxy for such a survey, as it is close enough to resolve many of the evolved companion stars and has a high nova rate accompanied by relatively good *HST* coverage. However, the project can be extended to M33 and Magellanic Clouds. In the Magellanic Clouds some of the MS-novae will be resolvable, although due to the large apparent size, *HST* coverage of the LMC and SMC is not anywhere near complete. However, due to their proximity to the Milky Way, ground-based images can be readily used to search for novae with evolved companions, as was done by Bode et al. (in preparation). While the entire red-giant branch is not resolvable in more distant galaxies, novae with more luminous red giant companions (like RS Oph for example) will be detectable. This certainly applies to galaxies like M81 and M83 and possibly even as far out as M101 for the most luminous systems.

The model to analyse the statistics and biases of the M31 nova progenitor survey described in Chapter 5 could also be improved in future. In can be seen from Figure 5.2 that slower novae tend to be more associated with the central regions of M31, as has been suggested by previous authors. However, the model presented here uses a general t_2 distribution, rather than one dependent on spatial position. In future, it would be possible to produce a basic model that reflects this, allowing the associated biases to be accounted for in the statistical analysis.

Ideally, a simple model of the LT scheduler should be created. As faster fading novae are more likely to be missed through scheduling constraints. This will also be affected by the priority a given telescope proposal had. The LT proposals are ranked A, B or C, with A being the highest priority and C being the lowest. The rank of the proposal is particularly significant early in the year, when M31 is only observable for a few hours early in the night.

A further study also needs to be conducted on the relationship between t_2 and the time it takes a nova to reach quiescence. For some M31 novae, it would be possible for *HST* data to have been taken before they had returned to quiescence, yet no source be visible in the data as it had faded beyond the limiting magnitude. This could be considered

in future refinements of the statistical model. The sensitivity of the model to assumed parameters, such as the proportion of novae associated with the disk, should also be tested.

7.3 Final Summary

This thesis has offered a simple theoretical explanation for the observed correlation between t_2 and the time it takes dust to form in novae, $t_{\rm cond}$. In a survey of 38 M31 novae, this work has recovered the likely progenitors for 11 systems. The resulting statistical analysis finds that a relatively high proportion ($0.38^{+0.16}_{-0.12}$) of M31 novae appear to be associated with a resolved quiescent source in the *HST* data. As this group of systems would be expected to be dominated by RG-novae, the result is important when considering such systems as SN Ia progenitors. This result was somewhat surprising given that only a few percent of Galactic novae had been found to be associated with red giant companions, implying RG-novae may contribute more significantly to the SN Ia progenitor population than previously thought.

Appendix A

Archival *HST* Coverage of M31

This appendix shows the archival *HST* coverage of M31 for each broad-band filter from F435W to F814W in each of the three wide-field cameras; ACS, WFPC2 and WFC3.

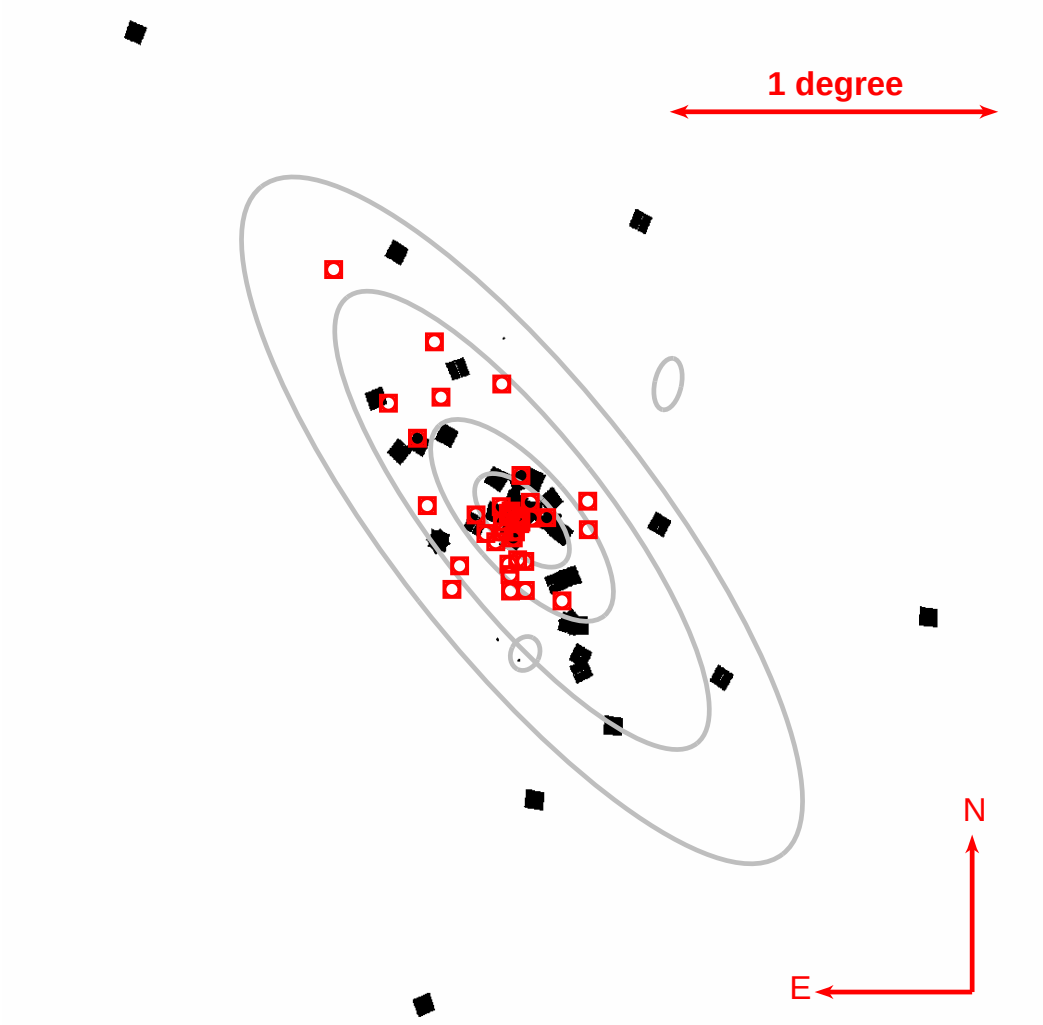

Figure A.1: The ACS *HST* coverage of M31 in F435W filter. The black regions have coverage, whereas the white regions do not. The red points represent the 38 novae from the progenitor survey catalogue presented in Chapter 3, with the grey ellipses showing isophotes from Kent (1987).

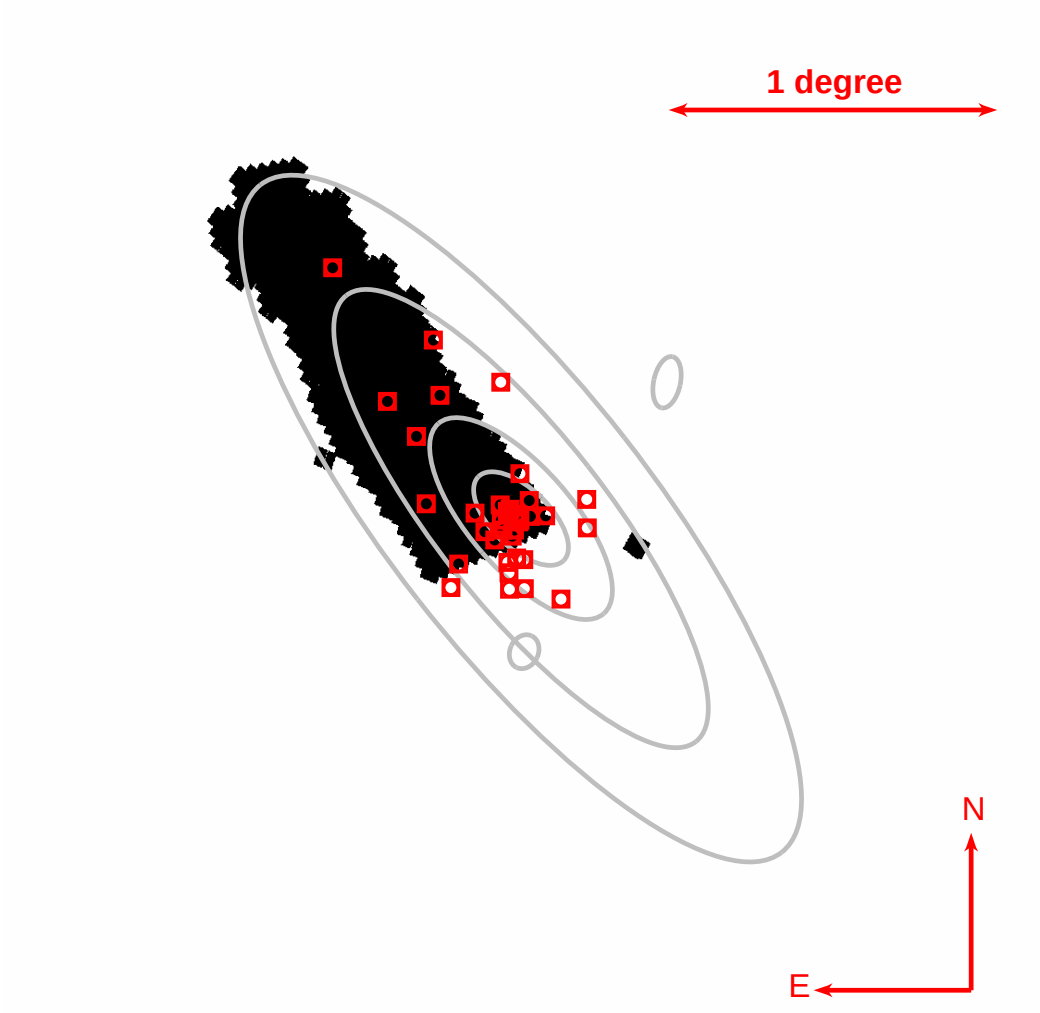

Figure A.2: The ACS *HST* coverage of M31 in F475W filter. Key as in Figure A.1.

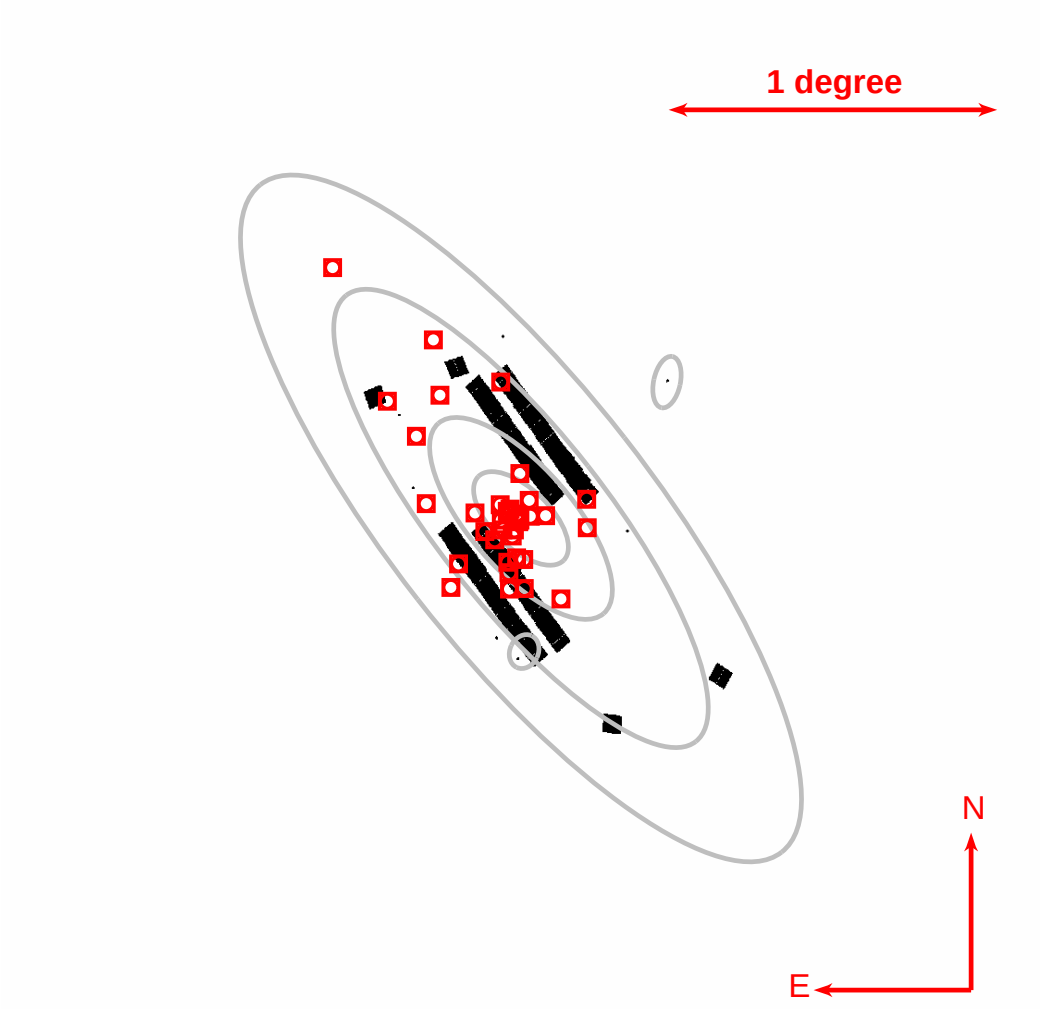

Figure A.3: The ACS *HST* coverage of M31 in F555W filter. Key as in Figure A.1.

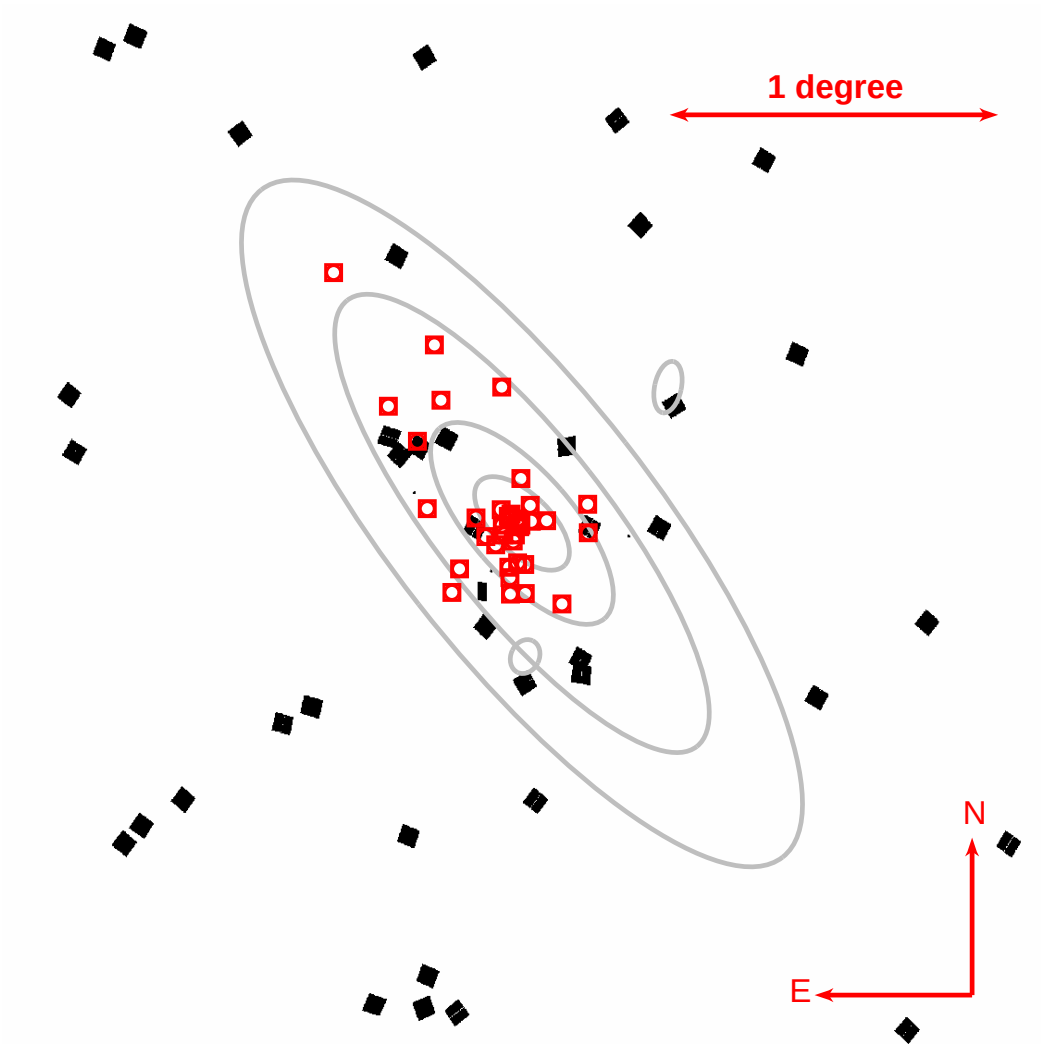

Figure A.4: The ACS *HST* coverage of M31 in F606W filter. Key as in Figure A.1.

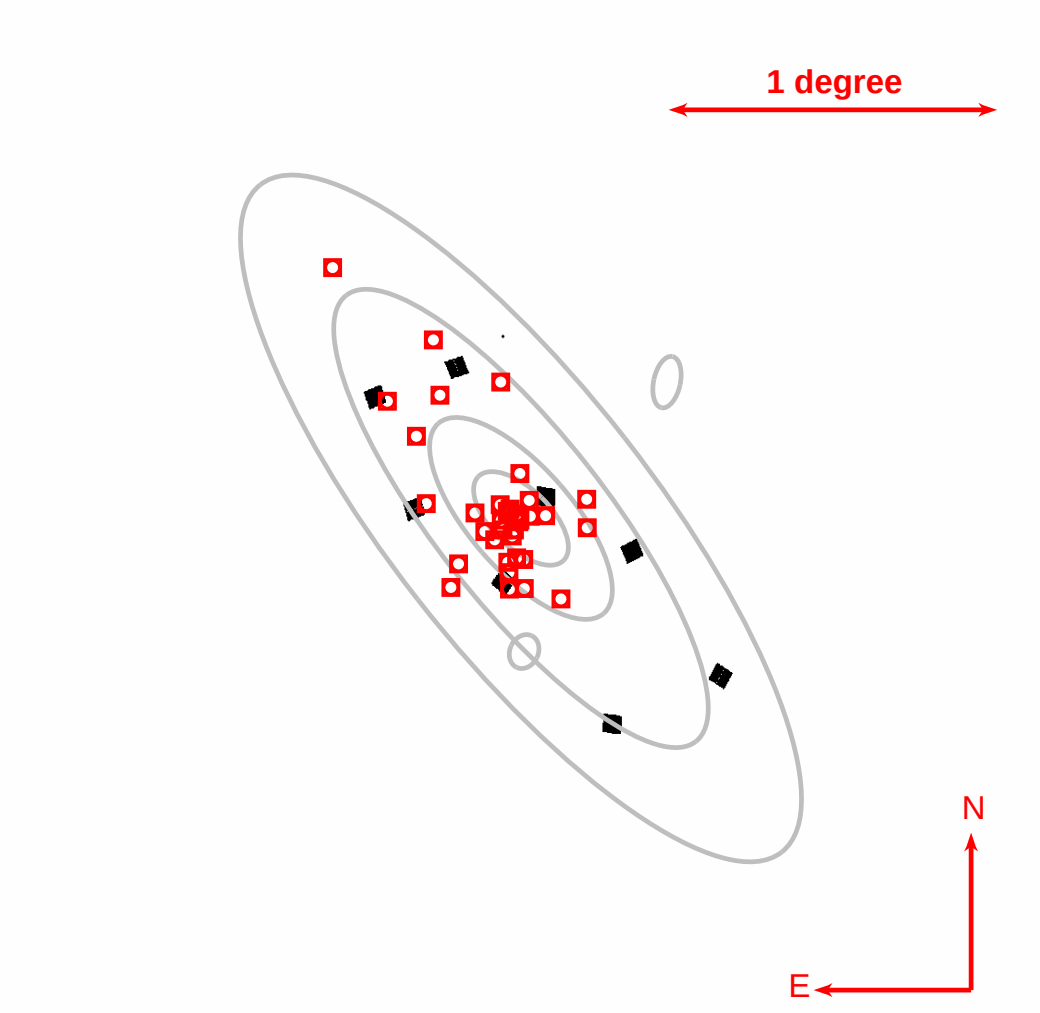

Figure A.5: The ACS *HST* coverage of M31 in F625W filter. Key as in Figure A.1.

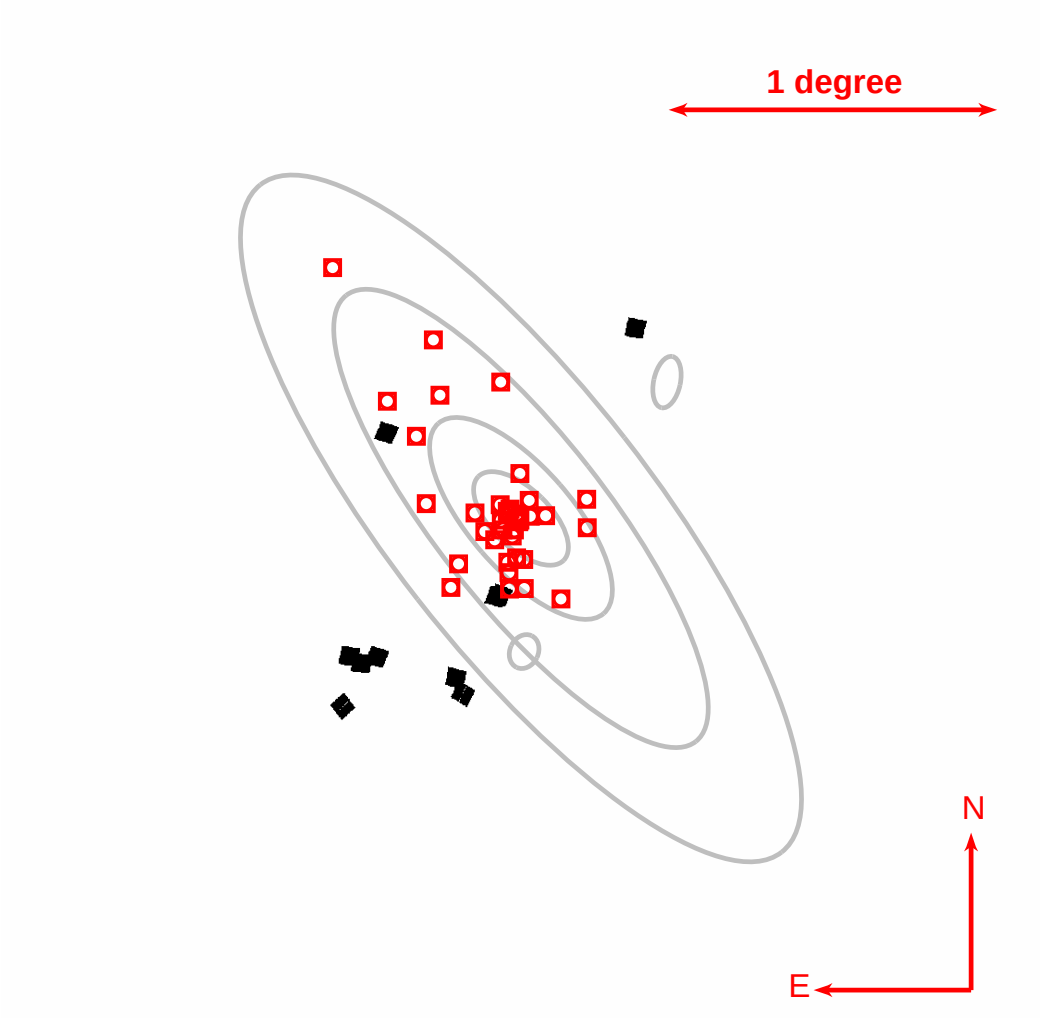

Figure A.6: The ACS *HST* coverage of M31 in F775W filter. Key as in Figure A.1.

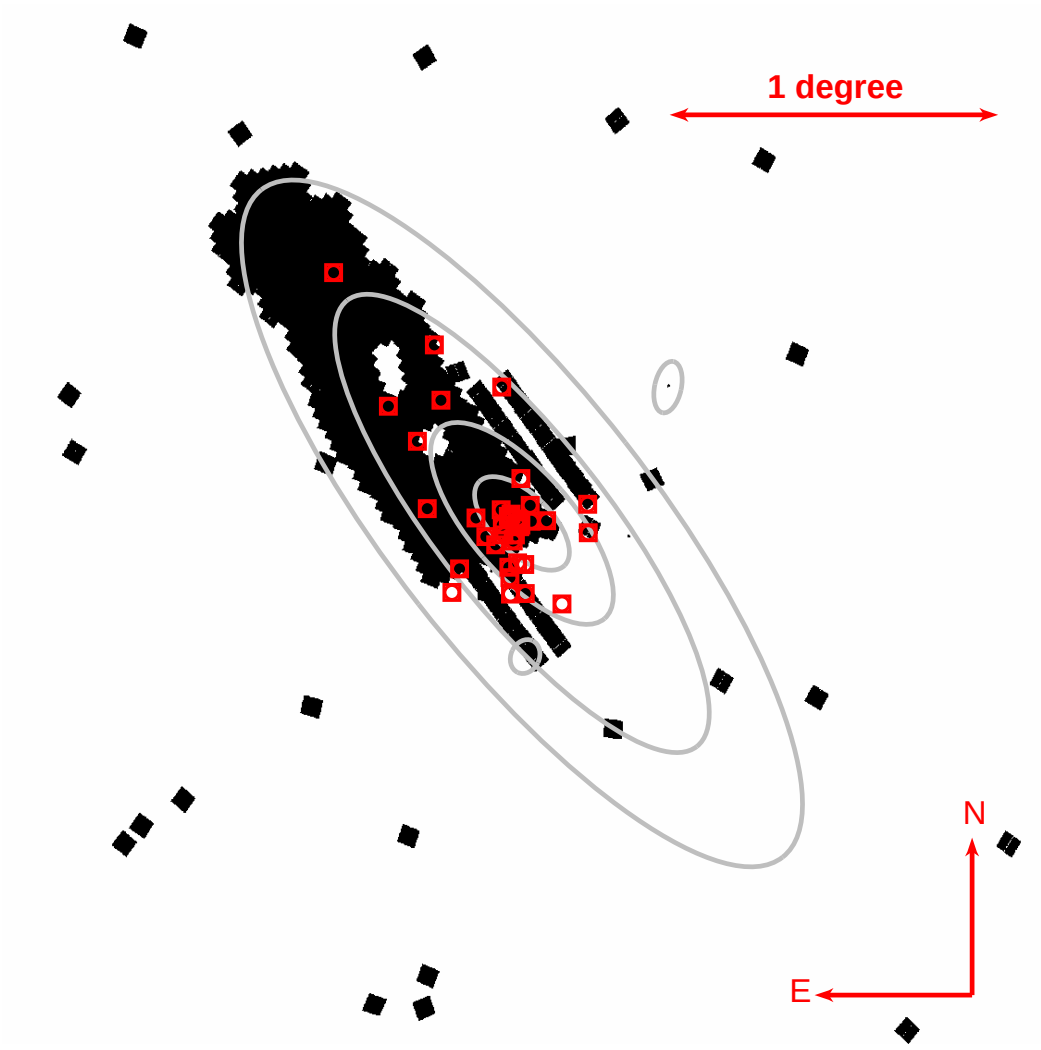

Figure A.7: The ACS *HST* coverage of M31 in F814W filter. Key as in Figure A.1.

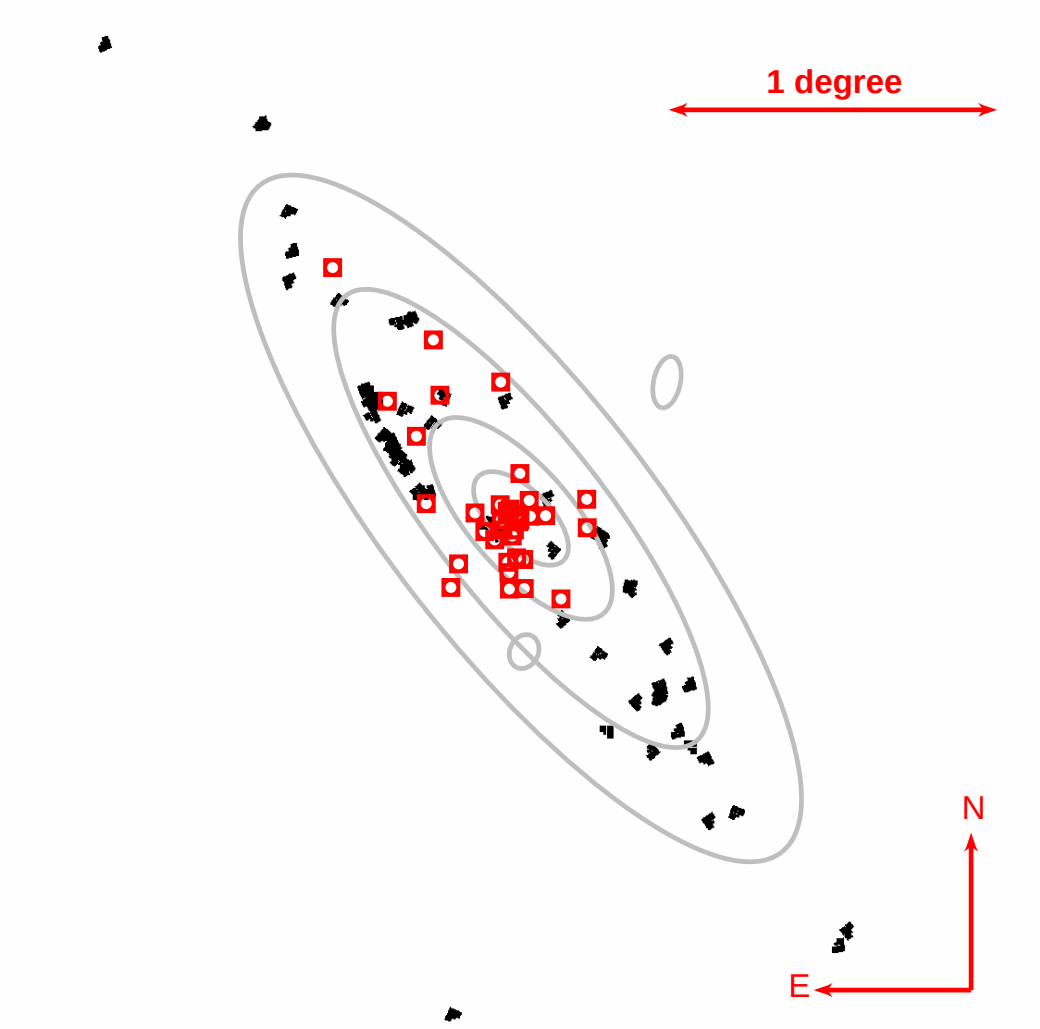

Figure A.8: The WFPC2 *HST* coverage of M31 in F439W filter. Key as in Figure A.1.

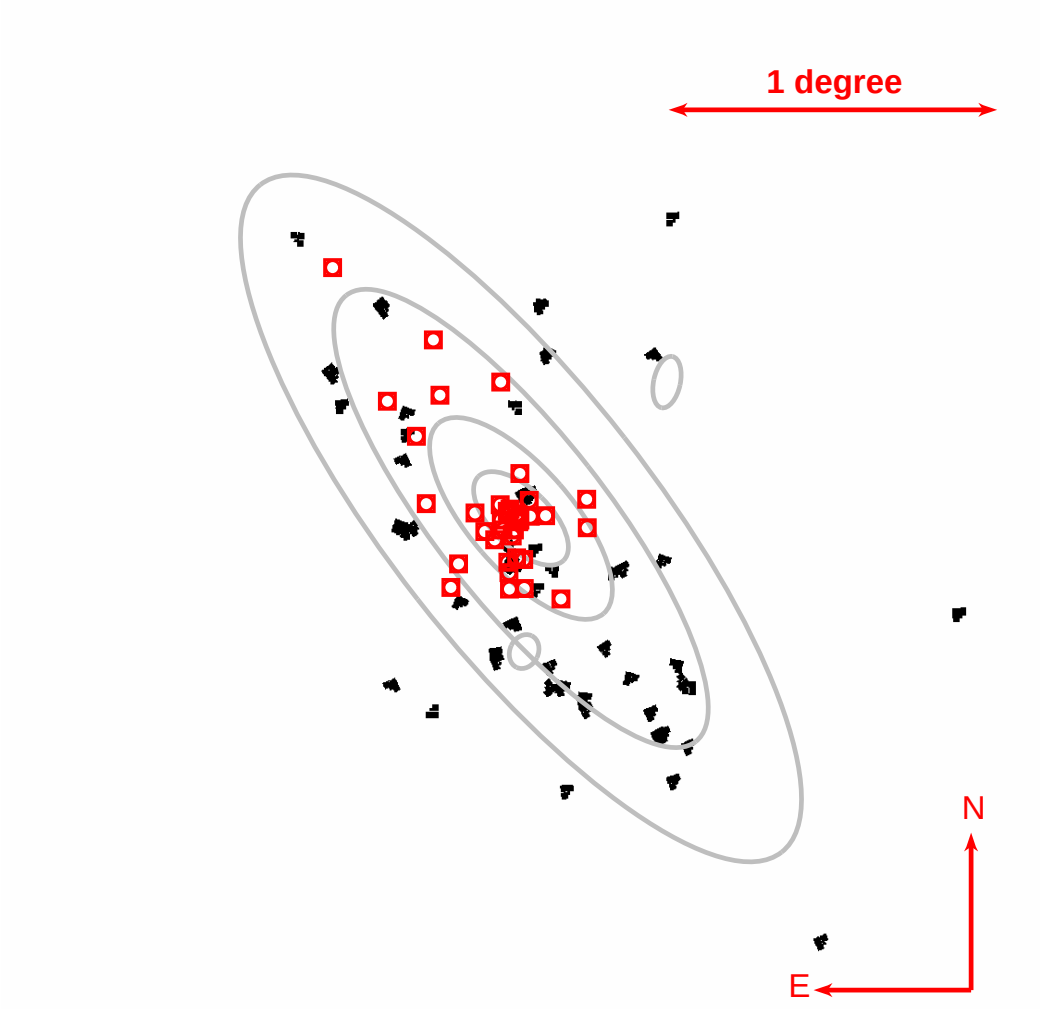

Figure A.9: The WFPC2 *HST* coverage of M31 in F450W filter. Key as in Figure A.1.

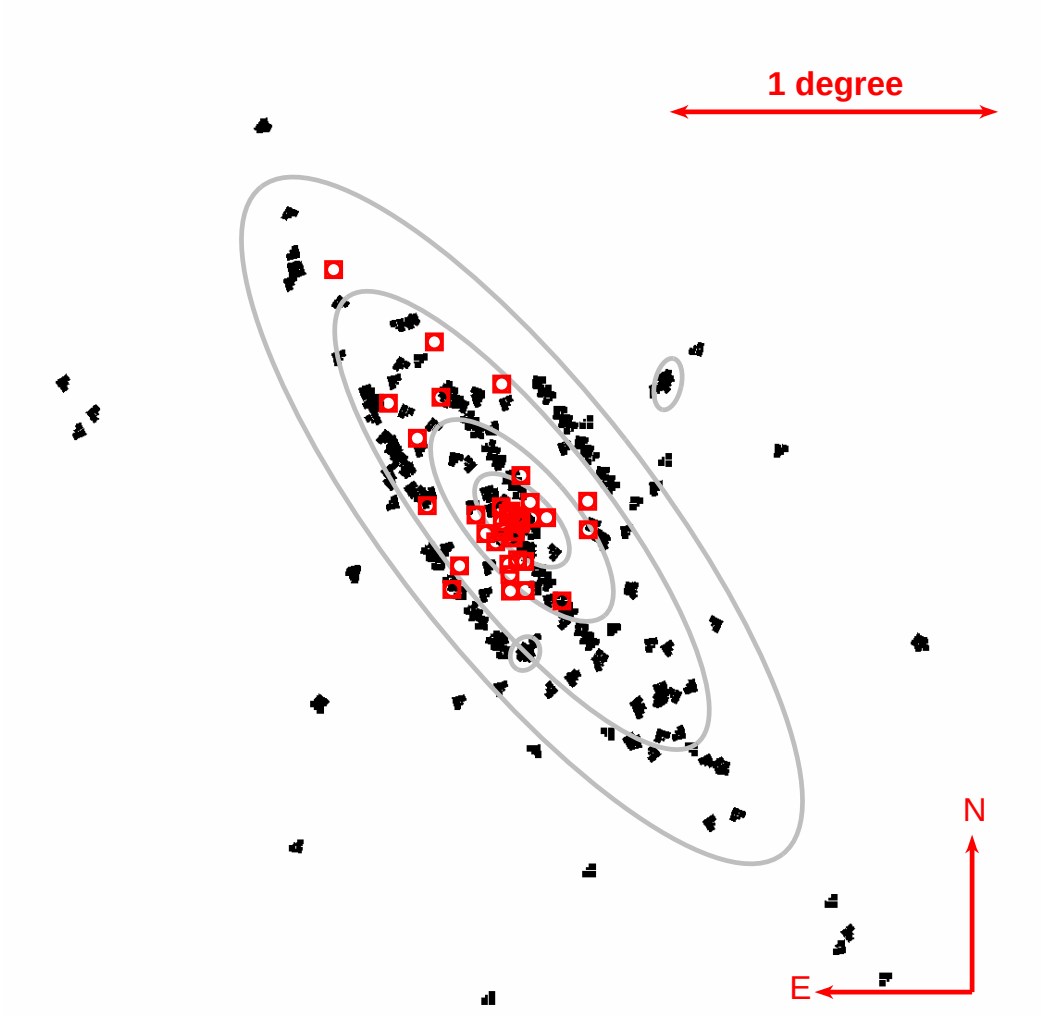

Figure A.10: The WFPC2 *HST* coverage of M31 in F555W filter. Key as in Figure A.1.

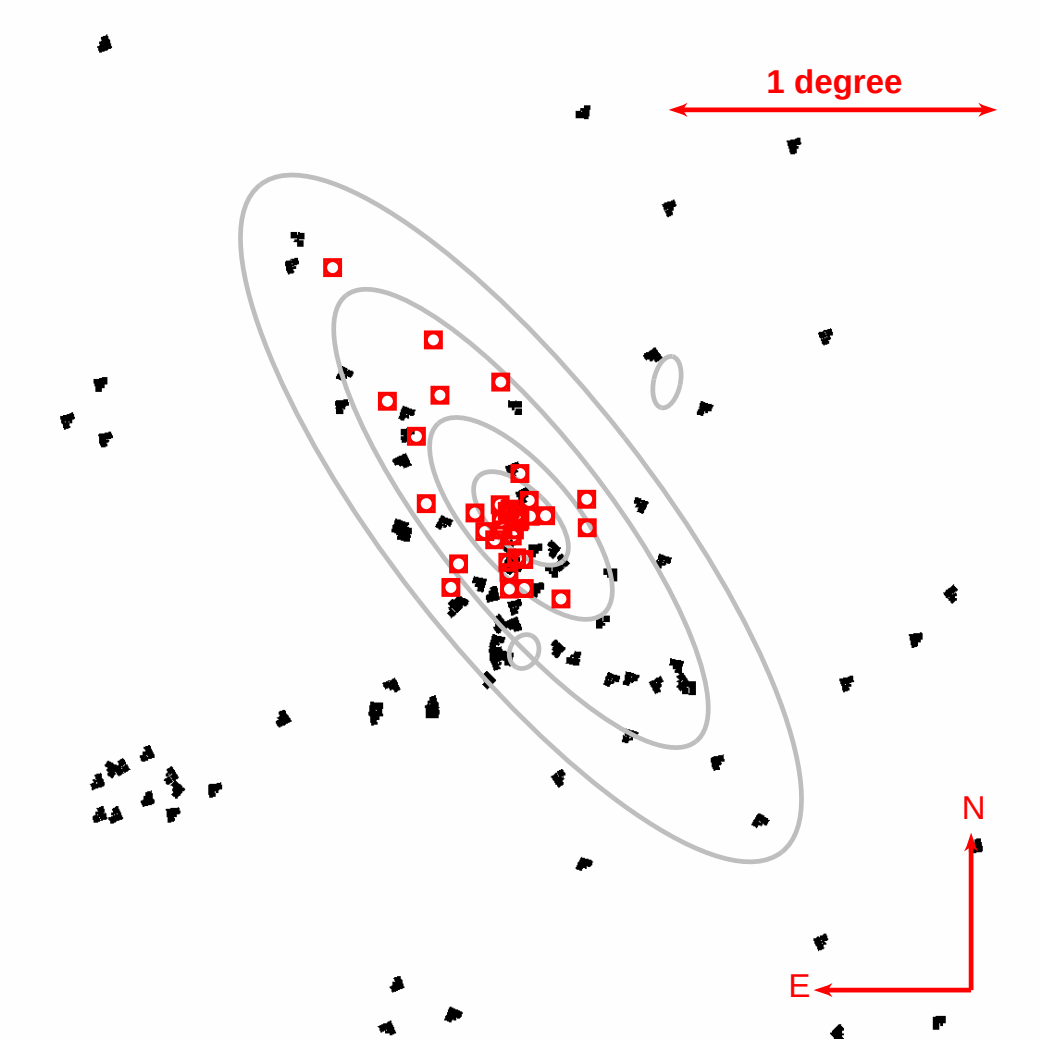

Figure A.11: The WFPC2 *HST* coverage of M31 in F606W filter. Key as in Figure A.1.

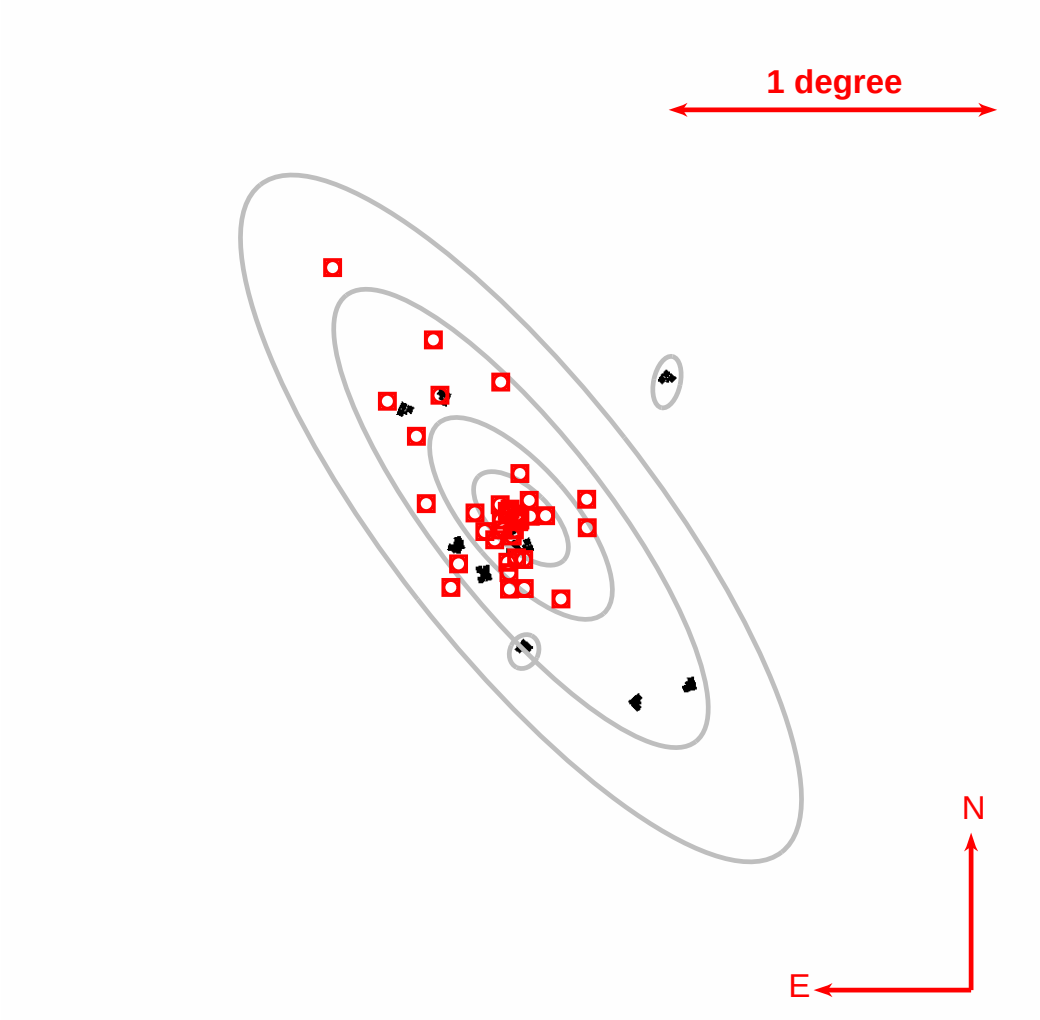

Figure A.12: The WFPC2 *HST* coverage of M31 in F675W filter. Key as in Figure A.1.

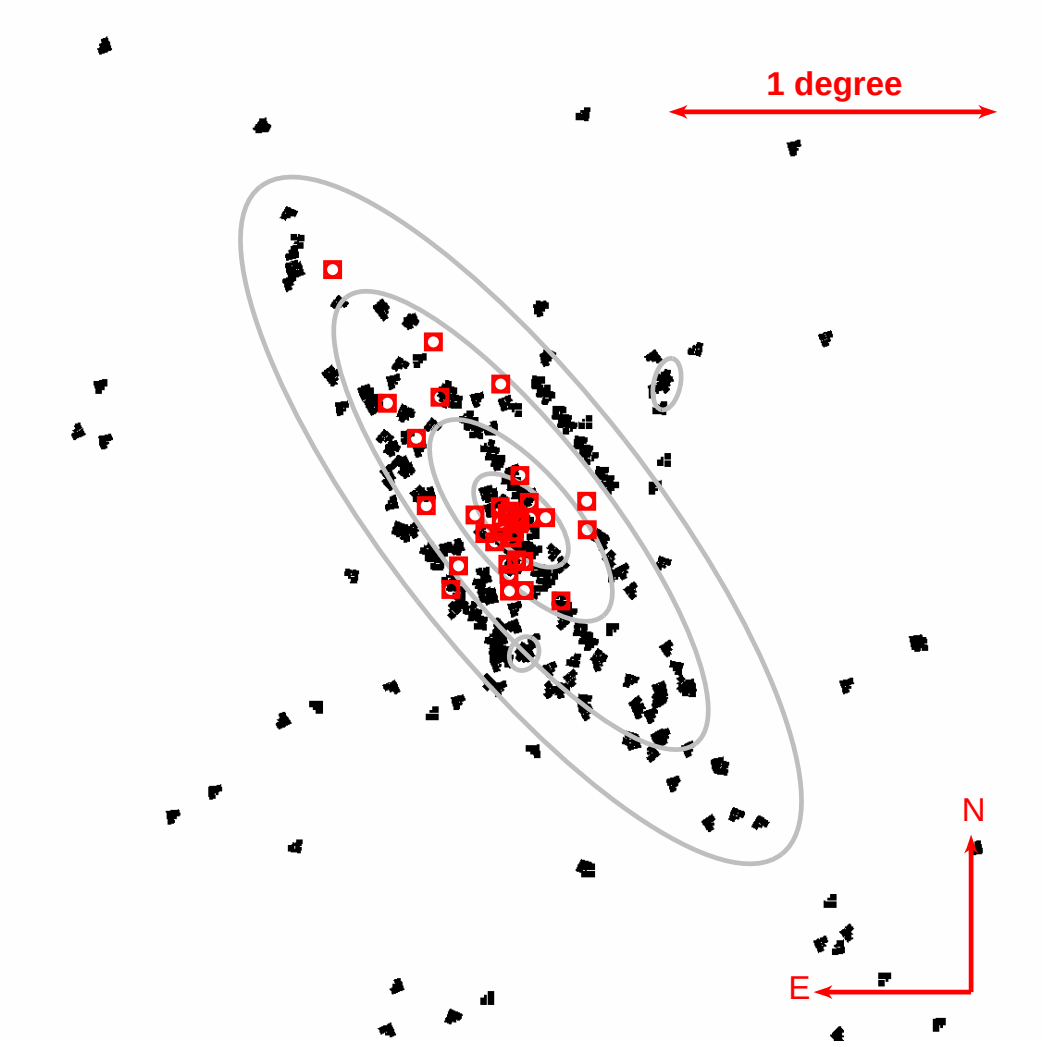

Figure A.13: The WFPC2 *HST* coverage of M31 in F814W filter. Key as in Figure A.1.

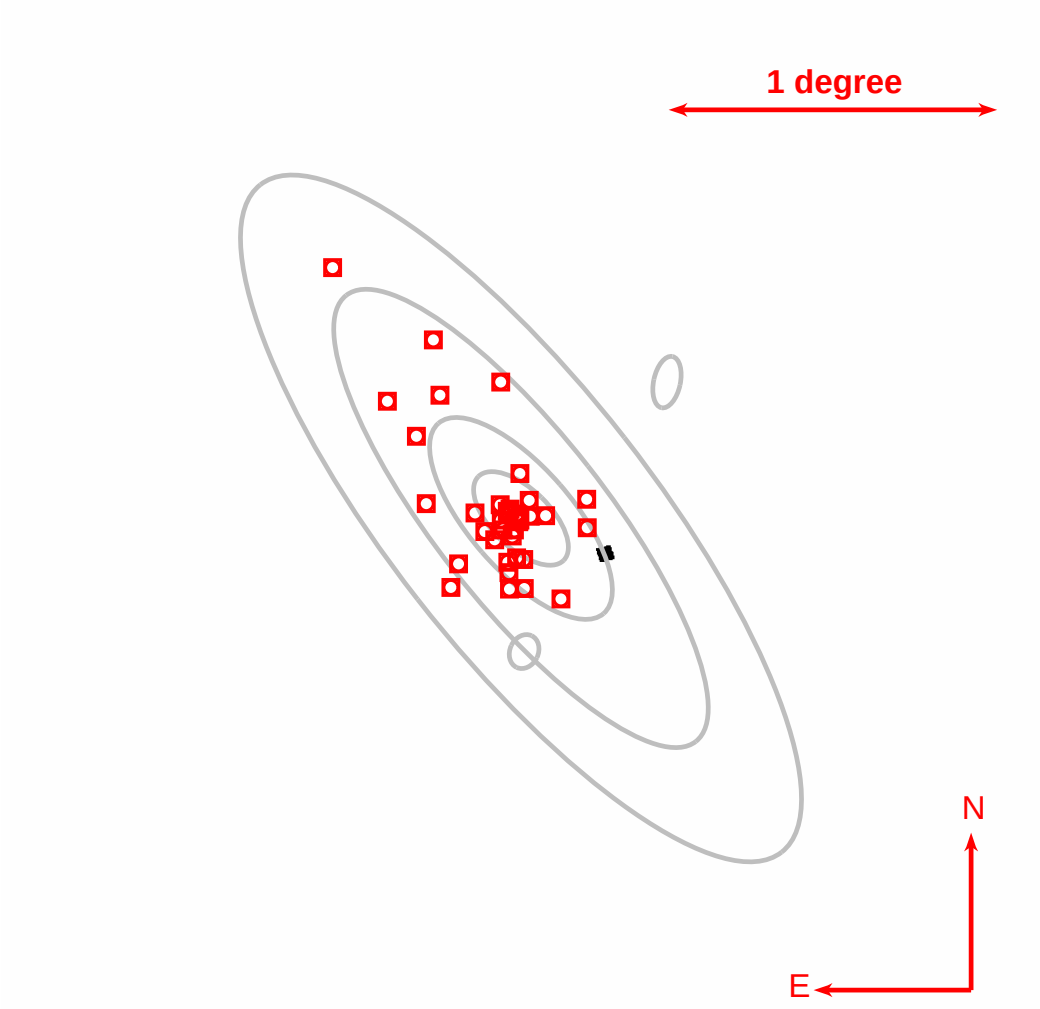

Figure A.14: The WFC3 *HST* coverage of M31 in F475X filter. Key as in Figure A.1.

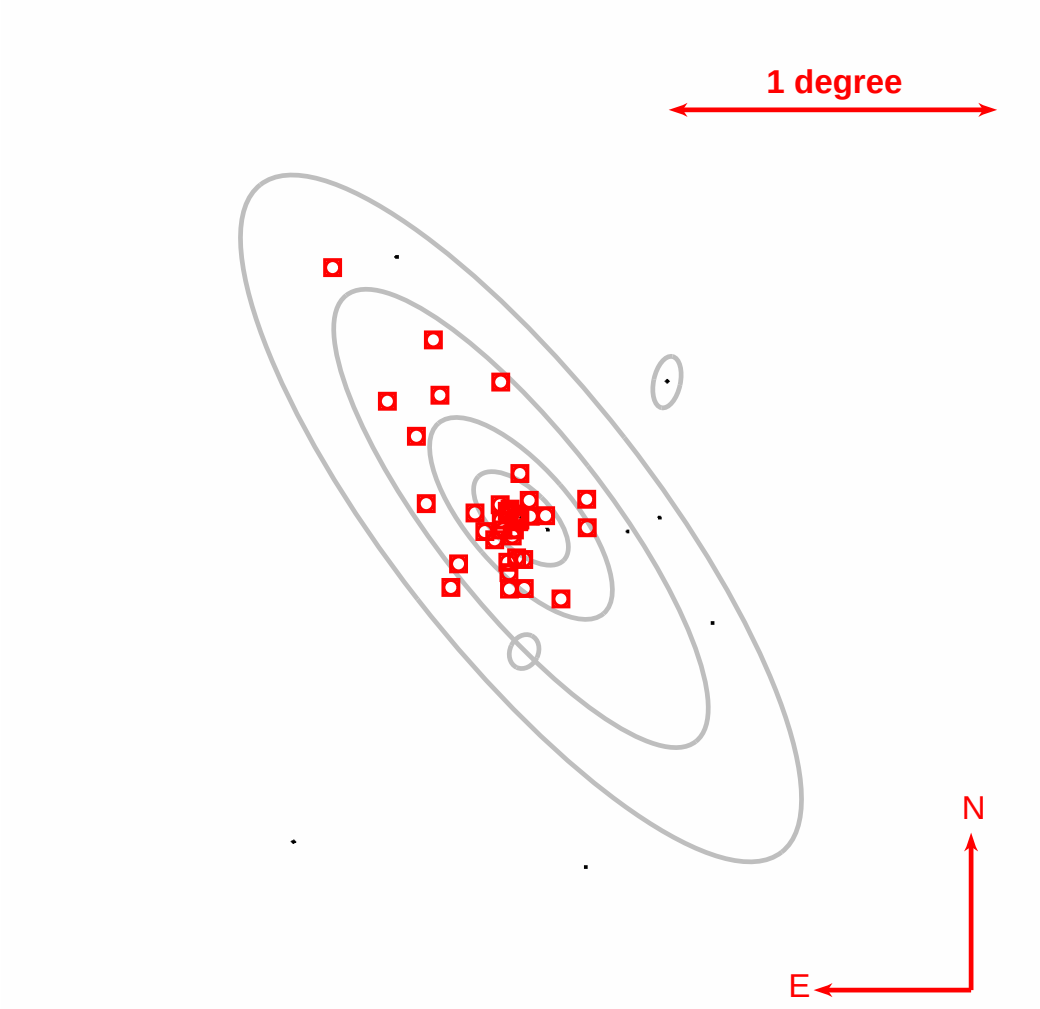

Figure A.15: The WFC3 *HST* coverage of M31 in F555W filter. Key as in Figure A.1.

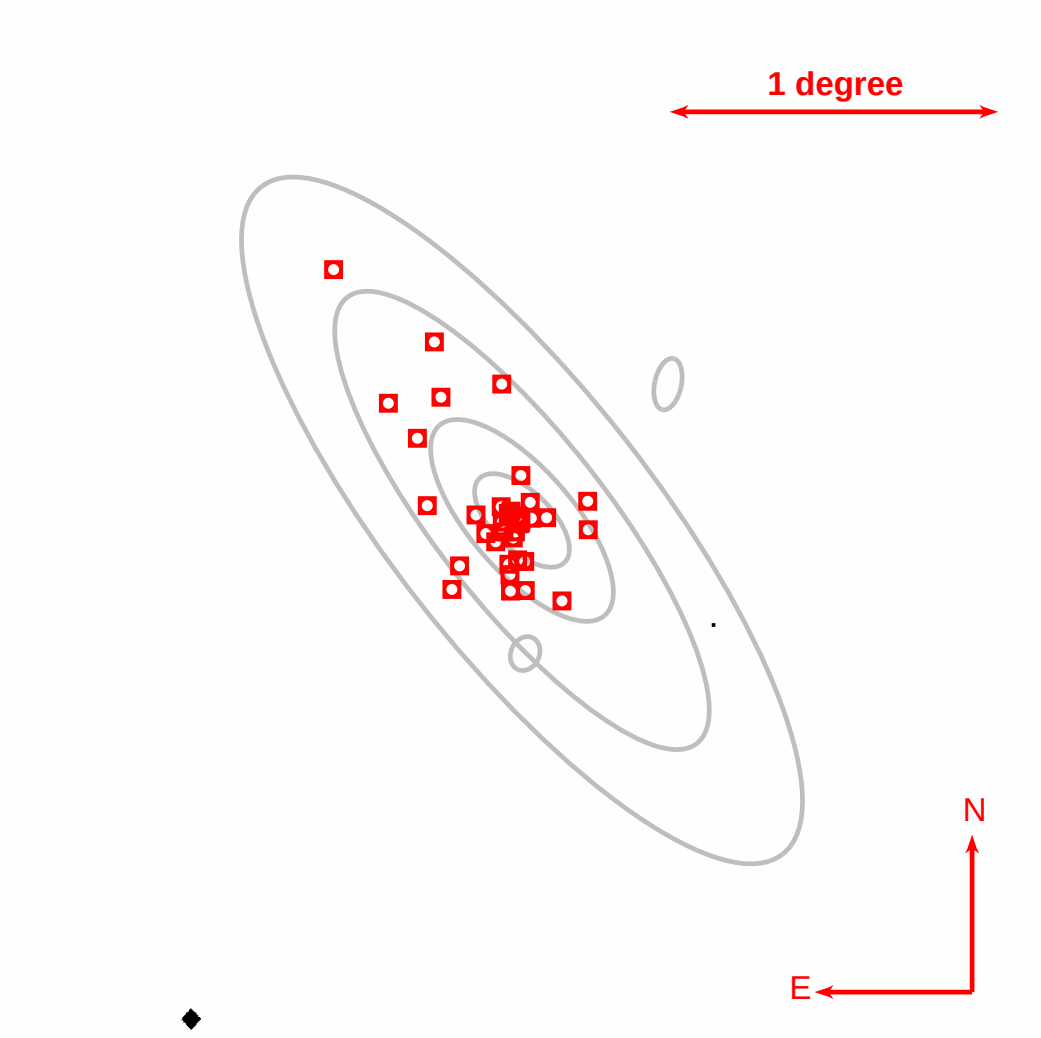

Figure A.16: The WFC3 *HST* coverage of M31 in F814W filter. Key as in Figure A.1.

Bibliography

Adamakis, S., Eyres, S. P. S., Sarkar, A., & Walsh, R. W. 2011, MNRAS, 414, 2195

Ansari, R., Aurière, M., Baillon, P., Bouquet, A., Coupinot, G., Coutures, C., Ghesquière, C., Giraud-Héraud, Y., Gillieron, D., Gondolo, P., Hecquet, J., Kaplan, J., Kim, A., Le Du, Y., Melchior, A. L., Moniez, M., Picat, J. P., & Soucail, G. 2004, A&A, 421, 509

Anupama, G. C. 2008, in Astronomical Society of the Pacific Conference Series, Vol. 401, RS Ophiuchi (2006) and the Recurrent Nova Phenomenon, ed. A. Evans, M. F. Bode, T. J. O'Brien, & M. J. Darnley, 31

Anupama, G. C. & Mikołajewska, J. 1999, A&A, 344, 177

Aurière, M., Baillon, P., Bouquet, A., Carr, B. J., Crézé, M., Evans, N. W., Giraud-Héraud, Y., Gould, A., Hewett, P. C., Kaplan, J., Kerins, E., Lastennet, E., Le Du, Y., Melchior, A.-L., Paulin-Henriksson, S., Smartt, S. J., & Valls-Gabaud, D. 2001, ApJ, 553, L137

Barsukova, E., Afanasiev, V., Fabrika, S., Valeev, A., Hornoch, K., & Pietsch, W. 2009, ATel, 2251

Barsukova, E., Fabrika, S., Hornoch, K., Fatkhullin, T., Sholukhova, O., & Pietsch, W. 2011, ATel, 3725

Bath, G. T., & Harkness, R. P. 1989, in Classical Novae, ed. M. F. Bode & A. Evans (1st ed.; Chichester: Wiley), 61

Bedin, L. R., Ruiz-Lapuente, P., González Hernández, J. I., Canal, R., Filippenko, A. V., & Mendez, J. 2014, MNRAS, 439, 354

Bode, M. F. 2010, Astronomische Nachrichten, 331, 160

Bode, M. F., Darnley, M. J., Shafter, A. W., Page, K. L., Smirnova, O., Anupama, G. C., & Hilton, T. 2009, ApJ, 705, 1056

Bode, M. F., & Evans, A. 1989, in Classical Novae, ed. M. F. Bode & A. Evans (1st ed.; Chichester: Wiley), 163

Bond, H. E., Walter, F., Espinoza, J., Gonzalez, D., Pasten, A., & Green, D. W. E. 2004, IAU Circ., 8424, 1

Burwitz, V., Pietsch, W., Henze, M., Updike, A., Milne, P., Williams, G., Hartmann, D. H., Rodriguez, J., Holmes, S., Kolb, U., & Lucas, R. 2010a, CBET, 2124, 1

—. 2010b, ATel, 2383

Burwitz, V., Pietsch, W., Updike, A., Hartmann, D., Milne, P., & Williams, G. 2007, ATel, 1238

Buscombe, W. & de Vaucouleurs, G. 1955, The Observatory, 75, 170

Cao, Y. 2011, ATel, 3702

Cao, Y. & Kasliwal, M. M. 2011, ATel, 3800

—. 2012, ATel, 3846

Cao, Y., Kasliwal, M. M., McKay, A., & Bradley, A. 2014, ATel, 5786

Cao, Y., Kasliwal, M. M., Neill, J. D., Kulkarni, S. R., Lou, Y.-Q., Ben-Ami, S., Bloom, J. S., Cenko, S. B., Law, N. M., Nugent, P. E., Ofek, E. O., Poznanski, D., & Quimby, R. M. 2012, ApJ, 752, 133

Cao, Y., Kasliwal, M. M., & Yaron, O. 2011, ATel, 3701

Cao, Y., Tang, S., Kasliwal, M. M., Cenko, S. B., & Clubb, K. I. 2013, ATel, 5260

Cardelli, J. A., Clayton, G. C., & Mathis, J. S. 1989, ApJ, 345, 245

Casanova, J., José, J., García-Berro, E., Calder, A., & Shore, S. N. 2011, A&A, 527, A5

Chesneau, O., Banerjee, D. P. K., Millour, F., Nardetto, N., Sacuto, S., Spang, A., Wittkowski, M., Ashok, N. M., Das, R. K., Hummel, C., Kraus, S., Lagadec, E., Morel, S., Petr-Gotzens, M., Rantakyro, F., & Schöller, M. 2008, A&A, 487, 223

Chesneau, O., Lagadec, E., Otulakowska-Hypka, M., Banerjee, D. P. K., Woodward, C. E., Harvey, E., Spang, A., Kervella, P., Millour, F., Nardetto, N., Ashok, N. M., Barlow, M. J., Bode, M., Evans, A., Lynch, D. K., O'Brien, T. J., Rudy, R. J., & Russell, R. W. 2012, A&A, 545, A63

Ciardullo, R., Ford, H. C., Neill, J. D., Jacoby, G. H., & Shafter, A. W. 1987, ApJ, 318, 520

Ciroi, S., Di Mille, F., Rafanelli, P., & Temporin, S. 2007, ATel, 1292

Coelho, E. A., Shafter, A. W., & Misselt, K. A. 2008, ApJ, 686, 1261

Collazzi, A. C., Schaefer, B. E., Xiao, L., Pagnotta, A., Kroll, P., Löchel, K., & Henden, A. A. 2009, AJ, 138, 1846

Cutri, R. M., Skrutskie, M. F., van Dyk, S., Beichman, C. A., Carpenter, J. M., Chester, T., Cambresy, L., Evans, T., Fowler, J., Gizis, J., Howard, E., Huchra, J., Jarrett, T., Kopan, E. L., Kirkpatrick, J. D., Light, R. M., Marsh, K. A., McCallon, H., Schneider, S., Stiening, R., Sykes, M., Weinberg, M., Wheaton, W. A., Wheelock, S., & Zacarias, N. 2003, 2MASS All Sky Catalog of point sources.

Darnley, M. J. 2005, PhD thesis, Liverpool John Moores University, UK

Darnley, M. J., Bode, M. F., Harman, D. J., Hounsell, R. A., Munari, U., Ribeiro, V. A. R. M., Surina, F., Williams, R. P., & Williams, S. C. 2013, in Stella Novae: Future and Past Decades, P. A. Woudt & V. A. R. M. Ribeiro (eds), ASPCS, in press (arXiv:1303.2711)

Darnley, M. J., Bode, M. F., Kerins, E., Newsam, A. M., An, J., Baillon, P., Belokurov, V., Calchi Novati, S., Carr, B. J., Crézé, M., Evans, N. W., Giraud-Héraud, Y., Gould, A., Hewett, P., Jetzer, P., Kaplan, J., Paulin-Henriksson, S., Smartt, S. J., Tsapras, Y., & Weston, M. 2006, MNRAS, 369, 257

Darnley, M. J., Bode, M. F., Kerins, E., Newsam, A. M., An, J., Baillon, P., Novati, S. C., Carr, B. J., Crézé, M., Evans, N. W., Giraud-Héraud, Y., Gould, A., Hewett, P., Jetzer, P., Kaplan, J., Paulin-Henriksson, S., Smartt, S. J., Stalin, C. S., & Tsapras, Y. 2004, MNRAS, 353, 571

Darnley, M. J., Kerins, E., Newsam, A., Duke, J. P., Gould, A., Han, C., Ibrahimov, M. A., Im, M., Jeon, Y.-B., Karimov, R. G., Lee, C.-U., & Park, B.-G. 2007, ApJ, 661, L45

Darnley, M. J., Ribeiro, V. A. R. M., Bode, M. F., Hounsell, R. A., & Williams, R. P. 2012, ApJ, 746, 61

Darnley, M. J., Williams, S. C., Bode, M. F., Henze, M., Ness, J.-U., Shafter, A. W., Hornoch, K., & Votruba, V. 2014, A&A, 563, L9

Das, R. K., Banerjee, D. P. K., & Ashok, N. M. 2009, MNRAS, 398, 375

de Vaucouleurs, G. 1958, ApJ, 128, 465

de Vaucouleurs, G. & Corwin, Jr., H. G. 1985, ApJ, 295, 287

della Valle, M., Bianchini, A., Livio, M., & Orio, M. 1992, A&A, 266, 232

della Valle, M. & Livio, M. 1996, ApJ, 473, 240

—. 1998, ApJ, 506, 818

Di Mille, F., Ciroi, S., Navasardyan, H., Orio, M., Rafanelli, P., & Bianchini, A. 2009, ATel, 2171

Di Mille, F., Ciroi, S., Orio, M., Rafanelli, P., Bianchini, A., Nelson, T., & Andreuzzi, G. 2008, ATel, 1818

Di Mille, F., Ciroi, S., Rafanelli, P., Navasardyan, H., & Bufano, F. 2007, ATel, 1325

Di Mille, F., Orio, M., Ciroi, S., Bianchini, A., Rafanelli, P., & Nelson, T. 2010, Astronomische Nachrichten, 331, 197

Dilday, B., Howell, D. A., Cenko, S. B., Silverman, J. M., Nugent, P. E., Sullivan, M., Ben-Ami, S., Bildsten, L., Bolte, M., Endl, M., Filippenko, A. V., Gnat, O., Horesh, A., Hsiao, E., Kasliwal, M. M., Kirkman, D., Maguire, K., Marcy, G. W., Moore, K., Pan, Y., Parrent, J. T., Podsiadlowski, P., Quimby, R. M., Sternberg, A., Suzuki, N., Tytler, D. R., Xu, D., Bloom, J. S., Gal-Yam, A., Hook, I. M., Kulkarni, S. R., Law, N. M., Ofek, E. O., Polishook, D., & Poznanski, D. 2012, Science, 337, 942

Dimitriadis, G., Chiotellis, A., & Vink, J. 2014, MNRAS, submitted (arXiv:1401.7332)

Dolphin, A. E. 2000, PASP, 112, 1383

—. 2009, PASP, 121, 655

Downes, R. A. & Duerbeck, H. W. 2000, AJ, 120, 2007

Duerbeck, H. W. 1981, PASP, 93, 165

Duerbeck, H. W. 1990, in Lecture Notes in Physics, Berlin Springer Verlag, Vol. 369, IAU Colloq. 122: Physics of Classical Novae, ed. A. Cassatella & R. Viotti, 34

Duerbeck, H. W. 2008, in Classical Novae, ed. M. F. Bode & A. Evans (2nd ed.; Cambridge: Cambridge Univ. Press), 1

Elias-Rosa, N., Greggio, L., & Botticella, M. T. 2014, ATel, 5849

Evans, A. 1993, The Dusty Universe (New York: Horwood)

—. 2001, Ap&SS, 275, 131

Evans, A., Geballe, T. R., Rawlings, J. M. C., Eyres, S. P. S., & Davies, J. K. 1997, MNRAS, 292, 192

Evans, A., Geballe, T. R., Rawlings, J. M. C., & Scott, A. D. 1996, MNRAS, 282, 1049

Evans, A. & Rawlings, J. M. C. 1994, MNRAS, 269, 427

Evans, A., & Rawlings, J. M. C. 2008, in Classical Novae, ed. M. F. Bode & A. Evans (2nd ed.; Cambridge: Cambridge Univ. Press), 308

Evans, A., Tyne, V. H., Smith, O., Geballe, T. R., Rawlings, J. M. C., & Eyres, S. P. S. 2005, MNRAS, 360, 1483

Fabrika, S., Barsukova, E. A., Valeev, A. F., Sholukhova, O., Hornoch, K., Shafter, A. W., & Henze, M. 2014, ATel, 5745

Fabrika, S., Barsukova, E. A., Valeev, A. F., Vinokurov, A., Goranskij, V. P., Hornoch, K., Henze, M., Shafter, A. W., & Pietsch, W. 2013, ATel, 5554

Fabrika, S., Sholukhova, O., Valeev, A., Hornoch, K., & Pietsch, W. 2009, ATel, 2240

Ferrarese, L., Côté, P., & Jordán, A. 2003, ApJ, 599, 1302

Fossey, J., Cooke, B., Pollack, G., Wilde, M., & Wright, T. 2014, CBET, 3792, 1

Fouqué, P., Solanes, J. M., Sanchis, T., & Balkowski, C. 2001, A&A, 375, 770

Freedman, W. L. & Madore, B. F. 1990, ApJ, 365, 186

Gal-Yam, A. & Quimby, R. 2007, ATel, 1236

Gaposchkin, C. H. P. 1957, The Galactic Novae ed. C. H. P. Gaposchkin (Amsterdam: North-Holland)

García-Berro, E. 2013, in IAU Symposium, Vol. 281, IAU Symposium, ed. R. Di Stefano, M. Orio, & M. Moe, 52

Garcia-Berro, E. & Iben, I. 1994, ApJ, 434, 306

Gehrz, R. D. 2008, in Classical Novae, ed. M. F. Bode & A. Evans (2nd ed.; Cambridge: Cambridge Univ. Press), 167

Gehrz, R. D., Truran, J. W., Williams, R. E., & Starrfield, S. 1998, PASP, 110, 3

Geisel, S. L., Kleinmann, D. E., & Low, F. J. 1970, ApJ, 161, L101

Gerke, J. R., Kochanek, C. S., & Stanek, K. Z. 2014, ATel, 5808

Gil-Pons, P., García-Berro, E., José, J., Hernanz, M., & Truran, J. W. 2003, A&A, 407, 1021

González Hernández, J. I., Ruiz-Lapuente, P., Filippenko, A. V., Foley, R. J., Gal-Yam, A., & Simon, J. D. 2009, ApJ, 691, 1

González Hernández, J. I., Ruiz-Lapuente, P., Tabernero, H. M., Montes, D., Canal, R., Méndez, J., & Bedin, L. R. 2012, Nature, 489, 533

Gutierrez, J., Garcia-Berro, E., Iben, Jr., I., Isern, J., Labay, J., & Canal, R. 1996, ApJ, 459, 701

Hachisu, I., Kato, M., Kato, T., & Matsumoto, K. 2000, ApJ, 528, L97

Hachisu, I., Kato, M., & Luna, G. J. M. 2007, ApJ, 659, L153

Haiman, Z., Magnier, E., Lewin, W. H. G., Lester, R. R., van Paradijs, J., Hasinger, G., Pietsch, W., Supper, R., & Truemper, J. 1994, A&A, 286, 725

Harrison, T. E., Johnson, J. J., & Spyromilio, J. 1993, AJ, 105, 320

Hauschildt, P. H. 2008, in Classical Novae, ed. M. F. Bode & A. Evans (2nd ed.; Cambridge: Cambridge Univ. Press), 102

Henize, K. G., Hoffleit, D., & McKibben Nail, V. 1954, Proceedings of the National Academy of Science, 40, 365

Henze, M., Burwitz, V., Pietsch, W., Hatzidimitriou, D., Reig, P., Primak, N., & Papamastorakis, G. 2008a, ATel, 1654

Henze, M. & Meusinger, H. 2014, ATel, 5933

Henze, M., Meusinger, H., & Pietsch, W. 2008b, A&A, 477, 67

Henze, M., Ness, J.-U., Bode, M. F., Darnley, M. J., & Williams, S. C. 2013, ATel, 5627

Henze, M., Ness, J.-U., Darnley, M. J., Bode, M. F., Williams, S. C., Shafter, A. W., Kato, M., & Hachisu, I. 2014a, A&A, 563, L8

Henze, M., Pietsch, W., Burwitz, V., Hatzidimitriou, D., Reig, P., Primak, N., & Papamastorakis, G. 2008c, ATel, 1790

Henze, M., Pietsch, W., Haberl, F., Della Valle, M., Sala, G., Hatzidimitriou, D., Hofmann, F., Hernanz, M., Hartmann, D. H., & Greiner, J. 2014b, A&A, 563, A2

Henze, M., Pietsch, W., Haberl, F., Hernanz, M., Sala, G., Hatzidimitriou, D., Della Valle, M., Rau, A., Hartmann, D. H., & Burwitz, V. 2011, A&A, 533, A52

Henze, M., Pietsch, W., Podigachoski, P., Burwitz, V., Haberl, F., Updike, A., Hartmann, D., Milne, P., Williams, G., Papamastorakis, G., Reig, P., & Strigachev, A. 2009, ATel, 2286

Hessman, F. V., Gänsicke, B. T., & Mattei, J. A. 2000, A&A, 361, 952

Hillman, Y., Prialnik, D., Kovetz, A., Shara, M. M., & Neill, J. D. 2014, MNRAS, 437, 1962

Hogg, F. S. 1937, JRASC, 31, 351

Hornoch, K. 2012, ATel, 4384

Hornoch, K., Corral-Santana, J., Casares, J., Hornochova, P., & Wolf, M. 2010a, CBET, 2487, 1

Hornoch, K. & Galad, A. 2012, ATel, 4653

Hornoch, K., Hornochova, P., & Wolf, M. 2010b, CBET, 2516, 3

Hornoch, K., Khan, R., Bird, J., Pejcha, O., Garnavich, P., Littlefield, C., Paul, N., & Bouzid, S. 2010c, CBET, 2319, 1

Hornoch, K. & Kucakova, H. 2013a, ATel, 5671

—. 2013b, ATel, 5414

Hornoch, K., Manilla-Robles, A., Tudor, V., Vaduvescu, O., & Ramsay, G. 2013, ATel, 5503

Hornoch, K. & Pejcha, O. 2009, CBET, 2061, 5

Hornoch, K., Pejcha, O., & Kusnirak, P. 2009a, CBET, 2058, 3

Hornoch, K., Pejcha, O., & Wolf, M. 2009b, CBET, 2062, 1

Hornoch, K., Pejcha, O., Zasche, P., & Kusnirak, P. 2009c, CBET, 2057, 3

Hornoch, K., Prieto, J., Khan, R., & Hornochova, P. 2010d, CBET, 2610, 1

Hornoch, K., Prieto, J., Khan, R., Pejcha, O., Kubanek, P., Gorosabel, J., Martorell, P., & Jelinek, M. 2010e, CBET, 2127, 1

Hornoch, K. & Vrastil, J. 2012, ATel, 4364

Hornoch, K., Wolf, M., Hornochova, P., Kubanek, P., Morales, N., Ortiz, J. L., Gorosabel, J., Jelinek, M., & Zasche, P. 2010f, CBET, 2305, 1

Hornoch, K., Wolf, M., Kubanek, P., Gorrosabel, J., & Jelinek, M. 2009d, CBET, 2057, 2

Hornoch, K., Zasche, P., Hornoch, K., Wolf, M., Hornochova, P., Kubanek, P., Gorosabel, J., Lara-Gil, O., & Jelinek, M. 2010g, CBET, 2341, 2

Hounsell, R., Bode, M. F., Hick, P. P., Buffington, A., Jackson, B. V., Clover, J. M., Shafter, A. W., Darnley, M. J., Mawson, N. R., Steele, I. A., Evans, A., Eyres, S. P. S., & O'Brien, T. J. 2010, ApJ, 724, 480

Hubble, E. P. 1926, ApJ, 63, 236

—. 1929, ApJ, 69, 103

Iben, I. & Fujimoto, M. Y. 2008, in Classical Novae, ed. M. F. Bode & A. Evans (2nd ed.; Cambridge: Cambridge Univ. Press), 34

Iben, Jr., I. 1985, QJRAS, 26, 1

INAF-Astronomical Observatory of Bologna. 2014, ATel, 5818

Jerjen, H., Binggeli, B., & Barazza, F. D. 2004, AJ, 127, 771

Jose, J. & Hernanz, M. 1998, ApJ, 494, 680

Jurdana-Šepić, R., Ribeiro, V. A. R. M., Darnley, M. J., Munari, U., & Bode, M. F. 2012, A&A, 537, A34

Kamath, U. S., Anupama, G. C., Ashok, N. M., & Chandrasekhar, T. 1997, AJ, 114, 2671

Karachentsev, I. D. & Kashibadze, O. G. 2006, Astrophysics, 49, 3

Kasliwal, M. M. 2009, CBET, 2015, 3

Kasliwal, M. M., Cenko, S. B., Kulkarni, S. R., Ofek, E. O., Quimby, R., & Rau, A. 2011, ApJ, 735, 94

Kasliwal, M. M., Rau, A., Salvato, M., Cenko, S. B., Ofek, E. O., Quimby, R., & Kulkarni, S. R. 2009, ATel, 1886

Kato, M., Saio, H., Hachisu, I., & Nomoto, K. 2014, ApJ, submitted (arXiv:1404.0582)

Kato, T., Uemura, M., Haseda, K., Yamaoka, H., Takamizawa, K., Fujii, M., & Kiyota, S. 2002, PASJ, 54, 1009

Kelly, P. L., Fox, O. D., Filippenko, A. V., Cenko, S. B., Prato, L., Schaefer, G., Shen, K. J., Zheng, W., Graham, M. L., & Tucker, B. E. 2014, ApJ, submitted (arXiv:1403.4250)

Kent, S. M. 1987, AJ, 94, 306

Kenyon, S. J. & Fernandez-Castro, T. 1987, AJ, 93, 938

Kerins, E., Darnley, M. J., Duke, J. P., Gould, A., Han, C., Jeon, Y.-B., Newsam, A., & Park, B.-G. 2006, MNRAS, 365, 1099

Kerzendorf, W. E., Schmidt, B. P., Asplund, M., Nomoto, K., Podsiadlowski, P., Frebel, A., Fesen, R. A., & Yong, D. 2009, ApJ, 701, 1665

Kerzendorf, W. E., Yong, D., Schmidt, B. P., Simon, J. D., Jeffery, C. S., Anderson, J., Podsiadlowski, P., Gal-Yam, A., Silverman, J. M., Filippenko, A. V., Nomoto, K., Murphy, S. J., Bessell, M. S., Venn, K. A., & Foley, R. J. 2013, ApJ, 774, 99

Kraft, R. P. 1964, ApJ, 139, 457

Lee, C.-H., Riffeser, A., Seitz, S., Bender, R., Fliri, J., Hopp, U., Ries, C., Bärnbantner, O., & Gössl, C. 2012, A&A, 537, A43

Leonard, D. C., Nied, P. M., Davis, M. R., Shafter, A. W., Norris, T. R., George, M. R., & Gal-Yam, A. 2006, CBET, 593, 1

Li, W., Bloom, J. S., Podsiadlowski, P., Miller, A. A., Cenko, S. B., Jha, S. W., Sullivan, M., Howell, D. A., Nugent, P. E., Butler, N. R., Ofek, E. O., Kasliwal, M. M., Richards, J. W., Stockton, A., Shih, H.-Y., Bildsten, L., Shara, M. M., Bibby, J., Filippenko, A. V., Ganeshalingam, M., Silverman, J. M., Kulkarni, S. R., Law, N. M., Poznanski, D., Quimby, R. M., McCully, C., Patel, B., Maguire, K., & Shen, K. J. 2011, Nature, 480, 348

Liller, W. 2009, IAU Circular, 9019, 1

Livio, M. & Truran, J. W. 1992, ApJ, 389, 695

Luyten, W. J. 1927, Harvard College Observatory Bulletin, 847, 8

Magnier, E. A., Lewin, W. H. G., van Paradijs, J., Hasinger, G., Jain, A., Pietsch, W., & Truemper, J. 1992, A&AS, 96, 379

Mason, E. 2011, A&A, 532, L11

Mason, E., Ederoclite, A., Williams, R. E., Della Valle, M., & Setiawan, J. 2012, A&A, 544, A149

Massey, P., Olsen, K. A. G., Hodge, P. W., Strong, S. B., Jacoby, G. H., Schlingman, W., & Smith, R. C. 2006, AJ, 131, 2478

McLaughlin, D. B. 1939, Popular Astronomy, 47, 410

—. 1945, PASP, 57, 69

McLaughlin, D. B. 1960, in Stellar Atmospheres, ed. J. L. Greenstein (Chicago: Univ. Chicago Press), 585

Mitchell, R. M. & Evans, A. 1984, MNRAS, 209, 945

Munari, U., Dallaporta, S., Cherini, G., Castellani, F., Cetrulo, G., Valisa, P., & Graziani, M. 2013, ATel, 4893

Munari, U., Joshi, V. H., Ashok, N. M., Banerjee, D. P. K., Valisa, P., Milani, A., Siviero, A., Dallaporta, S., & Castellani, F. 2011, MNRAS, 410, L52

Nakano, S. 2007, IAU Circular, 8898, 2

Nakano, S. & Yusa, T. 2009, CBET, 1967, 1

Neill, J. D. & Shara, M. M. 2004, AJ, 127, 816

—. 2005, AJ, 129, 1873

Ness, J.-U., Schwarz, G., Starrfield, S., Osborne, J. P., Page, K. L., Beardmore, A. P., Wagner, R. M., & Woodward, C. E. 2008, AJ, 135, 1328

Newsham, G., Starrfield, S., & Timmes, F. 2013, in Stella Novae: Future and Past Decades, P. A. Woudt & V. A. R. M. Ribeiro (eds), ASPCS, in press (arXiv:1303.3642)

Nishiyama, K. & Kabashima, F. 2009a, CBET, 2003, 1

—. 2009b, CBET, 2058, 1

—. 2010, CBET, 2305, 2

Nishiyama, K., Kabashima, F., Hornoch, K., Kubanek, P., Gorrosabel, J., & Jelinek, M. 2009, CBET, 2015, 1

Nishiyama, K., Kabashima, F., Sun, G., Yusa, T., & Pietsch, W. 2010a, CBET, 2472, 1

Nishiyama, K., Kabashima, F., & Yusa, T. 2010b, CBET, 2483, 1

Nomoto, K. & Iben, Jr., I. 1985, ApJ, 297, 531

Nugent, P. E., Sullivan, M., Cenko, S. B., Thomas, R. C., Kasen, D., Howell, D. A., Bersier, D., Bloom, J. S., Kulkarni, S. R., Kandrashoff, M. T., Filippenko, A. V., Silverman, J. M., Marcy, G. W., Howard, A. W., Isaacson, H. T., Maguire, K., Suzuki, N., Tarlton, J. E., Pan, Y.-C., Bildsten, L., Fulton, B. J., Parrent, J. T., Sand, D., Podsiadlowski, P., Bianco, F. B., Dilday, B., Graham, M. L., Lyman, J., James, P., Kasliwal, M. M., Law, N. M., Quimby, R. M., Hook, I. M., Walker, E. S., Mazzali, P., Pian, E., Ofek, E. O., Gal-Yam, A., & Poznanski, D. 2011, Nature, 480, 344

O'Brien, T. J. & Bode, M. F. 2008, in Classical Novae, ed. M. F. Bode & A. Evans (2nd ed.; Cambridge: Cambridge Univ. Press), 285

Ovcharov, E., Valcheva, A., Kostov, A., Nikolov, Y., & Nedialkov, P. 2011, ATel, 3693

Page, K. L., Osborne, J. P., Beardmore, A. P., & Mukai, K. 2014, ATel, 5870

Pagnotta, A. & Schaefer, B. E. 2014, ApJ, accepted (arXiv:1405.0246)

Patterson, J. 1994, PASP, 106, 209

Perryman, M. A. C. & ESA, eds. 1997, ESA Special Publication, Vol. 1200, The HIPPARCOS and TYCHO catalogues. Astrometric and photometric star catalogues derived from the ESA HIPPARCOS Space Astrometry Mission

Piersanti, L., Gagliardi, S., Iben, Jr., I., & Tornambé, A. 2003, ApJ, 598, 1229

Pietsch, W. 2010, Astronomische Nachrichten, 331, 187

Pietsch, W., Burwitz, V., Greiner, J., Barsukova, E., Fabrika, S., Moiseev, A., Valeev, A., Goranskij, V., & Hornoch, K. 2007a, ATel, 1009

Pietsch, W., Haberl, F., Sala, G., Stiele, H., Hornoch, K., Riffeser, A., Fliri, J., Bender, R., Bühler, S., Burwitz, V., Greiner, J., & Seitz, S. 2007b, A&A, 465, 375

Pietsch, W., Henze, M., Burwitz, V., Kaur, A., Hartmann, D. H., Milne, P., & Williams, G. 2010a, ATel, 3001

Pietsch, W., Henze, M., Haberl, F., & Burwitz, V. 2010b, ATel, 3038

Pietsch, W., Henze, M., Haberl, F., Hernanz, M., Sala, G., Hartmann, D. H., & Della Valle, M. 2011, A&A, 531, A22

Pietsch, W., Kaduk, F., Henze, M., Burwitz, V., Papamastorakis, G., Reig, P., & Strigachev, A. 2009a, ATel, 2147

Pietsch, W., Lloyd, J., Henze, M., Burwitz, V., Knaur, A., Hartmann, D., Milne, P., Williams, G., Liakos, A., Hatzidimitriou, D., & Niarchos, P. 2010c, ATel, 2896

Pietsch, W., Podigachoski, P., Haberl, F., Henze, M., Burwitz, V., Updike, A., Milne, P., Williams, G., & Hartmann, D. H. 2009b, ATel, 2308

Planck Collaboration, Ade, P. A. R., Aghanim, N., Armitage-Caplan, C., Arnaud, M., Ashdown, M., Atrio-Barandela, F., Aumont, J., Baccigalupi, C., Banday, A. J., & et al. 2013 (arXiv:1303.5076)

Podigachoski, P., Henze, M., Pietsch, W., Burwitz, V., Papamastorakis, G., Reig, P., & Strigachev, A. 2009a, ATel, 2234

Podigachoski, P., Pietsch, W., Henze, M., Burwitz, V., Updike, A., Milne, P., Williams, G., & Hartmann, D. H. 2009b, ATel, 2304

Podsiadlowski, P. 2010, Astronomische Nachrichten, 331, 218

Pontefract, M. & Rawlings, J. M. C. 2004, MNRAS, 347, 1294

Prialnik, D. & Kovetz, A. 1984, ApJ, 281, 367

—. 1995, ApJ, 445, 789

Pritchet, C. J. & van den Bergh, S. 1987, ApJ, 318, 507

Qiao, Q. Y., Qiu, Y. L., Hu, J. Y., Li, W. D., Esamdin, A., Zhang, Y., Wei, J. Y., Cao, L., & Gu, Q. S. 1997, IAU Circ., 6777, 1

Quimby, R. 2006, ATel, 887

Quimby, R., Shafter, A., Rau, A., Kasliwal, M., Ofek, E., Yuan, F., Akerlof, C., & Wheeler, J. C. 2007, ATel, 1299

Raj, A., Ashok, N. M., & Banerjee, D. P. K. 2011, MNRAS, 415, 3455

Raj, A., Ashok, N. M., Banerjee, D. P. K., Munari, U., Valisa, P., & Dallaporta, S. 2012, MNRAS, 425, 2576

Rau, A. 2007, ATel, 1276

Rau, A., Burwitz, V., Cenko, S. B., Updike, A., Hartmann, D., Milne, P., & Williams, G. 2007, ATel, 1242

Ritchey, G. W. 1917, PASP, 29, 257

Robinson, E. L. 1975, AJ, 80, 515

Rodríguez-Gil, P., Ferrando, R., Rodríguez, D., Bode, M. F., Huxor, A., Giles, P., & Mackey, D. 2009, ATel, 2166

Rosino, L. 1973, A&AS, 9, 347

Ruan, J., Gao, X., Nishiyama, K., Kabashima, F., Itagaki, K., Nakano, S., & Yusa, T. 2010, CBET, 2500, 1

Rudy, R. J., Dimpfl, W. L., Lynch, D. K., Mazuk, S., Venturini, C. C., Wilson, J. C., Puetter, R. C., & Perry, R. B. 2003, ApJ, 596, 1229

Ruiz-Lapuente, P., Comeron, F., Méndez, J., Canal, R., Smartt, S. J., Filippenko, A. V., Kurucz, R. L., Chornock, R., Foley, R. J., Stanishev, V., & Ibata, R. 2004, Nature, 431, 1069

Sala, G. & Hernanz, M. 2005, A&A, 439, 1061

Schaefer, B. E. 2005, ApJ, 621, L53

—. 2010, ApJS, 187, 275

Schaefer, B. E., Landolt, A. U., Linnolt, M., Stubbings, R., Pojmanski, G., Plummer, A., Kerr, S., Nelson, P., Carstens, R., Streamer, M., Richards, T., Myers, G., & Dillon, W. G. 2011 (arXiv:1109.0065)

Schaefer, B. E. & Pagnotta, A. 2012, Nature, 481, 164

Schaefer, B. E., Pagnotta, A., & Shara, M. M. 2010a, ApJ, 708, 381

Schaefer, B. E., Pagnotta, A., Xiao, L., Darnley, M. J., Bode, M. F., Harris, B. G., Dvorak, S., Menke, J., Linnolt, M., Templeton, M., Henden, A. A., Pojmański, G., Pilecki, B., Szczygieł, D. M., & Watanabe, Y. 2010b, AJ, 140, 925

Selvelli, P., González-Riestra, R., Gilmozzi, R., & Cassatella, A. 2010, Mem. Societa Astronomica Italiana, 81, 388

Shafter, A. 2008, in Classical Novae, ed. M. F. Bode & A. Evans (2nd ed.; Cambridge: Cambridge Univ. Press), 335

Shafter, A. W. 1997, ApJ, 487, 226

—. 2007, ATel, 1332

—. 2013, AJ, 145, 117

Shafter, A. W., Bode, M. F., Darnley, M. J., Ciardullo, R., Cao, Y., & Hornoch, K. 2011a, ATel, 3825

Shafter, A. W., Bode, M. F., Darnley, M. J., Ciardullo, R., & Misselt, K. A. 2010a, ATel, 3006

Shafter, A. W., Bode, M. F., Darnley, M. J., Misselt, K. A., Rubin, M., & Hornoch, K. 2011b, ApJ, 727, 50

Shafter, A. W., Ciardullo, R., Bode, M. F., & Darnley, M. J. 2011c, ATel, 3699

Shafter, A. W., Ciardullo, R., Bode, M. F., Darnley, M. J., & Misselt, K. A. 2010b, ATel, 2987

Shafter, A. W., Ciardullo, R., Bode, M. F., Darnley, M. J., Misselt, K. A., Nishiyama, K., & Kabashima, F. 2008a, ATel, 1834

Shafter, A. W., Ciardullo, R., Burwitz, V., Henze, M., Pietsch, W., Milne, P., Misselt, K. A., Williams, G., Hartmann, D. H., Updike, A., Bode, M. F., & Darnley, M. J. 2008b, ATel, 1851

Shafter, A. W., Ciardullo, R., Darnley, M. J., & Bode, M. F. 2011d, ATel, 3727

Shafter, A. W., Ciardullo, R., Darnley, M. J., Bode, M. F., & Misselt, K. A. 2010c, ATel, 2898

—. 2010d, ATel, 2949

—. 2010e, ATel, 2909

Shafter, A. W., Ciardullo, R., & Pritchet, C. J. 2000, ApJ, 530, 193

Shafter, A. W., Coelho, E. A., Misselt, K. A., Bode, M. F., Darnley, M. J., & Quimby, R. 2006, ATel, 923

Shafter, A. W., Curtin, C., Pritchet, C. J., Bode, M. F., & Darnley, M. J. 2013, in Stella Novae: Future and Past Decades, P. A. Woudt & V. A. R. M. Ribeiro (eds), ASPCS, in press (arXiv:1307.2296)

Shafter, A. W., Darnley, M. J., Bode, M. F., & Ciardullo, R. 2012a, ApJ, 752, 156

Shafter, A. W., Darnley, M. J., Bode, M. F., Ciardullo, R., & Hornoch, K. 2012b, ATel, 3850

Shafter, A. W., Darnley, M. J., Bode, M. F., Williams, S. C., Hornoch, K., & Ciardullo, R. 2011e, ATel, 3806

Shafter, A. W., Darnley, M. J., Hornoch, K., Filippenko, A. V., Bode, M. F., Ciardullo, R., Misselt, K. A., Hounsell, R. A., Chornock, R., & Matheson, T. 2011f, ApJ, 734, 12

Shafter, A. W., Hornoch, K., Ciardullo, J. V. R., Darnley, M. J., & Bode, M. F. 2012c, ATel, 4503

Shafter, A. W., Hornoch, K., Ciardullo, R., Darnley, M. J., & Bode, M. F. 2012d, ATel, 4368

—. 2012e, ATel, 4658

—. 2012f, ATel, 4391

Shafter, A. W., Hornoch, K., Darnley, M. J., Bode, M. F., Ciardullo, R., & Misselt, K. A. 2010f, ATel, 3039

Shafter, A. W. & Irby, B. K. 2001, ApJ, 563, 749

Shafter, A. W., Rau, A., Quimby, R. M., Kasliwal, M. M., Bode, M. F., Darnley, M. J., & Misselt, K. A. 2009, ApJ, 690, 1148

Shore, S. N., Sonneborn, G., Starrfield, S. G., Hamuy, M., Williams, R. E., Cassatella, A., & Drechsel, H. 1991, ApJ, 370, 193

Siess, L. 2006, A&A, 448, 717

Sirianni, M., Jee, M. J., Benítez, N., Blakeslee, J. P., Martel, A. R., Meurer, G., Clampin, M., De Marchi, G., Ford, H. C., Gilliland, R., Hartig, G. F., Illingworth, G. D., Mack, J., & McCann, W. J. 2005, PASP, 117, 1049

Skrutskie, M. F., Cutri, R. M., Stiening, R., Weinberg, M. D., Schneider, S., Carpenter, J. M., Beichman, C., Capps, R., Chester, T., Elias, J., Huchra, J., Liebert, J., Lonsdale, C., Monet, D. G., Price, S., Seitzer, P., Jarrett, T., Kirkpatrick, J. D., Gizis, J. E., Howard, E., Evans, T., Fowler, J., Fullmer, L., Hurt, R., Light, R., Kopan, E. L., Marsh, K. A., McCallon, H. L., Tam, R., Van Dyk, S., & Wheelock, S. 2006, AJ, 131, 1163

Stark, A. A., Gammie, C. F., Wilson, R. W., Bally, J., Linke, R. A., Heiles, C., & Hurwitz, M. 1992, ApJS, 79, 77

Starrfield, S. 2008, in Astronomical Society of the Pacific Conference Series, Vol. 401, RS Ophiuchi (2006) and the Recurrent Nova Phenomenon, ed. A. Evans, M. F. Bode, T. J. O'Brien, & M. J. Darnley, 4

Starrfield, S., Iliadis, C., & Hix, W. R. 2008, in Classical Novae, ed. M. F. Bode & A. Evans (2nd ed.; Cambridge: Cambridge Univ. Press), 77

Starrfield, S., Timmes, F. X., Iliadis, C., Hix, W. R., Arnett, W. D., Meakin, C., & Sparks, W. M. 2012, Baltic Astronomy, 21, 76

Starrfield, S., Truran, J. W., Sparks, W. M., & Kutter, G. S. 1972, ApJ, 176, 169

Steele, I. A., Smith, R. J., Rees, P. C., Baker, I. P., Bates, S. D., Bode, M. F., Bowman, M. K., Carter, D., Etherton, J., Ford, M. J., Fraser, S. N., Gomboc, A., Lett, R. D. J., Mansfield, A. G., Marchant, J. M., Medrano-Cerda, G. A., Mottram, C. J., Raback, D., Scott, A. B., Tomlinson, M. D., & Zamanov, R. 2004, in Society of Photo-Optical Instrumentation Engineers (SPIE) Conference Series, Vol. 5489, ed. J. M. Oschmann, Jr., 679

Stockman, H. S., Schmidt, G. D., & Lamb, D. Q. 1988, ApJ, 332, 282

Strope, R. J., Schaefer, B. E., & Henden, A. A. 2010, AJ, 140, 34

Sturm, R., Haberl, F., Pietsch, W., & Greiner, J. 2013a, ATel, 5528

Sturm, R., Hofmann, F., Pietsch, W., & Greiner, J. 2013b, ATel, 5384

Sturm, R., Pietsch, W., Hofmann, F., & Greiner, J. 2013c, ATel, 5256

Surina, F. 2014, PhD thesis, Liverpool John Moores University, UK

Tang, S., Bildsten, L., Wolf, W. M., Li, K. L., Kong, A. K. H., Cao, Y., Cenko, S. B., De Cia, A., Kasliwal, M. M., Kulkarni, S. R., Laher, R. R., Masci, F., Nugent, P. E., Perley, D. A., Prince, T. A., & Surace, J. 2014, ApJ, 786, 61

Tang, S., Cao, Y., & Kasliwal. 2013a, ATel, 5607

Tang, S., Cao, Y., & Kasliwal, M. M. 2013b, ATel, 5341

Tang, S., Cao, Y., Kasliwal, M. M., Waszczak, A., Johansson, J., O'Sullivan, D., & Ben-Ami, S. 2013c, ATel, 5367

Thoroughgood, T. D., Dhillon, V. S., Littlefair, S. P., Marsh, T. R., & Smith, D. A. 2001, MNRAS, 327, 1323

Tody, D. 1986, in Society of Photo-Optical Instrumentation Engineers (SPIE) Conference Series, Vol. 627, Instrumentation in astronomy VI, ed. D. L. Crawford, 733

Truran, J. W. & Livio, M. 1986, ApJ, 308, 721

Valeev, A., Barsukova, E., Sholukhova, O., Medvedev, A., Hornoch, K., Kusnirak, P., Pietsch, W., & Fabrika, S. 2009, ATel, 2208

Valeev, A. F., Barsukova, E. A., Fabrika, S., Sholukhova, O., Hornoch, K., Kusnirak, P., Vrastil, J., Kucakova, H., Henze, M., & Shafter, A. W. 2013, ATel, 5461

van den Bergh, S. & Pritchet, C. J. 1986, PASP, 98, 110

Waagan, E., Linnolt, M., Bolzoni, S., Amorim, A., Plummer, A., Williams, P. F., Matsuyama, H., Kerr, S., & Pearce, A. 2011, CBET, 2700, 1

Walker, M. F. 1954, PASP, 66, 230

Walter, F. M. & Battisti, A. 2011, in Bulletin of the American Astronomical Society, Vol. 43, American Astronomical Society Meeting Abstracts 217, 338.11

Warner, B. 1995, Cataclysmic Variable Stars (Cambridge: Cambridge Univ. Press)

Warner, B. 2008, in Classical Novae, ed. M. F. Bode & A. Evans (2nd ed.; Cambridge: Cambridge Univ. Press), 16

Whelan, J. & Iben, Jr., I. 1973, ApJ, 186, 1007

White, N. E., Giommi, P., Heise, J., Angelini, L., & Fantasia, S. 1995, ApJ, 445, L125

Williams, B. F., Garcia, M. R., Kong, A. K. H., Primini, F. A., King, A. R., Di Stefano, R., & Murray, S. S. 2004, ApJ, 609, 735

Williams, R., Liller, W., Shara, M., Moffat, A., Wells, L., & Heathcote, S. 1990, IAU Circular, 4964, 1

Williams, R. & Mason, E. 2010, Ap&SS, 327, 207

Williams, R. E. 1992, AJ, 104, 725

Williams, S. C., Bode, M. F., Darnley, M. J., Evans, A., Zubko, V., & Shafter, A. W. 2013, ApJ, 777, L32

Williams, S. C., Darnley, M. J., Bode, M. F., Keen, A., & Shafter, A. W. 2014, ApJS, accepted (arXiv:1405.4874)

Williams, S. J. & Shafter, A. W. 2004, ApJ, 612, 867

Worters, H. L., Eyres, S. P. S., Bromage, G. E., & Osborne, J. P. 2008, in Astronomical Society of the Pacific Conference Series, Vol. 401, RS Ophiuchi (2006) and the Recurrent Nova Phenomenon, ed. A. Evans, M. F. Bode, T. J. O'Brien, & M. J. Darnley, 223

Wynn, G. 2008, in Astronomical Society of the Pacific Conference Series, Vol. 401, RS Ophiuchi (2006) and the Recurrent Nova Phenomenon, ed. A. Evans, M. F. Bode, T. J. O'Brien, & M. J. Darnley, 73

Yamaoka, H., Itagaki, K., Guido, E., Sostero, G., Maehara, H., Fujii, M., Arai, A., Isogai, M., Imamura, K., Rudy, R. J., Prater, T. R., Russell, R. W., Puetter, R. C., Perry, R. B., & Kazarovets, E. V. 2009, IAU Circular, 9098, 1

Yaron, O., Prialnik, D., Shara, M. M., & Kovetz, A. 2005, ApJ, 623, 398

Yuan, F., Quimby, R., Akerlof, C., Aretakis, J., Rykoff, E., & Wheeler, J. C. 2007, ATel, 1311

Ze-Zong, X. & Shu-Jen, P. 1966, Science, 154, 597

Zheng, W., Shivvers, I., Filippenko, A. V., Itagaki, K., Clubb, K. I., Fox, O. D., Graham, M. L., Kelly, P. L., & Mauerhan, J. C. 2014, ApJ, 783, L24

Zubko, V. G., Mennella, V., Colangeli, L., & Bussoletti, E. 1996, MNRAS, 282, 1321